Thermodynamic properties of liquid ^{3}He-^{4}He mixtures between 0.15 K and 1.8 K

by

Gunaranjan Chaudhry

B. Tech., Mechanical Engineering, IIT Delhi, 2003
S.M., Mechanical Engineering, MIT, 2005

Submitted to the Department of Mechanical Engineering
in partial fulfilment of the requirements for the degree of

Doctor of Philosophy

at the

Massachusetts Institute of Technology

September 2009

© 2009 Gunaranjan Chaudhry. All rights reserved.
The author hereby grants to MIT permission to reproduce and to distribute publicly paper and electronic copies of this thesis document in whole or in part in any medium now known or hereafter created.

Signature of Author_____
Department of Mechanical Engineering
August 21, 2009

Certified by_____
John Brisson
Professor of Mechanical Engineering
Thesis Supervisor

Accepted by_____
David Hardt
Chairman, Department Committee on Graduate Students

Thermodynamic properties of liquid ^{3}He-^{4}He mixtures between 0.15 K and 1.8 K

by

Gunaranjan Chaudhry

Submitted to the Department of Mechanical Engineering on August 21, 2009
in partial fulfilment of the requirements for the degree of Doctor of Philosophy

Abstract

Thermodynamic property relations for liquid ^{3}He-^{4}He mixtures between temperatures of 0.15 K and 1.8 K are determined. The relations are valid over the entire concentration range. Thermodynamic properties are first calculated at saturated pressure (which is more or less equal to zero pressure) in the two-phase region, and then extended to the single-phase He-II (up to 1.8 K) and He-I (up to 1.5 K) regions. The calculations at saturated pressure are based on available specific heat data and previously determined sub-0.15 K properties. The property relations are then extended to higher pressures (up to 10 bar) between 0.15 K and 1.5 K, using available molar volume data. The results are largely in good agreement with some other ^{3}He-^{4}He mixture property data, though the scarcity of experimental data in large parts of the region of interest precludes a more thorough comparison. Applications of the derived properties to components of sub-Kelvin refrigerators, specifically He-II mixture heat exchangers and He-II mixture throttles, are also discussed.

Thesis Supervisor: John Brisson
Title: Professor of Mechanical Engineering

Thesis Committee Member: Joseph Smith
Title: Professor of Mechanical Engineering

Thesis Committee Member: Ernest Cravalho
Title: Professor of Mechanical Engineering

Contents

List of Figures

List of Tables

List of Symbols

C or $C_{x,p}$: Specific heat at constant x and constant pressure (per mole of mixture)

$C_{x,svp}$: Specific heat at constant x and at saturated pressure (per mole of mixture)

C_{μ_4} : Specific heat at constant μ_4 and constant pressure (per mole of ^{3}He)

g : Molar Gibbs free energy, per mole of mixture

h : Molar enthalpy, per mole of mixture

h^{os} : Osmotic enthalpy, per mole of ^{3}He

p : Pressure

s : Molar entropy, per mole of mixture

T : Temperature

v : Molar volume, per mole of mixture

x : Mole fraction (concentration) of ^{3}He in ^{3}He-^{4}He mixture

μ_3 : Chemical potential of ^{3}He in ^{3}He-^{4}He mixture

μ_4 : Chemical potential of ^{4}He in ^{3}He-^{4}He mixture

Subscripts

I : Properties in the He-I region

II : Properties in the He-II region

2ϕ : Properties in the two-phase region

3 : ^{3}He property (either of the pure fluid, or of the ^{3}He component in the mixture)

4 : ^{4}He property (either of the pure fluid, or of the ^{4}He component in the mixture)

$\sigma-$: Properties on the dilute-phase surface

$\sigma+$: Properties on the concentrated-phase surface

λ : Properties on the λ-surface

Superscripts

0 : Properties of a pure fluid (either ^{3}He or ^{4}He)

Chapter 1: Introduction

^{3}He-^{4}He mixtures are widely used in dilution refrigerators to achieve cooling to temperatures below 10 mK. Dilution refrigerators work by utilising the heat of solution of ^{3}He in ^{4}He – at sub-Kelvin temperatures, the transfer of ^{3}He atoms from a pure ^{3}He phase to a dilute solution of ^{3}He in ^{4}He results in a cooling effect.

Since the working fluids in dilution refrigerators are pure ^{3}He and dilute ^{3}He-^{4}He mixtures that are usually less than about 7% ^{3}He (on a molar basis) and at pressures of less than 250 millibar (typically), knowledge of thermodynamic properties of the ^{3}He-^{4}He mixtures at low concentrations and low pressure, and those of pure ^{3}He is all that is needed to design, predict and model the performance of these machines. As interest in the properties of ^{3}He-^{4}He mixtures has been largely driven by applications to dilution refrigeration, the thermodynamic tables for ^{3}He-^{4}He mixtures currently available [1,2] are restricted to low ^{3}He concentrations, saturated pressure and mostly to low temperature.

Recent efforts have been made to develop other sub-Kelvin refrigeration cycles [3, 4, 5] (which use ^{3}He-^{4}He mixtures as the working fluid) that could prove to be more efficient than dilution refrigerators by eliminating many of the losses associated with the latter [6]. These newer cycles use mixtures of ^{3}He and ^{4}He with much higher concentrations of ^{3}He, which fall outside the range of available property tables. The proper design of these machines requires knowledge of ^{3}He-^{4}He mixture properties over the entire concentration range (from pure ^{3}He to pure ^{4}He) and up to temperatures in excess of 1.2 K. (A thermal reservoir at 1.2 K – the temperature of a pumped ^{4}He "pot" – is a natural choice for the high temperature reservoir for a sub-Kelvin refrigerator.)

The intent of this work is to provide a complete set of tables of thermodynamic properties of liquid ^{3}He-^{4}He mixtures that span the entire concentration range up to temperatures of 1.8 K and pressures of 10 bar.

1.1 ^{4}He and ^{3}He

^{4}He and ^{3}He, the two stable isotopes of helium, have markedly different behaviour at low temperatures. The ^{4}He atom has integer spin and is governed by Bose-Einstein statistics. At temperatures of about 2 K (2.17 K at saturated pressure) ^{4}He goes through what is known as a "λ-transition", named after the shape of the specific heat-vs.-temperature plot in the vicinity of 2.17 K. This transition is analogous to Bose-Einstein condensation. Above the λ-transition temperature, ^{4}He behaves like a regular, "normal" fluid (which is designated He-I). Its behaviour, however, is quite different below the λ-transition temperature (where it is designated He-II). He-II exhibits a viscosity several orders of magnitude less than that of regular liquids (in certain experiments) and an apparent thermal conductivity several orders of magnitude greater than regular liquids. It is frequently modelled as being made up of two fluids – a "superfluid" and a normal fluid. The superfluid carries no entropy and exhibits no viscosity. The normal fluid has a viscosity and an entropy equal to the actual liquid entropy. The densities of the superfluid and the normal fluid sum up to the density of the fluid. The superfluid density is 0 at 2.17 K; the normal fluid density is 0 at 0 K, when all the liquid ^{4}He is in the ground state.

^{3}He, on the other hand, has a half-integer spin and is governed by Fermi-Dirac statistics. Although superfluidity is also observed in ^{3}He, it occurs at much lower temperatures (below about 2.6 mK). Since this is beyond the operating range of sub-Kelvin refrigerators using ^{3}He-^{4}He mixtures, ^{3}He will be assumed to be a normal fluid all the way down to 0 K in this work.

1.2 Mixtures of ^{3}He and ^{4}He

The phase diagram for liquid ^{3}He-^{4}He mixtures is shown in Figure 1.1. Three independent thermodynamic properties are required for this binary mixture; in this case, they are chosen to be the temperature (T), pressure (p) and ^{3}He mole fraction of the mixture (x). Mixtures of ^{3}He and ^{4}He also exhibit a λ-transition, at ^{3}He mole fractions of less than approximately 0.67, at the λ-surface shown in the figure. Below the λ-surface, in the He-II region, the ^{4}He in the mixture has a superfluid component. There is no superfluid above the λ-surface, in the He-I region. For pure ^{4}He, the λ-transition occurs under saturated conditions (almost zero pressure) at 2.17 K, the intersection of the λ-surface with the temperature axis in Figure 1.1a. The λ-transition temperature T_λ decreases with increasing x at a given pressure.

In addition to the λ-transition, a phase separation is also observed at temperatures below 0.87 K. At certain ^{3}He concentrations, the mixture separates into a He-II phase (with a superfluid ^{4}He component) and a He-I phase (all normal fluid). The He-I phase has a higher concentration of ^{3}He, and is referred to as the concentrated phase; the He-II phase, with a lower ^{3}He concentration is referred to as the dilute phase. Above the concentrated-phase surface, the mixture is all normal fluid.

The tricritical line represents the intersection of the λ-transition surface with the phase separation surfaces.

The feature of the ^{3}He-^{4}He phase diagram that is responsible for practical dilution refrigeration is the finite solubility of ^{3}He in ^{4}He at 0 K. The non-zero solubility is a result of a ^{3}He atom (in a dilute solution of ^{3}He in ^{4}He) being more strongly bound to ^{4}He than it is to ^{3}He. (With an increasing concentration of ^{3}He atoms, however, the binding energy of ^{3}He in ^{4}He decreases.) At 0 K and saturated pressure, the solubility is 6.6% ^{3}He (on a molar basis). The entropy of cooling associated with ^{3}He atoms going from pure ^{3}He into a dilute solution of ^{3}He in ^{4}He is exploited to provide cooling at very low temperatures.

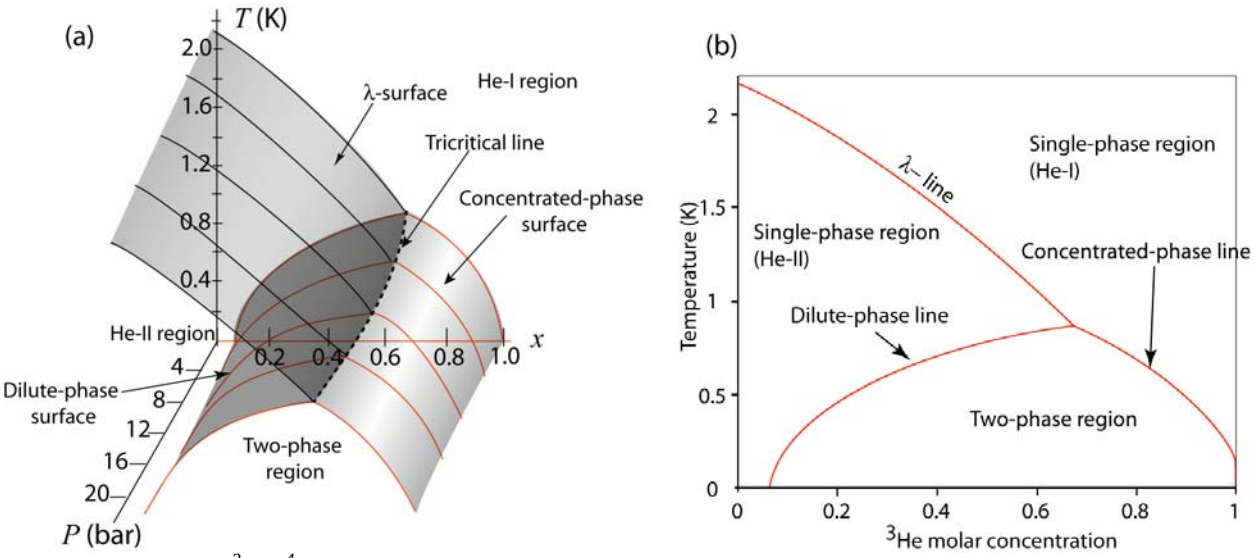

Figure 1.1: *(a) The ^{3}He-^{4}He phase diagram. (b) The cross section of the phase-diagram at saturated pressure.*

Vapour pressures associated with ^{3}He-^{4}He mixtures are extremely small at temperatures below 2 K – of the order of a few tens of torrs [7,8,9] (750 torr ≈ 1 bar). The data of Sydoriak and Roberts [7] indicates that for the highest temperatures covered in this work (1.8 K in the He-II region, 1.5 K in the He-I region), the vapour pressure is about 50 torr (0.07 bar). At temperatures below 1.2 K, the vapour pressure is less than 20 torr (0.03 bar). Therefore, it will be assumed that the saturated pressure surface is coincident with a constant pressure surface where the pressure is 0 bar. Because gaseous ^{3}He-^{4}He mixtures exist only at very small pressures, we will not concern ourselves with them in this work.

1.3 Review of available property tables of ^{3}He-^{4}He mixtures

One of the earliest attempts to characterize the properties of ^{3}He-^{4}He mixtures was by de Bruyn Ouboter et al [10] in the early 1960s. They made extensive measurements of the specific heat between 0.4 K and 2 K and used that data, along with some vapour-liquid equilibrium data, to calculate the excess enthalpy and excess Gibbs free energy as a function of ^{3}He concentration and temperature at saturated pressure. In theory, these properties are sufficient to derive all other thermodynamic properties, provided the properties of pure ^{3}He and pure ^{4}He are known. However, the properties were calculated only at certain values of temperature and ^{3}He concentration; properties at other values need to be interpolated, which is a problem since the calculated values do not appear to be smooth functions of ^{3}He concentration and temperature. In addition, the calculations were based on extrapolations (they calculated the excess enthalpy relative to 15%-^{3}He and 95.4%-^{3}He solutions from experimental data, and extrapolated the results down to 0%-^{3}He and 100%-^{3}He solutions to obtain the actual excess enthalpy) and other approximations (the assumed form of the excess Gibbs free energy was quite simplistic). London et al [11] point out a discrepancy between de Bruyn Ouboter et al's calculated values and other data above 1 K (but also note that a change in the extrapolation scheme brings them into "good agreement"). de Bruyn Ouboter et al's values also do not extend to temperatures below 0.4 K, which limits their usefulness as design tools for refrigerators supposed to cool down to below 0.1 K. Nevertheless, their specific heat data are more extensive than most and are widely used in this thesis, although with reservation in certain cases. There is a lot of noise in some of their specific heat measurements near the λ-line and the phase-separation curves; in addition, some specific heat values near the λ-line, as well as measured co-ordinates of the λ-line and the phase-separation curves, are not completely consistent with later measurements.

Investigations into the thermodynamic properties of ^{3}He-^{4}He mixtures in the late 1960s through the early 1980s were driven by interest in dilution refrigeration. Dilution refrigerators are commonly used to cool down to temperatures in the milli-Kelvin range (the most efficient ones can cool down to just below 10 mK). The working fluid in these machines consists of pure ^{3}He and dilute mixtures of ^{3}He in ^{4}He – cooling is achieved by the transfer of ^{3}He atoms from the pure ^{3}He phase to the dilute ^{3}He phase, as explained in the previous section. Consequently, most property tabulations in this time frame are restricted to the low ^{3}He-concentration, low temperature region of the phase diagram, at saturated pressure. Thermodynamic properties in this region were derived largely from a theoretical model of the behaviour of ^{3}He in dilute solutions of ^{4}He. The ^{3}He component is treated as an ideal Fermi gas of "quasiparticles" in a solution of ^{4}He; the "quasiparticles" have a mass different from that of a ^{3}He atom, but otherwise have the same properties. This model is borne out by experimental ^{3}He-^{4}He mixture data at low temperatures and concentrations, but deviates from experiments at high temperatures and concentrations.

The most extensive set of thermodynamic property tables for ^{3}He-^{4}He mixtures were developed by Radebaugh [1] in 1967, who calculated mixture properties at saturated pressure for temperatures below 1.5 K and ^{3}He mole fractions below 30%. His properties were based on the ideal-Fermi-gas model discussed above – a model which becomes increasingly inappropriate at high temperatures and high ^{3}He

concentrations. The calculation scheme also involved the use of other theoretical models (specifically, the chemical potential of ^{3}He at 0 K).

Some of Radebaugh's property values were later found to be inconsistent with subsequent experimental measurements of the osmotic pressure and osmotic enthalpy [2]. In 1985, Kuerten et al [2] developed a calculation scheme quite similar to Radebaugh's, in that they treated the ^{3}He component as an ideal Fermi gas too. However, they used experimentally determined values of the osmotic pressure in lieu of Radebaugh's theoretical model for the chemical potential. They determined the thermodynamic properties only for temperatures below 0.25 K and ^{3}He mole fractions below 8%, because it was clear by that time (from experiments) that the theory for dilute solutions of ^{3}He in ^{4}He did not extend up to the temperatures and concentrations covered by Radebaugh.

There are also tabulations of properties of ^{3}He-^{4}He mixtures near the tricritical point, notably by Islander and Zimmermann [12] (1973) and Goellner et al [13] (1973). These properties are based on experimental data; the former on specific heat measurements made by Alvesalo et al [14] and the latter on specific heat and vapour pressure measurements. However, the tabulations are only for a few properties (entropy, the chemical potential difference $\Phi = \mu_3 - \mu_4$ and its derivatives) and are limited to a small portion of the T - x plane. They are not particularly useful for engineering purposes.

To our knowledge, there are no calculated properties at high pressures. To a first approximation, the (liquid) mixtures can be treated as being incompressible; however, the isothermal compressibilities of pure ^{4}He (about 0.01 bar^{-1} [15]) and pure ^{3}He (about 0.02-0.04 bar^{-1} [16]) at 1 K and 1-10 bar are quite high; as a comparison, water at room temperature and atmospheric pressure has an isothermal compressibility that is two to three orders of magnitude smaller (about 5×10^{-5} bar^{-1} [17]). This suggests that for ^{3}He-^{4}He mixtures, the errors associated with the assumption of an incompressible liquid could be very significant.

In summary, mixture thermodynamic properties (such as the internal energy, entropy, enthalpy, etc.) at saturated pressure are rather limited, and there are none whatsoever at high pressures. In addition, a feature of a lot of the available properties is that they are based largely on theoretical models, rather than experimental data. (Of course, the theoretical models are validated by experimental data in certain cases, but they fail to capture the real behaviour as the boundaries are pushed). The thermodynamic properties in this work are (a) calculated over a much wider range of the x - T - p space, and (b) based on actual experimental data in regions of "non-ideal" behaviour.

1.4 Thermodynamic state equations for binary mixtures

As stated earlier, three independent properties are required to specify the state of a binary mixture, such as the ^{3}He-^{4}He mixture under investigation. This is in accordance with the Gibbs phase rule, which states that the number of independent properties is equal to $c - \phi + 2$, where c is the number of components of the system and ϕ the number of phases. For a pure substance (one component), two independent properties are required; the sets of properties most typically designated as being independent are the temperature T and the specific volume v, or the temperature T and the pressure p. For a binary mixture, an obvious choice for the third additional property is the fraction of one of the components in the system. For ^{3}He-^{4}He mixtures, the commonly used property is the mole fraction of the ^{3}He component, designated x. (The ^{3}He mole fraction will also be interchangeably referred to as the "concentration").

A choice now needs to be made between the (x, T, p) and the (x, T, v) sets of independent properties. The former is used in this work. The choice is largely dictated by the experimental data that is available. A review of the available experimental data that can be used to determine a state equation reveals that most experimental work on ^{3}He-^{4}He mixtures has been restricted to saturated pressure. (In particular, two areas of the phase diagram at saturated pressure are well covered – dilute solutions of ^{3}He in ^{4}He, and mixtures in the vicinity of the tricritical point and the λ-line. The work in the former is due to applications to dilution refrigerators; the work in the latter is due to an interest in critical phenomena.) It has been previously stated that the saturated pressure surface is nearly coincident with a constant (zero) pressure surface for the temperature range of interest. If the pressure is chosen as an independent variable, properties can first be calculated at saturated (virtually constant) pressure, as a function of two variables – T and x – only. The reduction of independent variables from three to two greatly simplifies the calculations. Once properties are known on the saturated pressure plane, they can be extended to higher pressures using available molar volume data (which, incidentally, is more or less the only useful data available at high pressures).

The choice of x, T and v as independent variables, on the other hand, does not lend itself to as convenient a calculation procedure.

In this work, expressions are developed for the specific heat at constant x and (constant) zero pressure, $C_{x,p=0}$, as a function of x and T, and the molar volume v as a function of x, T and p. These are used in conjunction with expressions for the phase-separation surfaces to determine thermodynamic properties. In essence, properties at a given x, T and p are calculated by first integrating across x at zero temperature and zero pressure (using existing models), then by integrating across T at zero pressure (using the specific heat data), and finally by integrating across p (using the molar volume data) .

At this point, we digress to note that a more rigorous approach would entail the determination of a characteristic function as the state equation. Thermodynamic state equations for pure substances typically involve the calculation of the Gibbs or Helmholtz free energy, from which all other properties are derived. The advantage of using a free energy as the characteristic function is that all other properties can be calculated from it by differentiation, which results in no undetermined constants. For a pure substance, the Helmholtz free energy f is based on T and the specific volume v; the Gibbs free energy g is based on T and p. The differential form of the Helmholtz free energy for a pure substance is:

$$df = -pdv - sdT \tag{1.1}$$

where s is the entropy. The differential form of the Gibbs free energy for a pure substance is:

$$dg = vdp - sdT . \tag{1.2}$$

For a binary mixture, the differential forms of the Helmholtz and Gibbs free energies are [18]:

$$df = -pdv - sdT + (\mu_3 - \mu_4)dx \tag{1.3}$$

and

$$dg = vdp - sdT + (\mu_3 - \mu_4)dx \tag{1.4}$$

where μ_3 and μ_4 are the chemical potentials of the ^{3}He and ^{4}He components respectively.

The Helmholtz free energy is more commonly used in equations of state. However, a Gibbs free energy approach, (with independent variables x, T and p) would be easier in this case, for reasons that have already been discussed. The Gibbs free energy could be calculated on a constant pressure surface (the saturated pressure surface) as a function of just two variables, T and x, since, on a surface of constant pressure, the Gibbs free energy is simply

$$dg = -sdT + (\mu_3 - \mu_4)dx. \quad (1.5)$$

It could then be extended to other pressures using the molar volume data, since along a line of constant T and constant x,

$$dg = vdp. \quad (1.6)$$

Since there are two distinct states over the temperature range of interest (the normal He-I region and the He-II region with the superfluid component), two different expressions for the Gibbs free energy would be required, one for each region. (Knowledge of the λ-surface is required to determine the boundary between the two regions.) The Gibbs free energies in the single-phase regions would have to be determined by fitting available data to a functional form (which may evolve over the fitting process). The two phase-separation surfaces would be calculated from the Gibbs free energies of the He-II and He-I states, by setting the chemical potentials of the ^{3}He and ^{4}He components in the two states equal to each other. (Experimental phase-separation data, therefore, would be part of the fitting functions for the two states; additionally, this would lead to the two fitting functions being coupled together).

The Gibbs free energy approach is not used in this work because it was originally unclear what an appropriate functional form for g would look like, since the range of available thermodynamic properties to refer to was so small. Therefore, properties were calculated in a sequential process (outlined a few paragraphs ago), rather than by attempting to fit an all-encompassing characteristic function. It is worth mentioning, though, that the procedure employed in this work is, in essence, the same as using a Gibbs free energy approach. Although an explicit functional form for the Gibbs free energy is not determined, the zero-temperature-zero-pressure model, and the expressions for $C_{x,p=0}$, v and the phase-separation surfaces can be combined to yield the Gibbs free energy implicitly. (The forms of these quantities calculated in this thesis are such that an explicit expression for g cannot be calculated from them.) Together, these quantities effectively play the same role as g and thus can be used to completely determine thermodynamic properties.

1.4.1 Layout of the thesis

In Chapter 2, properties are determined across the zero-pressure surface as a function of x and T. To do this, (1) expressions for the dilute- and concentrated-phase lines are determined from experimental data; (2) properties along the dilute- and concentrated-phase lines at zero pressure are then calculated from experimental measurements of the specific heat in the two-phase region, as well as the idealized models of ^{3}He-^{4}He mixtures used by Radebaugh and Kuerten et al, only in the regions where they are applicable; and (3) properties along the phase-separation lines are then used with single-phase specific heat measurements to determine properties in the single-phase He-I and He-II regions.

The zero-pressure properties are extended to higher pressures in Chapter 3. Expressions for the dilute- and concentrated-phase surfaces at all pressures are first determined. Thermodynamic properties at high pressures are then calculated on the basis of high-pressure molar volume measurements (in conjunction with the phase-separation surface fits and the zero-pressure results of Chapter 2). It is worth emphasising though, that high-pressure molar volume data for mixtures is only available below 0.7 K and in the He-II region. At high temperatures, the data available is for mixtures at zero pressure and for pure ^{3}He and pure ^{4}He (at all pressures). While some of the calculated mixture properties at high pressure and high temperature are expected to be reasonably accurate, others must be used with caution. This is discussed in greater detail in Chapter 3, and later in Chapter 5.

Applications of the calculated properties to the design of sub-Kelvin refrigerators are discussed in Chapter 4.

Chapter 5 presents a comparison of our results with some other experimental measurements that were not used in determining the equation of state. The expected accuracies and inaccuracies associated with our results in regions where the lack of experimental data precludes a comparison are also discussed.

Chapter 6 presents a summary of the work done in this thesis and looks at the road ahead to get a more complete state equation.

1.4.2 Thermodynamic properties calculated in this work

In this section, we list the thermodynamic properties calculated in this work and present some relations between properties that will be used at various points in this work. As with pure substances, the entropy s and the enthalpy h play an important role in thermodynamic analysis. They are related to the Gibbs free energy through:

$$g = h - Ts . \tag{1.7}$$

For a pure substance, the enthalpy and entropy are related to the constant-pressure specific heat C_p through:

$$\left(\frac{\partial h}{\partial T}\right)_p = C_p \tag{1.8}$$

and

$$T\left(\frac{\partial s}{\partial T}\right)_p = C_p , \tag{1.9}$$

respectively. The analogous relations for a binary mixture involve the specific heat at constant pressure and constant concentration, $C_{x,p}$:

$$\left(\frac{\partial h}{\partial T}\right)_{x,p} = C_{x,p} \tag{1.10}$$

and

$$T\left(\frac{\partial s}{\partial T}\right)_{x,p} = C_{x,p} . \tag{1.11}$$

For the sake of brevity, $C_{x,p}$ will be shortened to C.

Since the substance under investigation is a binary mixture, the chemical potentials of the two species (especially that of ^{4}He, for reasons that will become clear) are also quite important. The chemical potentials of ^{3}He and ^{4}He are defined as [18]:

$$\mu_3 = g + (1-x)\left(\frac{\partial g}{\partial x}\right)_{T,p} \tag{1.12}$$

and

$$\mu_4 = g - x\left(\frac{\partial g}{\partial x}\right)_{T,p} , \tag{1.13}$$

respectively. Note that the chemical potentials satisfy:

$$g = x\mu_3 + (1-x)\mu_4 . \tag{1.14}$$

In addition to these "regular" thermodynamic properties, there are some other properties of significance, specifically in the He-II region, due to the superfluid behaviour of the ^{4}He. These are the osmotic pressure and the osmotic enthalpy.

Consider the two chambers shown in Figure 1.2 connected by a "superleak". One chamber is filled with a ^{3}He-^{4}He mixture; the other with pure ^{4}He. The superleak (a porous plug, with nanometer-scale pores) effectively acts as a semi-permeable membrane. It offers no resistance to the flow of superfluid ^{4}He, but does not allow ^{3}He (or the normal component of the ^{4}He) to pass. At equilibrium the pressure in the pure ^{4}He chamber is less than the pressure in the mixture chamber by an amount known as the osmotic pressure (Π). From the equation of motion of a superfluid (at low velocities v_s) [19]:

$$\frac{\partial v_s}{\partial t} = -\nabla\mu_4 , \tag{1.15}$$

it is evident that the superfluid component flows to equalize the ^{4}He chemical potential. At equilibrium, therefore, the ^{4}He chemical potentials are equal in both chambers. This is used as a definition of the osmotic pressure:

$$\mu_4(p,T,x) = \mu_4^0(p-\Pi,T) \tag{1.16}$$

where μ_4 is the chemical potential of the ^{4}He in the mixture, and μ_4^0 is the chemical potential of the pure ^{4}He. A Taylor expansion of the above equation yields:

$$\mu_4(p,T,x) = \mu_4^0(p,T) - \Pi\frac{\partial\mu_4^0}{\partial p} + \frac{\Pi^2}{2}\frac{\partial^2\mu_4^0}{\partial p^2} + \text{ higher order terms.} \tag{1.17}$$

At this point we note that the chemical potential of pure ^{4}He is simply its Gibbs free energy, and its pressure derivative is simply the molar volume of pure ^{4}He, v_4^0. The above equation becomes

$$\mu_4(p,T,x) = \mu_4^0(p,T) - \Pi v_4^0 + \frac{\Pi^2}{2}\frac{\partial v_4^0}{\partial p} + \text{ higher order terms.} \tag{1.18}$$

For superfluid mixtures in the temperature range covered in this work, the second order term is at least two orders of magnitude smaller than the first order term. Consequently, an explicit definition of the osmotic pressure is:

$$\Pi(p,T,x) = \frac{\mu_4^0(p,T) - \mu_4(p,T,x)}{v_4^0(p,T)} . \tag{1.19}$$

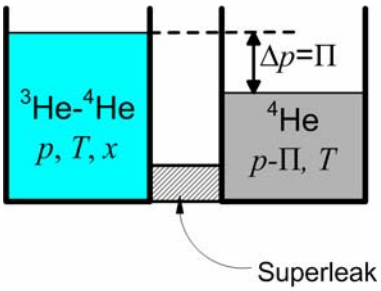

Figure 1.2: *The osmotic pressure of a ^{3}He-^{4}He mixture*

The osmotic pressure is, therefore, directly related to the mixture ^{4}He chemical potential. As x increases, μ_4 decreases, and the osmotic pressure increases.

Another quantity of significance in superfluid ^{3}He-^{4}He mixtures is the osmotic enthalpy. The osmotic enthalpy of a mixture (per mole of ^{3}He), first introduced by London, Clarke and Mendoza [11], and later rigorously derived by Ebner and Edwards [20], is defined as

$$h^{os} = \frac{h-(1-x)\mu_4}{x} \tag{1.20}$$

and is useful for First Law analysis of flowing superfluid mixtures. The osmotic enthalpy does not appear in the usual statement of the First Law of Thermodynamics,

$$\frac{dE}{dt} = \dot{Q} - \dot{W} + \sum_{ports} \dot{N}h, \tag{1.21}$$

where E is the total energy in the control volume, $\dot{Q}$ is the rate of heat transfer into the control volume, $\dot{W}$ is the rate of work transfer from the control volume, $\dot{N}$ is the total molar flow rate into the control volume, and h is the enthalpy of the mixture per mole of the mixture. In the He-I region (where there is no superfluid), the enthalpy flow term ($\dot{N}h$) is easily evaluated since viscous effects ensure that the ^{3}He and ^{4}He components flow at the same velocity. In contrast, in the He-II region, the presence of a superfluid moving at a velocity different from that of the normal fluid means that the enthalpy flow term actually consists of two separate terms. The effective enthalpy flow in this case can be derived by considering the Gedanken apparatus shown in Figure 1.3. (The following derivation of the effective enthalpy flow is a duplication of the analysis done by Ebner and Edwards [20] and by Miller and Brisson [21]).

The flowing He-II mixture with the (unknown) enthalpy flow rate enters the control volume through the port on the right and flows into two cylinders. The top cylinder is directly connected to the entering flow. It contains a ^{3}He-^{4}He mixture at the same pressure, temperature and ^{3}He concentration as the flowing mixture. The bottom cylinder is connected to the entering flow through a superleak through which only superfluid can flow. It contains pure ^{4}He at a pressure $p-\Pi$ (where Π is the osmotic pressure) and is maintained at the same temperature as the mixture through thermal contact with a heat reservoir at T.

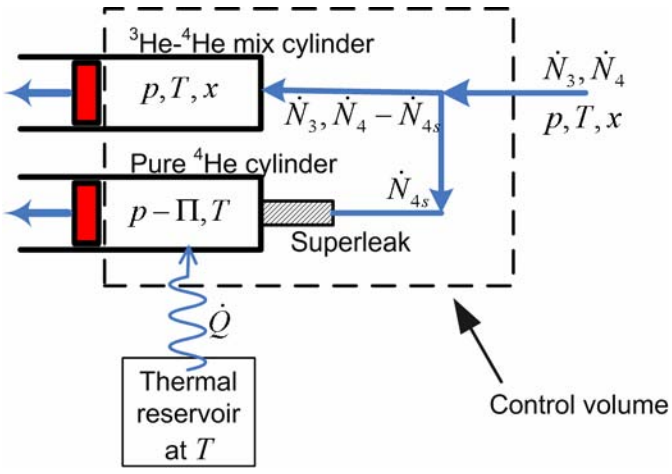

Figure 1.3: *Gedanken experiment to determine the effective enthalpy of a superfluid flow*

The flow rates of ^{3}He and ^{4}He entering the control volume are $\dot{N}_3$ and $\dot{N}_4$ respectively. The superfluid flow rate into the bottom piston is $\dot{N}_{4s}$. The total ^{4}He flow rate into the top piston is therefore $\dot{N}_4 - \dot{N}_{4s}$. (All the ^{3}He flows into the top cylinder.) We will now attempt to find an expression for the enthalpy flow rate into the control volume, $\dot{N}_{total} h_{flow} = (\dot{N}_3 + \dot{N}_4) h_{flow}$.

The ^{3}He concentration in the top cylinder is

$$x = \frac{\dot{N}_3}{\dot{N}_3 + \dot{N}_4 - \dot{N}_{4s}}. \tag{1.22}$$

Since the flow through the top cylinder crossing the control volume boundary is a bulk flow, its enthalpy is well defined. The enthalpy flow rate out through the top cylinder is $(\dot{N}_3 + \dot{N}_4 - \dot{N}_{4s}) h(p,T,x)$. In the bottom cylinder, the only flow crossing the control volume is that of pure ^{4}He. The enthalpy flow rate out through the bottom cylinder is $\dot{N}_{4s} h_4^0(p - \Pi, T)$.

The (usual form of the) First Law can now be applied to the control volume. Since the system is at steady state and there are no work transfers, the First Law simplifies to

$$0 = \dot{Q} + \dot{N}_{total} h_{flow} - (\dot{N}_3 + \dot{N}_4 - \dot{N}_{4s}) h(p,T,x) - \dot{N}_{4s} h_4^0(p - \Pi, T). \tag{1.23}$$

$\dot{Q}$ is the heat transfer into the bottom cylinder which is required to maintain its temperature at T, since the flow into the bottom cylinder is a superfluid flow, while the flow "out" is a bulk flow. The heat transfer can be calculated by applying the Second Law to the bottom cylinder only. The inflowing superfluid does not carry any entropy. The only entropy transferred by a mass flow is by the pure ^{4}He leaving the system. Since the system is at steady state and there is no entropy generation,

$$0 = \frac{\dot{Q}}{T} - \dot{N}_{4s} s_4^0(p - \Pi, T) \tag{1.24}$$

which yields

$$\dot{Q} = \dot{N}_{4s} T s_4^0(p - \Pi, T). \tag{1.25}$$

Plugging this back into Eq. 1.23, we get

$$\dot{N}_{total} h_{flow} = (\dot{N}_3 + \dot{N}_4 - \dot{N}_{4s}) h(p,T,x) + \dot{N}_{4s} h_4^0(p - \Pi, T) - \dot{N}_{4s} T s_4^0(p - \Pi, T) \tag{1.26}$$

which simplifies to

$$\dot{N}_{total} h_{flow} = (\dot{N}_3 + \dot{N}_4 - \dot{N}_{4s}) h(p,T,x) + \dot{N}_{4s} \mu_4^0(p - \Pi, T). \tag{1.27}$$

Since the superfluid ensures equal ^{4}He chemical potential on both sides of the superleak, the ^{4}He chemical potential of the mixture in the top cylinder must be equal to the chemical potential of the pure ^{4}He, i.e., $\mu_4(p,T,x) = \mu_4^0(p - \Pi, T)$. Therefore,

$$\dot{N}_{total} h_{flow} = (\dot{N}_3 + \dot{N}_4 - \dot{N}_{4s}) h(p,T,x) + \dot{N}_{4s} \mu_4(p,T,x). \tag{1.28}$$

The definition of the mixture concentration x (Eq. 1.22) is now used to substitute in for $\dot{N}_{4s}$, which results in

$$\dot{N}_{total} h_{flow} = \frac{\dot{N}_3}{x} h(p,T,x) + \left(\dot{N}_3 + \dot{N}_4 - \frac{\dot{N}_3}{x} \right) \mu_4(p,T,x). \tag{1.29}$$

Rearranging, we get

$$\dot{N}_{total} h_{flow} = \dot{N}_3 \left(\frac{h(p,T,x)}{x} + \frac{x-1}{x} \mu_4(p,T,x) \right) + \dot{N}_4 \mu_4(p,T,x) \tag{1.30}$$

which can be rewritten as

$$\dot{N}_{total} h_{flow} = \dot{N}_3 h^{os}(p,T,x) + \dot{N}_4 \mu_4(p,T,x) . \tag{1.31}$$

Therfore, the enthalpy flow term is equivalent to $\dot{N}_3 h^{os} + \dot{N}_4 \mu_4$, where h^{os} is the osmotic enthalpy of the mixture per mole of ^{3}He as defined in Eq. 1.20 and μ_4 is the ^{4}He chemical potential. As a result, the First Law for a superfluid ^{3}He-^{4}He mixture can be written as:

$$\frac{dE}{dt} = \dot{Q} - \dot{W} + \sum_{ports} \dot{N}_3 h^{os} + \sum_{ports} \dot{N}_4 \mu_4 . \tag{1.32}$$

Therefore, the osmotic enthalpy is required for the analysis of flows with a superfluid component. For normal mixtures, this form of the First Law reduces to the usual form, a fact that can be checked by substituting the expression for the osmotic enthalpy into Eq. 1.32.

For completeness, we also derive a form of the Second Law that is appropriate for He-II mixtures. The derivation has previously been presented by Miller and Brisson [21]. Their analysis is repeated here. Applying the usual form of the Second Law

$$\frac{dS}{dt} = \sum \frac{\dot{Q}}{T} + \sum_{ports} \dot{N} s + \dot{S}_{gen} \tag{1.33}$$

to the control volume in Figure 1.3 yields

$$0 = \frac{\dot{Q}}{T} + \dot{N}_{total} s_{flow} - (\dot{N}_3 + \dot{N}_4 - \dot{N}_{4s}) s(p,T,x) - \dot{N}_{4s} s_4^0(p - \Pi, T) . \tag{1.34}$$

Substituting the expression for $\dot{Q}$ from Eq. 1.25 into the above equation, we get

$$\dot{N}_{total} s_{flow} = -\dot{N}_{4s} s_4^0(p - \Pi, T) + (\dot{N}_3 + \dot{N}_4 - \dot{N}_{4s}) s(p,T,x) + \dot{N}_{4s} s_4^0(p - \Pi, T) \tag{1.35}$$

or

$$\dot{N}_{total} s_{flow} = (\dot{N}_3 + \dot{N}_4 - \dot{N}_{4s}) s(p,T,x) . \tag{1.36}$$

The definition of x can now be substituted in to get

$$\dot{N}_{total} s_{flow} = \dot{N}_3 \frac{s(p,T,x)}{x} = \dot{N}_3 s_{3He} \tag{1.37}$$

where s_{3He} is the mixture entropy per mole of ^{3}He, and is equal to the mixture entropy per mole of mixture, s, divided by x, the moles of ^{3}He per mole of mixture.

The usual statement of the Second Law can therefore be rewritten as

$$\frac{dS}{dt} = \sum \frac{\dot{Q}}{T} + \sum_{ports} \dot{N}_3 s_{3He} + \dot{S}_{gen} . \tag{1.38}$$

This form of the Second Law can be applied to He-II mixtures.

1.4.3 Units and notation

A note on the units of the various properties calculated in the subsequent chapters: the entropy, enthalpy, Gibbs free energy and specific volume are calculated per mole of the mixture, the ^{4}He chemical potential per mole of ^{4}He, and the osmotic enthalpy per mole of ^{3}He. The use of "mol" in the units indicates properties calculated on a per-mole-of-mixture basis; "mol-^{4}He" and "mol-^{3}He" indicate properties calculated per mole of ^{4}He and per mole of ^{3}He respectively.

Finally, a word on the notation: properties on the dilute-phase surface will be subscripted with "$\sigma-$"; properties on the concentrated-phase surface will be subscripted with "$\sigma+$".

Chapter 2: Properties of ^{3}He-^{4}He mixtures at zero pressure

Most ^{3}He-^{4}He mixture experimental data are restricted to the saturated pressure surface, which, as discussed in the previous chapter, is more or less coincident with the zero pressure surface. In this chapter, thermodynamic properties along this constant pressure surface are determined.

It is worth pointing out that although the specific heat data used in this chapter is treated as a constant-pressure specific heat, it was actually measured at saturated pressure rather than at constant pressure. However, the saturated-pressure specific heats are practically equal to specific heats at constant pressure over the temperature range covered in this work, and are therefore treated that way. The relation between the constant-x specific heat at saturated-pressure, $C_{x,svp}$, and the specific heat at constant x and pressure, C is:

$$C = T\left.\frac{\partial s}{\partial T}\right|_{x,p} = T\left(\left.\frac{\partial s}{\partial T}\right|_{x,svp} - \left.\frac{\partial s}{\partial P}\right|_{x,T}\left.\frac{\partial p_{sat}}{\partial T}\right|_{x}\right) = T\left.\frac{\partial s}{\partial T}\right|_{x,svp}\left(1 - \frac{\left.\frac{\partial s}{\partial P}\right|_{x,T}\left.\frac{\partial p_{sat}}{\partial T}\right|_{x}}{\left.\frac{\partial s}{\partial T}\right|_{x,svp}}\right)$$

$$= C_{x,svp}\left(1 + \frac{T}{C_{x,svp}}\left.\frac{\partial v}{\partial T}\right|_{x,p}\left.\frac{\partial p_{sat}}{\partial T}\right|_{x}\right) \qquad (2.1)$$

Over the range of temperatures and pressures of interest, the second term in the parenthesis is maximum at high values of x and T. At a temperature of 1.5 K and x ~0.8-0.9, $\partial v / dT$ is about 10^{-6} m^3/mol-K [22], $\partial p_{sat} / \partial T$ is about 1.5 x 10^4 Pa/K [7], and $C_{x,svp}$ is about 5 J/mol-K [10]. The order of magnitude of the second term in the parenthesis is therefore no more than about 0.005. Given that the error bounds associated with some of the available data as well as discrepancies between different sets of data are much larger, it is fair to assume that C is equal to $C_{x,svp}$.

2.1 Properties at low temperatures (sub-150 mK) at all ^{3}He concentrations

The calculations in this chapter are restricted to temperatures above 0.15 K (and below 1.8 K). The reason for the choice of this lower extreme is that accurate low-temperature properties (below 0.15 K) can be calculated from other sources.

Properties in the He-II region at low temperatures are available from two sources – Radebaugh [1] and Kuerten et al [2]. The calculation schemes used by these authors, based on an idealized model of dilute solutions of ^{3}He in ^{4}He, are very similar. However, unlike Radebaugh's calculations, which are based on a theoretical model for the ^{3}He chemical potential at 0 K, Kuerten et al's calculations are based on very-low-temperature osmotic pressure measurements (which were made subsequent to Radebaugh's calculations). Kuerten et al's properties are consequently more consistent with experimental data. Their calculations are limited to ^{3}He concentrations below 8% and temperatures below 0.25 K, and are restricted to the single-phase He-II region.

At temperatures below 0.15 K, the solubility of ^{3}He in ^{4}He is less than 8% (about 8.014% at 0.15 K, decreasing to 6.6% at 0 K, according to Kuerten et al). Therefore, Kuerten et al's calculations cover the

entire single-phase He-II region at sub-150 mK temperatures. In addition, at temperatures below 0.15 K, the solubility of ^{4}He in ^{3}He is very low (about 1000 ppm at 0.15 K [23,24], and even lower at lower temperatures). As a result, the He-I region below 0.15 K can be reasonably approximated to be pure ^{3}He.

The properties of two-phase mixtures below 0.15 K are simply weighted averages of the corresponding (He-II) dilute phase and the (He-I) concentrated phase, at the same temperature. (For temperatures below 0.15 K, properties of the concentrated phase are assumed to be identical to ^{3}He properties.)

Consequently, properties at low temperatures (sub-150 mK) are known at all concentrations. The T >0.15 K properties calculated in the following sections are consistent with these properties.

These low-temperature properties are actually quite critical to the calculation procedure. Effectively, they provide the only means for calculating variations of properties with respect to the ^{3}He concentration. There seem to be no measurements at high temperatures that would allow the direct calculation of variations of properties with respect to x. One of the measurements that would allow that is the osmotic pressure. The most extensive osmotic pressure measurements we could find are those by Landau et al [25], London et al [11], and Wilson and Tough [26]. The measurements of Landau et al are restricted to temperatures below 0.2 K for ^{3}He concentrations above 2.5% and are therefore not very useful. The measurements of Wilson and Tough are at 0.32 K, 0.65 K and 1.16 K, but only for ^{3}He concentrations of less than 2%. The measurements of London et al are at temperatures of 0.8 K, 1.0 K and 1.2 K and ^{3}He concentrations between 20% and 30%. They are potentially useful, but were not used in the calculation procedure since they were discovered much too late by the author. They are compared with results of the calculations in Section 5.1.

In the following sections, available specific heat data is used in conjunction with the low temperature ($T \leq 0.15$ K) thermodynamic property models of Kuerten et al to determine the properties of saturated liquid ^{3}He-^{4}He mixtures. We begin by analysing the phase diagram at saturated pressure.

2.2 The phase diagram at zero pressure

The first step in the process is the determination of the equations of the two phase-separation curves as well as the λ-line. The tricritical point at zero pressure is assumed to lie at a temperature T_t = 0.867 K and ^{3}He concentration x_t = 0.674 [27]. The ^{3}He concentration along the phase-separation curves was determined as a function of the temperature by curve-fits to available experimental data. For the dilute phase-separation curve, a curve was fitted to the experimental phase-separation data of Qin et al [27], Kierstead [28], Roe et al [29], Goellner et al [13], Yorozu et al [30], and Ahlers and Greywall [31]. Roe et al suggest that the phase-separation temperature data of Goellner et al is consistently high by about 5 mK. Consequently, we shifted Goellner et al's data downward by 5 mK. The following equation was obtained for the ^{3}He mole fraction ($x_{\sigma-}$) along the dilute phase-separation curve (for temperatures above 0.15 K):

$$x_{\sigma-} - x_t = \frac{-0.209148(T - T_t)}{T - T_t - 0.080280} + 0.960222(T - T_t) + 0.549920(T - T_t)^2 . \qquad (2.2)$$

This fit reduces to $x_{\sigma-} = x_t$ at $T = T_t$. It was also ensured that the fit yields the same value of $x_{\sigma-}$ at T = 0.15 K as Kuerten et al's model. For temperatures below 0.15 K, phase-separation data is available from Kuerten et al.

For the concentrated phase-separation curve, He et al [23] recommend the following fit above 0.04 K:

$$\log_{10}(1-x_{\sigma+}) = -0.36 + 1.92(\log_{10} T) - 0.85(\log_{10} T)^2 + 0.59(\log_{10} T)^3 . \quad (2.3)$$

where $x_{\sigma+}$ is the ^{3}He mole fraction along the concentrated phase-separation curve.

In order to get an equation that is easier to manipulate, a curve was fitted to the experimental phase-separation data of Qin et al [27], Kierstead [28], Roe et al [29], Goellner et al [13] (whose data was once again shifted downward by 5 mK) and Lahuerte [32], resulting in the following expression for $x_{\sigma+}$ as a function of temperature:

$$x_{\sigma+} - x_t = 0.316170\ (T - T_t)^3 - 0.180743\ (T - T_t)^2 - 0.746805\ (T - T_t) . \quad (2.4)$$

This expression also reduces to $x_{\sigma+} = x_t$ at $T = T_t$. At T = 0.15 K, this expression yields $x_{\sigma+}$ = 1. ($x_{\sigma+}$ is actually around 0.999 at 0.15 K [23].) This concentrated phase-separation curve expression is also used only at temperatures above 0.15 K, since x is approximately 1 for temperatures below 0.15 K.

The derivative of the dilute phase-separation curve (dT / dx) at the tricritical point predicted by Eq. 2.2 is slightly lower than experimental data (the fit predicts 0.28; measured values [13,28,29] range from 0.31 to 0.33). The derivative of the concentrated phase-separation curve at the tricritical point predicted by Eq. 2.4 lies within the range of experimental data (the fit predicts -1.34; measured values [13,28,29] range from -1.31 to -1.47).

The fits of Eqs. 2.2 and 2.4 are shown with the underlying experimental data in Figure 2.1.

To find the dependence of temperature on x along the λ-line, the λ-transition data of Roberts and Sydoriak [33], Alvesalo et al [14], Goellner et al [13], Qin et al [27], and Ahlers and Greywall [31] was used to get:

$$T_\lambda(x) - T_t = -2.620259(x - x_t) - 1.023726(x - x_t)^2 . \quad (2.5)$$

The fit of Eq. 2.5 is shown with the underlying data in Figure 2.2.

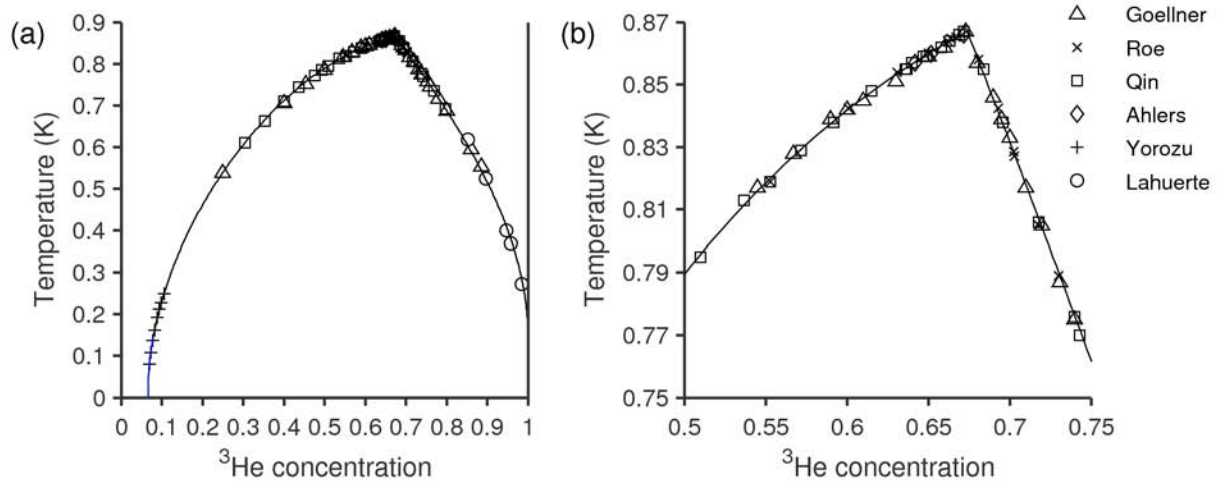

Figure 2.1: *Fits to the phase-separation curves, shown by solid lines, (a) over the entire T - x plane, and (b) in the vicinity of the tricritical point. The markers represent experimental data: Goellner et al [13] (shifted – see text), Roe et al [29], Qin et al [27], Ahlers and Greywall [31], Yorozu et al [30], and Lahuerte [32]. The dilute phase-separation curve is extended from 0.15 K to 0 K using values calculated by Kuerten et al [2].*

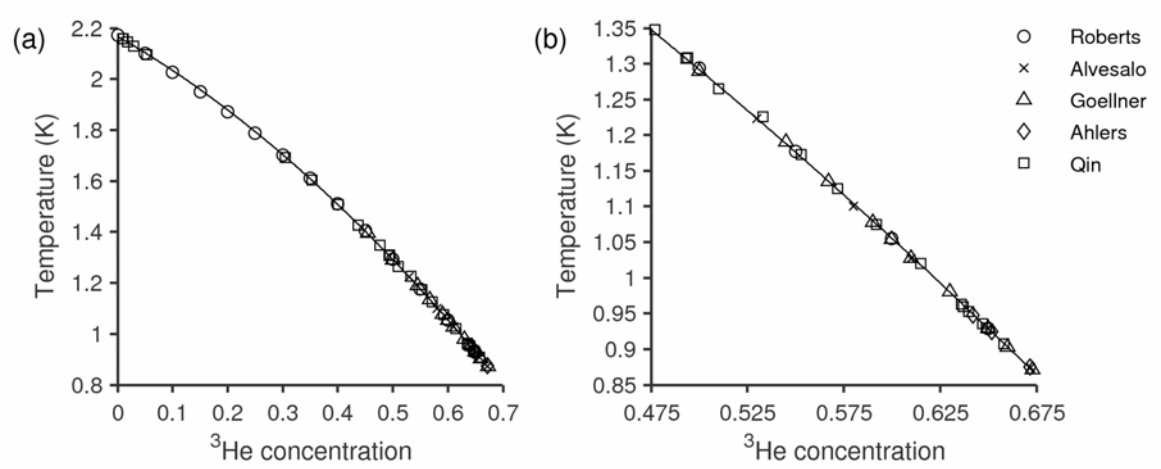

Figure 2.2: *Fit to the λ-curve shown by a solid line, (a) over the entire T - x plane, and (b) near the tricritical point. The markers represent experimental data: Roberts and Sydoriak [33], Alvesalo et al [14], Goellner et al [13], Ahlers and Greywall [31],and Qin et al [27].*

2.3 Available specific heat data

The range of some of the available specific heat data at saturated pressure is shown in Figure 2.3. Just about all of the specific heat data that are available are restricted either to dilute solutions of ^{3}He in ^{4}He at low temperatures, to near the tricritical point, or to near the lambda line. Anderson et al [34] measured the specific heat below temperatures of 0.2 K for mixtures with ^{3}He concentrations of 1.3% and 5%. Edwards et al [35] measured the specific heat between 0.1 K and 0.5 K for mixtures with ^{3}He concentrations between 3.9% and 15.1%. de Bruyn Ouboter et al [10] made measurements of the specific heat across the entire concentration range (they used 14 different mixtures) for temperatures between 0.4 K and 2 K. Alvesalo et al [14] made measurements of the specific heat in the vicinity of the tricritical point. In addition, Gasparini and Moldover [36] made measurements of the specific heat in the vicinity of the λ-line (within ± 0.1 K) for 1.1%-, 9.97%-, 20%- and 39%-^{3}He mixtures.

This specific heat data will now be used to calculate properties, first in the two-phase region, and then in the single-phase He-II and He-I regions. The discrepancies and contradictions between different sets of data (of which there are quite a few) will also be pointed out along the way.

A note on notation: in the following sections, the subscript "2ϕ" will be used for specific heats of two-phase mixtures, "$1\phi, II$" for single-phase, He-II mixtures, and "$1\phi, I$" for single-phase, He-I mixtures.

2.4 Thermodynamic properties in the two-phase region

In the two-phase region, it is possible to determine the thermodynamic properties at saturated pressure simply from a knowledge of the mixture molar specific heat at constant pressure and constant ^{3}He concentration, $C_{x,p}$ (or C), provided that properties at 0 K are known. Thermodynamic property calculations in the two-phase region are based on the fact that the properties of a mixture, such as the enthalpy, entropy, Gibbs free energy, and the molar volume in the two-phase region are a weighted average of the properties of the dilute phase and the concentrated phase.

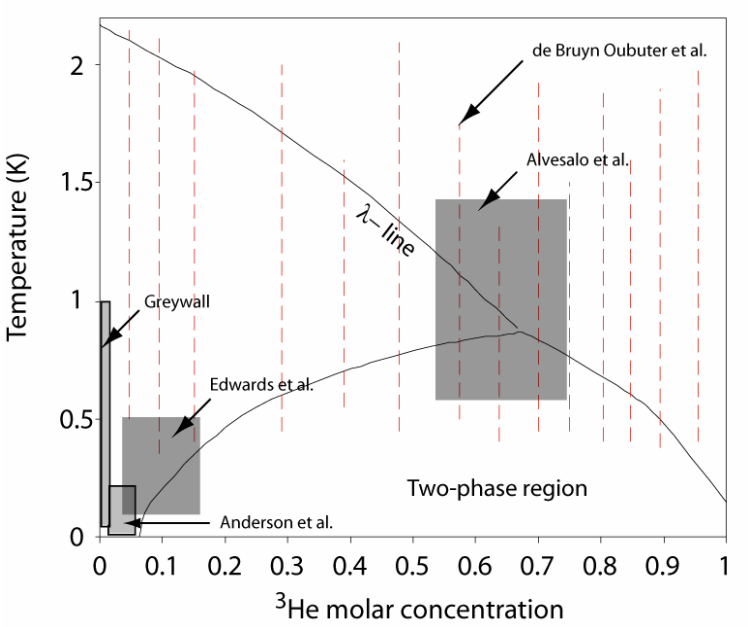

Figure 2.3: *Plot of the available specific heat data at saturated pressure on a T - x plot. The data by de Bruyn Oubuter et al [10] is shown as dashed lines. This representation of data is not exhaustive but is representative of the range of available data.*

According to the lever rule, the molar enthalpy $h(x,T)$ at any point in the two-phase region at a temperature T and a ^{3}He mole fraction x can be written as the weighted average of the enthalpies of the concentrated (^{3}He-rich) phase and the dilute phase at the same temperature T,

$$h(x,T) = \frac{x_{\sigma+}(T) - x}{x_{\sigma+}(T) - x_{\sigma-}(T)} h(x_{\sigma-}(T),T) + \frac{x - x_{\sigma-}(T)}{x_{\sigma+}(T) - x_{\sigma-}(T)} h(x_{\sigma+}(T),T) \tag{2.6}$$

where $x_{\sigma+}(T)$ and $x_{\sigma-}(T)$ are the ^{3}He mole fractions of the concentrated and dilute phases respectively, at a temperature T.

Therefore, at a fixed temperature T, h varies linearly with x in the two-phase region; hence

$$\left(\frac{\partial h}{\partial x}\right)_T = \frac{h(x_{\sigma+}(T),T) - h(x_{\sigma-}(T),T)}{x_{\sigma+}(T) - x_{\sigma-}(T)}. \tag{2.7}$$

Since the order of differentiation does not influence the value of a mixed derivative,

$$\frac{\partial}{\partial x}\left(\frac{\partial h}{\partial T}\right) = \frac{\partial}{\partial T}\left(\frac{\partial h}{\partial x}\right) = \frac{\partial}{\partial T}\left(\frac{h(x_{\sigma+}(T),T) - h(x_{\sigma-}(T),T)}{x_{\sigma+}(T) - x_{\sigma-}(T)}\right). \tag{2.8}$$

The derivative of the specific heat with respect to x in the two-phase region can be determined by substituting Eq. 1.10 into Eq. 2.8.

$$\frac{\partial C_{2\phi}}{\partial x} = \frac{\partial}{\partial T}\left(\frac{\partial h}{\partial x}\right) = \frac{\partial}{\partial T}\left(\frac{h(x_{\sigma+}(T),T) - h(x_{\sigma-}(T),T)}{x_{\sigma+}(T) - x_{\sigma-}(T)}\right). \tag{2.9}$$

Since the right hand side of the above equation is constant for all x at a given temperature T, the specific heat also varies linearly with x at a fixed temperature in the two-phase region.

The enthalpy in the two-phase region will now be determined in terms of specific heats. Treating x and T as independent variables, the differential enthalpy can be written as

$$dh = \left(\frac{\partial h}{\partial x}\right)_T dx + \left(\frac{\partial h}{\partial T}\right)_x dT \,. \tag{2.10}$$

Starting from the point ($x = x_t, T = 0$), Eq. 2.10 is integrated first along a line of constant temperature (T = 0 K) from x_t to x and then along a line of constant ^{3}He mole fraction (x) from 0 to T. (x_t is the ^{3}He concentration at the tricritical point: 67.4%.) The path of integration is shown in Figure 2.4. The enthalpy at x and T is therefore

$$h(x,T) - h(x_t,0) = \left(\frac{\partial h}{\partial x}\right)_{0\mathrm{K}} (x - x_t) + \int_0^T \left(\frac{\partial h}{\partial T}\right)_x dT \,. \tag{2.11}$$

Since the specific heat is linear at a fixed temperature in the two-phase region, the specific heat at x and T can be written as

$$\left(\frac{\partial h}{\partial T}\right)_x = C_{2\phi}(x,T) = C_{2\phi,t}(T) + \frac{\partial C_{2\phi}}{\partial x}(x - x_t) \tag{2.12}$$

where $C_{2\phi,t}(T)$ is the specific heat of a two-phase mixture at a temperature T and a ^{3}He fraction of x_t = 0.674.

Substituting Eq. 2.12 into Eq. 2.11 results in

$$h(x,T) = \left(\left(\frac{\partial h}{\partial x}\right)_{0\mathrm{K}} + \int_0^T \frac{\partial C_{2\phi}}{\partial x} dT\right)(x - x_t) + \int_0^T C_{2\phi,t} dT + h(x_t,0) \,. \tag{2.13}$$

Since the ^{3}He mole fractions at the concentrated and dilute phase separation curves are 1 and 0.066 respectively at 0 K, the value of $(\partial h / \partial x)_{0\mathrm{K}}$ and $h(x_t,0)$ can be determined from

$$\left(\frac{\partial h}{\partial x}\right)_{0\mathrm{K}} = \frac{h_3^0(0\ \mathrm{K}) - h(x = 0.066, 0\ \mathrm{K})}{1 - 0.066} \tag{2.14}$$

and

$$h(x_t,0) = h_3^0(0\ \mathrm{K}) - (1 - x_t)\left(\frac{\partial h}{\partial x}\right)_{0\mathrm{K}} \,, \tag{2.15}$$

where h_3^0 is the enthalpy of pure ^{3}He. The values of h_3^0 and $h(x = 0.066)$ at 0 K are taken from Kuerten et al's tables [2].

An expression for the entropy in the two-phase region in terms of specific heats at constant x can be found using a similar analysis. Going through the same steps and integrating along the same path, the following equation is obtained for entropy, which is similar to the enthalpy expression in Eq. 2.13:

$$s(x,T) = \left(\left(\frac{\partial s}{\partial x}\right)_{0\mathrm{K}} + \int_0^T \frac{1}{T}\frac{\partial C_{2\phi}}{\partial x} dT\right)(x - x_t) + \int_0^T \frac{C_{2\phi,t}}{T} dT + s(x_t,0) \,. \tag{2.16}$$

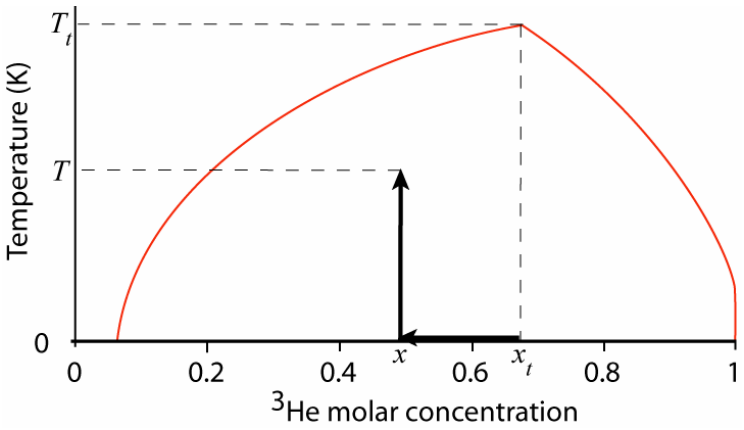

Figure 2.4: *Path of integration used to calculate the enthalpy (and entropy) at a given x and T in the two-phase region*

In accordance with the Third Law of Thermodynamics, the entropy at zero temperature, $s(x, T = 0)$, is equal to 0 for all values of x. This is a consequence of the statistical definition of entropy,

$$s = k \ln \Omega \tag{2.17}$$

where Ω is the number of available microstates. As the temperature approaches zero, the system goes into its ground state. As a consequence, Ω equals 1, and the entropy goes to zero. This is discussed in detail by Reif [37]. The seeming contradiction between the limiting solubility of ^{3}He in ^{4}He at 0 K and the non-zero entropy of mixing is discussed by Lounasmaa [38].

In order that the entropy calculated from Eq. 2.16 be zero at 0 K at all values of x, it is required that

$$\left(\frac{\partial s}{\partial x}\right)_{0\,\mathrm{K}} = 0 \tag{2.18}$$

and

$$s(x_t, 0) = 0\,. \tag{2.19}$$

Substituting Eqs. 2.18 and 2.19 into Eq. 2.16, we get

$$s(x,T) = (x - x_t)\int_0^T \frac{1}{T}\frac{\partial C_{2\phi}}{\partial x} dT + \int_0^T \frac{C_{2\phi,t}}{T} dT\,. \tag{2.20}$$

It is evident from Eqs. 2.13 and 2.20 that a knowledge of the specific heats at constant x and p is all that is necessary to determine properties within the two-phase region, provided that the value of $\partial h / \partial x$ is known at 0 K. Unfortunately, as is clear from Figure 2.3, specific heat data is not available over the entire range of temperatures (0 K to 0.867 K).

Specific heats at temperatures below 0.15 K were inferred from the thermodynamic models of Kuerten et al [2] and from properties of pure ^{3}He. $C_{2\phi,t}$ was estimated from

$$C_{2\phi,t} \approx T\left(\frac{s(x_t, T + \Delta T) - s(x_t, T)}{\Delta T}\right), \tag{2.21}$$

where

$$s(x_t,T) = \frac{x_t - x_{\sigma-}(T)}{1 - x_{\sigma-}(T)}\left(s_3^0(T) - s_{\sigma-}(T)\right) + s_{\sigma-}(T), \tag{2.22}$$

where $s_3^0(T)$ is the entropy of pure ^{3}He and $s_{\sigma-}(T)$ is the entropy of the mixture on the dilute-phase curve. The magnitude of ΔT was chosen to be 0.001 K. Note that this procedure could also have been carried out with the enthalpy rather than the entropy; however, the values obtained by using the entropy were a lot more insensitive to the chosen value of ΔT.

$\partial C_{2\phi} / \partial x$ was calculated from

$$\frac{\partial C_{2\phi}}{\partial x} = \frac{C_{2\phi}(x_{arb},T) - C_{2\phi,t}(T)}{x_{arb} - x_t} \tag{2.23}$$

where x_{arb} is an arbitrarily chosen value of x that lies within the two-phase region. The choice of x_{arb} does not affect the calculated value of $\partial C_{2\phi} / \partial x$, since the latter only depends on temperature. $C_{2\phi}(x_{arb},T)$ was estimated in much the same way as $C_{2\phi,t}$ above.

Alvesalo et al [14] made measurements of the specific heat of two-phase mixtures at temperatures above 0.5 K. However, there is not a lot of data available between 0.15 K and 0.5 K. de Bruyn Ouboter et al [10] made specific heat measurements of two-phase mixtures at temperatures above 0.45 K, but their data is quite noisy. In addition, de Bruyn Ouboter et al's data does not appear to be completely consistent with Alvesalo et al's data at temperatures below 0.6 K (see Figure 2.5). Edwards et al [35] made measurements of specific heats of two-phase mixtures of low overall ^{3}He concentration in the temperature range 0.15 K to 0.30 K. Unfortunately, there is considerable scope for error in the determination of the slope of the specific heat ($\partial C_{2\phi} / \partial x$) from Edwards et al's data, since the (closely-spaced) data must be read off a graph (which is shown below in Figure 2.6, directly reproduced from Edwards et al's paper) rather than from a table. Also, some of Edwards et al's data seems to be inconsistent with the conclusion that that the specific heat must vary linearly with x at constant temperature. This can also be seen from Figure 2.6. Specific heats are plotted as functions of temperature for 5 different mixtures. The 3.9% and 6% mixtures stay in the single-phase He-II region at all temperatures. The 8.1%, 12.1% and 15.1% mixtures transition from the two-phase region to the single-phase region. (The transition is very clear for the 12.1% and 15.1% mixtures; for the 8.1% mixture, it occurs at about 0.16 K.) From the figure, it appears that in the two-phase region, at about 0.15 K, the specific heat does not vary linearly from 8.1% to 12.1% to 15.1%. (Admittedly there isn't any actual data for the 12.1% mixture at 0.15 K, but there would have a marked change in the trend of the 12.1% mixture specific heat values for the linearity criterion to be satisfied.)

Polynomial fits for $C_{2\phi,t} / T$ and $(\partial C_{2\phi} / dx) / T$ were obtained by interpolating between the low temperature data of Kuerten et al, the high temperature data of Alvesalo et al, and some of Edwards et al's and de Bruyn Ouboter et al's data. The behaviour of the single-phase He-II model (which will be discussed in the following section) depends significantly on the specifics of these quantities. Several fitting schemes were considered and the resulting behaviour of the single-phase model was studied. In particular, for some of the fits, the resulting lines of constant ^{4}He chemical potential were found to be non-physical. Constraints were also placed on the two-phase specific heats to ensure consistency with the single-phase specific heats and with Kuerten et al's model. The fit finally chosen is shown in Figure 2.7, where the quantities $C_{2\phi,t} / T$ and $(\partial C_{2\phi} / dx) / T$ are plotted as functions of T. The fits for $C_{2\phi,t} / T$ and $(\partial C_{2\phi} / dx) / T$ are both piecewise: there is one fit each for temperatures below 0.15 K and one each for temperatures above 0.15 K. The fits are continuous and differentiable at the transition. The fits are

listed in Appendix A.2.1. (The fitting procedure will be discussed in the following section since all the specific heat fits, both in the two-phase and single-phase regions, were determined simultaneously.)

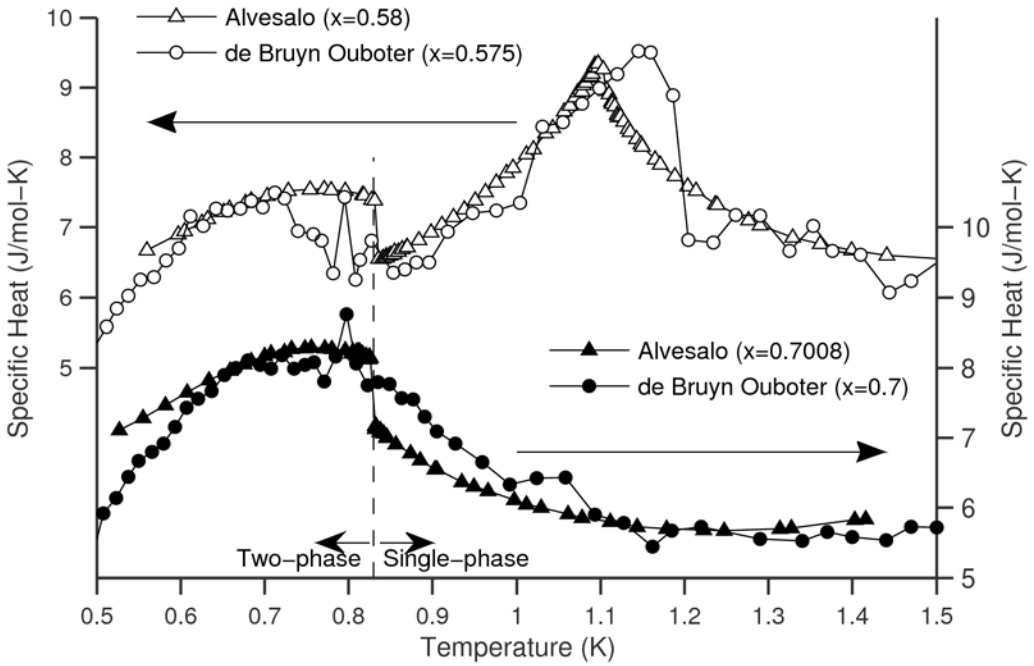

Figure 2.5: *A comparison of specific heat data of Alvesalo et al [14] and de Bruyn Ouboter et al [10]*

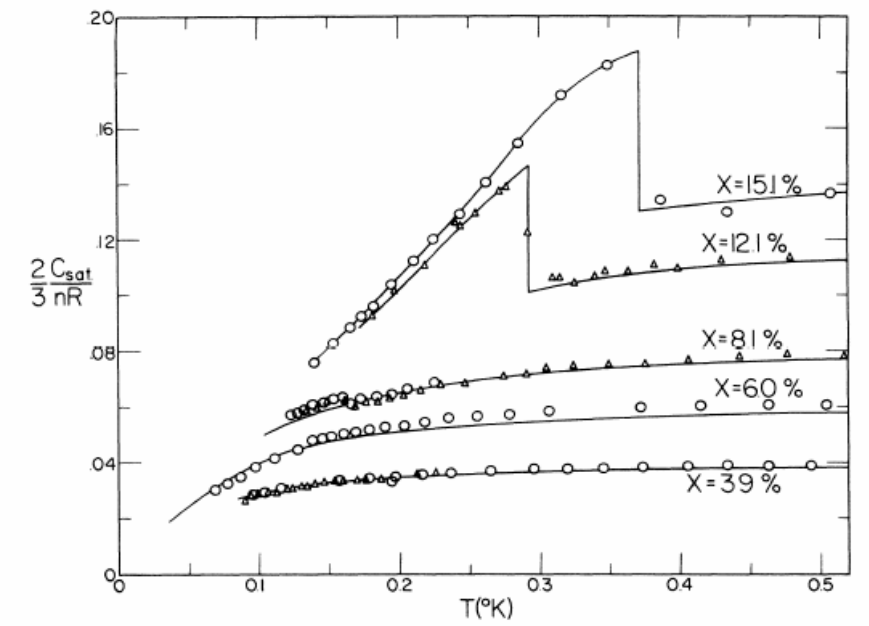

Figure 2.6: *The specific heat data of Edwards et al [35]*

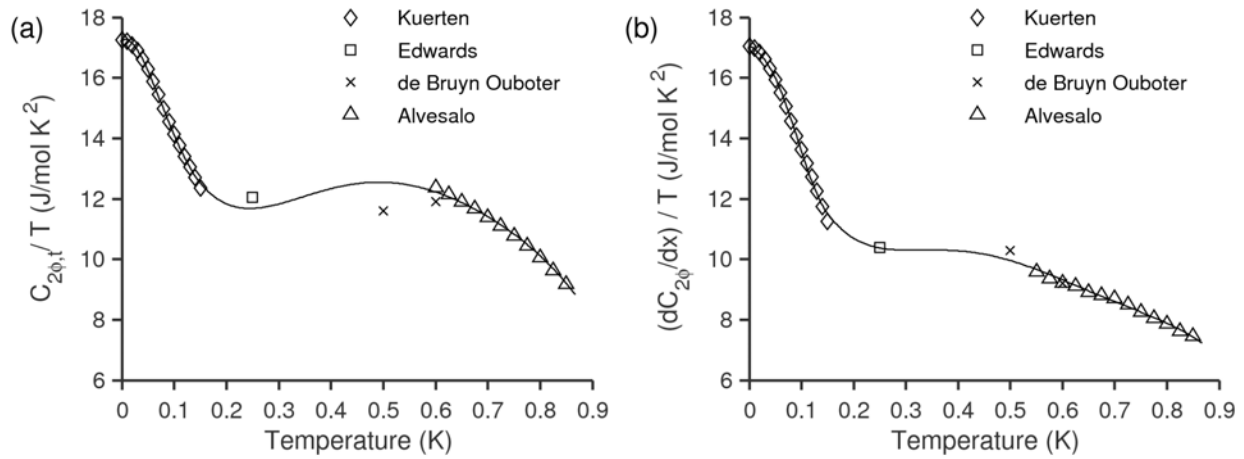

Figure 2.7: *(a)* $C_{2\phi,t}/T$ *and (b)* $(\partial C_{2\phi}/dx)/T$ *plotted as functions of* T*, in the two-phase region. The data points are from Kuerten et al [2], Edwards et al [35], de Bruyn Ouboter et al [10], and Alvesalo et al [14]. The solid lines represent the curve fits.*

With these fits, the enthalpy and entropy can be calculated from Eqs. 2.13 and 2.20 respectively. The Gibbs free energy g can be calculated from Eq. 1.7. The ^{4}He chemical potential can then be calculated from the Gibbs free energy of the mixture using Eq. 1.13.

In the two-phase region, g is a linear function of x at constant temperature, since both h and s are linear functions of x at constant temperature. Therefore, the Gibbs free energy $g(x,T)$ has the same form as the enthalpy in Eq. 2.6. Substituting that form into Eq. 1.13, the ^{4}He chemical potential at a temperature T, in terms of the Gibbs free energies of the dilute and concentrated phases, is

$$\mu_4(T) = \frac{x_{\sigma+}(T)g(x_{\sigma-}(T),T) - x_{\sigma-}(T)g(x_{\sigma+}(T),T)}{x_{\sigma+}(T) - x_{\sigma-}(T)}. \tag{2.24}$$

As expected, the ^{4}He chemical potential does not depend on x, since chemical potentials of both species must be the same in both phases of a two-phase mixture.

The ^{3}He chemical potential can be similarly calculated using Eq. 1.12. In terms of the Gibbs free energies of the dilute and concentrated phases, the ^{3}He chemical potential is

$$\mu_3(T) = \frac{\big(1-x_{\sigma-}(T)\big)g(x_{\sigma+}(T),T) - \big(1-x_{\sigma+}(T)\big)g(x_{\sigma-}(T),T)}{x_{\sigma+}(T) - x_{\sigma-}(T)}. \tag{2.25}$$

The osmotic enthalpy can be calculated from Eq. 1.20. Since values of h and μ_4 are already known, finding the osmotic enthalpy is quite straightforward.

Since the osmotic enthalpy is calculated on a per-mole-of-^{3}He basis, it is not a linear function of x at constant temperature in the two-phase region, unlike the enthalpy, entropy and the Gibbs free energy. However, since the mixture enthalpy is a linear function of x at constant temperature and μ_4 is constant at constant temperature, the product xh^{os} is a linear function of x in the two-phase region.

Experimental data on molar volumes of two-phase ^{3}He-^{4}He mixtures are quite limited. However, since the molar volume in the two-phase region is also just a weighted average of the molar volumes of the

concentrated and dilute phases, only the molar volumes along the phase separation curves are required. Molar volumes are discussed in greater detail in the next chapter.

The complete set of equations used to calculate the entropy, enthalpy, Gibbs free energy and ^{4}He chemical potential in the two-phase region is listed in Appendix B.1. In addition, Table 11 in Appendix E.1 lists the properties of ^{3}He-^{4}He mixtures in the two-phase region as a function of the temperature. At a given temperature, the ^{3}He concentration (x), molar volume (v), entropy (s), enthalpy (h), Gibbs free energy (g), and the product xh^{os} for both the dilute and the concentrated phases are tabulated. (The molar volumes are calculated from the model developed in Chapter 3). The properties in the two-phase region at a given x are determined by linearly interpolating between the properties of the dilute and concentrated phases at the appropriate temperature. The table also lists the ^{4}He chemical potential, which depends only on the temperature T and is the same for both concentrated and dilute phases.

2.5 Thermodynamic properties in the single-phase He-II region

One of the big difficulties in determining the properties in the single-phase region is the lack of consistent experimental data spanning the phase diagram. Before proceeding to the calculation procedure, it is worth discussing some of these inconsistencies.

In his thermodynamic property calculations, Radebaugh [1] used a simplifying model in which the specific heat of a mixture with a ^{3}He concentration of less than 30% can be written as the sum of a pure-^{4}He specific heat and the specific heat of an ideal Fermi gas of quasiparticles that have the same density as the ^{3}He in the mixture and an effective mass m^* calculated from the interaction potential between ^{3}He atoms. This model, used by Radebaugh for temperatures up to 1.5 K, is in good agreement [1] with the measurements of Anderson et al [34] and Edwards et al [35]. However, subsequent specific heat measurements on very dilute solutions (< 1% ^{3}He concentration) made by Greywall [39] in the temperature range 0.07 K to 1 K showed that this model was valid only for temperatures below about 0.25 K. This is why Kuerten et al [2], who used the same model as Radebaugh, restricted their thermodynamic property tables to below 0.25 K. For temperatures greater than about 0.25 K, Greywall suggests a correction term to the ideal model used by Radebaugh and Kuerten et al:

$$C_{non-ideal} = C_{ideal} + \frac{3}{2} xRS(T - T_o) \tag{2.26}$$

where $C_{non-ideal}$ is the mixture specific heat proposed by Greywall, C_{ideal} is the mixture specific heat predicted by the ideal model, R is the universal gas constant, T_o = 0.245 K and S = 0.20 K^{-1}. In Figure 2.8, we compare Greywall's "non-ideal" model and the ideal model with experimental measurements made by de Bruyn Ouboter et al [10] at a ^{3}He concentration of 4.7%. There are differences between the experimental measurements and the predicted values; however, the ideal model appears to be more consistent with the experimental measurements than the non-ideal model. If we believe de Bruyn Ouboter et al's values, it is debatable whether Greywall's correction, proposed for very dilute mixtures (<1%), can be extended to mixtures with higher ^{3}He concentrations.

In addition, Radebaugh's values (calculated from the ideal model) are inconsistent with the experimental specific heat data of de Bruyn Ouboter et al (see Figure 2.9), both at higher ^{3}He concentrations (10% and greater) and at higher temperatures (greater than 1.2 K). Radebaugh acknowledges that his tabulated specific heat values are not consistent with de Bruyn Ouboter et al's data. Specific heat measurements by Edwards et al of 15.1% solutions between 0.4 K and 0.5 K are in agreement with Radebaugh's model and inconsistent with de Bruyn Ouboter et al's data, as is also evident from Figure 2.9. There seem to be no

other specific heat measurements in the 15 to 30% ^{3}He-mole-fraction range which could possibly resolve these inconsistencies.

The data finally chosen to obtain a specific heat fit is from three sources – (a) Radebaugh [1], at low values of x (where it is in agreement with experimental measurements), and (b) Alvesalo et al [14] and (c) de Bruyn Ouboter et al [10], which are the only data sources at higher values of x. The specifics of the data chosen in the model will be discussed later, after developing expressions for thermodynamic properties as functions of the specific heat.

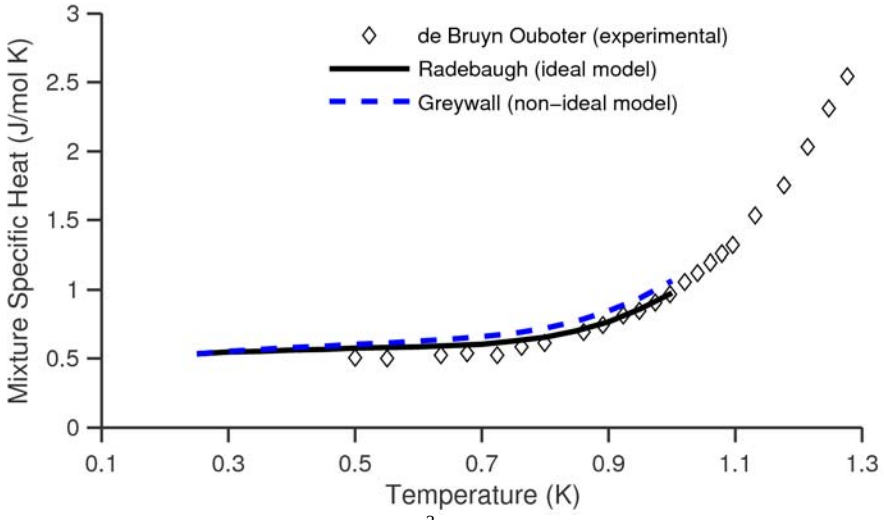

Figure 2.8: *Specific heats of a 4.7%-^{3}He mixture measured by de Bruyn Ouboter et al [10]. Also shown are specific heats predicted by the ideal specific heat model used by Radebaugh [1], and by the non-ideal model proposed by Greywall [39].*

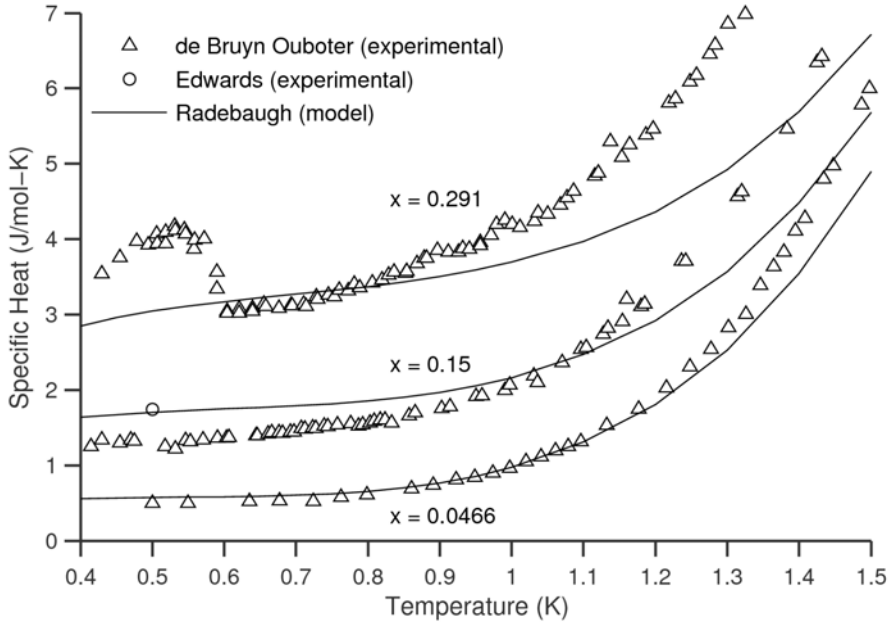

Figure 2.9: *Differences between the specific heats measured by de Bruyn Ouboter et al [10] and those from Radebaugh's model [1] at three different ^{3}He concentrations: 4.66%, 15% and 29.1%. On the other hand, the measurements of Edwards et al [35] (one data point shown) agree with Radebaugh's model.*

Properties in the He-II region are calculated from the known properties along the lower boundary of the region of interest, as shown in Figure 2.10. At 0.15 K, phase separation occurs at ^{3}He concentrations of above 8% (8.014%, according to Kuerten et al's model [2]). Properties for mixtures at 0.15 K with ^{3}He concentrations of less than 8% are known from Kuerten et al's tables. Properties for the dilute-phase saturated states (with ^{3}He concentrations of above 8%) were calculated in the previous section.

Using the relation between the entropy and the specific heat at constant p and x (Eq. 1.11), the entropy in the single-phase He-II region can be calculated from:

$$s(x,T) = s_l(x) + \int_{T_l(x)}^{T} \frac{C_{1\phi,II}(x,T)}{T} dT \tag{2.27}$$

where

$$T_l(x) = \begin{cases} For\ \ x < 0.08,\ \ 0.15\ \ K \\ For\ \ x > 0.08,\ \ T_{\sigma-}(x) \end{cases} \tag{2.28}$$

and

$$s_l(x) = \begin{cases} For\ \ x < 0.08,\ \ s(x,0.15\ \ K) \\ For\ \ x > 0.08,\ \ s_{\sigma-}(x) \end{cases}. \tag{2.29}$$

(Recall that the subscript $\sigma-$ refers to properties on the dilute phase-separation curve.)

Using Eq. 1.10, the enthalpy can similarly be calculated using:

$$h(x,T) = h_l(x) + \int_{T_l(x)}^{T} C_{1\phi,II}(x,T) dT \tag{2.30}$$

where $T_l(x)$ is the same as above, and

$$h_l(x) = \begin{cases} For\ \ x < 0.08,\ \ h(x,0.15\ \ K) \\ For\ \ x > 0.08,\ \ h_{\sigma-}(x) \end{cases}. \tag{2.31}$$

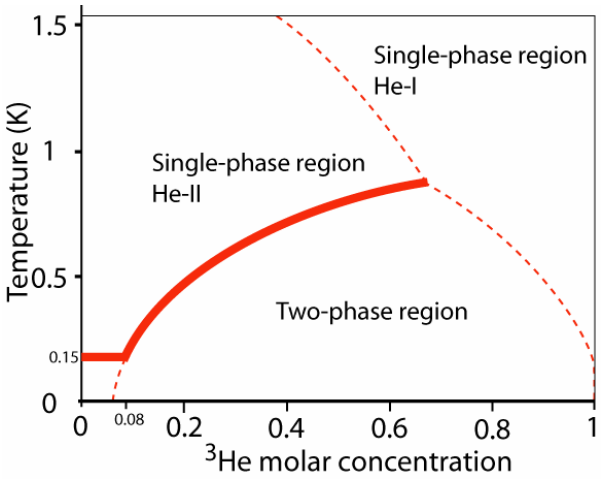

Figure 2.10: *Properties in the single-phase He-II region are determined by integrating up from the darkened line in this phase diagram. Thermodynamic properties are completely known along this line - from Kuerten et al for the horizontal portion and from the two-phase model for the curved portion.*

The values of entropy and enthalpy at 0.15 K and ^{3}He fractions of less than 8% are calculated from Kuerten et al's model (some representative values are listed in Table 9 in Appendix B.2.1); values at the phase-separation curve are calculated using the two-phase model of the previous section.

The Gibbs free energy g is calculated from the entropy and the enthalpy using Eq. 1.7:

$$g(x,T) = h_l(x) - Ts_l(x) + \int_{T_l(x)}^{T} C_{1\phi,II}(x,T)dT - T\int_{T_l(x)}^{T} \frac{C_{1\phi,II}(x,T)}{T}dT \,. \tag{2.32}$$

The ^{4}He and ^{3}He chemical potentials can then be derived from Eqs. 1.13 and 1.12 respectively.

To get an expression for the specific heat, available data were fitted to a single function of x and T. The specific heat at constant pressure and ^{3}He concentration was written as:

$$C_{1\phi,II}(x,T) = xC_3^0(T) + (1-x)C_4^0(T) + x(1-x)C_{r,II}(x,T) \tag{2.33}$$

where $C_3^0(T)$ is the specific heat of pure ^{3}He, $C_4^0(T)$ is the specific heat of pure ^{4}He, and $C_{r,II}(x,T)$ represents the deviation from the specific heat of an "ideal" mixture (not to be confused with the "ideal" model used by Radebaugh). The mixture specific heat reduces to the specific heat of pure ^{3}He and pure ^{4}He at x = 1 and x = 0 respectively. To write the mixture specific heat this way, expressions are required for the specific heats of pure ^{3}He and ^{4}He.

The specific heat of pure ^{3}He was measured by Greywall [40]. He proposed an empirical relation for the specific heat as a function of the molar volume v_3^o and temperature T above 0.1 K:

$$C_3^0(v_3^o,T) = \sum_{i=0}^{i=3}\sum_{j=0}^{j=2} a_{1,ij}\left(v_3^o\right)^j T^{-i} + \exp\left(-\frac{1}{T}\sum_{j=0}^{2} a_{2,j}\left(v_3^o\right)^j\right)\sum_{i=1}^{i=3}\sum_{j=0}^{j=2} a_{3,ij}\left(v_3^o\right)^j T^{-i} \tag{2.34}$$

where $a_{1,ij}$, $a_{2,j}$ and $a_{3,ij}$ are constants. At a constant molar volume v_3^o = 36.82 cm^3/mol, (which corresponds to $p \approx 0$), this reduces to the form

$$C_3^0(T) = \sum_{i=0}^{i=3} a'_{1i}T^{-i} + \exp\left(-\frac{a'_2}{T}\right)\sum_{i=1}^{i=3} a'_{3i}T^{-i} \,. \tag{2.35}$$

To get an expression for $C_3^0(T)$ that could be easily integrated, the pure ^{3}He specific heat was rewritten as

$$C_3^0(T) = \sum_{i=0}^{3} A_{31,i}T^i + \frac{A_{32}}{T^2}e^{-\frac{\Delta_3}{T}} \,. \tag{2.36}$$

The coefficients $A_{31,i}$, A_{32} and Δ_3 were determined from a least squares fit to Greywall's tabulated values [40]. The maximum difference between the fit of Eq. 2.36 and Greywall's fit is about 0.7%. The values of $A_{31,i}$, A_{32} and Δ_3 are listed in Table 3 in Appendix A.2.2.

According to Khalatnikov [41], the specific heat of pure ^{4}He at low temperatures can be written as a sum of the phonon specific heat and the roton specific heat:

$$C_4^0(T) = A_{41,1}T^3 + A_{42}\left(\frac{\Delta_r}{T}\right)^{\frac{3}{2}} e^{-\frac{\Delta_r}{T}}\left(1 + \frac{T}{\Delta_r} + \frac{3}{4}\left(\frac{T}{\Delta_r}\right)^2\right) \tag{2.37}$$

where the first term corresponds to the phonon contribution and the second term to the roton contribution.

Greywall measured the specific heat of pure ^{4}He up to temperatures of 0.85 K [42]. He added correction terms to the phonon contribution and fitted his data to an expression of the form:

$$C_4^0(T) = \left(A_{41,1}T^3 + A_{41,3}T^5 + A_{41,4}T^6 + A_{41,5}T^7\right) + A_{42}\left(\frac{\Delta_r}{T}\right)^{\frac{3}{2}} e^{-\frac{\Delta_r}{T}}\left(1 + \frac{T}{\Delta_r} + \frac{3}{4}\left(\frac{T}{\Delta_r}\right)^2\right). \qquad (2.38)$$

To improve the ^{4}He fit at higher temperatures (T > 1 K), Brisson and Patel [43] added a "maxon" contribution to Khalatnikov's expression (Eq. 2.37). Including both the phonon correction terms and the maxon contribution, the specific heat of pure ^{4}He is

$$C_4^0(T) = \sum_{i=1}^{5} A_{41,i}T^{i+2} + A_{42}\left(\frac{\Delta_r}{T}\right)^{\frac{3}{2}} e^{-\frac{\Delta_r}{T}}\left(1 + \frac{T}{\Delta_r} + \frac{3}{4}\left(\frac{T}{\Delta_r}\right)^2\right) + \frac{A_{43}}{T}\left(\frac{\Delta_m}{T}\right)^2 e^{-\frac{\Delta_m}{T}}\left(1 - 2\frac{T}{\Delta_m}\right) \qquad (2.39)$$

where the "Δ_m" terms correspond to the maxon contribution. The coefficients $A_{41,i}$, A_{42}, A_{43}, Δ_r and Δ_m were determined from a least squares fit to Greywall's values [42] and ^{4}He data from HEPAK [15]. The values of these coefficients are listed in Table 3 in Appendix A.2.2. The maximum difference between the fit of Eq. 2.39 and the underlying data is approximately 1%.

Having determined expressions for the specific heats of pure ^{3}He and pure ^{4}He between 0.15 K and 1.8 K, we now need to find an expression for $C_{r,II}(x,T)$ based on mixture specific heat data. It is important to note that mixtures of ^{3}He concentrations of greater than about 25% undergo a λ-transition at temperatures of less than 1.8 K. Therefore, the expression for $C_{r,II}(x,T)$ must take into account the sharp changes in specific heat near the λ-line.

In fitting the specific heat of pure ^{4}He near the λ-line, Arp [44] used an expression of the form

$$C_4^0 = \sum\sum a_{1,ij}T^i\left(v_4^o\right)^j + \sum a_{2,i}T^i \ln(T - T_\lambda(v_4^o)). \qquad (2.40)$$

where v_4^o is the molar volume of pure ^{4}He, and $T_\lambda(v_4^o)$ is the λ-transition temperature at v_4^o. The logarithmic terms were required for a good fit near the λ-line. A similar form was adopted for the correction term $C_{r,II}(x,T)$. Since the specific heat is a function of T and x for the (zero-pressure) ^{3}He-^{4}He mixture, $C_{r,II}(x,T)$ was initially written as

$$C_{r,II}(x,T) = \sum_{i=0}^{4}\sum_{j=0}^{4} A_{II,1,ij}x^iT^j + \sum_{i=0}^{4}\sum_{j=1}^{2} A_{II,2,ij}x^iT^j \ln(T - T_\lambda(x) + \varepsilon) \qquad (2.41)$$

where $T_\lambda(x)$ is the λ-transition temperature at x, and ε is a positive constant used to ensure a finite value at $T = T_\lambda$. It turned out, however, that in the He-II region, the logarithmic terms did not significantly improve the fit to experimental data for the mixtures. Therefore, we finally simply used

$$C_{r,II}(x,T) = \sum_{i=0}^{4}\sum_{j=0}^{4} A_{II,1,ij}x^iT^j \; . \qquad (2.42)$$

The He-II specific heat was fitted to the smoothed specific heat data of Alvesalo et al [14] (^{3}He concentrations of 53%, 58%, 61%, 65%) and de Bruyn Ouboter et al [10] (^{3}He concentrations of 4.7%, 9.4%, 15%, 29%, 47.8%). (The specific heat data at each value of x was smoothed by fitting a third- or fourth-order polynomial function of temperature to it.) The 39%-^{3}He data of de Bruyn Ouboter et al was not used because it is quite noisy and has much fewer data points than their other measurements. Their 4.7%-^{3}He specific heat data only extends down to 0.5 K, and, in addition, the data in the temperature range 0.5 K-0.8 K is very limited. Since their data is in reasonable agreement with Radebaugh's values over the temperature range 0.6 K-1.2 K, de Bruyn Ouboter et al's 4.7%-^{3}He data was included in the

fitting function only at temperatures above 1.2 K, and Radebaugh's specific heat values for 5%-^{3}He mixtures (as well as for 1% and 2.5%-^{3}He mixtures) at temperatures between 0.2 K and 1 K. Radebaugh's values were included because there is not much experimental data in the x = 0.01–0.05 and T = 0.2–1 K region of the T - x plane.

There were certain constraints on the specific heat fits employed in this model (which were briefly alluded to in the previous section). Kuerten et al's data was used to calculate properties at ^{3}He concentrations below 8%, and data along the phase-separation curve to calculate properties at ^{3}He concentrations above 8%. It needed to be ensured that the entropy and enthalpy thus calculated (and their derivatives) were continuous across the x = 0.08 boundary. Constraints were included to ensure continuity up to a second derivative. These constraints are listed in Appendix D.1.

For consistency, the values predicted by the specific heat fit were constrained to be continuous with the specific heats from Kuerten et al's model at 0.15 K. The temperature derivatives of the specific heat were not constrained to be continuous.

The fitting procedure was implemented in Matlab using the non-linear data fitting function *lsqnonlin*. *lsqnonlin* operates on a user-defined function – it minimises the sum of the squares of all the elements in a vector returned by that user-defined function. The fitting program was set up to calculate specific heat parameters that would minimise the difference between the values calculated from the various fitting formulas and the underlying experimental data, while satisfying all the constraints on the fits. The constraints were implemented using Lagrange multipliers. In essence, the fitting program minimised the function

$$F = \sum_i w_i \left(y_{fitted,i} - y_{data,i} \right)^2 + \sum_j \lambda_j G_j \qquad (2.43)$$

where the y's were the various data points (mostly specific heats), the w's the associated weights, the G_j's the various constraints and the λ_j's the Lagrange multipliers.

It has been mentioned previously that all specific heat fits (in the two-phase, and in both the He-II and He-I regions) were determined simultaneously. The fitted data included the two-phase $C_{2\phi,t} / T$ and $(\partial C_{2\phi} / dx) / T$ values, the He-II specific heat values, and the He-I specific heat values, which will be discussed in the following section. The constraints included the ones discussed above, and additional constraints for the He-I region, which will also be discussed in the following section.

The coefficients $A_{II,1,ij}$ for use in Eq. 2.42 (i.e., for the single-phase He-II region) calculated from the fitting procedure are tabulated in Table 4 in Appendix A.2.2. This fit is valid for temperatures between 0.15 K and 1.8 K. The smoothed experimental specific heat data and the specific heats calculated from the fit are plotted in Figure 2.11, at various concentrations. The r.m.s. error associated with the data is about 5% (and the maximum error is about 14%). The errors associated with the entropy, enthalpy and Gibbs free energy are expected to be smaller, since these quantities are obtained by integrating the specific heat.

We now discuss some some of the limitations of the calculated fit.

The model results may be inaccurate in the values of μ_4 at ^{3}He concentrations between 10% and 25%. This is due to the sensitivity of μ_4 to the value of $(C_{2\phi})_{T_{\sigma-}}$, the two-phase specific heat at x and $T_{\sigma-}$. An explicit expression for $\mu_4(x,T)$ is given in Appendix B.2.2 (Eq. B.12). The sensitivity to $(C_{2\phi})_{T_{\sigma-}}$ is contained in one term, i.e.,

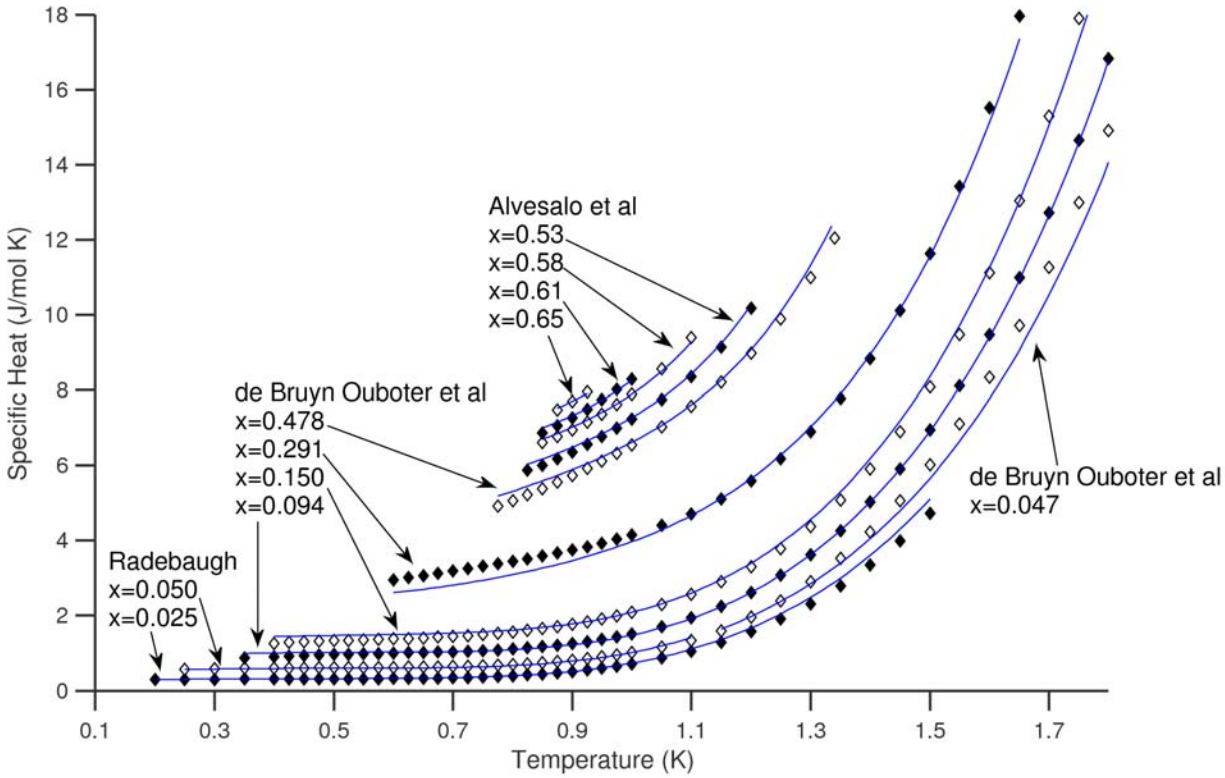

Figure 2.11: *Specific heats in the He-II region as a function of temperature. The markers represent smoothed experimental data of de Bruyn Ouboter et al [10] and Alvesalo et al [14], and the values of Radebaugh [1]. The solid lines represent the fit of Eq. 2.33.*

$$\mu_4(x,T) = -x\frac{dT_{\sigma-}}{dx}\left(1-\frac{T}{T_{\sigma-}}\right)\left(\left(C_{2\phi}\right)_{T_{\sigma-}} - \left(C_{1\phi,II}\right)_{T_{\sigma-}}\right) + \text{other terms.} \qquad (2.44)$$

Since the calculated value of $\mu_4(x,T)$ depends on the two-phase specific heat at x and $T_{\sigma-}(x)$, errors in its estimation can lead to significant errors in μ_4. Recall that in the two-phase region, we were forced to interpolate between low (< 0.2 K) and high (> 0.55 K) temperatures to fit the specific heats and the slopes of the specific heats as functions of temperature. These temperature limits correspond to ^{3}He concentrations of between 10% and 25% on the phase-separation curve. (At 0.2 K, phase separation takes place at about x = 0.09; at 0.55 K, phase separation takes place at about x = 0.25). Since our fits to the two-phase specific heats are based on sparse experimental data in this region, it is quite possible that they are not accurate enough for the purposes of calculating μ_4. The errors are magnified at high temperatures, since the expression for μ_4 involves a product of $(C_{2\phi})_{T_{\sigma-}}$ and $(1-T/T_{\sigma-})$. Errors in the two-phase fits do not pose as much of a problem when calculating quantities such as the entropy or the enthalpy. Since those depend on the integral of the specific heat, they are less sensitive to errors in the fits. However, errors in the fits could substantially affect the calculated values of the ^{4}He chemical potential. Depending on the specifics of the fit, it was found that in this ^{3}He-concentration range at high temperatures (around 1.5 K), the calculated value of x for a given value of μ_4 and T varied by up to 0.05. The fit finally chosen yields results that seem to be in reasonable agreement with other low-^{3}He concentration data; however, there are errors when the fit is compared with some data at ^{3}He concentrations in the vicinity of 20-30%. (A comparison of osmotic pressures is presented in Chapter 5.)

In addition, the shapes of lines of constant μ_4 (which will be discussed in Chapter 4) in the area of 15%-25% ^{3}He concentration seem rather peculiar, but this was a characteristic of all the fits that were tried. A more rigorous fitting procedure could conceivably resolve the issue. It is also worth noting that any errors in the values of μ_4 in the neighbourhood of x =0.15-0.25 also lead to errors in the values of h^{os}.

The first and second derivatives of entropy were constrained to be continuous at the x = 0.08 boundary; the third derivatives, however, are not continuous, even though in reality, they are expected to be continuous everywhere in the single-phase He-II region. In other words, the second derivatives of the entropy and enthalpy with respect to x have different slopes on either side of the x = 0.08 boundary. Also, since the second derivatives were forced to be equal at the boundary, there may be some error associated with them in the vicinity of x = 0.08. This means that the quantity $(\partial\mu_4 / \partial x)_T$, which is equal to $-x\left(\partial^2 g / \partial x^2\right)_T$, is not differentiable at the boundary. $(\partial\mu_4 / \partial x)_T$ is not likely to be accurate near x = 0.08; the error is expected to be about 10-15%. $(\partial\mu_4 / \partial x)_T$ is plotted as a function of x around x = 0.08 at various temperatures in Figure 2.12.

During the fitting procedure, it was attempted to ensure continuity of the third derivatives by including additional constraints (similar to those used to ensure continuity of the first and second derivatives) in the specific heat fit. This attempt failed miserably; the error associated with the ensuing specific heat fit (i.e., the differences between the experimental specific heat data and the predicted values) was too large for it to be seriously considered. It was unclear why the error would become so large with the addition of the two constraints. One possibility is that the Matlab function *lsqnonlin* did not do a good job of finding an acceptable solution. Another possibility is that this is an offshoot of the splicing procedure that is employed, wherein properties at an x just below 0.08 are calculated based on Kuerten et al's calculated values, and properties at an x just greater than 0.08 are calculated based on values on the dilute-phase curve, which in turn were calculated from a combination of Kuerten et al's values, actual experimental data and pure ^{3}He properties. Kuerten et al's (theoretical) model becomes increasingly inapplicable at higher temperatures and ^{3}He concentrations; however, it is treated as a given, and it is the specific heat fits that are fiddled around with to ensure continuity. This is not a problem with lower derivatives; however, since Kuerten et al's higher derivatives could be off by quite a bit, it is possible that it is infeasible to find a specific heat fit that ensures continuity with these derivatives while still reasonably approximating the given experimental data. In any case, whatever the cause, the end result is that there are kinks in functions that should behave smoothly. However, from a practical point of view, the quantities with the kinks are not particularly important with regard to refrigerator design.

The specific heat fit is not valid at temperatures below 0.15 K. However, below this temperature, single-phase mixtures have ^{3}He concentrations of less than 8%. At these low concentrations and temperatures, the specific heat model used by Kuerten et al can be applied with good accuracy. For thermodynamic properties below 0.15 K, we refer the reader back to Kuerten et al [2]. (Portions of their tabulated values are reproduced in Table 10 in Appendix E.1.) Kuerten et al's tables actually extend to 0.25 K and there is a slight mismatch between their calculated properties and ours. The reason for these differences is that our specific heat model is designed to encompass a very large area of the phase-diagram and is not as accurate as theirs in the narrow region of overlap (between temperatures of 0.15 K and 0.25 K, and ^{3}He mole fractions of less than 7%). The maximum difference between the specific heat values is less than 3%. Because of the specific heat differences, there are minor discrepancies between Kuerten et al's and our tabulated values of entropy, enthalpy, etc. in the region of overlap. However, the differences are small (less than 0.5% for the entropy and ^{4}He chemical potential, less than 3% for the enthalpy). Comparisons of entropies at 0.25 K and enthalpies at 0.25 K are shown in Figure 2.13. Also shown are comparisons of the specific heats at 0.15 K, which were constrained to be equal in the fitting procedure; the differences between Kuerten et al's values and the fitted values are less than 1%.

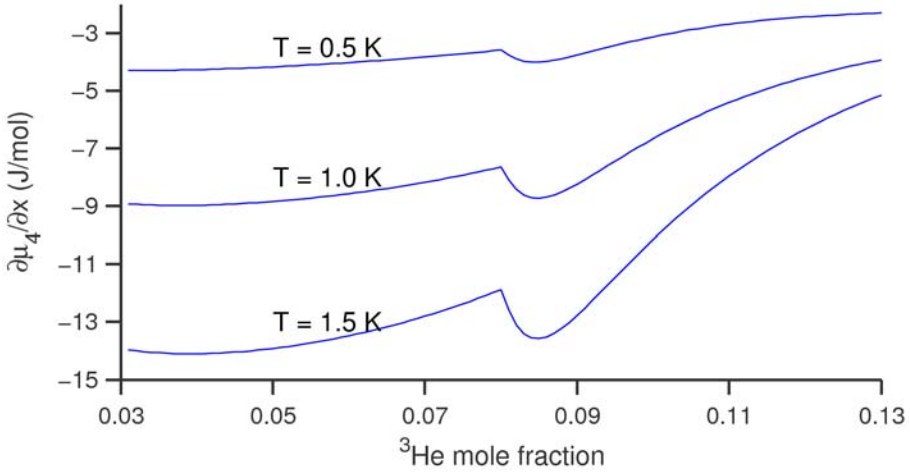

Figure 2.12: $(\partial\mu_4/\partial x)_T$ *as a function of* x *at 0.5 K, 1 K and 1.5 K. The slope is discontinuous at* $x \approx 0.08$.

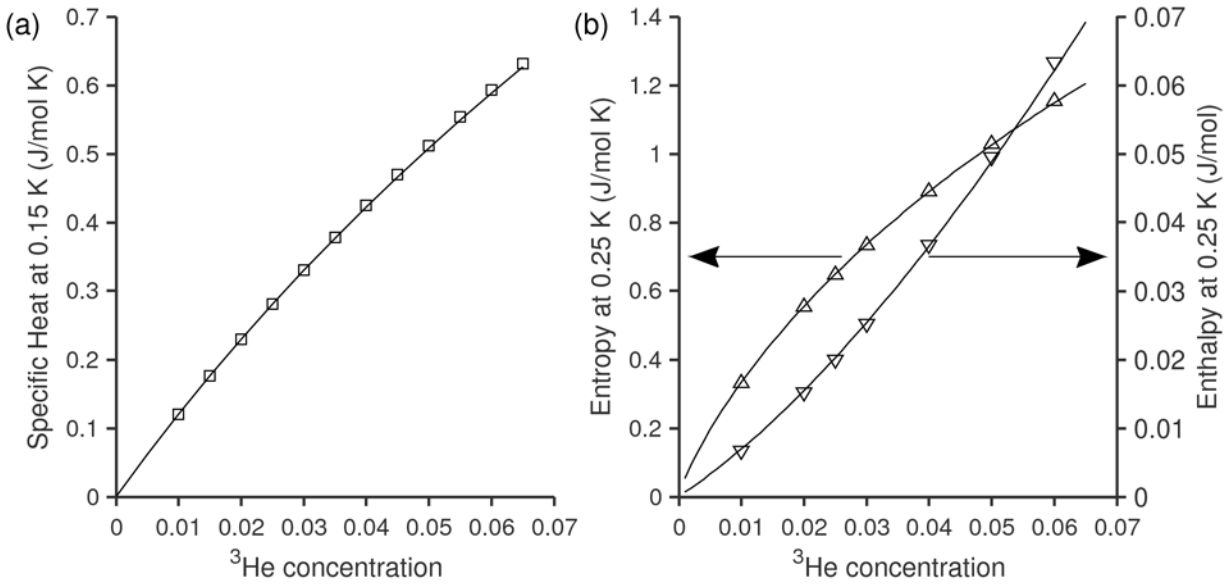

Figure 2.13: *A comparison of (a) single-phase mixture specific heats at 0.15 K, and (b) the entropies and enthalpies at 0.25 K, predicted by Kuerten et al's model (markers) and the fit of Eq. 2.33 (solid lines).*

The entropy, enthalpy, Gibbs free energy, ^{4}He chemical potential and osmotic enthalpy derived from this formulation are tabulated in Table 12 through Table 16, in Appendix E.1. The full equations for these quantities based on the specific heat model are listed in Appendix B.2.

2.6 Thermodynamic properties in the single-phase He-I region

To the best of our knowledge, the only measurements of specific heat in the He-I region were made by Alvesalo et al [14] (53%, 58%, 61%, 65%, 67.2%, 68%, 70% and 73% ^{3}He solutions) and de Bruyn

Ouboter et al [10] (70%, 75%, 80.5%, 84.7%, 89.4% and 95.4% solutions). All of Alvesalo et al's data, and de Bruyn Ouboter et al's data for more than 75%-^{3}He solutions, were used to generate thermodynamic properties for temperatures of up to 1.5 K. de Bruyn Ouboter et al also list specific heat data in the He-I region at lower ^{3}He concentrations. The noise associated with some of the data limits their usefulness.

The approach used to determine properties in the He-I region is similar to that in the He-II region. The entropy and enthalpy are calculated by integrating up from known properties along the phase-separation curves (Figure 2.14). For ^{3}He concentrations of greater than 67.4% (the tricritical point concentration), properties in the He-I region can be obtained by integrating up from the concentrated phase-separation curve (much like properties in the He-II region, which were obtained by integrating up from the dilute phase-separation curve). The entropy, enthalpy and Gibbs free energy are therefore

$$s(x,T) = s_{\sigma+}(x) + \int_{T_{\sigma+}(x)}^{T} \frac{C_{1\phi,I}(x,T)}{T} dT\,, \tag{2.45}$$

$$h(x,T) = h_{\sigma+}(x) + \int_{T_{\sigma+}(x)}^{T} C_{1\phi,I}(x,T) dT\,, \tag{2.46}$$

and

$$g(x,T) = h_{\sigma+}(x) - Ts_{\sigma+}(x) + \int_{T_{\sigma+}(x)}^{T} C_{1\phi,I}(x,T) dT - T\int_{T_{\sigma+}(x)}^{T} \frac{C_{1\phi,I}(x,T)}{T} dT \tag{2.47}$$

where the subscript $\sigma+$ refers to properties on the concentrated phase-separation curve. The values of entropy and enthalpy on the concentrated phase separation curve were calculated from the two-phase model as outlined previously (using Eqs. 2.20 and 2.13).

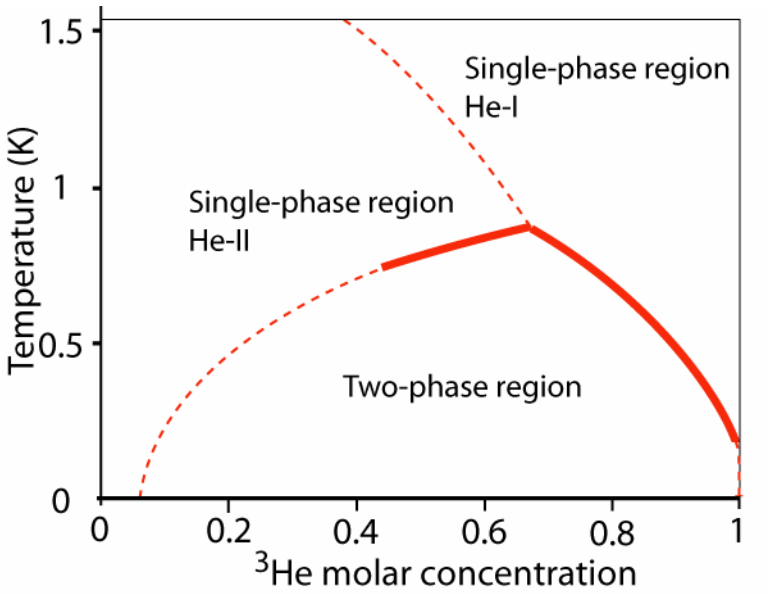

Figure 2.14: *Properties in the single-phase He-I region are determined by integrating up from the darkened line in this phase diagram. Thermodynamic properties are completely known along this line from the two-phase model for the curved portion. Properties in the He-I region are only calculated for ^{3}He concentrations of more than 50%.*

For ^{3}He concentrations below 67.4%, properties in the He-I region are obtained by integrating up from the dilute phase-separation curve, and across the λ-line from the He-II region into the He-I region. The entropy, enthalpy and Gibbs free energy are now calculated from

$$s(x,T) = s_{\sigma-}(x) + \int_{T_{\sigma-}(x)}^{T_\lambda(x)} \frac{C_{1\phi,II}(x,T)}{T} dT + \int_{T_\lambda(x)}^{T} \frac{C_{1\phi,I}(x,T)}{T} dT , \tag{2.48}$$

$$h(x,T) = h_{\sigma-}(x) + \int_{T_{\sigma-}(x)}^{T_\lambda(x)} C_{1\phi,II}(x,T) dT + \int_{T_\lambda(x)}^{T} C_{1\phi,I}(x,T) dT , \tag{2.49}$$

and

$$g(x,T) = h_{\sigma-}(x) - Ts_{\sigma-}(x) + \int_{T_{\sigma-}(x)}^{T_\lambda(x)} C_{1\phi,II}(x,T) dT - T\int_{T_{\sigma-}(x)}^{T_\lambda(x)} \frac{C_{1\phi,II}(x,T)}{T} dT + \int_{T_\lambda(x)}^{T} C_{1\phi,I}(x,T) dT - T\int_{T_\lambda(x)}^{T} \frac{C_{1\phi,I}(x,T)}{T} dT . \tag{2.50}$$

In both cases, the ^{4}He and ^{3}He chemical potentials can be determined from Eqs. 1.13 and 1.12.

Once again, an expression for the specific heat is required. The same form of specific heat (Eq. 2.33) that was used for the He-II region was also used for the He-I region:

$$C_{1\phi,I}(x,T) = xC_3^0(T) + (1-x)C_4^0(T) + x(1-x)C_{r,I}(x,T) . \tag{2.51}$$

Expressions for $C_3^0(T)$ and $C_4^0(T)$ are given in equations 2.36 and 2.39. The correction term $C_{r,I}(x,T)$ has the same form as the original expression for $C_{r,II}(x,T)$:

$$C_{r,I}(x,T) = \sum_{i=0}^{4}\sum_{j=0}^{4} A_{I,1,ij} x^i T^j + \sum_{i=0}^{4}\sum_{j=1}^{2} A_{I,2,ij} x^i T^j \ln(T - T_\lambda(x) + 0.0005) . \tag{2.52}$$

In the He-I region, the logarithmic terms were retained in the specific heat expression (unlike the He-II region), since the polynomial terms could not adequately capture the drop in specific heat near the λ-line, for ^{3}He concentrations of less than x_t. The constant ε in the logarithm is used to ensure a finite value of the specific heat at $T = T_\lambda$. However, the logarithmic term presents a problem for $x > x_t$ – since there is no λ-transition beyond $x = x_t$, it is unclear what $T_\lambda(x)$ should be at ^{3}He concentrations of greater than 67.4%. It was found that using Eq. 2.5 as the expression for $T_\lambda(x)$ worked quite well all the way up to x = 1. This is because the T_λ predicted by Eq. 2.5 at a certain value of x becomes increasingly smaller than the actual phase-separation temperature $T_{\sigma+}$ at that value of x (Figure 2.15). Therefore, as x increases beyond 0.674, the difference between T and (the fictional) T_λ in the single-phase He-I region becomes larger (of the order of 1), and the contribution of the logarithmic terms becomes smaller. For ^{3}He concentrations of less than 0.674, the magnitudes of the logarithmic terms are large near the λ-line (when $T - T_\lambda$ is small, the argument of the logarithm is close to zero and therefore its magnitude is quite large), to capture the steep drop in specific heat at temperatures just greater than T_λ. It is emphasised again that for values of x greater than 0.674, T_λ has no physical meaning, since there is no λ-transition at those concentrations. It is used simply as a modelling aid.

The He-I specific heat was fitted to the smoothed data of Alvesalo et al (^{3}He concentrations of 53%, 58%, 61%, 65%, 67.2%, 68%, 70%, 73%) and de Bruyn Ouboter et al (^{3}He concentrations of 80.5%, 84.7%, 89.4%, 95.4%).

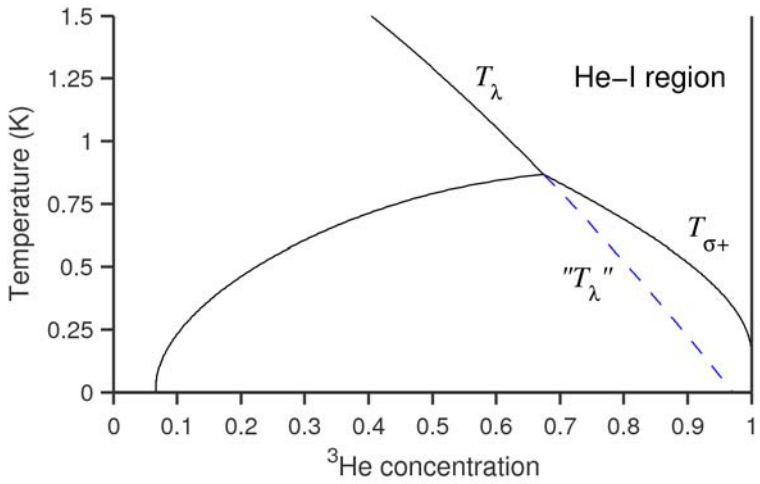

Figure 2.15: *The extension of T_λ to values of x greater than x_t. As x becomes larger, the difference between temperatures in the He-I region and T_λ becomes larger.*

The early measurements of de Bruyn Ouboter et al near the λ-line suggested that the specific heat was discontinuous across the λ-line. However, later measurements by Alvesalo et al and Gasparini and Moldover [36] (especially those by the latter, which were performed to within 0.01 mK of the λ-temperature) indicated that the specific heat is continuous across the λ-line. Therefore, the specific heat fits in the He-II (Eq. 2.33; Table 4) and He-I (Eq. 2.51; Table 5) regions were also constrained to be continuous across the λ-line (over the concentration range 0.5 - 0.674).

Because two different equations are used to determine properties for $x < 0.674$ and $x > 0.674$, constraints were added to ensure that the entropy and enthalpy, and their derivatives were continuous across the boundary. As in the He-II region at $x = 0.08$, the added constraints ensured continuity up to a second derivative.

The data points and the constraints were included in the fitting procedure that was described in the previous section. The coefficients $A_{1,1,ij}$ and $A_{1,2,ij}$ calculated from the fitting program for use in Eq. 2.52 are listed in Table 5 in Appendix A.2.2; ε is chosen to be 0.0005. Even though the available data points are restricted to temperatures between 0.4 K and 1.5 K, the calculated specific heats are valid even at lower temperatures. This is a consequence of the form of the specific heat chosen (Eq. 2.51) – at low temperatures in the He-I region, where x is very close to 1, the $C_3^0(T)$ term (which is known all the way down to 0 K) dominates the correction term. The r.m.s. error associated with the fit is about 2.2%, and the maximum error is about 6%. The fit also reasonably predicts de Bruyn Ouboter et al's 47.8% data, though with slightly higher errors. We use it only for ^{3}He concentrations of more than 50%. The smoothed experimental specific heat data and the predicted specific heats are plotted in Figure 2.16, at various concentrations. The He-II and He-I fits are in agreement along the λ-line; they are shown in Figure 2.17.

Since the third derivatives of entropy and enthalpy are not continuous at $x = 0.674$ (much like the He-II region at $x = 0.08$), $(\partial\mu_4/\partial x)_T$ is not differentiable at the boundary, even though it should be. Therefore, $(\partial\mu_4/\partial x)_T$ is not expected to be accurate in the vicinity of $x = 0.674$. Figure 2.18 shows the quantity $(\partial\mu_4/\partial x)_T$ as a function of x. The error in $(\partial\mu_4/\partial x)_T$ is small at low temperatures (about 1 K) but increases with increasing temperature. The error is expected to be about 15% near $x = 0.674$ at 1.4 K.

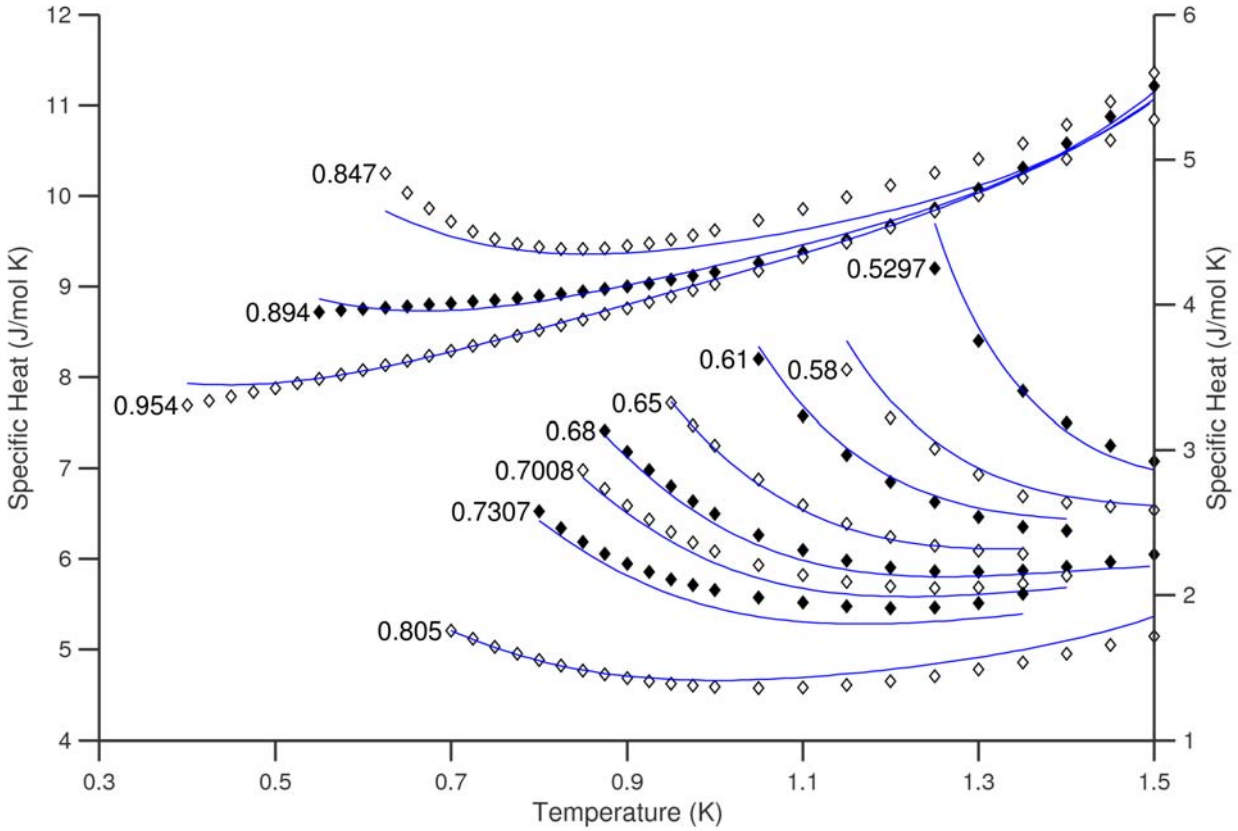

Figure 2.16: *Specific heats in the He-I region as a function of temperature. The markers represent smoothed experimental data of de Bruyn Ouboter et al [10] (x = 0.805, 0.847, 0.894, 0.954) and Alvesalo et al [14] (x = 0.5297, 0.58, 0.61, 0.65, 0.68, 0.701, 0.731). The solid lines represent values calculated from the fit of Eq. 2.51. The x = 0.5297, 0.58, 0.61, 0.65, 0.68, 0.701, 0.731 and 0.805 data are plotted on the left vertical axis. The x = 0.847, 0.894 and 0.954 data are plotted on the right vertical axis.*

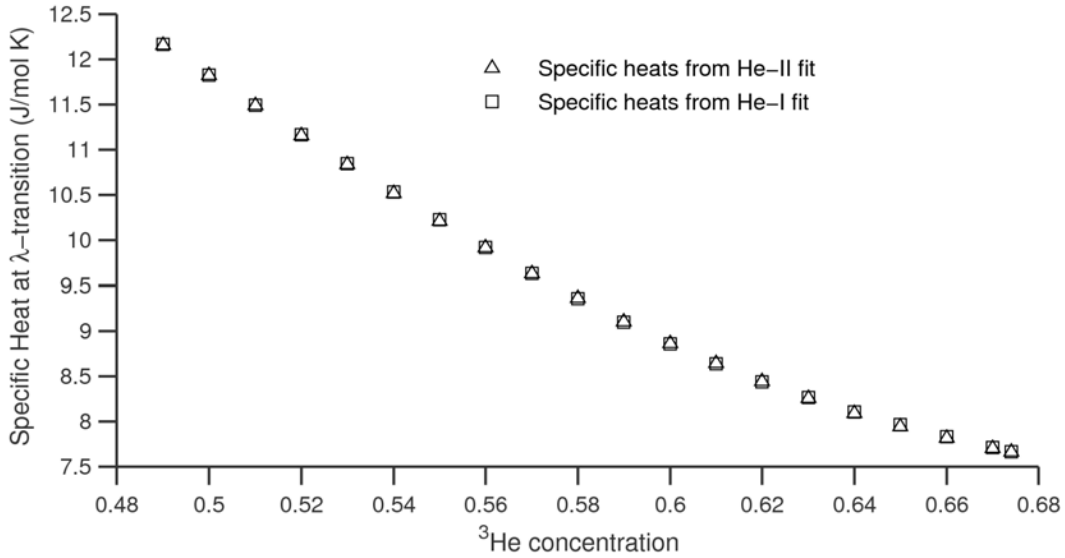

Figure 2.17: *A comparison of specific heats along the λ-line predicted by the He-II and He-I fits (Eqs. 2.33 and 2.51 respectively).*

Properties in the He-I region are tabulated in Table 12 through Table 15, in Appendix E.1, alongside the He-II properties. Complete expressions for the entropy, enthalpy, Gibbs free energy and the ^{4}He chemical potential are listed in Appendix B.3.

We now have thermodynamic properties of ^{3}He-^{4}He mixtures in the two-phase, single-phase He-II, and the single-phase He-I region, at saturated pressure. The range of temperatures and concentrations covered is shown in Figure 2.19. Molar specific volumes are discussed in greater detail in the next chapter, when we discuss the extension of these properties to higher pressures.

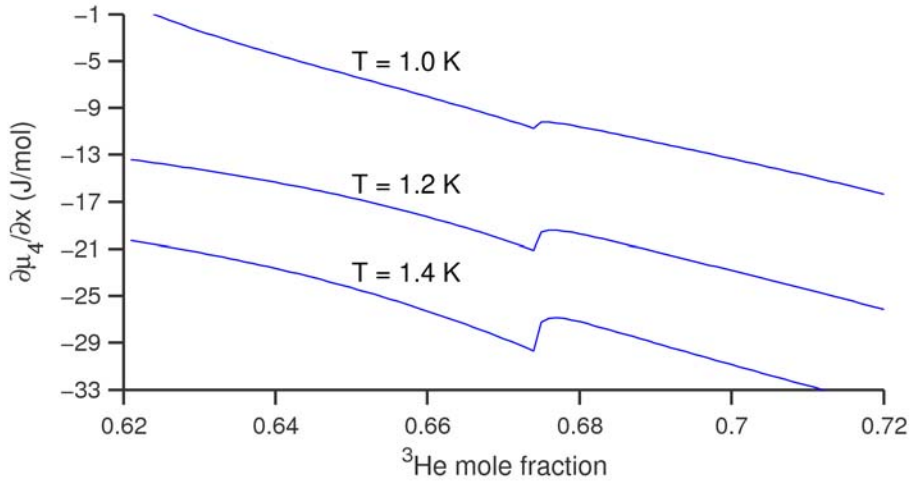

Figure 2.18: $(\partial\mu_4/\partial x)_T$ *as a function of* x*, at 1 K, 1.2 K and 1.4 K. The slope is discontinuous at* x = *0.674.*

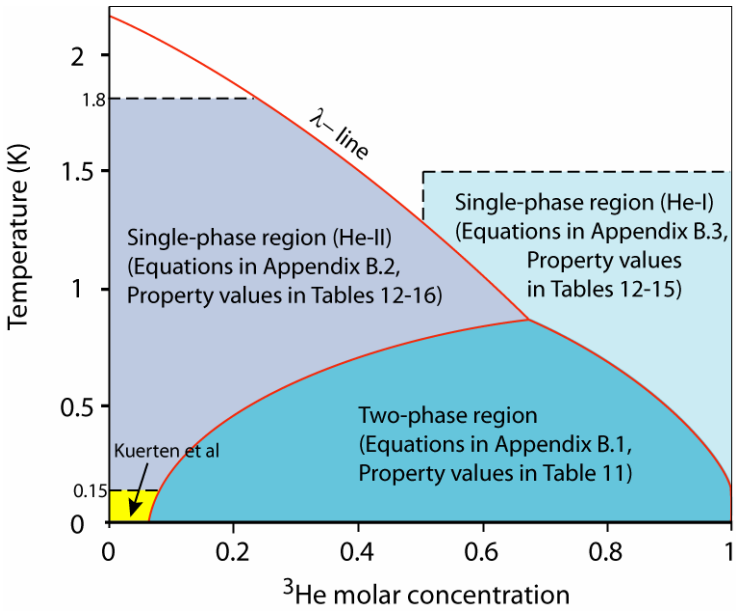

Figure 2.19: *The range of temperatures and* ^{3}*He concentrations over which properties of* ^{3}*He-*^{4}*He mixtures have been calculated in this chapter. Properties in the single-phase He-II region below 0.15 K are calculated by Kuerten et al.*

Chapter 3: Properties of ^{3}He-^{4}He mixtures at high pressures

In the previous chapter, properties were determined as a function of temperature and composition, at a constant value of pressure. The procedure used to determine properties at zero pressure cannot be used to calculate properties at higher pressures because of the lack of specific heat and osmotic pressure data at these pressures. The only specific heat measurements we could find at higher pressures were made by Polturak and Rosenbaum [45], who measured the specific heats of 5% and 3% solutions of ^{3}He in ^{4}He at 10 and 20 atmospheres. However, their measurements were restricted to temperatures below 0.1 K.

Other experimental data is also quite sparse at high pressures. The only osmotic pressure measurements at high pressure that we could find were made by Landau et al [25], at only two pressures – 10 and 20 atmospheres. Their data is also restricted to low temperatures (below 0.2 K) except at ^{3}He fractions of less than 2.5%. Since it covers a rather small region of the phase-space, it is not particularly useful.

Fortunately, however, there do exist more extensive measurements of the molar volume. This is crucial, since variations of the Gibbs free energy with pressure can be calculated from the molar volume:

$$\left(\frac{\partial g}{\partial p}\right)_{T,x} = v\,. \tag{3.1}$$

Since the Gibbs free energy is known at zero pressure, the molar volume allows the calculation of the Gibbs free energy at higher pressures. Since all thermodynamic properties can be obtained from derivatives of the Gibbs free energy, it follows that pressure derivatives of all thermodynamic properties can be obtained from the molar volume and its derivatives. For example, the pressure derivative of entropy can be determined using the Maxwell relation

$$\left(\frac{\partial s}{\partial p}\right)_{T,x} = -\left(\frac{\partial v}{\partial T}\right)_{p,x}. \tag{3.2}$$

Similarly, the pressure derivatives of enthalpy, ^{4}He chemical potential and osmotic enthalpy can be determined using

$$\left(\frac{\partial h}{\partial p}\right)_{T,x} = v + T\left(\frac{\partial s}{\partial p}\right)_{T,x} = v - T\left(\frac{\partial v}{\partial T}\right)_{p,x}, \tag{3.3}$$

$$\left(\frac{\partial \mu_4}{\partial p}\right)_{T,x} = v - x\left(\frac{\partial v}{\partial x}\right)_{T,p}, \tag{3.4}$$

and

$$\left(\frac{\partial h^{os}}{\partial p}\right)_{T,x} = \frac{1}{x}\left(\frac{\partial h}{\partial p}\right)_{T,x} - \frac{1-x}{x}\left(\frac{\partial \mu_4}{\partial p}\right)_{T,x} = v + (1-x)\left(\frac{\partial v}{\partial x}\right)_{T,p} - \frac{T}{x}\left(\frac{\partial v}{\partial T}\right)_{p,x}. \tag{3.5}$$

The pressure derivative of the specific heat is

$$\left(\frac{\partial C}{\partial p}\right)_{T,x} = \frac{\partial}{\partial p}\left(T\frac{\partial s}{\partial T}\right)_{T,x} = T\frac{\partial}{\partial p}\left(\frac{\partial s}{\partial T}\right) = T\frac{\partial}{\partial T}\left(\frac{\partial s}{\partial p}\right) = -T\frac{\partial^2 v}{\partial T^2}. \tag{3.6}$$

Therefore, if the mixture molar volume v is known as a function of temperature, pressure and ^{3}He concentration, the general thermodynamic property m (which may be s, h, g, μ_4, etc.) can be calculated at any pressure using

$$m(p,T,x) = m(0,T,x) + \int_0^p \frac{\partial m}{\partial p} dp \tag{3.7}$$

where $m(0,T,x)$ is the value of the property at T and x on the saturated (zero) pressure surface and is available from the zero-pressure model. The partial derivative (which, from Eqs. 3.1 through 3.6, is clearly only a function of the mixture molar volume and its derivatives, as well as the independent variables x, T and p) is integrated along a line of constant x and constant T. We will return to the specifics of the evaluation of the integral later, in Section 3.3.

In the following section, expressions for the phase-separation surfaces and λ-surface will be determined. These are extensions of the two-dimensional curves determined in Chapter 2. The phase-separation surfaces are necessary since the integral in Eq. 3.7 has different forms in the single- and two-phase regions; this will be clearer later. Following the calculation of the phase-separation surfaces, we will obtain a fit for the molar volume and then use it to calculate properties up to pressures of 10 bar.

3.1 Phase diagram

Expressions for the phase-separation surfaces and the λ-surface at high pressures will now be calculated. In his PhD thesis, Deng [46] calculated expressions for the phase-separation surfaces; however, his expressions are valid only at temperatures above 0.6 K. The expressions derived in this section can be used down to lower temperatures.

The equation of the tricritical line was first determined. Hoffer and Sinha [47] propose the following equation for the tricritical line between the saturated pressure and the freezing pressure:

$$x_t(p) - x_t(0) = 0.3037124\left[T_t(0) - T_t(p)\right] - 4.41225\times10^6\left[T_t(0) - T_t(p)\right]^9 \tag{3.8}$$

where $x_t(0)$ and $T_t(0)$ are the tricritical co-ordinates at zero (saturated) pressure – $x_t(0)$=0.674; $T_t(0)$=0.867 K. (In the previous chapter, they were simply referred to as x_t and T_t.) However, this equation does not specify the pressure dependence of x or T along the tricritical line. In order to find the pressure dependence of T along the tricritical line, the data of del Cueto et al [48] – who measured the pressure dependence of the tricritical point, and the concentrated- and dilute-phase separation lines in the vicinity of the tricritical point at high pressure, up to 22 bar – was used to get:

$$T_t(p) - T_t(0) = -\frac{0.12992576\,p}{p + 2.5967345} - 6.457263\times10^{-4}\,p \tag{3.9}$$

where the pressure p is in units of bar. Equations 3.8 and 3.9 can together be used to determine the equation of the tricritical line. The projection of the calculated tricritical line onto the T - x plane is plotted in Figure 3.1.

To get an expression for the dilute-phase surface at high pressures, we used the same form of the equation as was used for the dilute-phase line (Eq. 2.2) at saturated pressure:

$$x_{\sigma-}(T,p) - x_t(p) = \frac{K_{\sigma-,0}(p)\ \left(T - T_t(p)\right)}{\left(T - T_t(p)\right) - K_{\sigma-,a}(p)} + K_{\sigma-,1}(p)\left(T - T_t(p)\right) + K_{\sigma-,2}(p)\left(T - T_t(p)\right)^2 \tag{3.10}$$

where $K_{\sigma-,0}(p)$, $K_{\sigma-,1}(p)$, $K_{\sigma-,2}(p)$ and $K_{\sigma-,a}(p)$ are now functions of pressure rather than constants. These were set as quadratic functions of pressure, with the constraint that they reduce to the constants of Eq. 2.2 when p = 0:

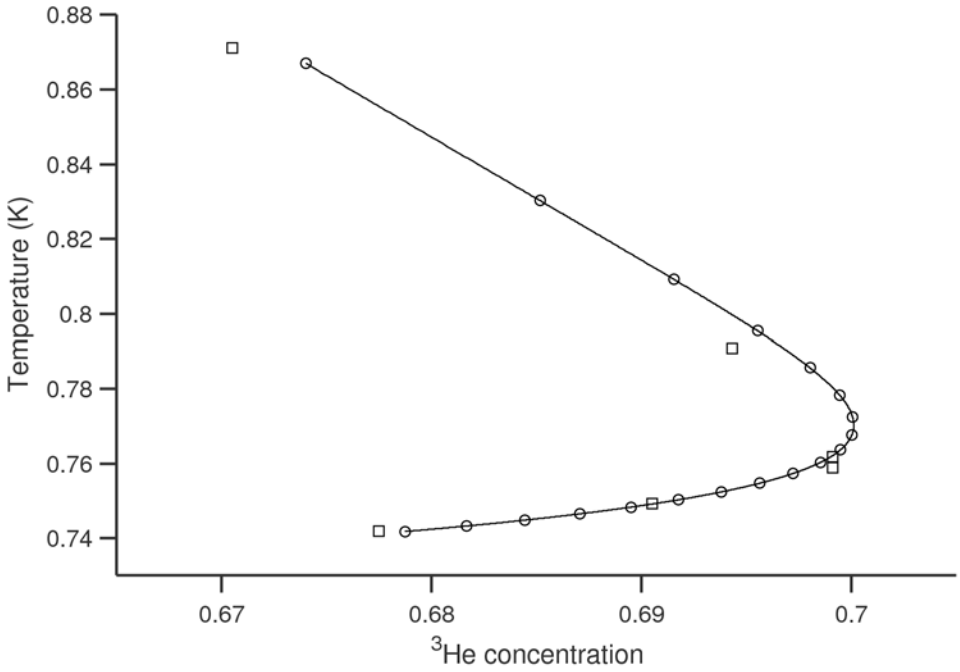

Figure 3.1: *Projection of the tricritical line onto the T - x plane. The square markers represent values from del Cueto et al [48], at pressures of 0 (sat. vap. pressure), 3.445, 8.207, 10.031, 13.172, and 17.935 bar (from top to bottom). The solid line represents values calculated from Eqs. 3.8 and 3.9. The circular markers, also calculated from Eqs. 3.8 and 3.9 are spaced at intervals of 1 bar, starting from 0 bar (sat. vap. pr.) to 18 bar.*

$$K_{\sigma-,i}(p) = K_{\sigma-,i0} + K_{\sigma-,i1}p + K_{\sigma-,i2}p^2 \quad (i = 0, 1, 2, a)\,. \tag{3.11}$$

To determine the remaining constants in Eq. 3.11, Eq. 3.10 was fitted to available high-pressure data. Yorozu et al [30] measured the dilute-phase separation curve at low temperatures (below 250 mK) at pressures of 0, 5, 10, 15 and 20 bar. Their 5 and 10 bar data was used in our fit. (Their 0 bar data had been used in determining the dilute-phase curve at saturated pressure.) In addition, Hatakeyama et al [49] suggest a functional dependence of $x_{\sigma-}$ on T and p, at low temperature. They work off the observation that at low temperatures, $x_{\sigma-}$ is proportional to T^2, and propose

$$x_{\sigma-}(T, p) = \frac{x_{s,w}(T = 0.05\,\mathrm{K}, p)}{1 + \beta(p)(0.05)^2}\left(1 + \beta(p)T^2\right) \tag{3.12}$$

where $x_{s,w}(T = 0.05\,\mathrm{K}, p)$ is the ^{3}He concentration along the dilute-phase line at 0.05 K, as a function of pressure, and $\beta(p)$ is a polynomial function of pressure that is used as a scaling function at low temperatures. The function $x_{s,w}(T = 0.05\,\mathrm{K}, p)$ is a polynomial fit to the data of Watson et al [50]. Values calculated from this function up to temperatures of about 250 mK were used in the fit.

In addition, it can also be shown (see Appendix D.2) that the dilute-phase surface must satisfy the equation

$$\frac{\partial x_{\sigma-}}{\partial p} = \frac{\left(\partial v/\partial x\right)_{2\phi, x=x_{\sigma-}} - \left(\partial v/\partial x\right)_{1\phi, x=x_{\sigma-}}}{\left(\partial^2 g/\partial x^2\right)_{x=x_{\sigma-}}} \tag{3.13}$$

where $\partial x_{\sigma-}/\partial p$ is the slope of the dilute-phase surface at constant temperature, $\left(\partial v/\partial x\right)_{1\phi,x=x_{\sigma-}}$ is the x-derivative of the molar volume at constant T and p in the single-phase region at $x = x_{\sigma-}$, and $\left(\partial^2 g/\partial x^2\right)_{x=x_{\sigma-}}$ is the second derivative of the Gibbs free energy at constant T and p in the single-phase region at $x = x_{\sigma-}$. The x-derivative of the molar volume at constant T and p in the two-phase region at $x = x_{\sigma-}$, $\left(\partial v/\partial x\right)_{2\phi,x=x_{\sigma-}}$, is equal to

$$\left(\frac{\partial v}{\partial x}\right)_{2\phi,x=x_{\sigma-}} = \frac{v(x_{\sigma+}) - v(x_{\sigma-})}{x_{\sigma+} - x_{\sigma-}}, \tag{3.14}$$

where $v(x_{\sigma+})$ and $v(x_{\sigma-})$ are the molar volumes at $x = x_{\sigma+}$ (the concentrated-phase concentration at T and p) and $x = x_{\sigma-}$ (the dilute-phase concentration at T and p).

The values of $\left(\partial^2 g/\partial x^2\right)_{x=x_{\sigma-}}$ at zero pressure are known from the saturated-pressure equation of state. The values of $v(x_{\sigma+})$, $v(x_{\sigma-})$ and $\left(\partial v/\partial x\right)_{1\phi,x=x_{\sigma-}}$ at zero pressure were calculated from data from various sources. Kierstead's molar volume data [22] was used to calculate these quantities at temperatures greater than 0.55 K. Hatakeyama et al's molar volume fit [49] was used to calculate $v(x_{\sigma-})$ and $\left(\partial v/\partial x\right)_{1\phi,x=x_{\sigma-}}$ at temperatures less than 0.6 K. Radebaugh's expression for the molar volume of a mixture [1],

$$v(\mathrm{cm}^3/\mathrm{mol}) = 27.58 + 7.6x + 1.65x^3, \tag{3.15}$$

was used to calculate $v(x_{\sigma+})$ at temperatures below 0.55 K, even though it is claimed to be applicable only for ^{3}He concentrations of less than 30%. (It was used since it matches Kierstead's high-x data quite well in the 0.6 K-1 K range, and there is no experimental data for high-x mixtures below 0.55 K.) Therefore, $\partial x_{\sigma-}/\partial p$ was known at zero pressure at temperatures up to the tricritical temperature. These values were included in the fitting function.

Zinov'eva [51] made measurements of the phase-separation surface of ^{3}He-^{4}He mixtures across a wide range of concentrations from saturated vapour pressure up to 24 bar. Her data is not in very good agreement with other measurements made at saturated vapour pressure (as is evident in Figure 3.2), but is the only data available at high pressures in the region of x = 0.5 – 0.7. The data was used only for pressures above 5 bar.

The constants $K_{\sigma-,i1}$ and $K_{\sigma-,i2}$ determined from a fit to the above data are listed in Table 1 in Appendix A.1.2. ($K_{\sigma-,i0}$ is already known from the zero-pressure fit of the last chapter.) The fit is valid for pressures of up to 10 bar.

A similar procedure was employed to determine an expression for the concentrated-phase surface at high pressures. The constants in Eq. 2.4 were replaced by functions of pressure:

$$x_{\sigma+}(T,p) - x_t(p) = K_{\sigma+,1}(p)\left(T - T_t(p)\right) + K_{\sigma+,2}(p)\left(T - T_t(p)\right)^2 + K_{\sigma+,3}(p)\left(T - T_t(p)\right)^3 \tag{3.16}$$

where $K_{\sigma+,1}(p)$, $K_{\sigma+,2}(p)$ and $K_{\sigma+,3}(p)$ are quadratic functions of pressure that reduce to the constants of Eq. 2.4 at zero pressure:

$$K_{\sigma+,i}(p) = K_{\sigma+,i0} + K_{\sigma+,i1}p + K_{\sigma+,i2}p^2 \quad (i = 1, 2, 3). \tag{3.17}$$

To calculate the undetermined constants in Eq. 3.17 , Eq. 3.16 was fitted to the data of Lahuerte [32], who measured the phase-separation temperature of high-^{3}He-concentration mixtures at high pressures, and the data of Zinov'eva. In addition, analogous to Eq. 3.13, the slope of the concentrated-phase curve must satisfy

$$\frac{\partial x_{\sigma+}}{\partial p} = \frac{\left(\partial v / \partial x\right)_{2\phi, x=x_{\sigma+}} - \left(\partial v / \partial x\right)_{1\phi, x=x_{\sigma+}}}{\left(\partial^2 g / \partial x^2\right)_{x=x_{\sigma+}}}. \tag{3.18}$$

In the above equation, $\left(\partial v / \partial x\right)_{2\phi, x=x_{\sigma+}}$ is identical to $\left(\partial v / \partial x\right)_{2\phi, x=x_{\sigma-}}$, which was calculated earlier. The concentration susceptibility ($\partial^2 g / \partial x^2$) at zero pressure was known from the saturated-pressure model developed in the previous chapter. $\left(\partial v / \partial x\right)_{1\phi, x=x_{\sigma+}}$ was calculated from the saturated-pressure molar volumes of Kierstead [22] at temperatures above 0.55 K, and from Radebaugh's formula (Eq. 3.15) at temperatures below 0.55 K. Thus, $\partial x_{\sigma+} / \partial p$ was known at p = 0, and was included in the fitting function.

The coefficients $K_{\sigma+,i1}(p)$ and $K_{\sigma+,i2}(p)$ determined from the fit are listed in Table 1 in Appendix A.1.2. The fit is valid for pressures of up to 10 bar. Due to there being no data at low temperatures (the lowest-temperature data point is from Lahuerte [32]: 0.246 K), the fit is possibly unphysical below 0.2 K.

The dilute- and concentrated-phase curves at 0, 5 and 10 bar, determined from the fits of Eqs. 3.10 and 3.16 are shown in Figure 3.2. The deviation of the values calculated from the fit from the underlying experimental data is shown in Figure 3.3.

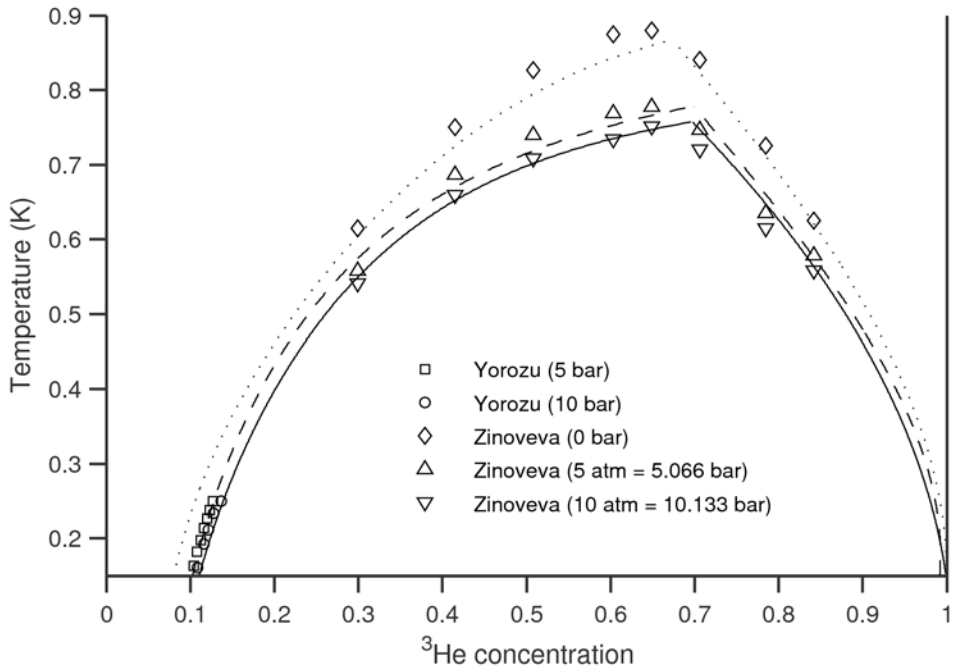

Figure 3.2: *The phase-separation curves calculated from the fits of Eqs. 3.10 and 3.16, at 5 bar (dashed line), and 10 bar (solid line). The markers represent the high-pressure data of Yorozu et al [30], and Zinov'eva [51]. Lahuerte's data [32], which was given greater weight than Zinov'eva's in the fitting function for the concentrated-phase surface, is not shown due it being irregularly spaced. Also shown is Zinov'eva's zero-pressure data, which is not in very good agreement with the zero-pressure phase-separation curves (dotted lines) calculated previously in Chapter 2 (Eqs. 2.2 and 2.4).*

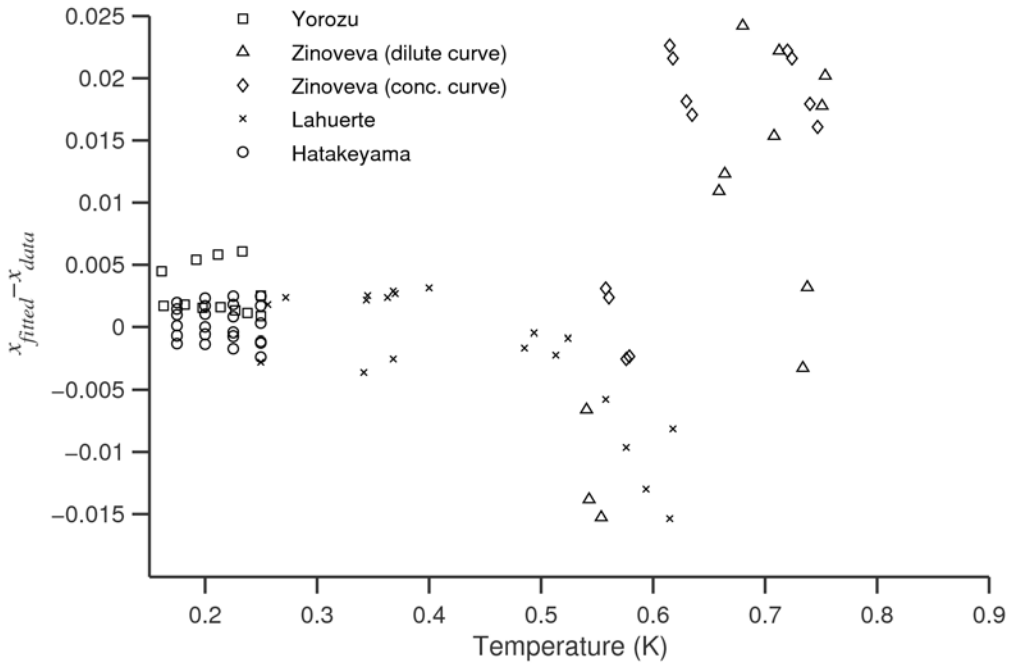

Figure 3.3: *The deviation of the values calculated from the phase-separation surface expressions of Eqs. 3.10 and 3.16 from the actual data,* $x_{fitted} - x_{data}$*, plotted as a function of temperature. Deviations from the data of Yorozu et al [30], Zinov'eva [51] and Lahuerte [32], and from the values calculated from the formula of Hatakeyama et al [49], are shown.*

The λ-surface was determined in similar fashion. The equation for the λ-surface was written as

$$T_\lambda(x,p) - T_t(p) = K_{\lambda 1}(p)\big(x - x_t(p)\big) + K_{\lambda 2}(p)\big(x - x_t(p)\big)^2 . \tag{3.19}$$

$K_{\lambda 1}(p)$ and $K_{\lambda 2}(p)$ are quadratic functions of pressure that reduce to the coefficients in Eq. 2.5 at p = 0:

$$K_{\lambda i}(p) = K_{\lambda i0} + K_{\lambda i1} p + K_{\lambda i2} p^2 \quad (i = 1, 2) . \tag{3.20}$$

Beal et al [52] measured the λ-transition temperature as a function of pressure (up to about 25 atm) for 5 different ^{3}He concentrations between 9% and 40%. Vignos and Fairbank [53] measured the λ-transition temperature as a function of pressure for 5%- and 25%-^{3}He mixtures. Le Pair et al [54] also made measurements of the λ-temperature for 8.9%, 22.8%, 50.5% and 64.5% ^{3}He mixtures. Equation 3.19 was fitted to data from these three sources.

The coefficients $K_{\lambda 1}$ and $K_{\lambda 2}$ are listed in Table 1 in Appendix A.1.2. The λ-curve at 0, 5 and 10 bar, as determined from the fit of Eq. 3.19 (valid for pressures up to 10 bar) is shown in Figure 3.4.

3.2 Calculation of the mixture molar volume

The next step is the determination of an appropriate form for the molar volume as a function of x, T and p. Although sources of high-pressure molar volume data are more abundant than other high-pressure mixture data, they are, in the overall scheme of things, quite limited. Boghosian and Meyer [55] measured

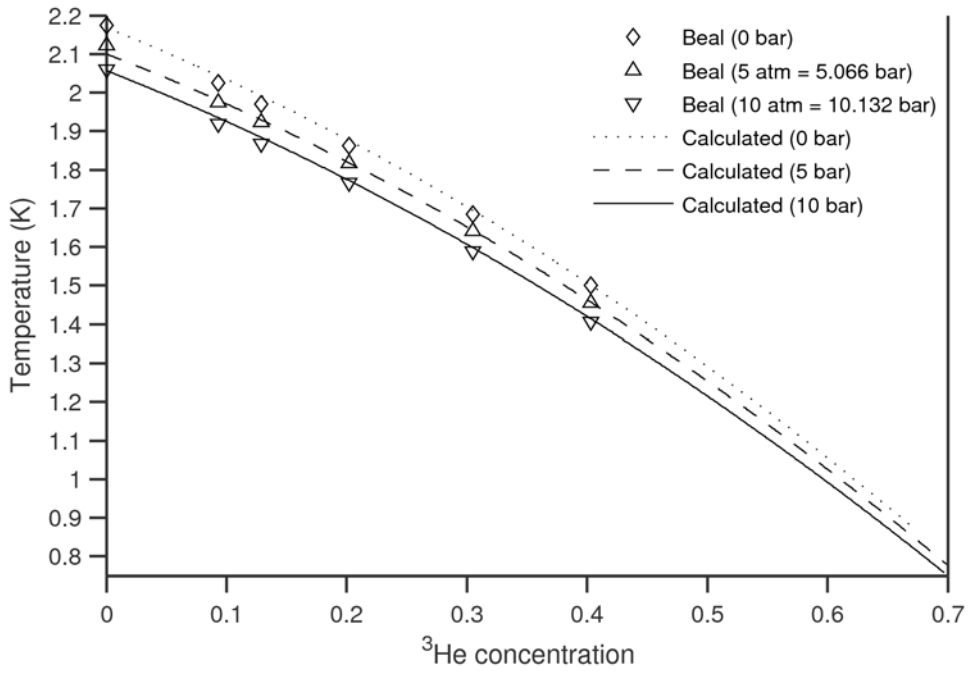

Figure 3.4: *λ-lines calculated from the fit of Eq. 3.19, at 0 bar, 5 bar and 10 bar. The markers represent the data of Beal et al [52].*

the molar volume of a 6% liquid solution of ^{3}He in ^{4}He, between temperatures of 1.25 – 2.2 K, and at pressures of up to 20 atmospheres. They tabulate their data only for mixtures at 1.25 K. Watson et al [50] measured molar volumes of pure ^{4}He and dilute ^{3}He-^{4}He mixtures (6.4%-10% ^{3}He concentration) at temperatures between 0.2 K and 0.5 K, up to pressures of 22 atmospheres. Hatakeyama et al [49] measured the molar volumes of ^{3}He-^{4}He mixtures in the single-phase He-II region at temperatures between 0.4 mK and 0.66 K, 7%-39% ^{3}He concentration, and pressures between 0.3 and 10 kgf/cm^2 (0.29 – 9.8 bar) and present an empirical fit to their data; they do not present their actual data.

There is hardly any mixture data at temperatures above about 0.7 K, and in the He-I region. The only available data in these regions is at saturated pressure. Kierstead [22] made measurements of the saturated-pressure molar volume over the entire concentration range for temperatures of more than 0.55 K. There are other sets of ^{3}He-^{4}He mixture molar volume data at saturated pressure, most notably by Kerr [56]; however, since they are not nearly as extensive as Kierstead's and are in good agreement with his values where they do overlap, we do not use them. There is no available mixture molar volume data at high pressure (above 0.7 K and in the He-I region). However, the high-temperature, high-pressure molar volumes of pure ^{3}He and pure ^{4}He are used to get a handle on properties in these regions. The range of the available molar volume data that is ultimately used in determining a molar volume function is shown in Figure 3.5. (Kierstead's saturated-pressure measurements are treated as zero-pressure measurements, just like the saturated-pressure specific heat measurements in the previous chapter. An estimate of the error associated with this approximation is provided in Appendix D.4.)

The molar volume formula determined in this section is used up to temperatures of 1.5 K. (This is because the property tables developed in this work are intended to be used as a design aid for sub-Kelvin refrigerators using a 1.2 K pumped ^{4}He pot as a high-temperature reservoir.) Since data above 0.7 K is quite scarce, some calculated high-pressure properties at high temperature must be used with caution. This will be discussed in detail in Section 5.2.

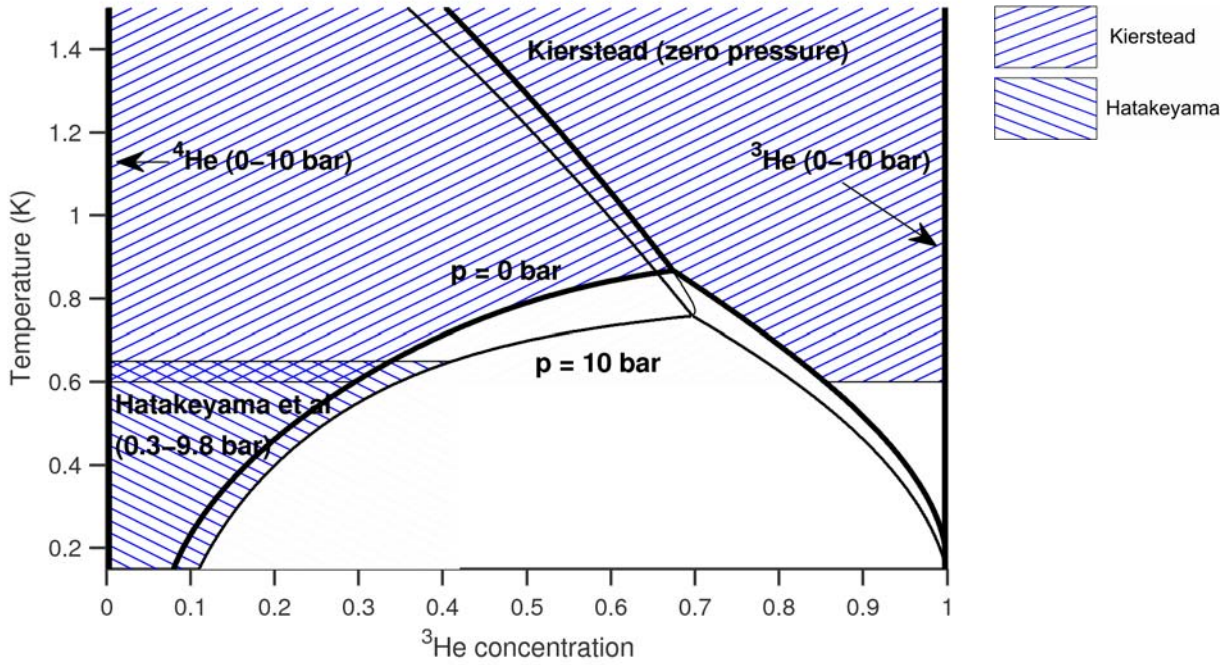

Figure 3.5: *Range of available molar volume data for ^{3}He-^{4}He mixtures. The data of Hatakeyama et al [49] extends from 0.3-9.8 bar. The data of Kierstead [22] is at zero pressure. Pure ^{3}He and ^{4}He data is available over the entire pressure and temperature range of interest in this work. Also shown are the phase diagram at 0 bar and 10 bar.*

In order to exploit the known molar volumes of pure ^{3}He and pure ^{4}He, the molar volume v of a ^{3}He-^{4}He mixture is written as

$$v(p,T,x) = xv_3^0(p,T) + (1-x)v_4^0(p,T) + x(1-x)v_r(p,T,x), \tag{3.21}$$

where v_3^0 and v_4^0 are the molar volumes of pure ^{3}He and pure ^{4}He respectively and the v_r term represents the deviation from the volume of an "ideal" mixture. With the $x(1-x)$ pre-factor multiplying the v_r term, the molar volume reduces to v_3^0 at $x = 1$ and v_4^0 at $x = 0$.

The molar volume of pure ^{4}He as a function of pressure and temperature is available from a number of sources. Tanaka et al [57] present an empirical formula for the molar volume of pure ^{4}He which is applicable for temperatures from 0.05 K to 1 K and for pressures from 0 to 15.7 bar. Brooks and Donnelly [58] tabulate thermodynamic properties of superfluid ^{4}He including the molar volume v_4^0, the isothermal compressibility $-(1/v_4^0)\left(\partial v_4^0/\partial p\right)_T$, and the thermal expansion coefficient $(1/v_4^0)\left(\partial v_4^0/\partial T\right)_p$. The ^{4}He property program HEPAK [15] can be used to calculate the molar volume, isothermal compressibility and expansion coefficient at temperatures above 0.8 K.

Tanaka et al's expression [57] for v_4^0 is

$$v_4^0(T,p) = \left(\sum_{i=0\text{ to }9} V_{40,i}\,p^i\right)\left[1 + \left(\frac{A_1}{(p-p_c)^2} + \frac{A_2}{(p-p_c)^{5/3}}\right)\frac{T^4}{4} - (B_0 + B_1 p)\,\mathrm{Erfc}\sqrt{\frac{\sum_{i=0\text{ to }2}\Delta_i p^i}{T}}\right] \tag{3.22}$$

They suggest that their formula is valid only up to temperatures of 1 K; however, it matches values (molar volumes, isothermal compressibilities and expansion coefficients) from other sources [58, 15] quite well all the way up to 1.8 K. (The maximum error associated with Tanaka et al's expression is about 0.1% for values between 1 K and 1.8 K.) Therefore, their formula for v_4^0 is used in Eq. 3.21 for the entire range of temperatures in this work. The constants for use in the above equation are reproduced in Table 6 in Appendix A.3.

The molar volume, isothermal compressibility and expansion coefficient of pure ^{3}He as a function of pressure and temperature is also available from a number of sources [16,59,60]. This data was fitted to the empirical formula

$$v_3^0(T, p) = \sum_{\substack{i=0 \text{ to } 3 \\ j=0 \text{ to } 2}} V_{31,ij} T^i p^j + \frac{1}{V_{32,2} p^2 + V_{32,0}} . \qquad (3.23)$$

The coefficients are listed in Table 7 in Appendix A.3. The r.m.s. error associated with the molar volumes is about 0.1%.

We now require an expression for v_r, based on ^{3}He-^{4}He mixture data. Before calculating this fit, it is important to note that since properties at high pressure, as determined in this work, are based on derivatives of the molar volume (see Eqs. 3.1 through 3.6), it is important that the fit for v_r be good enough to calculate accurate first and second derivatives of the molar volume with respect to T and x.

In theory, separate fits are required for v_r in the He-I and He-II regions. This is because the second derivatives of v are discontinuous across the λ-surface. (The first derivatives are continuous but not differentiable.) However, it is worth determining two separate fits only if the resulting fits can be expected to be reasonably accurate. Given the mixture data that are available, this is extremely unlikely. To our knowledge, the only mixture data crossing the λ-line are Kierstead's experimental data [22] at saturated pressure – specifically, polynomial fits to the experimentally measured Clausius-Mossotti parameter as a function of temperature at three different values of x: 0.4004, 0.532 and 0.602. (The Clausius-Mossotti parameter is very nearly inversely proportional to the molar volume; the exact relationship is detailed in Ref. 22.) Kierstead also presents a fitting function for $v(x,T)$ from x = 0 to x = 1, and 0.55 K to 1.95 K, but one that is clearly only appropriate to determine the molar volume, and not its derivatives near the λ-line. The fitting function is a polynomial function of x and T and yields continuous values of $\partial^2 v / \partial T^2$ across the λ-line. These values do not match the corresponding experimental values for 40%-, 53%- and 60%-^{3}He mixtures, as seen in Figure 3.6. Values of $\partial v / \partial T$ calculated from the fitting function do not match the experimental values near the λ-line either (although the correspondence is quite good away from the λ-line). In light of this, the only reasonably reliable values of $\partial v / \partial T$ and $\partial^2 v / \partial T^2$ near the λ-surface that are available are for 40%-, 53%- and 60%-^{3}He mixtures at saturated pressure.

The situation is worse with regard to $\partial v / \partial x$ and $\partial^2 v / \partial x^2$. Kierstead's actual experimental data cannot be used to calculate these derivatives, and it is unclear how good the values calculated from his fitting function are. Like the temperature derivatives, they are not expected to be accurate.

In summary, there isn't enough data to get accurate derivatives near the λ-surface. In view of this, we calculate a single fit for v_r across the entire p-T-x space, while recognising that properties calculated from this fit are not expected to be accurate in the vicinity of the λ-surface.

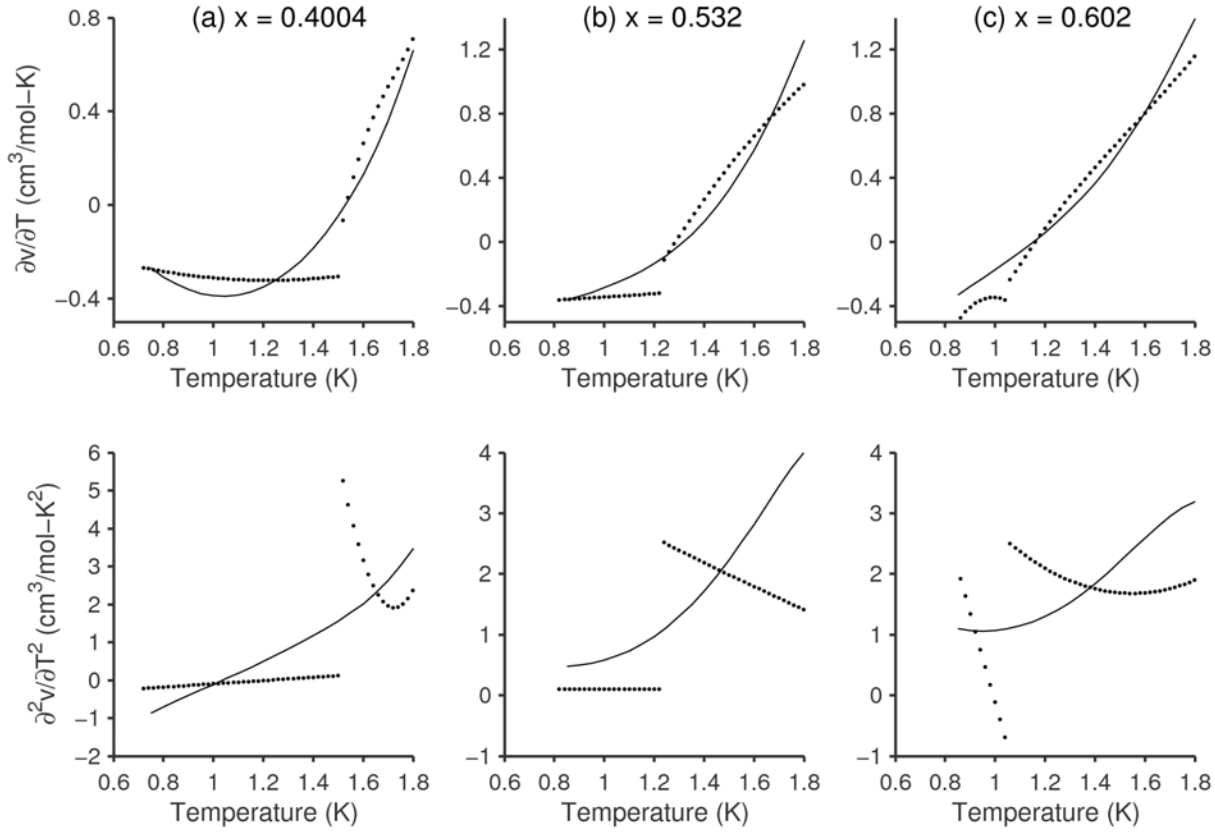

Figure 3.6: *The temperature derivatives $\partial v / \partial T$ and $\partial^2 v / \partial T^2$, as calculated from (i) Kierstead's [22] general fitting function for molar volume (solid lines), and from (ii) Kierstead's [22] polynomial fits to experimentally measured values of the Clausius-Mossotti parameter (dotted lines). The λ-transition can be clearly seen from the experimental data (where the second derivatives are discontinuous). The first derivatives, $\partial v / \partial T$, are reasonably consistent everywhere except near the λ-transition. The second derivatives, $\partial^2 v / \partial T^2$, are not consistent.*

We now turn our attention to the first and second derivatives elsewhere in the p-T-x space, i.e., away from the λ-surface. The values of $\partial v / \partial T$ calculated from Kierstead's fit are in good agreement with his experimental data (at 7 different mixture concentrations, including the 40%-, 53%- and 60%-^{3}He data mentioned earlier), as seen in Figure 3.6 and Figure 3.7. Therefore, it is reasonable to assume that the fit reasonably predicts $\partial v / \partial T$ everywhere (except, of course, near the λ-surface). Values of $\partial^2 v / \partial T^2$ calculated from the fit, however, are quite flaky (see Figure 3.6 and Figure 3.7). They match the experimental data quite well for some mixtures, but not for others. There is no experimental data with which to compare values of $\partial v / \partial x$ and $\partial^2 v / \partial x^2$ calculated from the fit, but, just like the temperature derivative, the first derivative is expected to be more accurate than the second.

The most extensive high-pressure molar volume data is available from Hatakeyama et al [49] (at temperatures below 0.7 K). In their paper, they present an empirical formula for the molar volume of ^{3}He-^{4}He mixtures as a function of x, T and p, for temperatures of less than 0.7 K. As with Kierstead, the first derivatives, $\partial v / \partial T$ and $\partial v / \partial x$, may be expected to be reasonably accurate but there are question marks over the precision of the calculated $\partial^2 v / \partial T^2$ and $\partial^2 v / \partial x^2$ values.

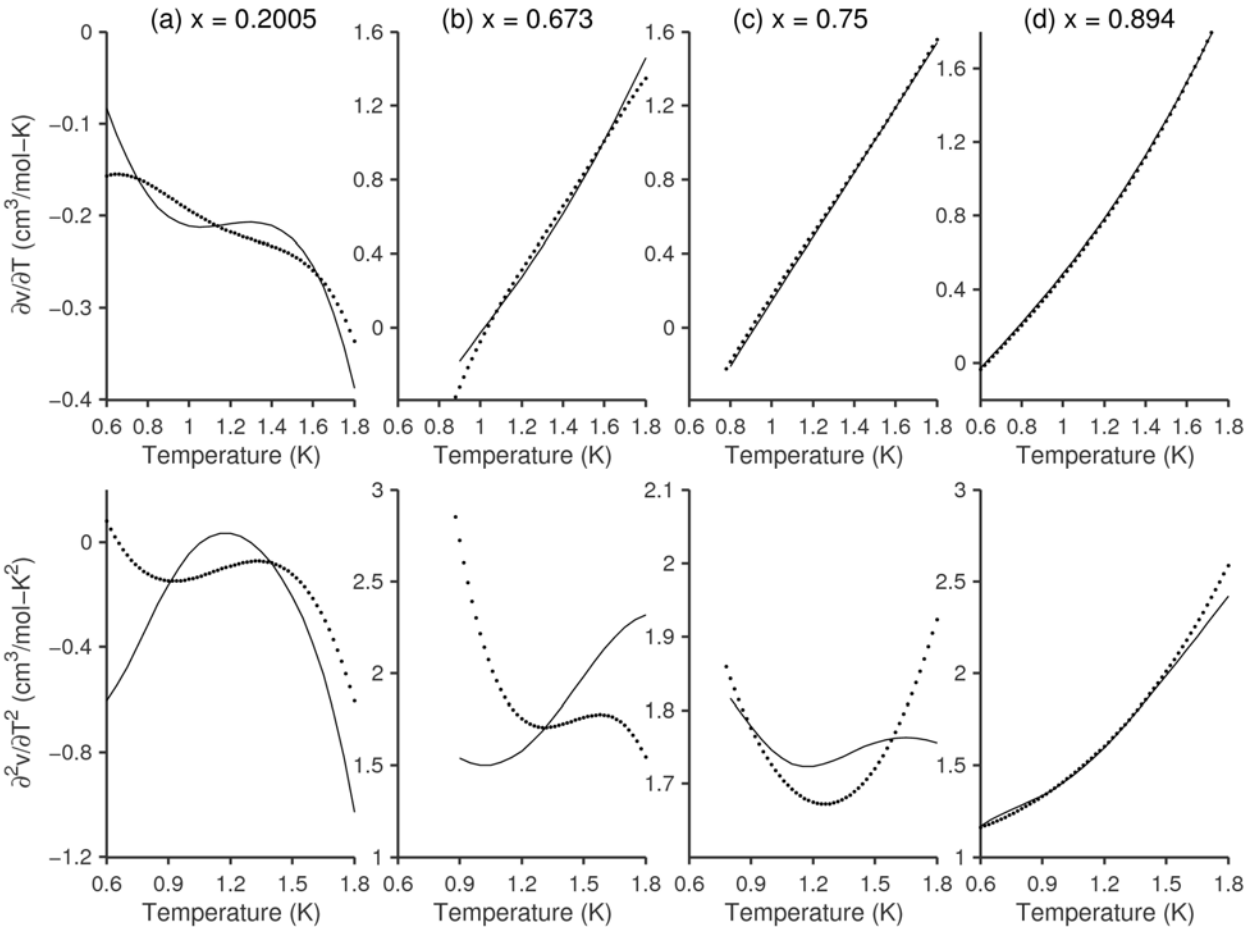

Figure 3.7: *The temperature derivatives $\partial v / \partial T$ and $\partial^2 v / \partial T^2$ for mixtures not undergoing a λ-transition at the temperatures shown, as calculated from (i) Kierstead's [22] general fitting function for molar volume (solid lines), and from (ii) Kierstead's [22] polynomial fits to experimentally measured values of the Clausius-Mossotti parameter (dotted lines). The first derivatives, $\partial v / \partial T$, are quite consistent. The second derivatives, $\partial^2 v / \partial T^2$, are not always consistent.*

Since there are substantial uncertainties associated with the second derivatives everywhere, our fit for v_r is based on available measurements of the molar volume v, and derivatives of the molar volume ($\partial v / \partial x$ and $\partial v / \partial T$) calculated from those measurements. The offshoot is that quantities based on a second derivative (the specific heat, and the concentration susceptibility, for example) may or may not be accurate.

However, the saving grace is that the quantity $\partial^2 v / \partial T^2$ is typically quite small, except near the λ-surface. The magnitude of $\partial^2 v / \partial T^2$, as calculated from Hatakeyama et al's formula (valid below 0.7 K in the He-II region), is about 10^{-7} m^3/mol-K^2. From Kierstead's experimental data for temperatures between 1 K and 1.5 K, the magnitude of $\partial^2 v / \partial T^2$ is similarly low for small x, and increases to about 10^{-6} m^3/mol-K^2 in the He-I region. The magnitude of $\partial C_p / \partial p$ is equal to that of $T(\partial^2 v / \partial T^2)$ (from Eq. 3.6), which translates to about 0.1 (J/mol-K)/bar. This indicates that the constant-pressure specific heat does not change very much with pressure, especially in the He-II region at temperatures below about 1.2 K (except in the vicinity of the λ-surface).

The data sources used to determine the fit for v_r include the data of Hatakeyama et al [49] and Kierstead [22]. The space spanned by the data of Watson et al [50] is a subset of that spanned by Hatakeyama et al's empirical formula. Since the two sources are consistent with each other, we use only Hatakeyama et al's formula. Since Hatakeyama et al's data [49] are restricted to low temperatures, and Kierstead's to saturated vapour pressure, there is no data at high pressures and high temperatures, except for a handful of measurements by Boghosian and Meyer [55] at 1.25 K and x = 0.06. This data was not used to calculate the fit; it will be compared against the results later (see Section 5.2).

One characteristic of all the high-pressure experimental data is that it is all in the single-phase He-II region. There is no data available in the single-phase He-I region except for Kierstead's data at saturated pressure. However, given the functional form of the molar volume along the dilute-phase surface, it is possible to estimate the molar volume of the corresponding concentrated phase using the previously derived relation for $\partial x_{\sigma-} / \partial p$ (Eq. 3.13). Using Eq. 3.13 and Eq. 3.14, the molar volume on the concentrated-phase surface at a given pressure and temperature is

$$v(x_{\sigma+}) = v(x_{\sigma-}) + \left(x_{\sigma+} - x_{\sigma-}\right)\left(\frac{\partial x_{\sigma-}}{\partial p}\left(\frac{\partial^2 g}{\partial x^2}\right)_{x=x_{\sigma-}} + \left(\frac{\partial v}{\partial x}\right)_{1\phi, x=x_{\sigma-}}\right). \tag{3.24}$$

The dilute-phase surface slope at constant temperature, $\partial x_{\sigma-} / \partial p$, can be calculated by differentiating Eq. 3.10. $(\partial v / \partial x)_{1\phi, x=x_{\sigma-}}$ is calculated from Hatakeyama et al's formula (after the value of $x_{\sigma-}$ has been calculated from Eq. 3.10). The molar volume on the dilute-phase surface at p and T, $v(x_{\sigma-})$, is also calculated from Hatakeyama et al's formula.

The second derivative $(\partial^2 g / \partial x^2)$ at some ^{3}He concentration x and pressure p can be calculated using

$$\left(\frac{\partial^2 g}{\partial x^2}\right)_{x,p} = \left(\frac{\partial^2 g}{\partial x^2}\right)_{x,p=0} + \int_0^p \frac{\partial}{\partial p}\left(\frac{\partial^2 g}{\partial x^2}\right) dp$$

$$= \left(\frac{\partial^2 g}{\partial x^2}\right)_{x,p=0} + \int_0^p \frac{\partial^2}{\partial x^2}\left(\frac{\partial g}{\partial p}\right) dp = \left(\frac{\partial^2 g}{\partial x^2}\right)_{x,p=0} + \int_0^p \frac{\partial^2 v}{\partial x^2} dp \tag{3.25}$$

where $\partial^2 g / \partial x^2$ at p = 0 is known from the saturated-pressure property model. Unfortunately, $\partial^2 g / \partial x^2$ at $x = x_{\sigma-}(p)$ cannot be accurately determined, for two reasons. The first reason is that at a given temperature, $x_{\sigma-}$ increases with pressure, for pressures of less than 10 bar. (This is apparent from Figure 3.2 and can also be seen by plotting the fit of Eq. 3.10.) As $\partial^2 g / \partial x^2$ is discontinuous across the phase-separation surface (and the magnitude of discontinuity is not known at high pressures), the integration in Eq. 3.25 must be restricted to the single-phase region. This allows us to calculate values of $\partial^2 g / \partial x^2$ at high-pressure only up to values of x less than $x_{\sigma-}(p = 0)$. The value of $\partial^2 g / \partial x^2$ at $x = x_{\sigma-}(p)$ must be extrapolated from these values. The extrapolation proceeds in the following fashion: (a) $\partial^2 g / \partial x^2$ is calculated at several values of x less than $x_{\sigma-}(p = 0)$, all at the same temperature, and (b) $\partial^2 g / \partial x^2$ is then plotted as a function of x, and the function is extrapolated to get the value at $x = x_{\sigma-}(p)$. At high pressures, $x_{\sigma-}(p)$ is quite different from $x_{\sigma-}(p = 0)$, which increases the likelihood of an error in the extrapolation. Another possible source of error lies in the calculated values of $\partial^2 v / \partial x^2$. These values are also calculated from Hatakeyama et al's formula. It was previously pointed

out that there are questions about the accuracy of the second derivatives calculated from the available data.

An example of the extrapolation procedure is shown in Figure 3.8. At 0.6 K, $\partial^2 g / \partial x^2$ is plotted as a function of x at pressures of 2, 6 and 10 bar. Values of $\partial^2 g / \partial x^2$ for $x \le x_{\sigma-}(p = 0) = 0.296$ are calculated from Eq. 3.25. Beyond $x = 0.296$, $\partial^2 g / \partial x^2$ is extrapolated to the appropriate value of $x_{\sigma-}(p)$. The extrapolated values of $\partial^2 g / \partial x^2$ at $x_{\sigma-}(p)$ at 2, 6 and 10 bar are about 5.8, 5.0, and 3.8 J/mol respectively.

The calculated value of $v(x_{\sigma+})$ in Eq. 3.24 does not strongly depend on the extrapolated value of $\partial^2 g / \partial x^2$. For example, at 10 bar, the extrapolated value of 3.8 J/mol yields $v(x_{\sigma+})$ = 29.53 cm^3/mol (using Eq. 3.24). An extrapolated value of 5 J/mol would have yielded 29.59 cm^3/mol; a value of 2 J/mol would have yielded 29.44 cm^3/mol. Therefore, a variation of about 30-40% in $\partial^2 g / \partial x^2$ yields only a about a 0.3% variation in the value of $v(x_{\sigma+})$.

The values of $v(x_{\sigma+})$ calculated from Eq. 3.24 were not expected to be spot on, but, in the absence of any other data in the He-I region at high pressure, were useful in determining a fit. They were calculated at temperatures of up to 0.7 K. (Hatakeyama et al suggest that their formula, which is used for determining $v(x_{\sigma-})$, is valid only up to 0.66 K. However, it appears to remain well-behaved up to 0.7 K, and we used it up to that temperature.) At low temperatures (0.3 K and below), however, $x_{\sigma+}$ is very close to 1, and the $v(x_{\sigma+})$ values are not very useful. Therefore the sub-0.3 K estimates were not included in the fitting function.

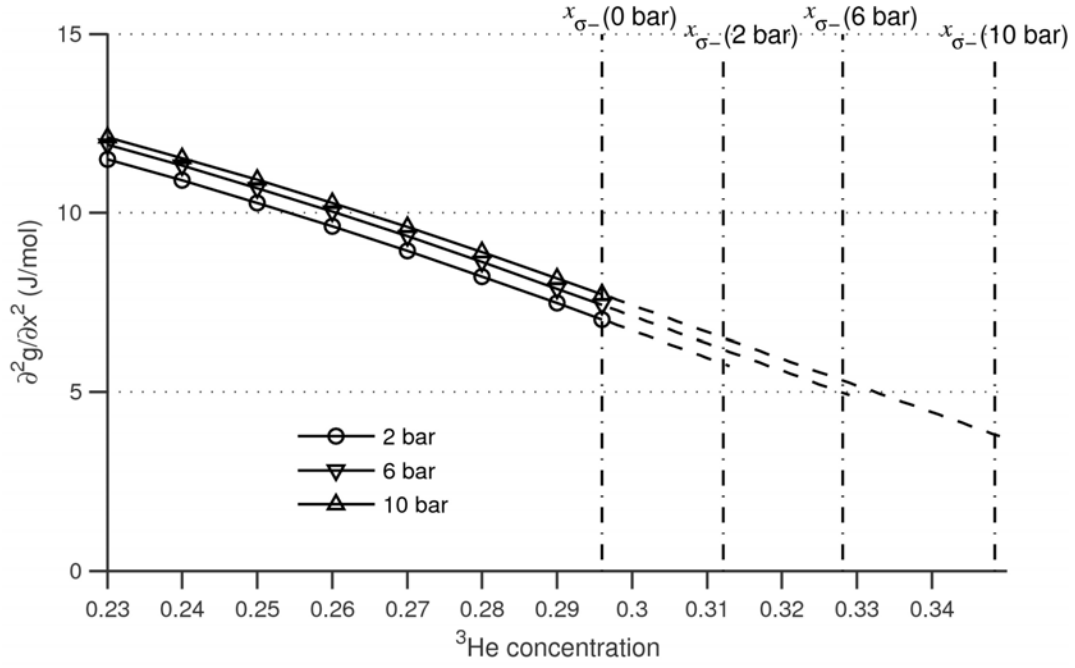

Figure 3.8: *$\partial^2 g / \partial x^2$ at 0.6 K as a function of x at 2 bar, 6 bar and 10 bar, and extrapolated (dashed lines) to the appropriate value of $x_{\sigma-}(p)$.*

The volume correction term v_r in Eq. 3.21 was written as

$$v_r(p,T,x) = \sum_{\substack{i=0 \text{ to } 3 \\ j=0 \text{ to } 3}} x^i T^j \left(\sum_{k=0 \text{ to } 2} V_{r1,ijk}\, p^k + V_{r2,ij} \frac{1}{p + p_{vr}} \right). \tag{3.26}$$

This expression for v_r was fitted to v_r calculated from data from Hatakeyama et al and Kierstead, as well as the concentrated-phase volumes estimated from Eq. 3.24. (The correction terms calculated from the various sources were based on the pure ^{3}He and ^{4}He molar volume expressions of Eq. 3.23 and 3.22 respectively.) In addition, values of $\partial v / \partial T$ and $\partial v / \partial x$ calculated from Eq. 3.21 are fitted to values of $\partial v / \partial T$ and $\partial v / \partial x$ calculated from Hatakeyama et al's and Kierstead's fits.

Although the only data available at high pressures and high temperatures are those of pure ^{3}He and pure ^{4}He, an effort was made to ensure that the mixture molar volume values predicted by the fit were not unreasonable in those regions. It was also ensured that the fit did not result in calculated thermodynamic properties (discussed in the following sections) that were unphysical. In particular, we looked at the behaviour of the ^{4}He chemical potential in the He-I region, and the values of the isothermal compressibility (which must always be positive).

The values of $\partial x_{\sigma-} / \partial p$ and $\partial x_{\sigma+} / \partial p$ at zero pressure calculated from Eqs. 3.13 and 3.18 (i.e., using the molar volume fit and the saturated pressure model) are not consistent with the values predicted by the fits of Eqs. 3.10 and 3.16. This is not surprising, since the molar volumes and the second derivatives of the Gibbs free energy at zero pressure are fairly involved functions of temperature, while the fits of Eqs. 3.10 and 3.16 are very simple functions of temperature. A comparison between the two sets of values is shown in Figure 3.9. However, these differences are not expected to have any practical implications.

The fitting was carried out using Microsoft Excel's Solver add-in. Matlab's *lsqnonlin* function did not come up with a better solution when the fit calculated by the Excel Solver was used as an initial guess for it. The constants in Eq. 3.26 calculated from the fit are listed in Table 8 in Appendix A.3. The values calculated from the fit of Eq. 3.21 are compared with the underlying data of Hatakeyama et al in Figure 3.10, and with that of Kierstead in Figure 3.11.

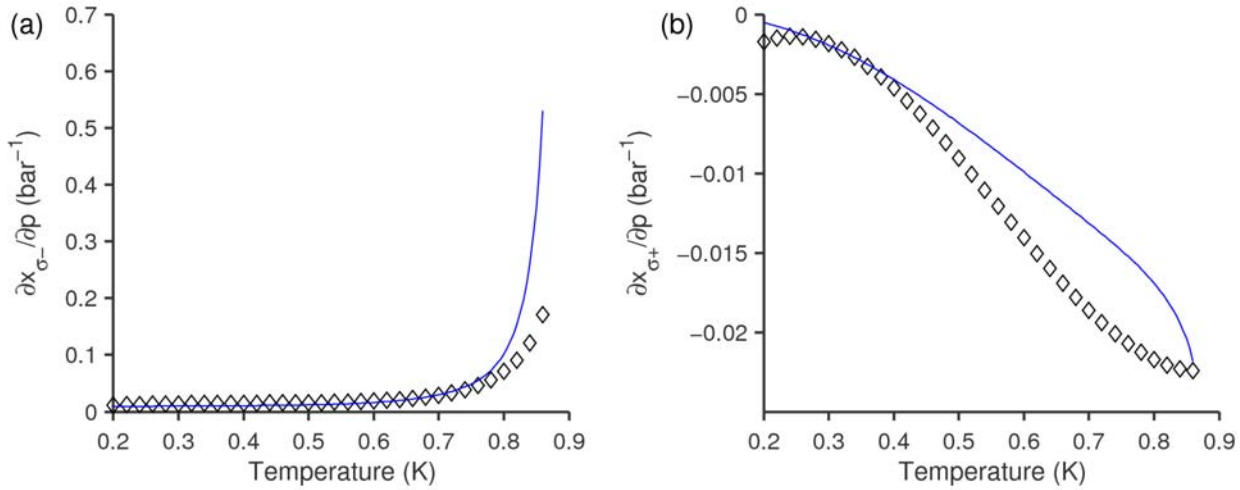

Figure 3.9: *The pressure-derivatives of the (a) dilute, and (b) concentrated phase-separation surfaces at p = 0 bar. The solid lines represent values calculated from (a) Eq. 3.13, and (b) Eq. 3.18. ($\partial^2 g / \partial x^2$ values were calculated from the saturated-pressure model of Chapter 2, molar volume derivatives from the fit of Eq. 3.21.) The markers represent values calculated from the fits of (a) Eq. 3.10 and (b) Eq. 3.16.*

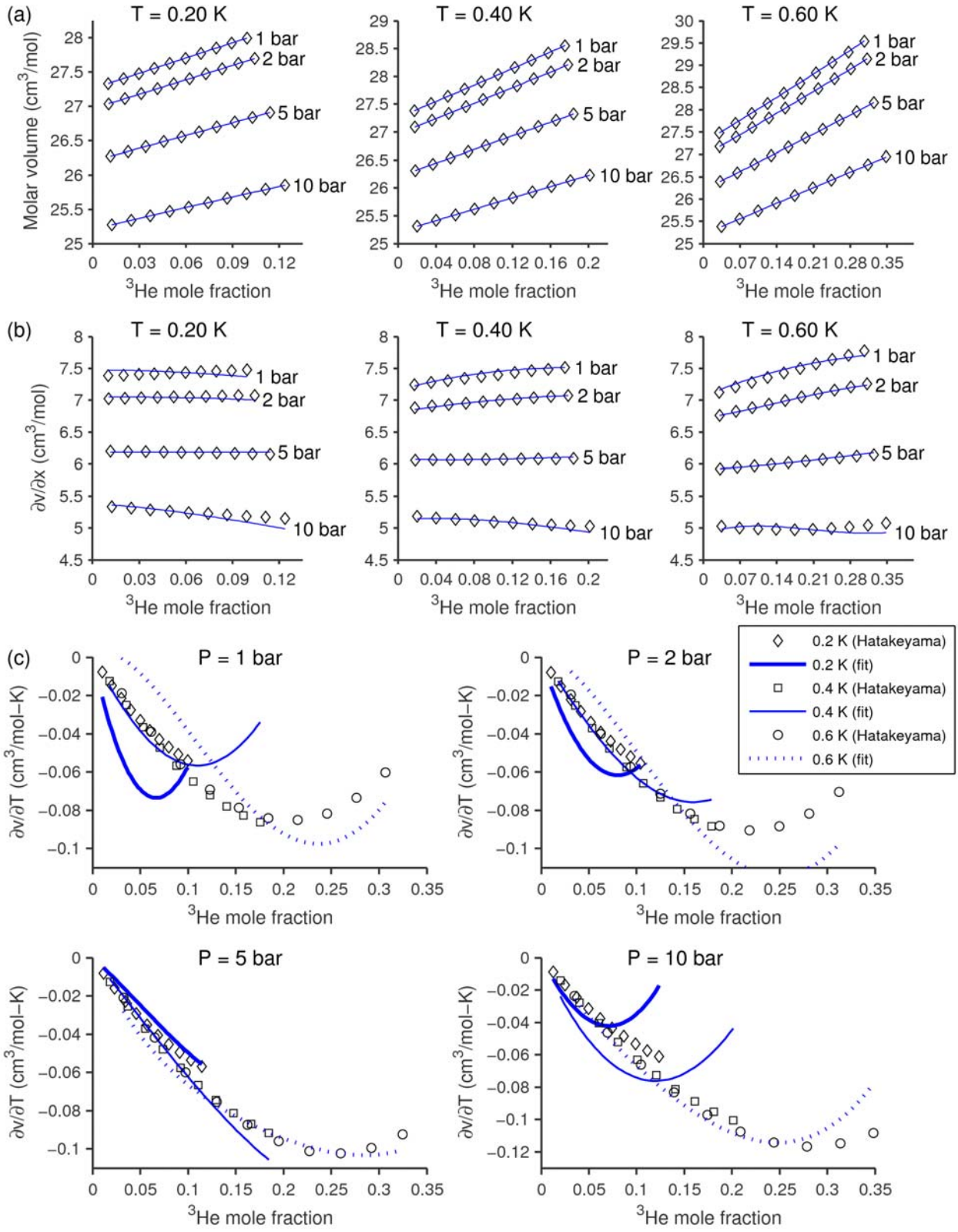

Figure 3.10: *Molar volumes, $\partial v/\partial x$, and $\partial v/\partial T$ from Hatakeyama et al [49] (markers) and from the fit of Eq. 3.21 (lines). The fits to v and $\partial v/\partial x$ are quite good; the fits to $\partial v/\partial T$ are better at high pressures than at low pressures. The magnitudes of $\partial v/\partial T$ are quite small.*

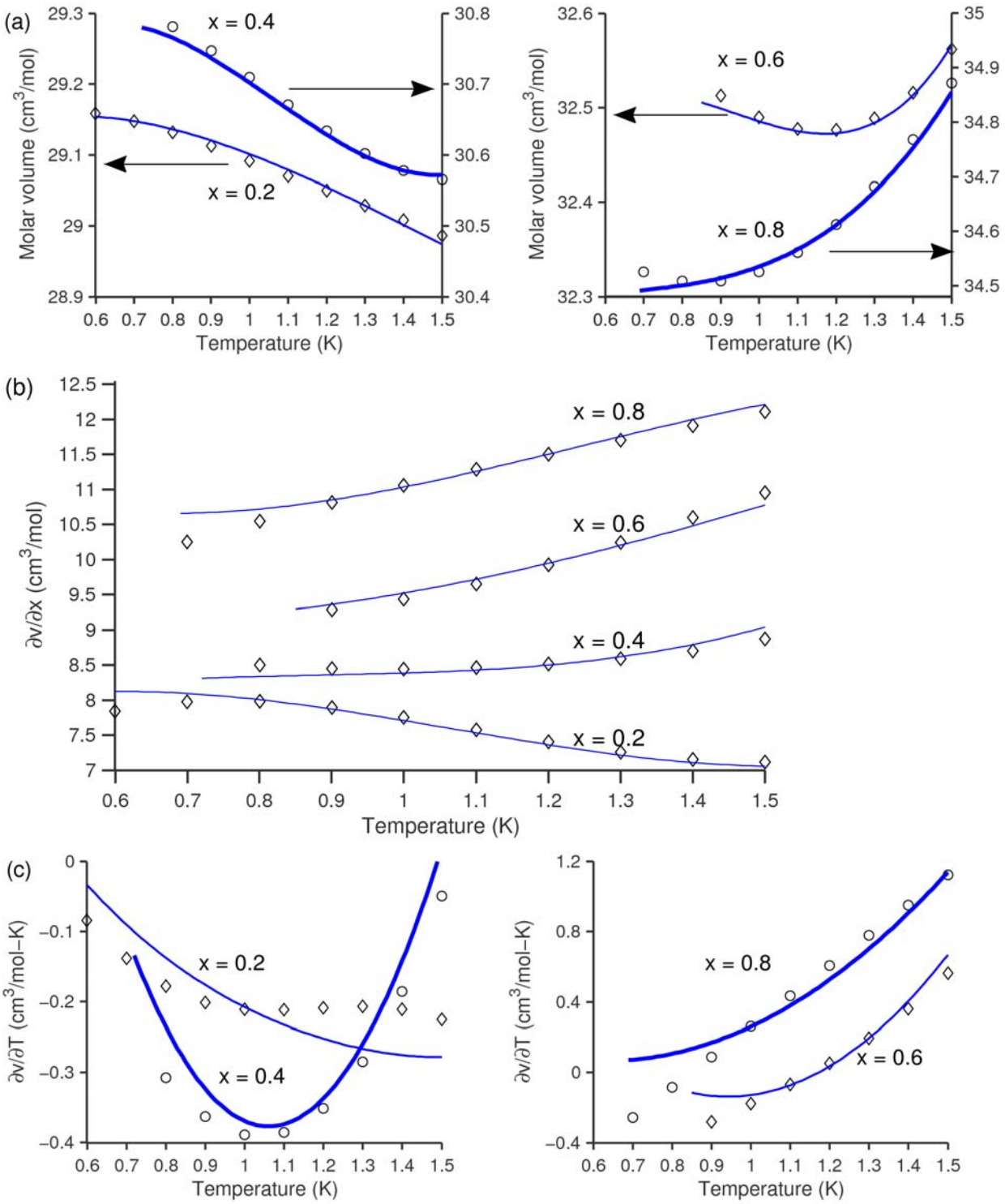

Figure 3.11: *(a) Molar volumes,(b) $\partial v / \partial x$, and (c) $\partial v / \partial T$ from Kierstead [22] (markers) and from the fit of Eq. 3.21 (solid lines).*

It is worth pointing out that despite there being no mixture data at high pressures and temperatures, the predicted molar volumes at those points are still expected to be quite reasonable, since the correction terms, $x(1-x)v_r(p,T,x)$, are much smaller in magnitude than the $xv_3^0(p,T)+(1-x)v_4^0(p,T)$ terms (about 0.5 cm^3/mol as compared to about 30 cm^3/mol), and reliable data is available for pure ^{4}He and pure ^{3}He at all temperatures and pressures. However, this does not hold true for derivatives of the molar volume.

The behaviour of the fit at high temperatures and pressures (i.e., in regions where the only data is for pure ^{3}He and pure ^{4}He) is shown in Figure 3.12. The molar volumes and the temperature derivatives are expected to be accurate at x = 0 and x = 1. There is no data to compare $\partial v/\partial x$ with.

3.3 Calculation of high-pressure thermodynamic properties

We now have an expression for the molar volume which will allow us to calculate and integrate the pressure partial derivatives of enthalpy, entropy, Gibbs free energy and chemical potential (which were listed in at the beginning of this chapter – Eqs. 3.1 through 3.6), and thus determine property values at high pressures. However, it is important to note that the expression for the molar volume that was calculated in the previous section is valid only for the single-phase region. In the two-phase region, the molar volume must be calculated from the lever rule:

$$v(x,T,p)=v(x_{\sigma+})\frac{(x-x_{\sigma-})}{(x_{\sigma+}-x_{\sigma-})}+v(x_{\sigma-})\frac{(x_{\sigma+}-x)}{(x_{\sigma+}-x_{\sigma-})}. \tag{3.27}$$

where $x_{\sigma+}$ and $x_{\sigma-}$ are the ^{3}He concentrations on the concentrated- and dilute-phase surfaces, respectively, at a temperature T and a pressure p, and $v(x_{\sigma+})$ and $v(x_{\sigma-})$ – the molar volumes at those concentrations – are calculated from the single-phase expression (Eq. 3.21).

The x-derivative of the molar volume at constant T and p in the two-phase region can be simply calculated from Eq. 3.14. The temperature-derivative is slightly more involved. It can be shown by differentiating Eq. 3.27 that the derivative $(\partial v/\partial T)$ varies linearly with x in the two-phase region when the temperature and pressure are held fixed. Therefore, $(\partial v/\partial T)_{2\phi,x}$ can be written as

$$\frac{\partial v}{\partial T}=\left(\frac{\partial v}{\partial T}\right)_{2\phi,x=x_{\sigma+}}\frac{(x-x_{\sigma-})}{(x_{\sigma+}-x_{\sigma-})}+\left(\frac{\partial v}{\partial T}\right)_{2\phi,x=x_{\sigma-}}\frac{(x_{\sigma+}-x)}{(x_{\sigma+}-x_{\sigma-})} \tag{3.28}$$

where $(\partial v/\partial T)_{2\phi,x=x_{\sigma-}}$ and $(\partial v/\partial T)_{2\phi,x=x_{\sigma+}}$ are the temperature derivatives in the two-phase region at $x=x_{\sigma-}$ and $x=x_{\sigma+}$ respectively. These can be written as

$$\left(\frac{\partial v}{\partial T}\right)_{2\phi,x=x_{\sigma-}}=\left(\frac{\partial v}{\partial T}\right)_{dil-\phi\ surf.}\Bigg|_{x=x_{\sigma-}}-\left(\frac{\partial x_{\sigma-}}{\partial T}\right)_p\left(\frac{\partial v}{\partial x}\right)_{2\phi,x=x_{\sigma-}}, \tag{3.29}$$

and

$$\left(\frac{\partial v}{\partial T}\right)_{2\phi,x=x_{\sigma+}}=\left(\frac{\partial v}{\partial T}\right)_{conc-\phi\ surf.}\Bigg|_{x=x_{\sigma+}}-\left(\frac{\partial x_{\sigma+}}{\partial T}\right)_p\left(\frac{\partial v}{\partial x}\right)_{2\phi,x=x_{\sigma+}}, \tag{3.30}$$

where $(\partial v/\partial T)_{dil-\phi\ surf.}\Big|_{x=x_{\sigma-}}$ and $(\partial v/\partial T)_{conc-\phi\ surf.}\Big|_{x=x_{\sigma+}}$ are the temperature-derivatives of molar

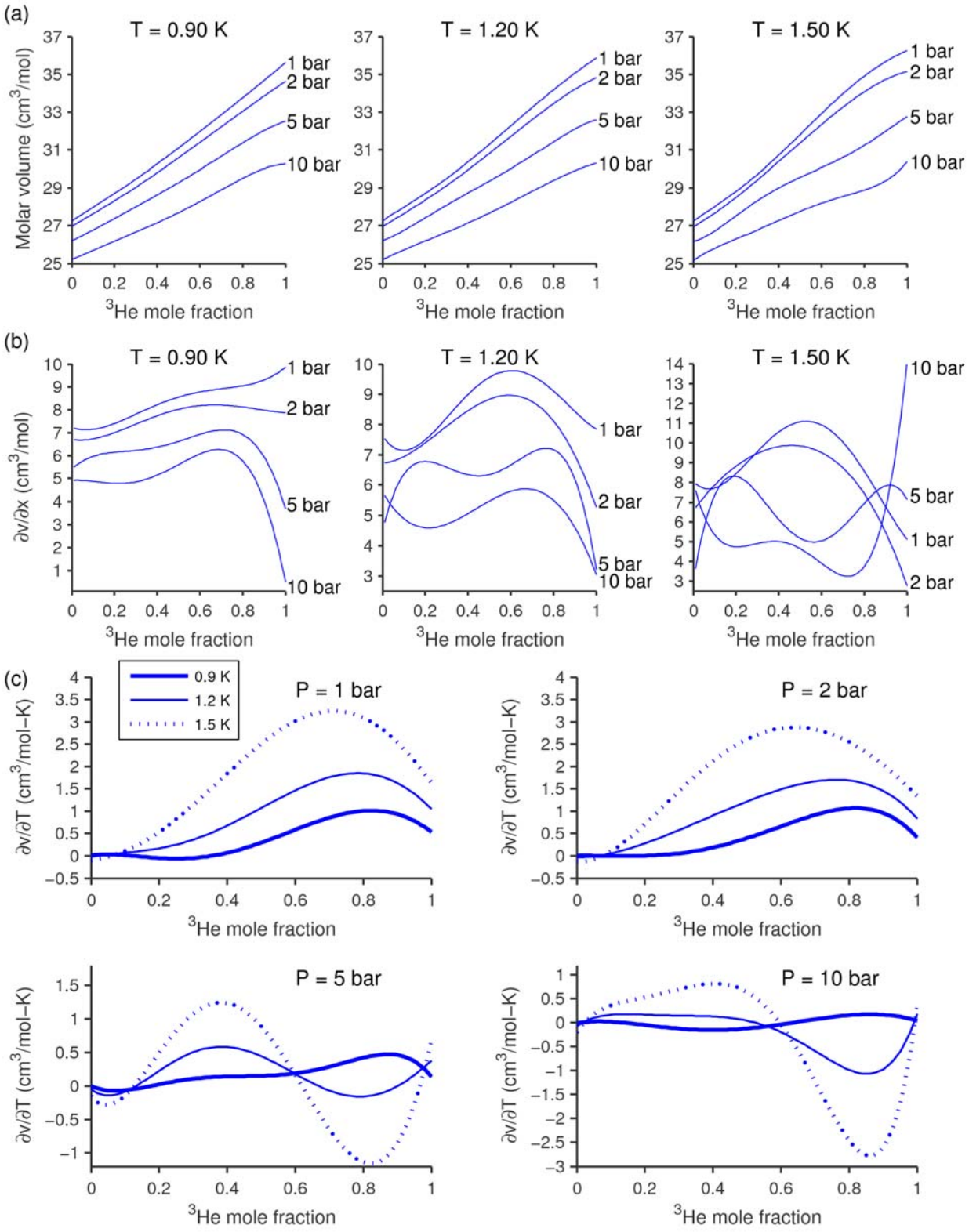

Figure 3.12: *(a) Molar volumes, (b) $\partial v / \partial x$, and (c) $\partial v / \partial T$ at 0.9 K, 1.2 K and 1.5 K predicted by the fit of Eq. 3.21. The only data available for fitting at these temperatures and pressures are v and $\partial v / \partial T$ values at $x = 0$ and $x = 1$.*

volume along the dilute- and concentrated-phase surfaces respectively, at constant pressure. The temperature-derivatives along the phase separation surfaces can in turn be written as

$$\left(\frac{\partial v}{\partial T}\right)_{dil-\phi\ surf.}\Bigg|_{x=x_{\sigma-}} = \left(\frac{\partial v}{\partial T}\right)_{1\phi,x=x_{\sigma-}} + \left(\frac{\partial x_{\sigma-}}{\partial T}\right)_p \left(\frac{\partial v}{\partial x}\right)_{1\phi,x=x_{\sigma-}} \tag{3.31}$$

and

$$\left(\frac{\partial v}{\partial T}\right)_{dil-\phi\ surf.}\Bigg|_{x=x_{\sigma+}} = \left(\frac{\partial v}{\partial T}\right)_{1\phi,x=x_{\sigma+}} + \left(\frac{\partial x_{\sigma+}}{\partial T}\right)_p \left(\frac{\partial v}{\partial x}\right)_{1\phi,x=x_{\sigma+}} . \tag{3.32}$$

Substituting Eq. 3.31 into Eq. 3.29, and Eq. 3.32 into Eq. 3.30, we can get expressions for $\left(\partial v/\partial T\right)_{2\phi,x=x_{\sigma-}}$ and $\left(\partial v/\partial T\right)_{2\phi,x=x_{\sigma+}}$:

$$\left(\frac{\partial v}{\partial T}\right)_{2\phi,x=x_{\sigma-}} = \left(\frac{\partial v}{\partial T}\right)_{1\phi,x=x_{\sigma-}} + \left(\frac{\partial x_{\sigma-}}{\partial T}\right)_p \left[\left(\frac{\partial v}{\partial x}\right)_{1\phi,x=x_{\sigma-}} - \left(\frac{\partial v}{\partial x}\right)_{2\phi,x=x_{\sigma-}}\right] \tag{3.33}$$

and

$$\left(\frac{\partial v}{\partial T}\right)_{2\phi,x=x_{\sigma+}} = \left(\frac{\partial v}{\partial T}\right)_{1\phi,x=x_{\sigma+}} + \left(\frac{\partial x_{\sigma+}}{\partial T}\right)_p \left[\left(\frac{\partial v}{\partial x}\right)_{1\phi,x=x_{\sigma+}} - \left(\frac{\partial v}{\partial x}\right)_{2\phi,x=x_{\sigma+}}\right], \tag{3.34}$$

which can be substituted back into Eq. 3.28, to calculate $(\partial v/\partial T)$ in the two-phase region.

Depending on the values of x and T, a mixture may retain the same phase in going from zero pressure to a pressure p at constant x and T, or it may change phase (for example, from the He-II region to the He-I region, or from two-phase to single-phase He-I or He-II). As we use a single (continuous, differentiable) molar volume fit for both He-II and He-I single-phase regions (with the caveat that it is not likely to be accurate in the vicinity of the λ-surface), we do not have to bother about transitions across the λ-surface.

Within the pressure range of interest (0-10 bar), the values of $(\partial x_{\sigma-}/\partial p)_T$ and $(\partial x_{\sigma+}/\partial p)_T$ from the fits of Eqs. 3.10 and 3.16 are always positive and negative respectively (except for a small region on the concentrated-phase surface, below 0.2 K; when deriving an expression for $x_{\sigma+}$, it had been indicated that the fit in this region was possibly non-physical due to the lack of experimental data). Therefore, in integrating along a line of constant x and T from zero pressure to a higher pressure, three possibilities emerge: (a) the constant-x, constant-T line stays exclusively in the single-phase region, (b) the constant-x, constant-T line stays exclusively in the two-phase region, and (c) the constant-x, constant-T line starts off in the two-phase region and ends in the single-phase region. These three possibilities are depicted in Figure 3.13.

For case (a), the integral of the pressure partial derivative of a thermodynamic property m in Eq. 3.7 is simply

$$\int_0^p \frac{\partial m}{\partial p}\,dp = \int_0^p \left(\frac{\partial m}{\partial p}\right)_{1\phi} dp . \tag{3.35}$$

Similarly, the integral of the pressure partial derivative for case (b) is

$$\int_0^p \frac{\partial m}{\partial p}\,dp = \int_0^p \left(\frac{\partial m}{\partial p}\right)_{2\phi} dp . \tag{3.36}$$

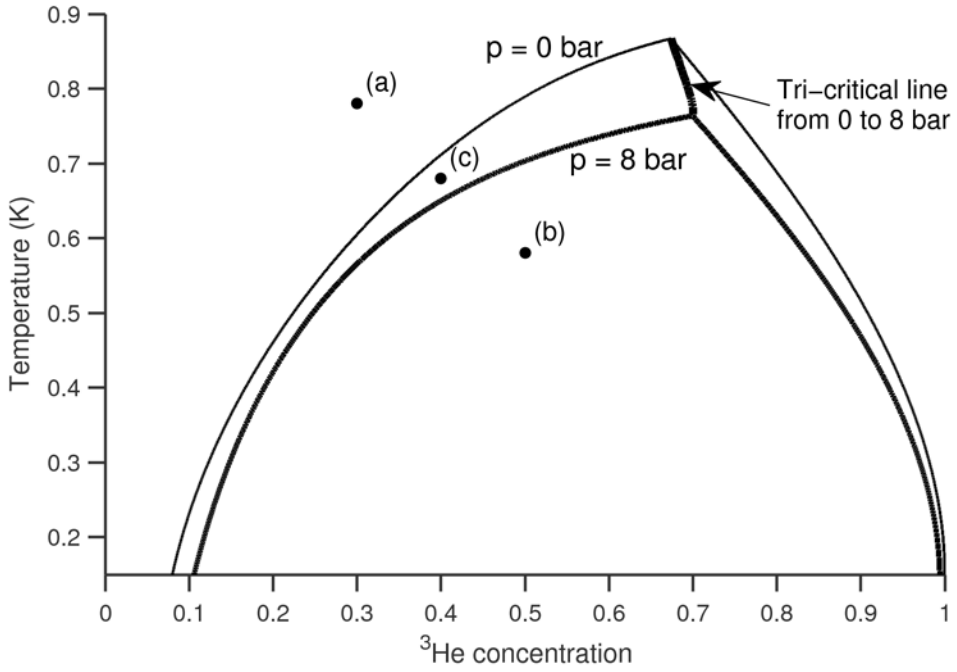

Figure 3.13: *The phase separation surfaces at p = 0 bar and p = 8 bar projected onto a T - x plane. Also shown are three lines of constant ^{3}He concentration and constant temperature from p = 0 bar to p = 8 bar. (On a T - x plane, they appear as points). Line (a) stays within the single-phase He-II region; line (b) stays within the two-phase region; line (c) starts in the two-phase region (at 0 bar), crosses the phase-separation surface and finishes in the single-phase region (at 8 bar).*

For case (c), it is necessary to determine the pressure p_{int} where the constant-x, constant-T line intersects the phase-separation surface. This is easily done by solving Eq. 3.10 or Eq. 3.16 (whichever is relevant) for p, given a specific x and T. The integral of the pressure partial derivative is then

$$\int_0^p \frac{\partial m}{\partial p}\,dp = \int_0^{p_{\text{int}}} \left(\frac{\partial m}{\partial p}\right)_{2\phi} dp + \int_{p_{\text{int}}}^{p} \left(\frac{\partial m}{\partial p}\right)_{1\phi} dp\,. \tag{3.37}$$

This integral can be evaluated if the partial derivative $\partial m / \partial p$ is a function of v and/or first derivatives of v, but not if it is a function of the second derivative of v (which, for example, is the case when m is the specific heat C_p; see Eq. 3.6). This is because the molar volume is continuous everywhere in the x - T - p space, but is not differentiable across the phase-separation surfaces. Therefore, first derivatives of the molar volume are finite everywhere in the x - T - p space, but are not continuous. As the first derivatives are not continuous across the phase-separation surfaces, the second derivatives are infinite at the boundary, and the integral of the pressure partial derivative cannot be split up as it has been in Eq. 3.37. So quantities like the specific heat (which is the second temperature derivative of the Gibbs free energy) and $\partial^2 g / \partial x^2$ cannot be directly computed everywhere using this integral. They can, however be computed in other ways. (The specific heat can be calculated from the temperature derivative of the entropy or enthalpy. $\partial^2 g / \partial x^2$ can be calculated from the x-derivative of the ^{4}He chemical potential.)

The values of enthalpy, entropy, ^{4}He chemical potential and osmotic enthalpy calculated from the molar volume fit are tabulated in Table 18 through Table 22 in Appendix E.2 at pressures of 2, 4, 6, 8 and 10 bar. Also tabulated are the properties on the dilute- and concentrated-phase surfaces, wherever applicable. These values can be used to calculate properties at any value of x in the two-phase region. (In the two-phase region, at a given temperature and pressure: (a) the enthalpy, entropy and molar volume vary linearly with x, from the dilute-phase surface to the concentrated-phase surface, (b) the ^{4}He chemical potential stays constant, (c) the osmotic enthalpy does not vary linearly with x; however, the product xh^{os} does vary linearly with x.)

The enthalpy, entropy and ^{4}He chemical potential are plotted at various temperatures at 3, 6 and 9 bar in Figure 3.14, Figure 3.15, and Figure 3.16. The enthalpy changes quite significantly from 3 bar to 9 bar; however, the entropy does not change very much with pressure. This is because $\partial s / \partial p$ is equal to $-\partial v / \partial T$, which is quite small in magnitude everywhere. The regions of linear variation of the enthalpy and entropy (and constant ^{4}He chemical potential) correspond to two-phase mixtures.

It is worth reiterating that high-temperature-high-pressure mixture properties are based on sparse data (pure component data and saturated-pressure mixture data). While some calculated properties (such as the enthalpy) are expected to be reasonably accurate, others (such as the entropy) must be used with caution. A detailed discussion of the accuracies and inaccuracies associated with the high-pressure property model is presented in Section 5.2.

We now have properties of ^{3}He-^{4}He mixtures up to pressures of 10 bar and between temperatures of 0.15 K and 1.5 K. Properties below 0.15 K are not calculated in this thesis; however, they can be calculated using the procedures outlined in this chapter. The work of Kuerten et al [2] (who present thermodynamic properties below 0.15 K at zero pressure) and Hatakeyama et al [49] (who present formulas for the molar volume and the dilute-phase surface below 0.15 K) can be used to calculate properties in the He-II region. Since the concentrated-phase surface is practically coincident with the pure ^{3}He surface at these temperatures, the He-II properties can be used with pure ^{3}He properties to get ^{3}He-^{4}He mixture properties in the two-phase region below 0.15 K.

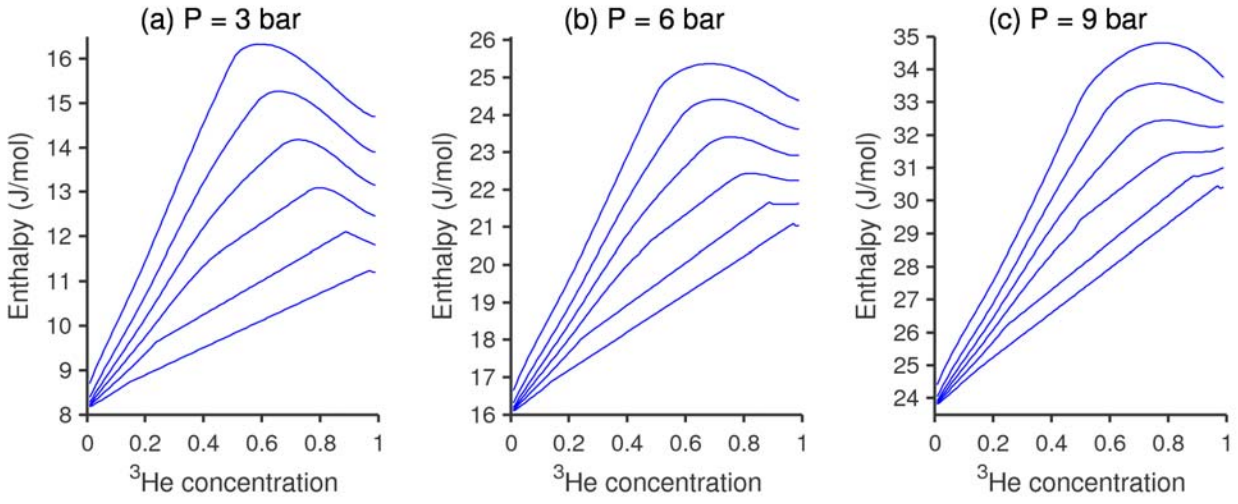

Figure 3.14: *Enthalpy as a function of x, at 3, 6 and 9 bar, at various temperatures (0.3 K, 0.5 K, 0.7 K, 0.9 K, 1.1 K and 1.3 K going upwards on each graph). At temperatures of 0.3 K, 0.5 K and 0.7 K, the two-phase region is identifiable by the linear variation of enthalpy with x.*

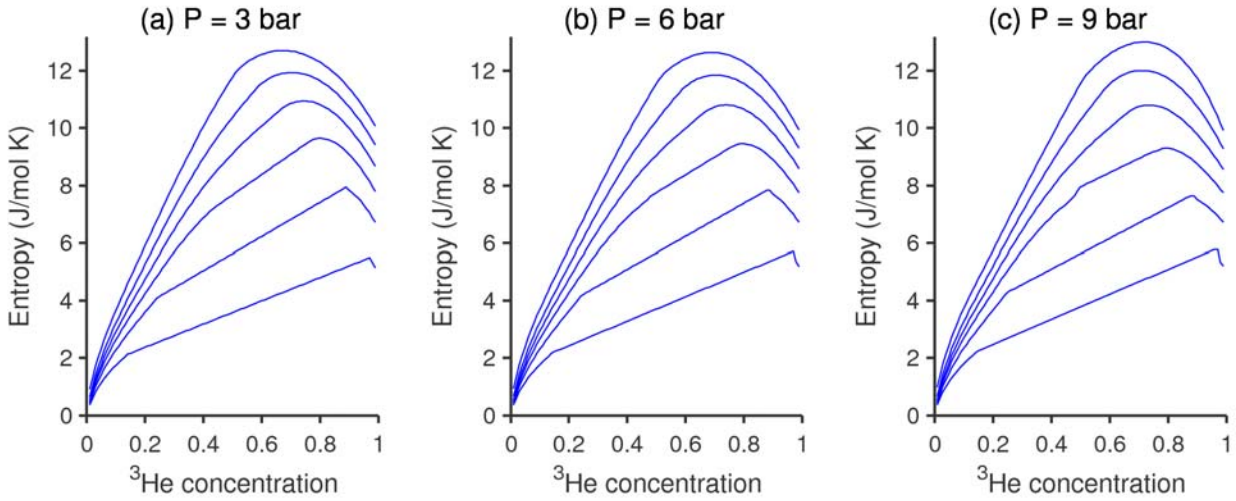

Figure 3.15: *Entropy as a function of x, at 3, 6 and 9 bar, at various temperatures (0.3 K, 0.5 K, 0.7 K, 0.9 K, 1.1 K and 1.3 K going upwards on each graph). At 0.3 K, 0.5 K and 0.7 K, the two-phase region is identifiable by the linear variation of entropy with x. The entropy does not change much with pressure.*

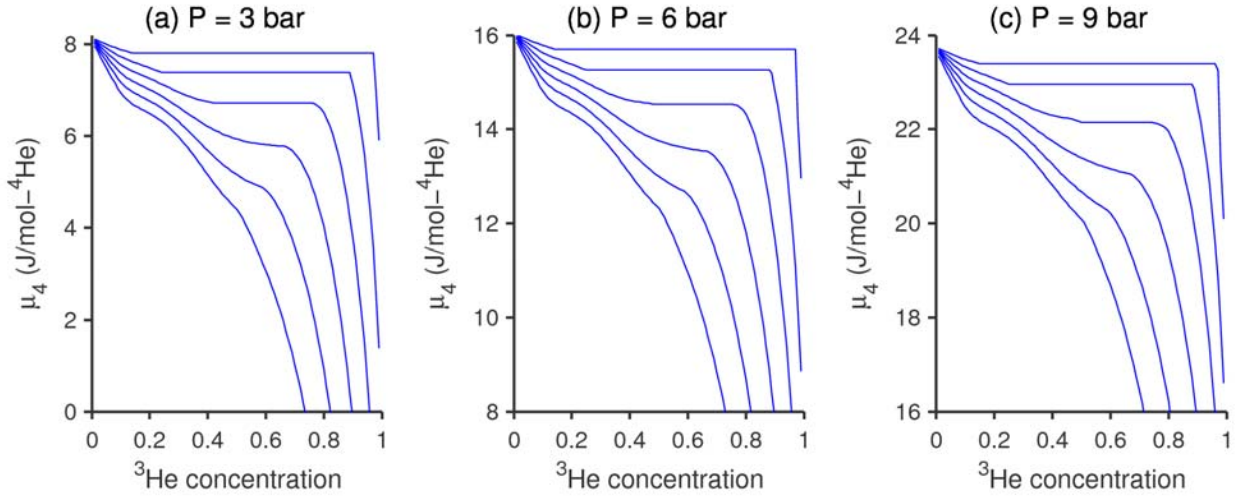

Figure 3.16: *^{4}He chemical potential as a function of x, at 3, 6 and 9 bar, at various temperatures (0.3 K, 0.5 K, 0.7 K, 0.9 K, 1.1 K and 1.3 K going downwards on each graph). At temperatures of 0.3 K, 0.5 K and 0.7 K, the two-phase region is identifiable by the constant value of μ_4.*

Chapter 4: Applications of ^{3}He-^{4}He properties to sub-Kelvin refrigeration

We now discuss applications of the calculated properties to components of sub-Kelvin refrigerators. In particular, we will look at superfluid heat exchangers and superfluid throttles. We also briefly discuss He-II mixture compression.

4.1 Heat Exchangers

The idealized model of a "standard" heat exchanger with normal fluids assumes that there is no pressure drop in the flowing streams due to friction. This condition will be assumed to also hold true for a heat exchanger with a He-II mixture flow.

In a flowing He-II mixture, the ^{3}He and the normal component of the ^{4}He are locked together [61]. If the velocity is below a critical value, however, the superfluid component of the ^{4}He flows independently of the normal component, with no viscosity. It has been discussed previously that the superfluid flows to equalize the ^{4}He chemical potential. (This is evident from the superfluid equation of motion at low velocities - Eq. 1.15.) Therefore, both the pressure and the ^{4}He chemical potential are constant across a He-II stream flowing in an "ideal" heat exchanger where the velocity is below the critical velocity. (The critical velocity will be discussed in some more detail at the end of this section.)

Diagrams of lines of constant μ_4 and constant pressure are therefore useful for the analysis of these heat exchangers. Lines of constant μ_4 at zero pressure (for various values of μ_4) are shown in Figure 4.1. (It is worth reiterating here that the values of μ_4 may be inaccurate between ^{3}He concentrations of 15%-25%; this point was discussed in Section 2.4, and will be revisited in Section 5.1.) These lines represent the dependence of x on temperature in a He-II mixture flowing through a heat exchanger. As it is being cooled, the mixture may also undergo phase separation; the change of phase from dilute to concentrated is analogous to condensation in normal fluids from the "dilute" vapour phase to the "concentrated" liquid phase.

Another useful quantity for the analysis of these heat exchangers is the specific heat of the mixture per mole of ^{3}He, at constant μ_4 and constant pressure. (It is more convenient to calculate the specific heat per mole of ^{3}He rather than per mole of mixture because, in steady flow, the flow rate of the ^{3}He component is constant throughout the stream from inlet to exit, unlike the flow rate of the total normal component.)

An apparatus to conceptualize this specific heat is shown in Figure 4.2. A piston-cylinder arrangement containing a ^{3}He-^{4}He mixture is connected to a ^{4}He reservoir by a superleak, through which only superfluid ^{4}He can flow. The free piston ensures that the mixture inside the cylinder stays at a constant pressure. The connection to the reservoir ensures that the ^{4}He chemical potential in the mixture stays constant. If a differential amount of heat δQ is now added to the cylinder, the heat capacity (at constant pressure and constant μ_4) is simply the heat added divided by the differential temperature change, $\delta Q / \delta T$. If we now apply the Second Law to the piston-cylinder control volume, and note that the superfluid flowing through the superleak carries no entropy, we get

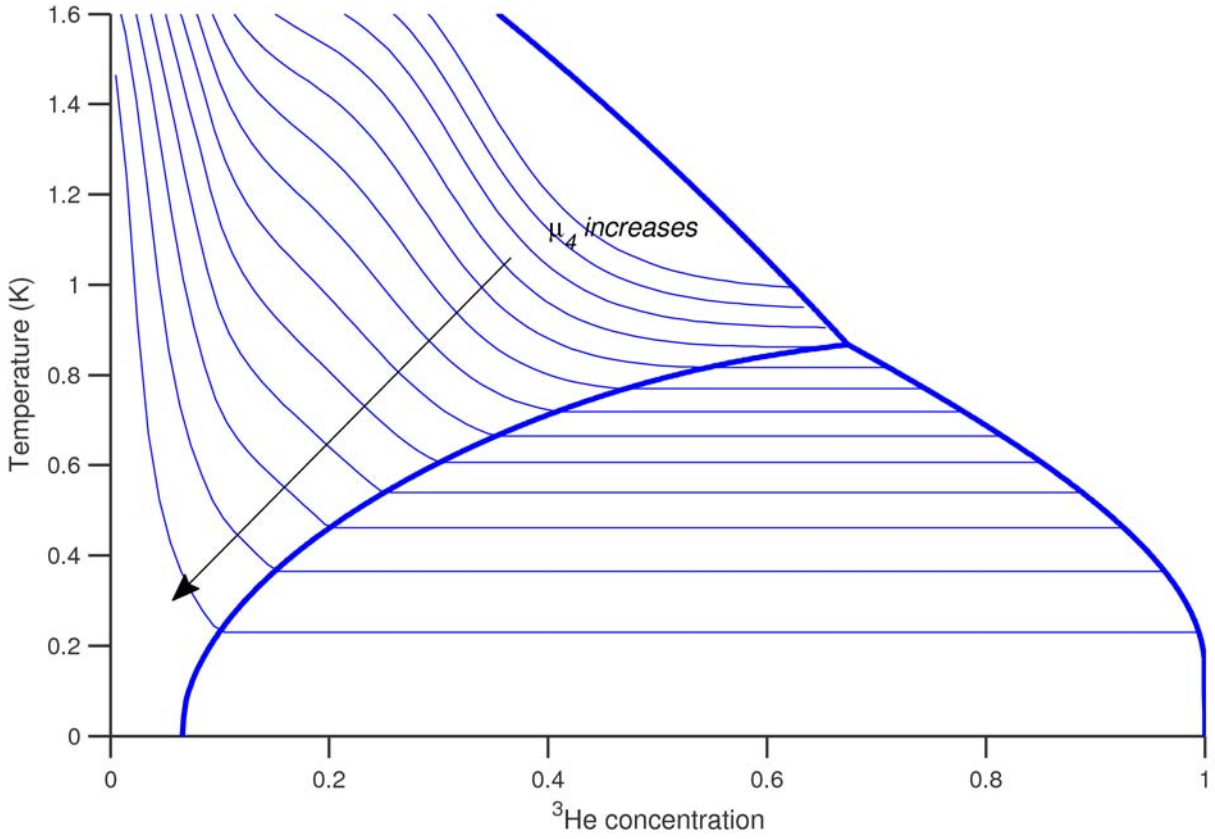

Figure 4.1: *Lines of constant μ_4 at zero pressure, as calculated in this work. The values of μ_4 along these lines are, going from left to right, -0.2, -0.4, -0.6, -0.8, -1.0, -1.2, -1.4, -1.6, -1.8, -2.0, -2.2, -2.4 and -2.6 J/mol-^{4}He, respectively.*

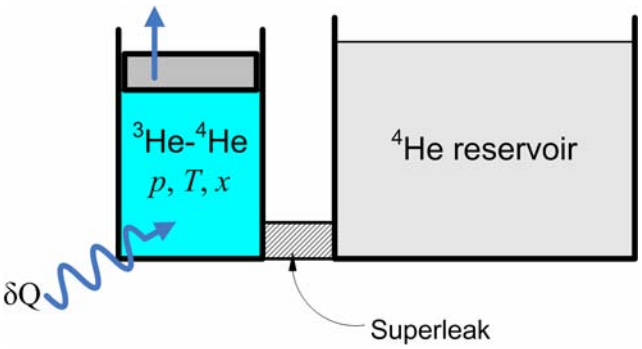

Figure 4.2: *An apparatus to measure the specific heat at constant pressure and constant μ_4*

$$dS_{mix} = \frac{\delta Q}{T}. \tag{4.1}$$

The heat capacity of the mixture of the mixture is therefore $T(\partial S_{mix} / \partial T)$. The specific heat, per mole of ^{3}He, is

$$C_{\mu_4} = T\left(\frac{\partial(S_{mix} / N_3)}{\partial T}\right)_{\mu_4, p} = T\left(\frac{\partial(s / x)}{\partial T}\right)_{\mu_4, p} = T\left(\frac{\partial s_{3He}}{\partial T}\right)_{\mu_4, p} \tag{4.2}$$

where s_{3He} is the total entropy of the mixture per mole of ^{3}He (and is therefore equal to the entropy per mole of mixture, s, divided by x).

An alternative form of C_{μ_4} can be derived by applying the First Law (Eq. 1.32) to the system:

$$dU = \delta Q - pdV + \mu_4 dN_4 . \tag{4.3}$$

Since the energy U is equal to $H - pV$, the above equation can be rewritten as

$$d(H - \mu_4 N_4) = \delta Q + Vdp - N_4 d\mu_4 . \tag{4.4}$$

The left side of this equation is equal to

$$H - \mu_4 N_4 = (N_3 + N_4)h - N_4\mu_4 = N_3\left(\frac{N_3 + N_4}{N_3}h - \frac{N_4}{N_3}\mu_4\right) = N_3\left(\frac{h}{x} - \frac{1-x}{x}\mu_4\right) = N_3 h^{os} \tag{4.5}$$

where we used the definition of osmotic enthalpy (Eq. 1.20) and that of x:

$$x = \frac{N_3}{N_3 + N_4} . \tag{4.6}$$

The First Law equation therefore reduces (at constant pressure and constant μ_4) to

$$d(N_3 h^{os}) = \delta Q . \tag{4.7}$$

The specific heat, per mole of ^{3}He, for this process is

$$C_{\mu_4} = \frac{1}{N_3}\frac{\delta Q}{\delta T} = \left(\frac{\partial h^{os}}{\partial T}\right)_{\mu_4, p} . \tag{4.8}$$

This is analogous to the C_p-h relation (Eq. 1.8) that holds for pure substances and is used for normal heat exchangers. The equivalence of Eqs. 4.2 and 4.8 can also be shown mathematically using the definition of osmotic enthalpy (see Appendix D.3).

The specific heat C_{μ_4} defined here is different from the specific heat C_{μ_4} defined by Radebaugh [1]. Radebaugh defines C_{μ_4} as $T(\partial s_3 / \partial T)_{\mu_4}$, where s_3 is the entropy of the ^{3}He component of the mixture only. Our definition of C_{μ_4} includes the contribution of the ^{4}He component. Below temperatures of about 0.7 – 0.8 K, the specific heat associated with the phonons and rotons in the ^{4}He component is very small and the ^{3}He component is the major contributor to the specific heat. In this temperature range, therefore, the difference between the C_{μ_4} defined here and Radebaugh's C_{μ_4} is quite small. At temperatures above about 0.9 K, the ^{4}He phonon-roton contribution to the specific heat starts becoming quite substantial. As a consequence, the values of C_{μ_4} calculated from Eq. 4.2 become increasingly greater than Radebaugh's C_{μ_4} values as the temperature increases. (A comparison is presented in Section 5.1.) Since the phonons and rotons (associated with the normal part of the ^{4}He component) are dragged along with the ^{3}He flow due to mutual friction [61], this definition of C_{μ_4} is more relevant to heat exchanger flow than that of Radebaugh.

The specific heat at constant μ_4 and pressure can be calculated by taking the derivative of the mixture entropy per mole of ^{3}He with respect to temperature, along a line of constant μ_4 at a fixed pressure. Values of specific heat at constant μ_4 in the single-phase He-II region at zero pressure are tabulated in Table 17 in Appendix E.1.

At high temperatures, low ^{3}He-concentration mixtures have a higher constant-μ_4 specific heat than high ^{3}He-concentration mixtures, while at lower temperatures, high-x mixtures have a higher specific heat than low-x mixtures. This is because at high temperatures, low ^{3}He-concentration streams have a greater amount of ^{4}He associated with them per mole of ^{3}He. At these temperatures, the specific heat associated with the phonons and rotons in the ^{4}He dominates, and therefore, low ^{3}He-concentration streams have a higher specific heat per mole of ^{3}He than high ^{3}He-concentration streams. On the other hand, at low temperatures, the specific heat associated with the ^{4}He phonon-roton component dies down, and the ^{3}He component makes the major contribution to the specific heat. Since high-concentration ^{3}He has a larger specific heat at low temperature than low-concentration ^{3}He, the specific heat per mole of ^{3}He is higher for the high ^{3}He-concentration stream [4]. An example of this can be seen in Figure 4.3, where we compare the behaviour of C_{μ_4} at two different values of the ^{4}He chemical potential (-1.6 J/mol-^{4}He and -2.0 J/mol-^{4}He). Note that at all temperatures, the μ_4 = -1.6 J/mol-^{4}He mixture has a lower ^{3}He concentration than the μ_4 = -2.0 J/mol-^{4}He mixture.

At low ^{3}He concentrations, however, (where the behaviour of the ^{3}He component of a ^{3}He-^{4}He mixture is expected to approach that of an ideal Fermi gas), the specific heat per mole of ^{3}He can be higher for the low ^{3}He-concentration stream at low temperatures. An example is shown in Figure 4.4, where we compare C_{μ_4} for μ_4 = -0.4 J/mol-^{4}He, μ_4 = -0.6 J/mol-^{4}He, and μ_4 = -0.8 J/mol-^{4}He. (At all temperatures, the μ_4 = -0.4 J/mol-^{4}He mixture has the lowest ^{3}He concentration, the μ_4 = -0.8 J/mol-^{4}He mixture has the highest ^{3}He concentration.) At high temperatures, a lower ^{3}He-concentration stream has a higher specific heat; at lower temperatures, the specific heat of a higher ^{3}He-concentration stream begins to dominate, for reasons discussed above. However, at even lower temperatures, the specific heats cross over once again. This is because the ^{3}He in the high-concentration stream has a higher Fermi temperature; as the temperature of the mixture falls below it, the specific heat of the high-concentration stream rapidly drops off. The low-x mixture has a lower Fermi temperature and therefore a higher specific heat.

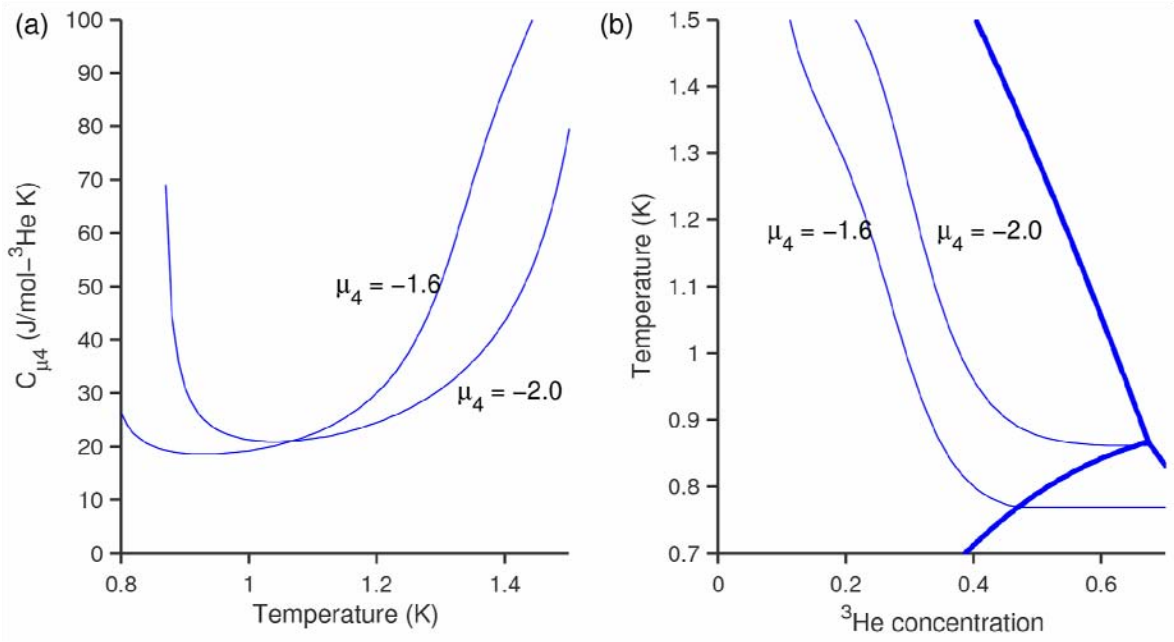

Figure 4.3: (a) *Specific heat (per mole of ^{3}He) at constant μ_4 and p, for μ_4 = -1.6 J/mol-^{4}He and μ_4 = -2.0 J/mol-^{4}He. (b) Lines of constant μ_4 on the T - x plane, for μ_4 = -1.6 J/mol-^{4}He and μ_4 = -2.0 J/mol-^{4}He*

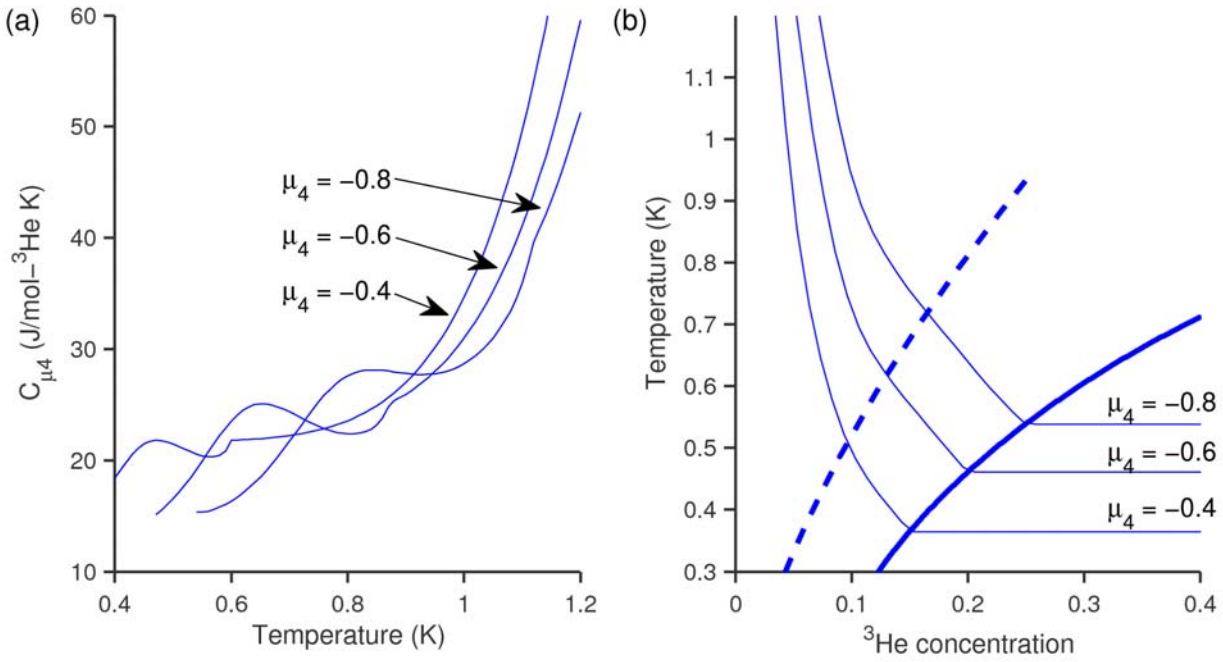

Figure 4.4: *(a) Specific heat (per mole of ^{3}He) at constant μ_4 and pressure, for μ_4 = -0.4 J/mol-^{4}He, -0.6 J/mol-^{4}He, and -0.8 J/mol-^{4}He; (b) Lines of constant μ_4 on the T - x plane, for μ_4 = -0.4 J/mol-^{4}He, -0.6 J/mol-^{4}He, and -0.8 J/mol-^{4}He. The dashed line represents the Fermi temperature for the ^{3}He component of the mixture, plotted as a function of x.*

The kinks in the C_{μ_4} plot in Figure 4.4 correspond to where the constant μ_4 lines intersect the $x = 0.08$ boundary and are a pathological result of the fitting procedure. It can be shown (by taking a temperature derivative of Eq. 4.2 at constant μ_4) that $\partial C_{\mu_4} / \partial T$ depends on the quantity $(\partial^2 \mu_4 / \partial x^2)_T$. As previously discussed, a limitation of the fitting procedure was that the derivative of $(\partial \mu_4 / \partial x)_T$ is discontinuous across $x = 0.08$. The calculated values of C_{μ_4} may not be very accurate in the vicinity of these kinks.

As stated at the beginning of this section, these results are applicable for heat exchangers where velocities are low enough that the superfluid ^{4}He ensures a uniform μ_4 throughout the stream. We now briefly discuss how low these velocities need to be for the uniform μ_4 assumption to be reasonable, and what happens when the velocities are not "low".

The magnitude of the critical velocity v_c in circular tubes of diameter d was measured by Zeegers [62] at temperatures below 0.1 K and by Mudde [63] at temperatures around 1.5 K. Zeegers found a logarithmic dependence of $v_c d$ on d. He observed critical velocities between 0.5 cm/s (in a 7.5 mm tube) and 10 cm/s (in a 0.1 mm tube). Mudde measured the critical velocity at various temperatures between 1.3 K and 1.7 K in a 0.1 mm tube. He observed critical velocities of about 3-8 cm/s; the higher critical velocities were observed at lower temperatures.

When the velocity of the normal component crosses the critical value, there is a "mutual friction" force between the normal fluid and the superfluid. This leads to a μ_4 gradient in the stream and the constant-μ_4 results are no longer apt. In this case, it is hard to define an appropriate specific heat for use in heat exchanger analysis; knowledge of the flow dynamics is now required. However, we can consider the limiting case of very high velocities, where all the superfluid ^{4}He is dragged along with the normal component of the mixture. Since all the components are locked together, the ^{3}He concentration of the mixture does not change across the length of the heat exchanger and so now, it is x and p that are uniform along the length of the heat exchanger, rather than μ_4 and p. The appropriate specific heat in this case is $C_{x,p}$. In addition, since the superfluid and normal components are flowing together, the modified form of the First Law (Eq. 1.32) reduces to the usual form (Eq. 1.21), and it is easier to work with the enthalpy of the mixture rather than its osmotic enthalpy.

Flow situations that lie between the limiting cases of low velocities (where μ_4 is constant) and very high velocities (where x is constant) are more complicated and will not be discussed here. The effect of the fluid dynamics in these cases on properties such as T, x, p and μ_4 are discussed by Zeegers [62] (at temperatures below 0.1 K) and by Mudde [63] (at temperatures between 1.3 K and 1.7 K).

4.2 Superfluid throttle

Recently, a new type of sub-Kelvin refrigeration cycle (the superfluid Joule-Thomson refrigerator [3, 4, 5]) was proposed that, unlike a dilution refrigerator, circulates the working fluid (a ^{3}He-^{4}He mixture) completely at low temperature. This cycle uses a throttle bypassed by a superleak to achieve cooling (Figure 4.5). For an adiabatic, zero-work, steady throttle, it can be shown using the First Law for a He-II mixture (Eq. 1.32) that the osmotic enthalpy stays constant across the throttle. (The superleak bypassing the throttle ensures that μ_4 is the same at the inlet and outlet.) The osmotic enthalpy, therefore, plays a role analogous to the enthalpy in "standard" room-temperature throttles commonly used in vapour-compression refrigerators. Lines of constant osmotic enthalpy at constant μ_4, therefore, can serve as a useful guide to the design of such machines.

The intersection of a constant μ_4 surface with a constant h^{os} surface in three dimensions is shown in Figure 4.6. It serves as a useful indicator of the amount of cooling that can be achieved with a throttle. For example, for the mixture shown in the figure (μ_4 = 1.5 J/mol-^{4}He, h^{os} = 12 J/mol-^{3}He), the temperature drops from 0.86 K to 0.6 K for a pressure drop of 1.3 to 0.7 bar.

The behaviour of lines of constant osmotic enthalpy at constant μ_4 at various temperatures is shown in Figure 4.7, where the lines are projected onto the T - x plane. (Note that any errors in μ_4 in the 10%-25% ^{3}He-concentration also afflict the osmotic enthalpy.) At high temperatures, throttling a mixture from high to low pressure decreases its temperature. The temperature drop is more pronounced in the two-phase region. It is also apparent that in the single-phase region at low temperatures, throttling a ^{3}He-^{4}He mixture from higher to lower pressure actually increases its temperature.

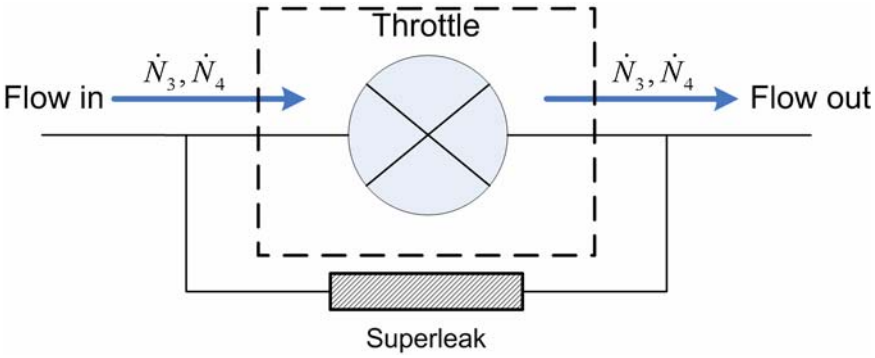

Figure 4.5: *A superleak-bypassed throttle operating in steady state*

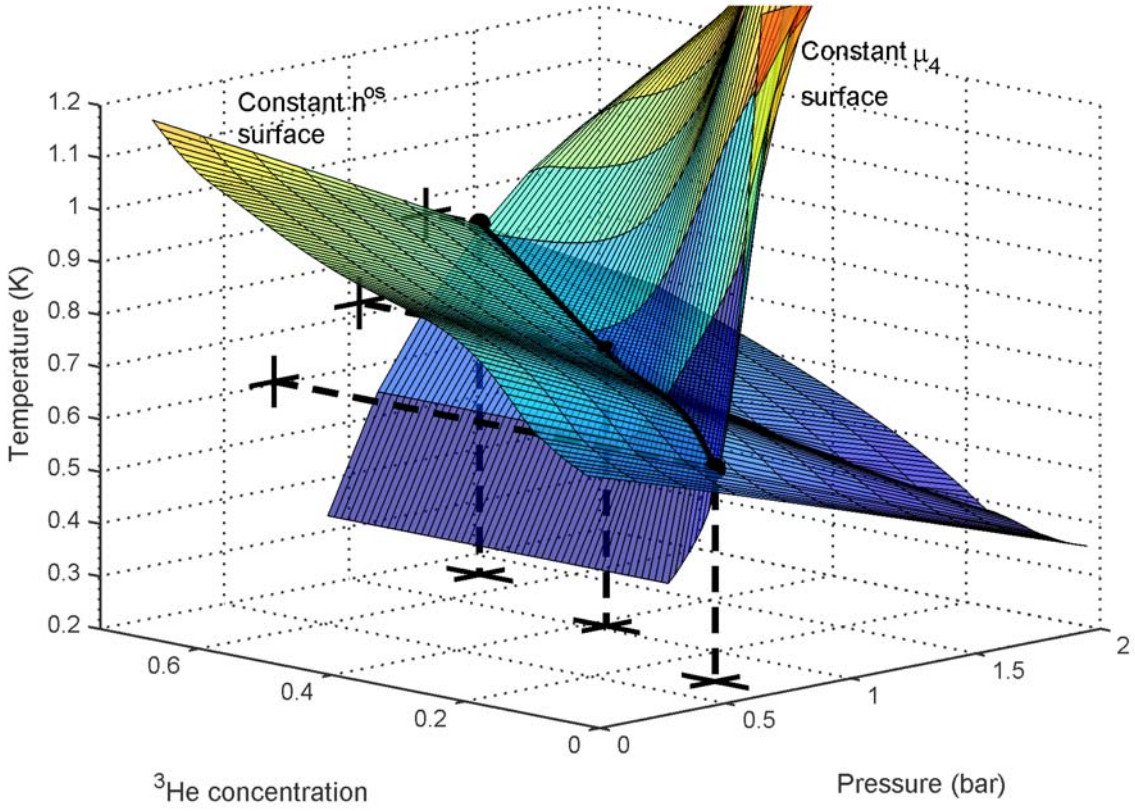

Figure 4.6: *The intersection of a surface of constant μ_4 (1.5 J/mol-^{4}He) with a surface of constant h^{os} (12 J/mol-^{3}He). The intersection – a line of constant μ_4 and constant h^{os} – is the locus of states followed by a ^{3}He-^{4}He mixture in a superfluid-bypassed throttle. The temperature drops from 0.86 K to 0.71 K if the pressure drops from 1.3 bar to 1 bar, and to 0.60 K, if the pressure drops further to 0.7 bar.*

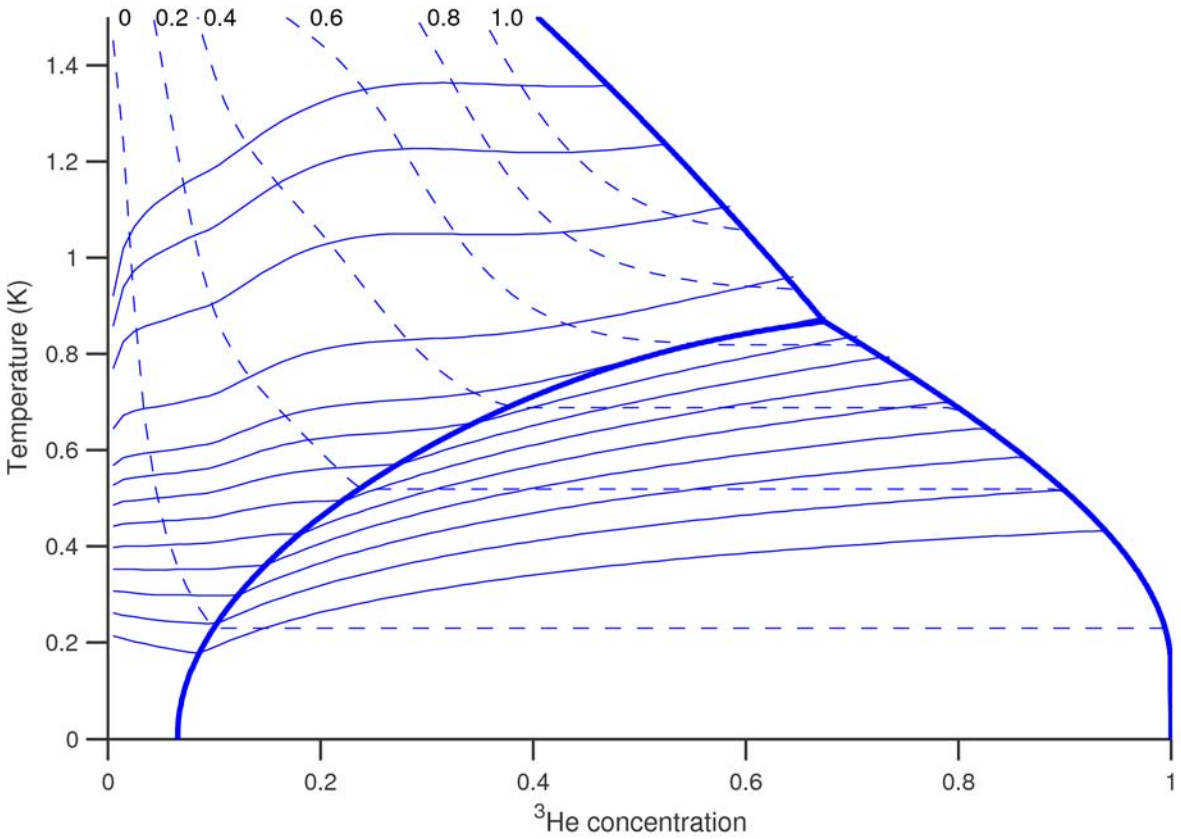

Figure 4.7: *Lines of constant osmotic enthalpy at constant* μ_4 *projected onto the* T *-* x *plane. Also shown for reference is the phase diagram at zero pressure. The values of osmotic enthalpy along the lines are, from the bottom up, 2, 3, 4, 5, 6, 7, 8, 9, 10, 12, 16, 20 and 24 J/mol-*^{3}*He respectively. The dashed lines are lines of constant pressure; the values adjacent to them represent the pressure in bar.*

4.3 ^{3}He compressor

One of the key components of a sub-Kelvin refrigerator that circulates the fluid at low temperature is a low-temperature compressor. A ^{3}He compressor was developed by Miller [4] for use in the superfluid Joule-Thomson refrigerator. The compressor increases the pressure and the ^{3}He concentration of the mixture. This discussion in this section is limited to a very basic compression process. The piston-cylinder arrangement in Figure 4.8 contains a ^{3}He-^{4}He mixture. It is connected to a ^{4}He reservoir through a superleak and is in good thermal contact with a heat reservoir. As the piston moves downward, increasing the pressure in the cylinder, superfluid ^{4}He flows through the superleak into the ^{4}He reservoir. The heat reservoir and the ^{4}He reservoir ensure that the process occurs at constant temperature and constant μ_4. The change in ^{3}He concentration of the mixture for a given change in pressure can be calculated by following a line of constant temperature on a surface of constant μ_4, an example of which is shown in Figure 4.9. A constant temperature cut (1.2 K) of this surface is shown in Figure 4.9c. The ^{3}He concentration of a mixture initially at 1.2 K, 1.5 bar and 5%-^{3}He (these properties correspond to μ_4 = 3.532 J/mol-^{4}He) increases to 16.5% when the pressure is increased to 1.8 bar and 29.2% when the

pressure is increased to 2.0 bar. A similar analysis can be performed at other temperatures using the projection of the constant-μ_4 surface onto the T - x plane shown in Figure 4.9b.

The modelling of an actual compressor is obviously more complicated. The compression cycle will consist of several processes. (A basic cycle would consist of an intake, a compression, an exhaust and a re-expansion.) The simplified isothermal compression process model here may not be apt for a practical compression process. For example, a relatively fast compression process would probably be more appropriately modelled as being isentropic than being isothermal. The size of the reservoir connected to the compressor via a superleak (the pure ^{4}He reservoir in the above example) would likely be of the same order as the compression volume, and so the compression would probably not be at a constant value of μ_4. These practical effects make the modelling more involved and will not be further discussed here. However, some of these more sophisticated compressor models are examined by Miller and Brisson [64].

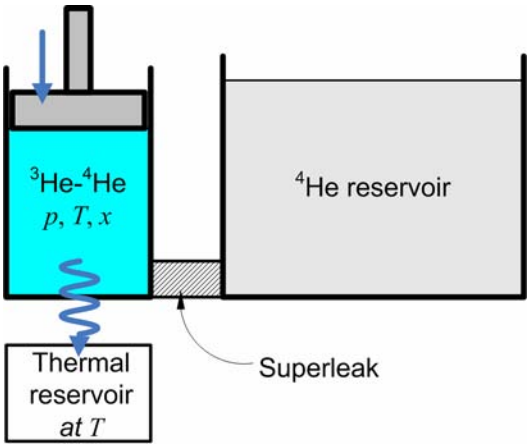

Figure 4.8: *A ^{3}He-^{4}He mixture undergoing a compression process at constant T and μ_4.*

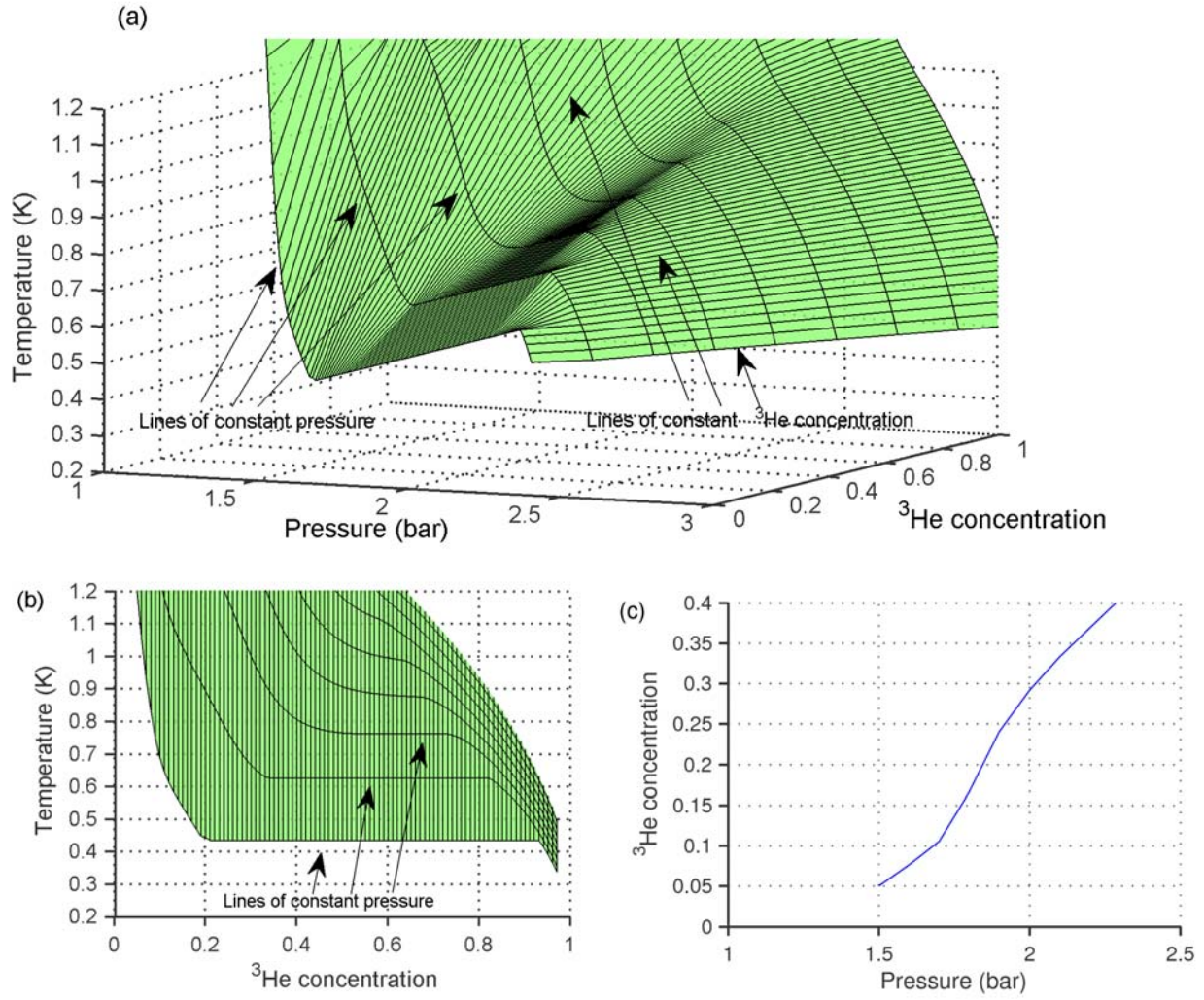

Figure 4.9: *(a) A surface of constant* μ_4 *(= 3.532 J/mol-*^{4}*He) in the* x *-* T *-* p *space. (b) The projection of the surface onto the* x *-* T *plane. (c) A constant-temperature (1.2 K) cut of the constant-* μ_4 *surface. In (a) and (b), the constant-pressure lines are spaced at intervals of 0.2 bar and the constant* x *lines are spaced at intervals of 0.01. The two-phase region is identifiable as that portion of the surface where both the temperature and pressure are constant.*

Chapter 5: Review of the mixture property model

In this chapter, results of the thermodynamic model are compared with other measurements on ^{3}He-^{4}He mixtures. A review of the high-pressure model in regions where there is no data for comparison is also presented.

5.1 Comparison with other data at saturated pressure

Figure 5.1 shows a comparison of entropies from Radebaugh's tables [1] and from this work. The values are quite similar to each other, although they are more consistent at $x = 0.1$, where the ideal specific heat model Radebaugh uses is more applicable than at $x = 0.3$.

Goellner et al [13] calculated the chemical potential difference, $\Phi - \Phi_t$, as a function of temperature and ^{3}He fraction, where Φ is equal to $\mu_3 - \mu_4$ and Φ_t is the value of Φ at the tricritical point. Their calculations, based on measurements of specific heat and vapour pressure in the vicinity of the tricritical point, were made between temperatures of 0.78 K and 1.22 K and ^{3}He fractions of 0.4 and 0.84. Results from this work show excellent correspondence with those values (Figure 5.2).

Goellner et al [13] also tabulate the quantity $\partial\Phi / \partial x$ (the inverse concentration susceptibility, which is also equal to $\partial^2 g / \partial x^2$), which they calculated from vapour pressure measurements. Their data is compared with results from our model in Figure 5.3. The results are in good agreement at temperatures below about 1 K, but not at higher temperatures. In particular, our model does not yield smooth values of the concentration susceptibility across $x = 0.674$. The reason for this has been discussed in Section 2.6.

Islander and Zimmermann [12] also calculated the entropy of ^{3}He-^{4}He mixtures in the vicinity of the tricritical point from the specific heat measurements of Alvesalo et al [14]. Their results are compared with ours in Figure 5.4. Figure 5.5 shows a comparison of the quantity $(\partial\Phi / \partial T)_x$, as calculated by Islander and Zimmermann, and in this work. There are slight differences between the two sets of data, but on the whole, the correspondence is quite good.

It should be pointed out, though, that the similarity of results in this work with Islander and Zimmermann is expected, because the specific heat data of Alvesalo et al [14] serves as the basis for their calculations too. The differences are due to (a) different interpolations for C_{x_t} / T and $(\partial C_{2\phi} / \partial x) / T$ as functions of temperature in the two-phase region, (b) different low-temperature data used in the calculations (they used Radebaugh's low-temperature data, which was the only data available at the time), and, to a small extent, (c) slight differences in the single-phase specific heats, since they use the actual experimental data and we use a fit that is designed to cover a large area of the T - x plane.

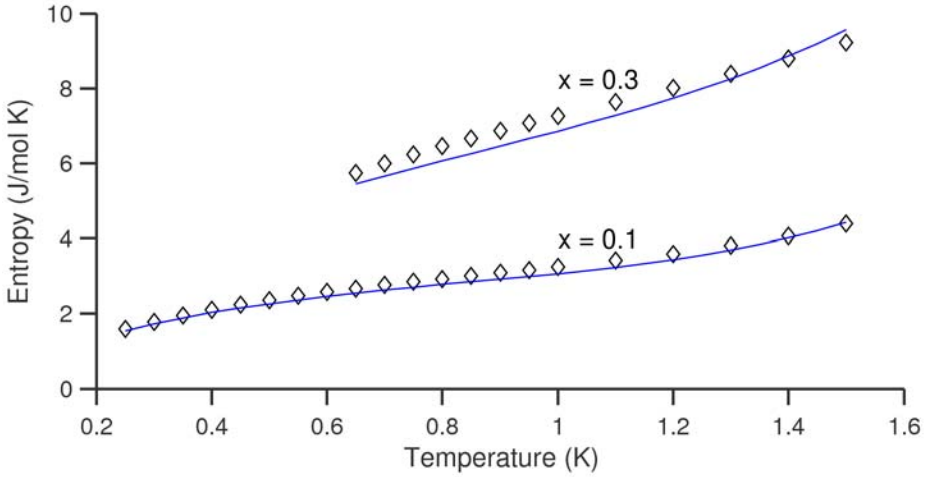

Figure 5.1: *A comparison of entropies – Radebaugh [1] (markers) and this work (solid lines)*

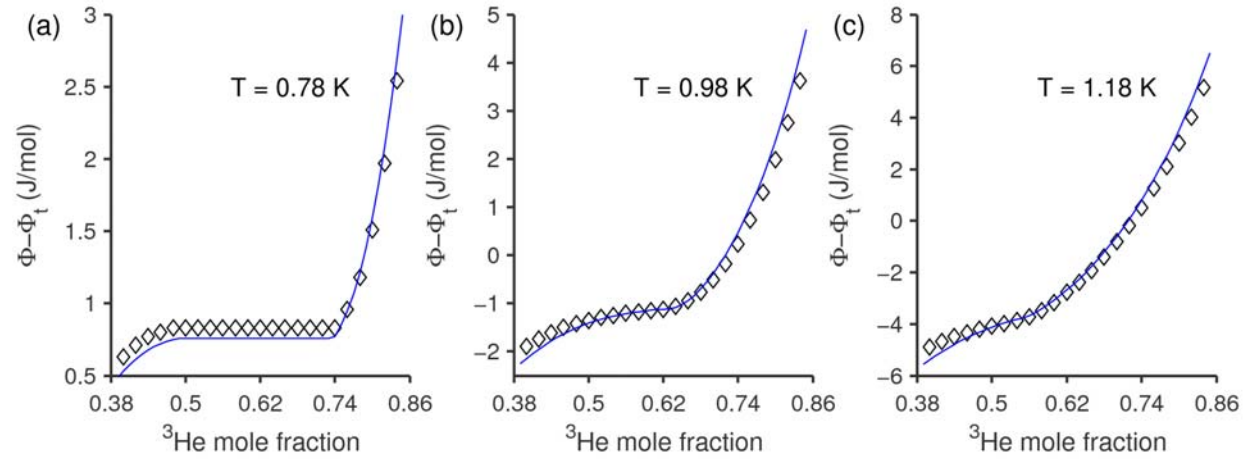

Figure 5.2: *A comparison of* $\Phi - \Phi_t$ *at 0.78 K, 0.98 K and 1.18 K from Goellner et al [13] (markers) and this work (solid lines).*

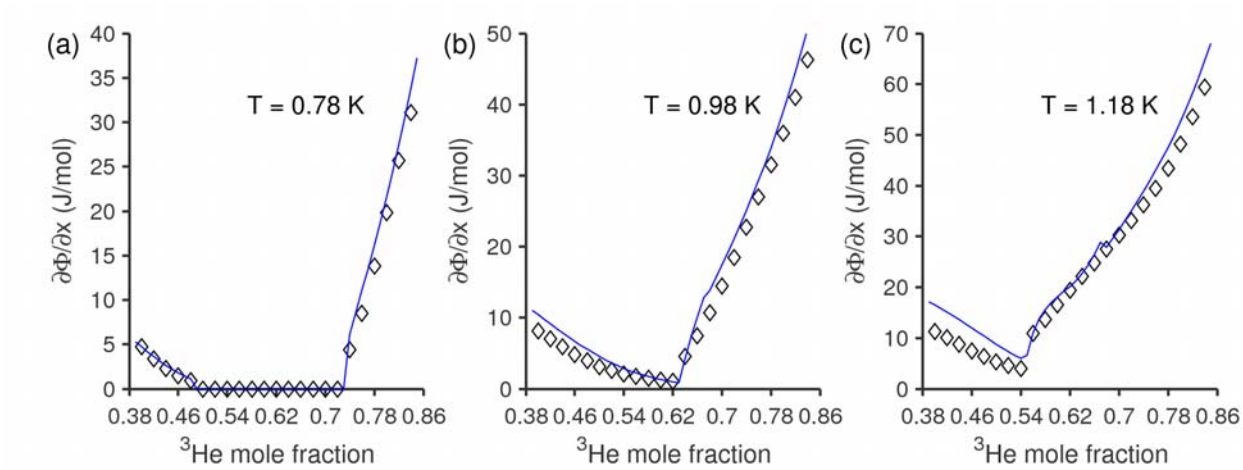

Figure 5.3: *A comparison of the inverse concentration susceptibility* $\partial\Phi / \partial x$ *from Goellner et al [13] (markers) and this work (solid lines).*

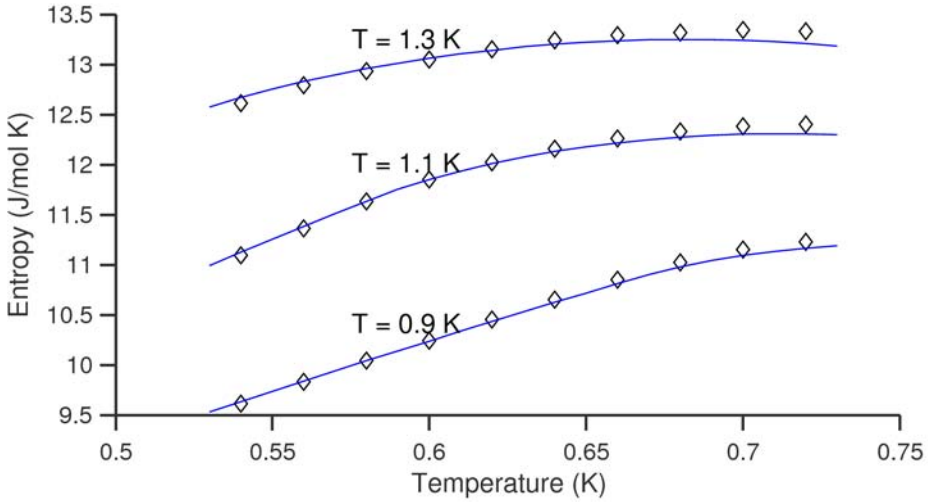

Figure 5.4: *A comparison of entropies at 0.9 K, 1.1 K and 1.3 K from Islander and Zimmermann [12] (markers) and this work (solid lines).*

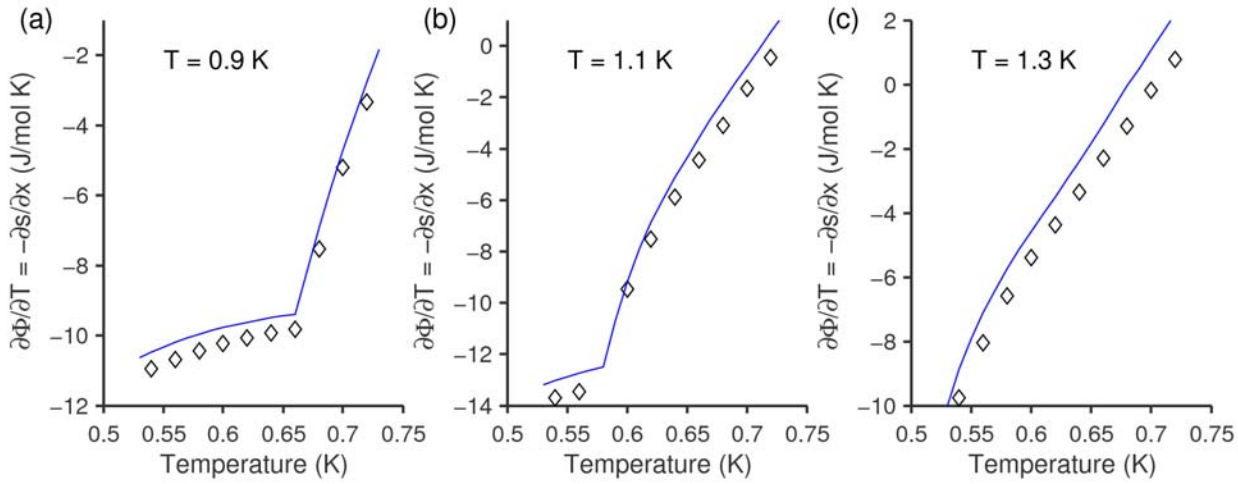

Figure 5.5: *A comparison of* $(\partial\Phi/\partial T)_x$ *(which is also equal to* $(-\partial s/\partial x)_T$ *by a Maxwell relation) from Islander and Zimmermann's [12] (markers) and this work (solid lines).*

Lines of constant μ_4 calculated from our model are compared with those tabulated by Radebaugh at four different values of μ_4, in Figure 5.6. The correspondence is quite good, which is not unexpected, since all the lines in this plot are at low values of x.

Figure 5.7 shows a comparison of C_{μ_4} from our model and from Radebaugh's tables. As discussed earlier (in Section 4.1), the values are expected to be very different at temperatures above about 0.8 K, when the ^{4}He excitations start contributing to C_{μ_4}. (Radebaugh's definition of C_{μ_4} does not incorporate the ^{4}He component of the mixture.) At lower temperatures, however, a comparison is appropriate. The C_{μ_4} values match well at low values of T_{ps} (the temperature at which the constant-μ_4 line intersects the dilute phase-separation curve), but not quite as well at higher values. The kinks in our calculated specific heats are relics of the kinks in $(\partial\mu_4/\partial x)_T$ across $x = 0.08$.

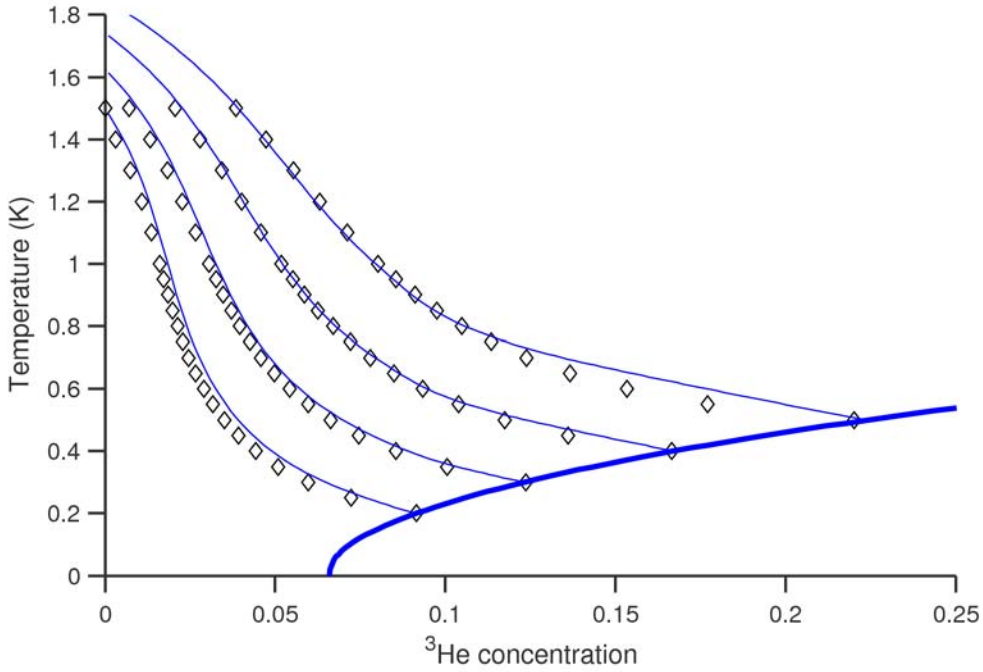

Figure 5.6: *Lines of constant μ_4. The solid lines represent values calculated in this work. The markers represent Radebaugh's tabulated values.*

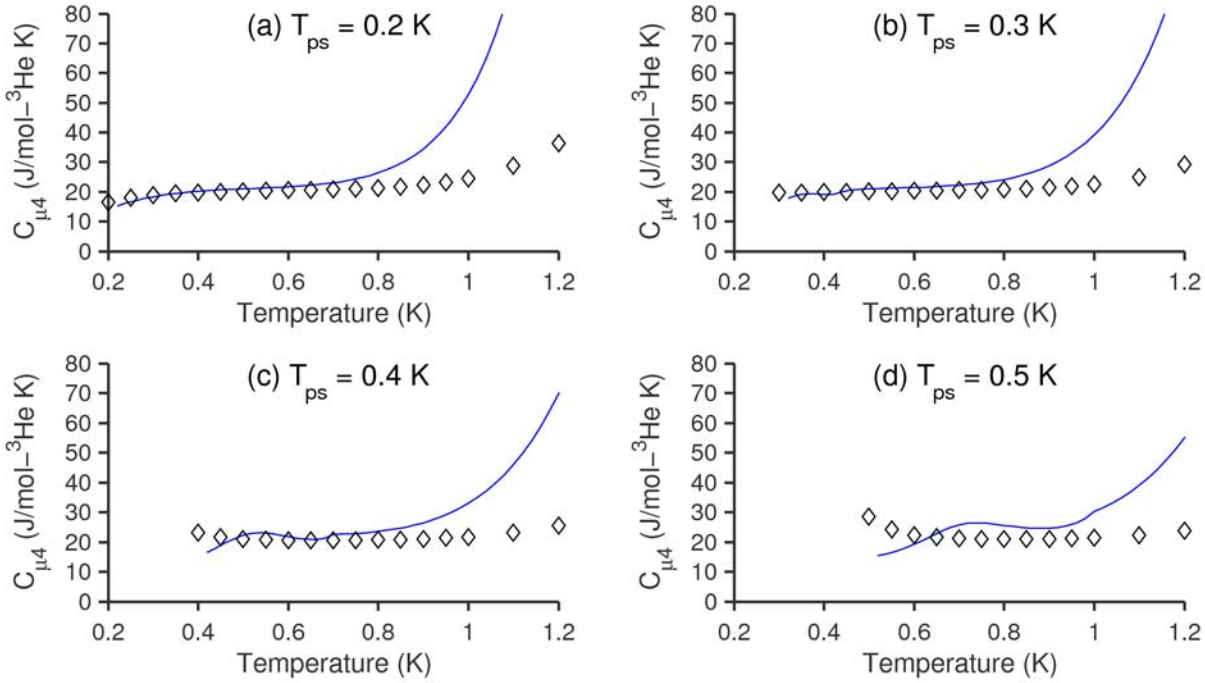

Figure 5.7: *A comparison of specific heats (per mole of ^{3}He) at constant μ_4 and pressure from Radebaugh (hollow markers) and this work (solid lines). The values of T_{ps} represent the temperatures at which the corresponding lines of constant μ_4 intersect the dilute phase-separation curve*

Figure 5.8 shows a comparison of calculated values of the specific heat at constant x and p (C) and the derivative $\partial C / \partial T$ very near the λ-line (within 0.1 K) with measurements made by Gasparini and Moldover [36]. The measurements that overlap with our calculated values are restricted to the He-II region (i.e., temperatures below the λ-transition) and include specific heats at x = 0.20 (only a slight overlap) and x = 0.39, and the derivatives at x = 0.39. The values of the specific heat are in good agreement; however, the temperature derivative is accurate only to within about $10^{-1.5}$ (or about 0.03) K of the λ-line. Our calculated temperature derivatives are much smaller; on reflection, this is not surprising, since in the He-II region, our specific heat fit contained only polynomial terms and not the rapidly changing logarithmic terms (see Section 2.5). However, it was always unlikely that the model would yield accurate derivatives of the specific heat near the λ-line, since the available experimental data used for fitting was really not good enough for that purpose. Nevertheless, this is not a major issue, given the intended applications of this work.

There are discrepancies with the data of London et al [11], who measured the osmotic pressure of ^{3}He-^{4}He mixtures at three temperatures – 0.8 K, 1.0 K and 1.2 K. Their data is shown in Figure 5.9 which is adapted from their paper. The osmotic pressure is plotted as a function of the mixture molar volume per mole of ^{3}He, (which we will call v_{3He} and which is equal to the molar volume per mole of mixture v divided by the ^{3}He concentration x). A value of v_{3He} = 150 cm^3/mol-^{3}He corresponds to a ^{3}He concentration of about 19%; v_{3He} = 70 cm^3/mol-^{3}He corresponds to a ^{3}He concentration of about 45%. Superimposed on it are osmotic pressure values calculated from our model. At 0.8 K, the correspondence is quite good at lower values of v_{3He}, below about 80 cm^3/mol-^{3}He (which corresponds to $x \approx 0.375$). At higher values of v_{3He}, the values diverge – the differences are about 5 cmHg (about 6500 Pa), which corresponds to a 10% error. Similar magnitudes of errors are seen at 1.0 K and 1.2 K, for which available data is restricted to more than 100 cm^3/mol-^{3}He ($x \approx 0.30$) and 125 cm^3/mol-^{3}He ($x \approx 0.25$) respectively. These errors seem to indicate that the calculated values of μ_4 in the region of x = 0.2-0.3 are not very accurate, a fault that was discussed previously, in Section 2.5. (Note that even at 1.0 K, the error starts reducing around the 100 cm^3/mol-^{3}He, or $x \approx 0.30$, mark.) If we assume that London et al's values are accurate, our calculated values of μ_4 are too high by about 0.2 J/mol-^{4}He around x = 0.25.

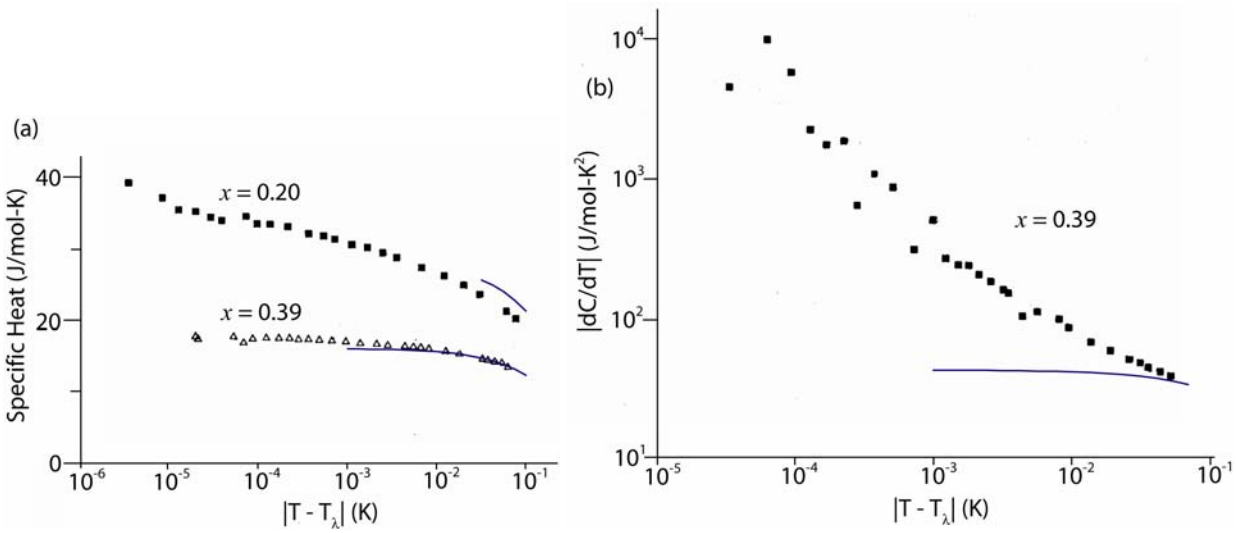

Figure 5.8: *Comparisons of (a) the specific heat, and (b) $\partial C / \partial T$ near the λ-line. The markers represent the data of Gasparini and Moldover [36]. The solid lines represent values calculated in this work.*

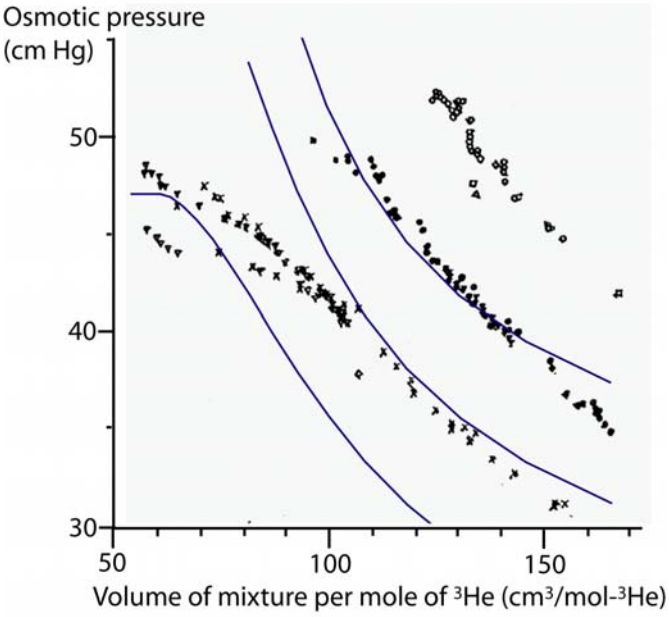

Figure 5.9: *Osmotic pressure as a function of molar volume per mole of ^{3}He at three different temperatures (from bottom to top): 0.8 K, 1.0 K and 1.2 K. The markers are from London et al [11]; the lines are the values calculated in this work. 1 cmHg = 1333 Pa.*

Interestingly, Radebaugh's calculated osmotic pressures [1] are in better agreement with London et al's data. His calculated values lie within the scatter of the data at 1.0 K and 1.2 K, and lie about midway between the data and our calculated values at 0.8 K.

The osmotic pressures are in much better agreement with experimental data at lower ^{3}He concentrations; a comparison with data at 0.26 atm and 10 atm is presented in the following section.

5.2 Review of the high-pressure model

Unfortunately, the lack of high-pressure measurements on ^{3}He-^{4}He mixtures precludes a thorough comparison of the calculated properties with experimental data. In Figure 5.10, the molar volume measurements of Boghosian and Meyer made at 1.25 K [55] are compared with results from our model. The correspondence is quite good, considering that the only high pressure data included in the fitting function to determine the molar volume was restricted to temperatures below 0.7 K.

The osmotic pressures calculated from the high-pressure model are in good agreement with the data of Landau et al [25] at 0.26 atm and 10 atm (Figure 5.11). Landau et al's data is all at low temperatures where molar volume data was available for use in the model; it doesn't help test the model at high temperatures.

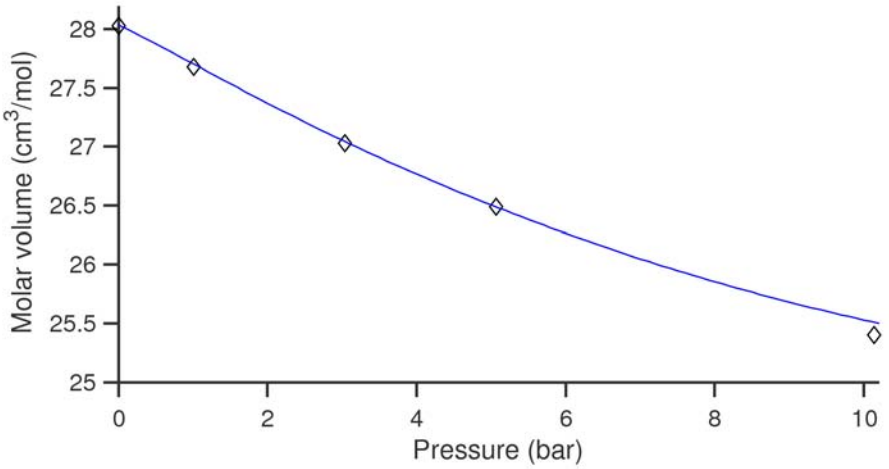

Figure 5.10: *Molar volumes for a 6%-^{3}He solution at 1.25 K, from Boghosian and Meyer [55] (diamond markers), and from the fit of Eq. 3.21 (solid line)*

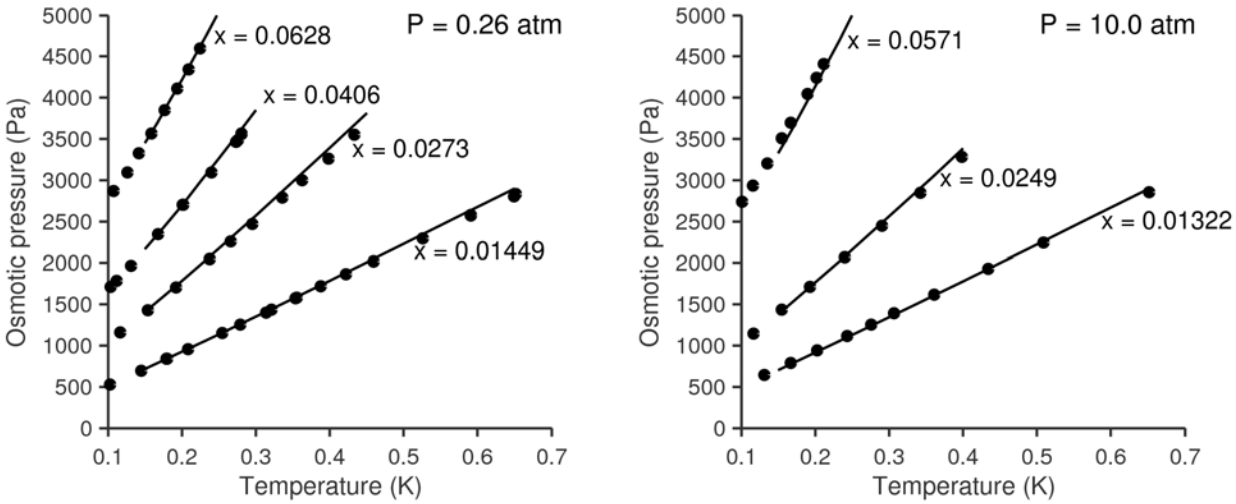

Figure 5.11: *A comparison of osmotic pressures from Landau et al [25] (markers), and from this work (solid lines).*

At this point, it is worth recapitulating where the property model is likely to be accurate and where it is questionable. The model is based on two sources of molar volume measurements: (i) in the He-II region, below 0.7 K and 10 bar, and, (ii) at saturated pressure, for all mixture concentrations and between 0.55 K and 1.5 K.

Since we basically ignore the λ-transition at high pressures, all the characteristics associated with the λ-transition appear at the temperature associated with the transition at zero pressure, rather than at the temperature associated with the transition at the appropriate pressure. This affects only a small area of the T - x plane though. From Figure 3.4, it is apparent that the λ-transition temperature does not change by more than 0.1 K from 0 to 10 bar.

The thermodynamic properties which depend exclusively or largely on the (integral of the) molar volume (and not its derivatives), such as g and h (the enthalpy depends on $\partial v / \partial T$ as well as the molar volume, but the derivative term is much smaller), are expected to be accurate in the high-pressure, low-

temperature He-II region, and low-pressure, high-temperature regions. In addition, since the deviation of the molar volume of a real mixture from that of an "ideal" mixture (i.e., $v - xv_3^0 - (1-x)v_4^0$) is quite small everywhere, these properties should be reasonably accurate even at high temperatures and pressures, where no actual experimental data was available and we were forced to extrapolate our fit. For example, at the beginning of this section, the fit was shown to be in very good agreement with the high-p, high-T molar volumes of Boghosian and Meyer [55].

Properties that depend on the integral of the derivatives of the molar volume (such as s and μ_4) are also expected to be accurate in the high-p, low-T (sub-0.7 K), He-II region and low-p, high-T region, except near the λ-surface. At high temperatures and high pressures (as well as at high pressures in the He-I region), the derivatives calculated from the fit may not be good enough to calculate accurate values of the entropy and ^{4}He chemical potential. Of course, the pressure derivative of entropy, $\partial s / \partial p$, which is equal to $-\partial v / \partial T$, is expected to be quite small; therefore, the entropy is not expected to change very much from low pressure to high pressure along a line of constant T and constant x (see Figure 3.15, for example). It is also worth adding that μ_4 depends on the values of v to a greater extent than those of $(\partial v / \partial x)$, especially in the He-II region. (Recall that $\partial \mu_4 / \partial p$ is equal to $v - x(\partial v / \partial x)$, from Eq. 3.4. Values of $(\partial v / \partial x)$ are typically 3-4 times less than the corresponding values of v. Additionally, in the He-II region, values of x are of the order of, or less than, 0.5; this further reduces the magnitude of the $(\partial v / \partial x)$ term.)

The uncertainties associated with properties that depend on the second derivatives of the molar volume (specific heat and $\partial^2 g / \partial x^2$) are greater, though, as discussed earlier, the specific heat is not expected to change very much with pressure except near the λ-surface. For small changes in pressure, the variation of the specific heat with pressure may be neglected.

Chapter 6: Conclusion

This thesis presents properties of liquid ^{3}He-^{4}He mixtures at temperatures below 1.8 K, pressures of up to 10 bar, and across the entire concentration range. Verily, this significantly extends the range of available thermodynamic data for these mixtures, the previous most extensive set of properties being restricted to saturated pressure and ^{3}He concentrations below 30%.

The calculations were performed in two stages. First, properties were calculated as a function of temperature and concentration at zero pressure, between temperatures of 0.15 K and 1.8 K in the He-II region, and between temperatures of 0.15 K and 1.5 K in the He-I region. Together with the calculations of Kuerten et al (below 0.15 K), these provide a complete set of thermodynamic properties up from 0 K. The calculated properties are generally in good agreement with other measurements, though there are discrepancies with the osmotic pressure at ^{3}He concentrations in the area of 25% at high temperatures. A shortcoming of the calculation procedure is that higher derivatives of properties (the third derivatives of entropy and enthalpy) are discontinuous at a couple of values of x.

Properties were then extended to pressures of up to 10 bar (between temperatures of 0.15 K and 1.5 K). The calculations were based on the zero-pressure model and available measurements of the molar volume. The calculations are expected to be quite good at low temperatures (below 0.7 K) in the He-II region, and also at low pressures everywhere. Because of the lack of experimental data at high temperatures and high pressures (the only available data at temperatures above 0.7 K was for zero-pressure mixtures, and for pure ^{4}He and pure ^{3}He), the calculated properties are based on extrapolations; consequently, some of them (specifically, the ones which strongly depend on derivatives of the molar volume) are quite questionable in those regions. Additionally, the high-pressure calculations are not expected to be accurate in the vicinity of the λ-surface.

6.1 Ruminations on a state equation for ^{3}He-^{4}He mixtures

It is worth emphasising the need for more data on ^{3}He-^{4}He mixtures, to determine an accurate equation of state. Most experimental investigations on these mixtures have been restricted to the saturated-pressure surface, which is reasonably well-covered, although some areas of the saturated-pressure surface have received more attention than others, and there are some discrepancies amongst available data. Additionally, as has been repeatedly emphasised, high-pressure data is quite limited. In theory, once properties are known at saturated-pressure, all that is needed to extend them to high pressure is a p-v-T-x relation for ^{3}He-^{4}He mixtures, provided that the λ- and phase-separation surfaces are completely known (which, currently, they are not). Therefore, the most urgent need is for (a) more widespread molar volume measurements at high pressures and high temperatures, and especially near the λ-surface, (b) specific heat measurements in certain parts of the saturated pressure surface – specifically, in the two-phase region below 0.5 K, where there is no reliable data, and in the single-phase region, to verify the data that is available and help decide whether more measurements are required – and, (c) measurements of the phase-separation and λ-surfaces.

Although they are not required in theory, specific heats and osmotic pressures at high pressures would also be very helpful, since they can be used to verify temperature derivatives and x-derivatives of properties determined from the p-v-T-x relation. This is especially true for properties in the vicinity of the λ-surface, because of sharp changes in properties in that area.

Finally, future work should focus on determining an actual state equation based on the Gibbs or Helmholtz free energy; there are kinks in the properties calculated in this work due to the somewhat fragmented nature of the calculation procedure. (A functional form of the Gibbs free energy can be inferred from this work.) The "overall" state equation would consist of an equation for the single-phase He-II region, an equation for the single-phase He-I region, and a p-T-x relation for the λ-surface.

Acknowledgements

I greatly appreciate the guidance and assistance of my thesis advisor Prof. John Brisson. I would also like to thank my thesis committee members Prof. Ernest Cravalho and Prof. Joseph Smith for their useful feedback, especially Prof. Smith, for some thought-provoking discussions.

Appendix A: Phase diagram, zero-pressure specific heats and molar volume

A.1 ^{3}He-^{4}He phase diagram

A.1.1 Saturated pressure

Tricritical point: $x_t(0) = 0.674,\ T_t(0) = 0.867$ K

Dilute phase-separation curve ($0.08014 < x < 0.674$; $0.15\text{ K} < T < 0.867$ K):

$$x_{\sigma-} - x_t = \frac{-0.209148(T - T_t)}{T - T_t - 0.080280} + 0.960222(T - T_t) + 0.549920(T - T_t)^2 \qquad \text{(A.1)}$$

Concentrated phase-separation curve ($0.674 < x < 1$; $0.15\text{ K} < T < 0.867$ K):

$$x_{\sigma+} - x_t = 0.316170\ (T - T_t)^3 - 0.180743\ (T - T_t)^2 - 0.746805\ (T - T_t) \qquad \text{(A.2)}$$

Lambda curve:

$$T_\lambda - T_t = -2.620259(x - x_t) - 1.023726(x - x_t)^2 \qquad \text{(A.3)}$$

A.1.2 All pressures

Tricritical line:

Temperature (in K) along the tricritical line as a function of pressure (in bar):

$$T_t(p) - T_t(0) = -\frac{0.12992576\,p}{p + 2.5967345} - 6.457263\times10^{-4}\,p \qquad \text{(A.4)}$$

Concentration along the tricritical line as a function of temperature (in K):

$$x_t(p) - x_t(0) = 0.3037124\left[T_t(0) - T_t(p)\right] - 4.41225\times10^{6}\left[T_t(0) - T_t(p)\right]^9 \qquad \text{(A.5)}$$

Dilute phase-separation surface:

$$x_{\sigma-}(T, p) - x_t(p) = \frac{K_{\sigma-,0}(p)\ \left(T - T_t(p)\right)}{\left(T - T_t(p)\right) - K_{\sigma-,a}(p)} + K_{\sigma-,1}(p)\left(T - T_t(p)\right) + K_{\sigma-,2}(p)\left(T - T_t(p)\right)^2 \qquad \text{(A.6)}$$

where $K_{\sigma-,i}(p) = K_{\sigma-,i0} + K_{\sigma-,i1}\,p + K_{\sigma-,i2}\,p^2 \quad (i = 0, 1, 2, a)$ (A.7)

Concentrated phase-separation surface:

$$x_{\sigma+}(T, p) - x_t(p) = K_{\sigma+,1}(p)\left(T - T_t(p)\right) + K_{\sigma+,2}(p)\left(T - T_t(p)\right)^2 + K_{\sigma+,3}(p)\left(T - T_t(p)\right)^3 \qquad \text{(A.8)}$$

where $K_{\sigma+,i}(p) = K_{\sigma+,i0} + K_{\sigma+,i1}\,p + K_{\sigma+,i2}\,p^2 \quad (i = 1,\ 2,\ 3)$ (A.9)

λ-surface:

$$T_\lambda(x,p) - T_t(p) = K_{\lambda 1}(p)\big(x - x_t(p)\big) + K_{\lambda 2}(p)\big(x - x_t(p)\big)^2 \tag{A.10}$$

where $K_{\lambda i}(p) = K_{\lambda i0} + K_{\lambda i1} p + K_{\lambda i2} p^2 \quad (i = 1,\ 2)$ (A.11)

Table 1: Coefficients for the dilute phase, concentrated phase, and λ-surface fits (Eqs. A.7, A.9 and A.11)

	j = 0	j = 1	j = 2
$K_{\sigma-,0j}$	-0.209148	-0.1269791 bar $^{-1}$	0.0102283 bar $^{-2}$
$K_{\sigma-,1j}$	0.960222 K^{-1}	-0.2165742 K^{-1} bar $^{-1}$	0.0169801 K^{-1} bar $^{-2}$
$K_{\sigma-,2j}$	0.549920 K^{-2}	-0.1198491 K^{-2} bar $^{-1}$	0.0092997 K^{-2} bar $^{-2}$
$K_{\sigma-,aj}$	0.080280 K	0.02291499 K bar $^{-1}$	-0.0020886 K bar $^{-2}$
$K_{\sigma+,1j}$	-0.746805 K^{-1}	0.0173549 K^{-1} bar $^{-1}$	-0.0028598 K^{-1} bar $^{-2}$
$K_{\sigma+,2j}$	-0.180743 K^{-2}	0.1120251 K^{-2} bar $^{-1}$	-0.0152076 K^{-2} bar $^{-2}$
$K_{\sigma+,3j}$	0.316170 K^{-3}	0.1723264 K^{-3} bar $^{-1}$	-0.0201411 K^{-3} bar $^{-2}$
$K_{\lambda 1j}$	-2.620259 K	0.0024823 K bar $^{-1}$	0.0009255 K bar $^{-2}$
$K_{\lambda 2j}$	-1.023726 K	0.0013175 K bar $^{-1}$	0.0009397 K bar $^{-2}$

A.2 Specific heats at zero pressure

A.2.1 Specific heat in the two-phase region

The specific heat fits in the two-phase region are:

$$\frac{C_{2\phi,t}}{T} = \begin{cases} \sum_{i=0}^{5} A_{2\phi,1i} T^i, & T < 0.15K \\ \sum_{i=0}^{5} A_{2\phi,2i} T^i, & T > 0.15K \end{cases} \tag{A.12}$$

and

$$\frac{1}{T}\left(\frac{\partial C_{2\phi}}{\partial x}\right)_T = \begin{cases} \sum_{i=0}^{5} B_{2\phi,1i} T^i, & T < 0.15K \\ \sum_{i=0}^{5} B_{2\phi,2i} T^i, & T > 0.15K \end{cases} \tag{A.13}$$

Table 2: Coefficients for the zero-pressure, two-phase specific heat fits (Eqs. A.12 and A.13)

	$C_{2\phi,t}/T$		$\left(\partial C_{2\phi}/dx\right)_T/T$	
i	$A_{2\phi,1i}$	$A_{2\phi,2i}$	$B_{2\phi,1i}$	$B_{2\phi,2i}$
5	44976.189 J/mol-K^7	-253.38487 J/mol-K^7	-116022.79 J/mol-K^7	-328.83486 J/mol-K^7
4	-27191.567 J/mol-K^6	748.45512 J/mol-K^6	56440.812 J/mol-K^6	927.34209 J/mol-K^6
3	7532.3747 J/mol-K^5	-867.12111 J/mol-K^5	-7421.4648 J/mol-K^5	-998.13371 J/mol-K^5
2	-963.11275 J/mol-K^4	466.88150 J/mol-K^4	74.625853 J/mol-K^4	500.33736 J/mol-K^4
1	12.661883 J/mol-K^3	-112.07332 J/mol-K^3	-13.057881 J/mol-K^3	-117.76463 J/mol-K^3
0	17.221625 J/mol-K^2	21.395625 J/mol-K^2	17.074164 J/mol-K^2	20.841016 J/mol-K^2

A.2.2 Specific heat in the single-phase region

Specific heat of pure ^{3}He:

$$C_3^0(T) = \sum_{i=0}^{3} A_{31,i} T^i + \frac{A_{32}}{T^2} e^{-\frac{\Delta_3}{T}} \tag{A.14}$$

Specific heat of pure ^{4}He:

$$C_4^0(T) = \sum_{i=1}^{5} A_{41,i} T^{i+2} + A_{42}\left(\frac{\Delta_r}{T}\right)^{\frac{3}{2}} e^{-\frac{\Delta_r}{T}}\left(1+\frac{T}{\Delta_r}+\frac{3}{4}\left(\frac{T}{\Delta_r}\right)^2\right) + \frac{A_{43}}{T}\left(\frac{\Delta_m}{T}\right)^2 e^{-\frac{\Delta_m}{T}}\left(1-2\frac{T}{\Delta_m}\right) \tag{A.15}$$

Table 3: Coefficients for the pure-^{3}He and pure-^{4}He specific heat fits (Eqs. A.14 and A.15)

^{3}He specific heat fit (Eq. A.14)		^{4}He specific heat fit (Eq. A.15)	
$A_{31,0}$	3.6851551 J/mol-K	$A_{41,1}$	0.082180127 J/mol-K^4
$A_{31,1}$	-1.9650072 J/mol-K^2	$A_{41,2}$	0
$A_{31,2}$	3.3601049 J/mol-K^3	$A_{41,3}$	-0.08745899 J/mol-K^6
$A_{31,3}$	-0.8351251 J/mol-K^4	$A_{41,4}$	0.12912758 J/mol-K^7
A_{32}	-0.0444842 J-K/mol	$A_{41,5}$	-0.0066314726 J/mol-K^8
Δ_3	0.0977175 K	A_{42}	70.198836 J/mol-K
		A_{43}	10244.198 J/mol
		Δ_r	8.8955141 K
		Δ_m	22.890183 K

Specific Heat in the He-II region:

$$C_{1\phi,II}(x,T) = xC_3^0(T) + (1-x)C_4^0(T) + x(1-x)C_{r,II}(x,T) \tag{A.16}$$

$$C_{r,II}(x,T) = \sum_{i=0}^{4}\sum_{j=0}^{4} A_{II,1,ij} x^i T^j \tag{A.17}$$

Table 4: Coefficients for the He-II specific heat correction term $C_{r,II}$ (Eq. A.17)

	$i = 0$	$i = 1$	$i = 2$	$i = 3$	$i = 4$
$A_{II,1,i0}$ (J/mol-K)	9.6988805	-84.656877	399.83199	534.18242	-694.57528
$A_{II,1,i1}$ (J/mol-K^2)	4.7441717	295.311	-2308.6299	-203.72526	945.31218
$A_{II,1,i2}$ (J/mol-K^3)	-14.794634	-291.36925	3456.284	-217.44213	526.21775
$A_{II,1,i3}$ (J/mol-K^4)	9.9291158	-116.30633	-854.18794	-1966.9463	-825.63046
$A_{II,1,i4}$ (J/mol-K^5)	0.9703338	150.36076	-389.46725	1305.9875	427.69316

Specific Heat in the He-I region:

$$C_{1\phi,I}(x,T) = xC_3^0(T) + (1-x)C_4^0(T) + x(1-x)C_{r,I}(x,T) \tag{A.18}$$

$$C_{r,I}(x,T) = \sum_{i=0}^{4}\sum_{j=0}^{4} A_{I,1,ij}\, x^i T^j + \sum_{i=0}^{4}\sum_{j=1}^{2} A_{I,2,ij}\, x^i T^j \ln(T - T_\lambda(x) + 0.0005) \tag{A.19}$$

Table 5: Coefficients for the He-I specific heat correction term $C_{r,I}$ (Eq. A.19)

	$i = 0$	$i = 1$	$i = 2$	$i = 3$	$i = 4$
$A_{I,1,i0}$ (J/mol-K)	760.89769	-503.0258	-809.27998	981.80849	-359.94357
$A_{I,1,i1}$ (J/mol-K^2)	-1333.1107	1131.8413	27.790349	-964.41177	963.42302
$A_{I,1,i2}$ (J/mol-K^3)	1.6484326	1248.4679	862.0627	-2190.7539	109.28068
$A_{I,1,i3}$ (J/mol-K^4)	540.59753	-1686.35	1133.5978	-1613.3837	1681.1155
$A_{I,1,i4}$ (J/mol-K^5)	107.16714	-1106.944	2728.7355	-2216.2144	523.34653
$A_{I,2,i1}$ (J/mol-K^2)	-1089.0449	4109.1861	-5393.9818	2533.6508	-9.4543704
$A_{I,2,i2}$ (J/mol-K^3)	361.81709	-352.22262	-2374.6527	5329.7792	-3305.5548

A.3 Molar volumes

Molar volume of a (single-phase) ^{3}He-^{4}He mixture:

$$v(p,T,x) = xv_3^0(p,T) + (1-x)v_4^0(p,T) + x(1-x)v_r(p,T,x) \tag{A.20}$$

$$v_4^0(T,p) = \left(\sum_{i=0\text{ to }9} V_{40,i}\, p^i\right)\left[1 + \left(\frac{A_1}{(p-p_c)^2} + \frac{A_2}{(p-p_c)^{5/3}}\right)\frac{T^4}{4} - (B_0 + B_1 p)\,\mathrm{Erfc}\sqrt{\frac{\sum_{i=0\text{ to }2}\Delta_i p^i}{T}}\right] \tag{A.21}$$

$$v_3^0 = \sum_{\substack{i=0\text{ to }3\\ j=0\text{ to }2}} V_{31,ij}\, T^i p^j + \frac{1}{V_{32,2}\,p^2 + V_{32,0}} \tag{A.22}$$

$$v_r(p,T,x) = \sum_{\substack{i=0 \text{ to } 3 \\ j=0 \text{ to } 3}} x^i T^j \left(\sum_{k=0 \text{ to } 2} V_{r1,ijk}\, p^k + V_{r2,ij} \frac{1}{p + p_{vr}} \right) \quad \text{(A.23)}$$

Table 6: Coefficients for the pure ^{4}He molar volume (Eq. A.21) from Tanaka et al [57]

$V_{40,0}$	2.757930 x 10^{-5} m^3/mol	Δ_0	8.618 K
$V_{40,1}$	-3.361585 x 10^{-12} m^3/mol-Pa	Δ_1	-7.487 x 10^{-7} K/Pa
$V_{40,2}$	1.602419 x 10^{-18} m^3/mol-Pa^2	Δ_2	5.308 x 10^{-14} K/Pa^2
$V_{40,3}$	-1.072604 x 10^{-24} m^3/mol-Pa^3	A_1	1.863 x 10^8 Pa^2/K^4
$V_{40,4}$	7.979064 x 10^{-31} m^3/mol-Pa^4	A_2	7.664 x 10^6 $Pa^{5/3}/K^4$
$V_{40,5}$	-5.356076 x 10^{-37} m^3/mol-Pa^5	p_c	-1.00170 x 10^6 Pa
$V_{40,6}$	2.703689 x 10^{-43} m^3/mol-Pa^6	B_0	2.191
$V_{40,7}$	-9.004790 x 10^{-50} m^3/mol-Pa^7	B_1	-1.702 x 10^{-7} 1/Pa
$V_{40,8}$	1.725962 x 10^{-56} m^3/mol-Pa^8		
$V_{40,9}$	-1.429411 x 10^{-63} m^3/mol-Pa^9		

Table 7: Coefficients for the pure ^{3}He molar volume (Eq. A.22)

	$j = 0$	$j = 1$	$j = 2$
$V_{31,0\,j}$	40.723012 cm^3 mol^{-1}	-1.3151948 cm^3 mol^{-1} bar^{-1}	0.0409498 cm^3 mol^{-1} bar^{-2}
$V_{31,1\,j}$	-0.6614794 cm^3 mol^{-1} K^{-1}	0.1275125 cm^3 mol^{-1} K^{-1} bar^{-1}	-0.0091931 cm^3 mol^{-1} K^{-1} bar^{-2}
$V_{31,2\,j}$	0.5542147 cm^3 mol^{-1} K^{-2}	-0.1527959 cm^3 mol^{-1} K^{-2} bar^{-1}	0.0113764 cm^3 mol^{-1} K^{-2} bar^{-2}
$V_{31,3\,j}$	0.1430724 cm^3 mol^{-1} K^{-3}	-0.0034712 cm^3 mol^{-1} K^{-3} bar^{-1}	-0.0008515 cm^3 mol^{-1} K^{-3} bar^{-2}
$V_{32,\,j}$	-0.2603492 mol cm^{-3}	-	-0.0051946 mol cm^{-3} bar^{-2}

Table 8: Coefficients for the ^{3}He-^{4}He mixture molar volume correction term v_r (Eq. A.23). These values yield v_r in cm^3/mol when the pressure is in bar and the temperature is in K.

$V_{r1,ij0}$	$i = 0$	$i = 1$	$i = 2$	$i = 3$	$V_{r1,ij1}$	$i = 0$	$i = 1$	$i = 2$	$i = 3$
$j = 0$	0.1389646	-4.933308	-4.4736292	-17.763600	$j = 0$	-0.0706271	2.0430264	1.9707327	1.2116373
$j = 1$	-2.5679051	40.217899	21.103275	-17.585800	$j = 1$	0.8984671	-13.570937	1.2376227	0.3340713
$j = 2$	0.5113374	-83.295844	42.535669	-2.7419703	$j = 2$	-0.1993514	18.303655	-9.101332	7.5264822
$j = 3$	3.9851834	16.616527	32.247635	-21.867304	$j = 3$	-1.372463	2.3961147	-18.726933	7.8044314
$V_{r1,ij2}$	$i = 0$	$i = 1$	$i = 2$	$i = 3$	$V_{r2,ij}$	$i = 0$	$i = 1$	$i = 2$	$i = 3$
$j = 0$	0.010287	-0.1641865	-0.2765908	0.0781768	$j = 0$	-1.1647447	-8.2289003	-5.7908683	62.107622
$j = 1$	-0.0599619	0.972759	0.2888217	-0.3641635	$j = 1$	-4.5046372	24.648775	-104.81653	8.1406542
$j = 2$	-0.0262424	-0.9242861	-0.6437575	0.5378945	$j = 2$	10.15904	31.640583	29.677981	4.3197622
$j = 3$	0.1356818	-0.5426784	2.2866511	-1.3449638	$j = 3$	-11.353903	4.2288385	-81.740459	32.623983
p_{vr}	1.7867623								

Appendix B: Thermodynamic properties at zero pressure

Figure 2.19 shows the relevant appendices where equations for the two-phase, single-phase He-II and single-phase He-I regions are listed.

B.1 Properties in the two-phase region:

$$s(x,T) = (x - x_t)\int_0^T \frac{1}{T}\frac{\partial C_{2\phi}}{\partial x}dT + \int_0^T \frac{C_{2\phi,t}}{T}dT \tag{B.1}$$

$$h(x,T) = \left(\left(\frac{\partial h}{\partial x}\right)_{2\phi,0K} + \int_0^T \frac{\partial C_{2\phi}}{\partial x}dT\right)(x - x_t) + \int_0^T C_{2\phi,t}dT + h(x_t,0) \tag{B.2}$$

$$g(x,T) = h - Ts = \left(\left(\frac{\partial h}{\partial x}\right)_{2\phi,0K} + \int_0^T \frac{\partial C_{2\phi}}{\partial x}dT - T\int_0^T \frac{1}{T}\frac{\partial C_{2\phi}}{\partial x}dT\right)(x - x_t) + \int_0^T C_{2\phi,t}dT - T\int_0^T \frac{C_{2\phi,t}}{T}dT + h(x_t,0) \tag{B.3}$$

$$\mu_4(T) = g - x\left(\frac{\partial g}{\partial x}\right)_T = -x_t\left(\left(\frac{\partial h}{\partial x}\right)_{2\phi,0K} + \int_0^T \frac{\partial C_{2\phi}}{\partial x}dT - T\int_0^T \frac{1}{T}\frac{\partial C_{2\phi}}{\partial x}dT\right) + \int_0^T C_{2\phi,t}dT - T\int_0^T \frac{C_{2\phi,t}}{T}dT + h(x_t,0) \tag{B.4}$$

In Eqs. B.1-B.4, $h(x_t,0) = -0.01986$ J/mol, and $(dh/dx)_{2\phi,0K} = 0.0609$ J/mol. The values were inferred from Kuerten et al's [2] tables.

B.2 Properties in the single-phase He-II region

Properties in the single-phase He-II region above 0.15 K can be obtained by substituting the He-II specific heat expression (Eq. A.16) into the following equations. For properties below 0.15 K, please refer to Kuerten et al [2]. Some of their properties are listed in Table 10 in Section E.1.

B.2.1 Properties for ^{3}He concentrations of less than 8.014%

$$g(x,T) = h_{0.15}(x) - Ts_{0.15}(x) + \int_{0.15K}^{T} C_{1\phi,II}(x,T)dT - T\int_{0.15K}^{T} \frac{C_{1\phi,II}(x,T)}{T}dT \tag{B.5}$$

$$s(x,T) = s_{0.15}(x) + \int_{0.15K}^{T} \frac{C_{1\phi,II}(x,T)}{T}dT \tag{B.6}$$

$$h(x,T) = h_{0.15}(x) + \int_{0.15K}^{T} C_{1\phi,II}(x,T)dT \tag{B.7}$$

$$\mu_4(x,T) = \left(h_{0.15} - x\left(\frac{\partial h}{\partial x}\right)_{0.15K} \right) - T\left(s_{0.15} - x\left(\frac{\partial s}{\partial x}\right)_{0.15K} \right) + \int_{0.15K}^{T} C_{1\phi,II}(x,T)dT$$
$$- T\int_{0.15K}^{T} \frac{C_{1\phi,II}(x,T)}{T}dT - x\left(\int_{0.15K}^{T} \frac{\partial C_{1\phi,II}(x,T)}{\partial x}dT - T\int_{0.15K}^{T} \frac{1}{T}\frac{\partial C_{1\phi,II}(x,T)}{\partial x}dT \right) \quad \text{(B.8)}$$

$h_{0.15}(x)$ and $s_{0.15}(x)$ are the enthalpy and entropy at 0.15 K, and $\left(\partial h/\partial x\right)_{0.15K}$ and $\left(\partial s/\partial x\right)_{0.15K}$ are the derivatives of the enthalpy and entropy with respect to x at constant temperature (T = 0.15 K). All these quantities are calculated from Kuerten et al's model. These quantities are tabulated in Table 9 for some values of x.

Table 9: Properties at 0.15 K calculated from Kuerten et al's model

^{3}He concentration	0.01	0.02	0.03	0.04	0.05	0.06	0.07	0.08
$h_{0.15}(x)$ (J/mol)	-0.0055	-0.0085	-0.0092	-0.0080	-0.0050	-0.0004	0.0056	0.0129
$s_{0.15}(x)$ (J/mol-K)	0.271	0.433	0.559	0.663	0.752	0.830	0.900	0.963
$\left(\partial h/\partial x\right)_{0.15K}$ (J/mol)	19.105	14.049	11.347	9.5776	8.3117	7.3626	6.6243	6.0332
$\left(\partial s/\partial x\right)_{0.15K}$ (J/mol-K)	-0.4166	-0.1811	0.0284	0.2143	0.3807	0.5309	0.666	0.7867

B.2.2 Properties for ^{3}He concentrations of more than 8.014%

$$g(x,T) = h_{\sigma-}(x) - Ts_{\sigma-}(x) + \int_{T_{\sigma-}(x)}^{T} C_{1\phi,II}(x,T)dT - T\int_{T_{\sigma-}(x)}^{T} \frac{C_{1\phi,II}(x,T)}{T}dT \quad \text{(B.9)}$$

$$s(x,T) = s_{\sigma-}(x) + \int_{T_{\sigma-}(x)}^{T} \frac{C_{1\phi,II}(x,T)}{T}dT \quad \text{(B.10)}$$

$$h(x,T) = h_{\sigma-}(x) + \int_{T_{\sigma-}(x)}^{T} C_{1\phi,II}(x,T)dT \quad \text{(B.11)}$$

$$\mu_4(x,T) = \left(h_{\sigma-} - x\left(\frac{\partial h}{\partial x}\right)_{2\phi,T=T_{\sigma-}} \right) - T\left(s_{\sigma-} - x\left(\frac{\partial s}{\partial x}\right)_{2\phi,T=T_{\sigma-}} \right) - x\frac{dT_{\sigma-}}{dx}\left(1 - \frac{T}{T_{\sigma-}}\right)\left(\left(C_{2\phi}\right)_{T_{\sigma-}} - \left(C_{1\phi,II}\right)_{T_{\sigma-}}\right)$$
$$+ \int_{T_{\sigma-}(x)}^{T} C_{1\phi,II}(x,T)dT - T\int_{T_{\sigma-}(x)}^{T} \frac{C_{1\phi,II}(x,T)}{T}dT$$
$$- x\left(\int_{T_{\sigma-}(x)}^{T} \frac{\partial C_{1\phi,II}(x,T)}{\partial x}dT - T\int_{T_{\sigma-}(x)}^{T} \frac{1}{T}\frac{\partial C_{1\phi,II}(x,T)}{\partial x}dT \right) \quad \text{(B.12)}$$

$T_{\sigma-}(x)$, the temperature at which phase separation occurs at the given value of x, is obtained from Eq. A.1. $h_{\sigma-}(x)$ and $s_{\sigma-}(x)$, the enthalpy and entropy on the dilute phase separation curve, are obtained by substituting $T = T_{\sigma-}(x)$ into Eqs. B.2 and B.1 respectively.

$\left(C_{1\phi,II}\right)_{T_{\sigma-}}$ is the specific heat in the 1-phase region at x and $T = T_{\sigma-}(x)$. $\left(C_{2\phi}\right)_{T_{\sigma-}}$ is the specific heat in the 2-phase region at x and $T = T_{\sigma-}(x)$, or more explicitly,

$$\left(C_{2\phi}\right)_{T_{\sigma-}} = T_{\sigma-}\left[\frac{C_{2\phi,t}}{T} + (x - x_t)\left(\frac{1}{T}\frac{\partial C_{2\phi}}{\partial x}\right)\right]_{T=T_{\sigma-}} \tag{B.13}$$

The 2-phase-region derivatives can be obtained by taking the derivatives (at a constant temperature $T = T_{\sigma-}(x)$) of Eqs. B.2 and B.1, resulting in

$$\left(\frac{\partial h}{\partial x}\right)_{2\phi,T=T_{\sigma-}} = \left(\left(\frac{\partial h}{\partial x}\right)_{2\phi,0K} + \int_0^{T_{\sigma-}} \frac{\partial C_{2\phi}}{\partial x} dT\right) \tag{B.14}$$

and

$$\left(\frac{\partial s}{\partial x}\right)_{2\phi,T=T_{\sigma-}} = \int_0^{T_{\sigma-}} \frac{1}{T}\frac{\partial C_{2\phi}}{\partial x} dT\,. \tag{B.15}$$

B.3 Properties in the single-phase He-I region

Properties in the single-phase He-I region can be obtained by substituting the He-II and He-I specific heat expressions (Eqs. A.16 and A.18) into the equations below.

B.3.1 Properties for ^{3}He concentrations of less than 67.4%

$$g(x,T) = h_{\sigma-}(x) - Ts_{\sigma-}(x) + \int_{T_{\sigma-}(x)}^{T_\lambda(x)} C_{1\phi,II}(x,T)dT - T\int_{T_{\sigma-}(x)}^{T_\lambda(x)} \frac{C_{1\phi,II}(x,T)}{T} dT + \int_{T_\lambda(x)}^{T} C_{1\phi,I}(x,T)dT - T\int_{T_\lambda(x)}^{T} \frac{C_{1\phi,I}(x,T)}{T} dT \tag{B.16}$$

$$s(x,T) = s_{\sigma-}(x) + \int_{T_{\sigma-}(x)}^{T_\lambda(x)} \frac{C_{1\phi,II}(x,T)}{T} dT + \int_{T_\lambda(x)}^{T} \frac{C_{1\phi,I}(x,T)}{T} dT \tag{B.17}$$

$$h(x,T) = h_{\sigma-}(x) + \int_{T_{\sigma-}(x)}^{T_\lambda(x)} C_{1\phi,II}(x,T)dT + \int_{T_\lambda(x)}^{T} C_{1\phi,I}(x,T)dT \tag{B.18}$$

$$\mu_4(x,T) = \left(h_{\sigma-} - x\left(\frac{\partial h}{\partial x}\right)_{2\phi,T=T_{\sigma-}}\right) - T\left(s_{\sigma-} - x\left(\frac{\partial s}{\partial x}\right)_{2\phi,T=T_{\sigma-}}\right) - x\frac{dT_{\sigma-}}{dx}\left(1 - \frac{T}{T_{\sigma-}}\right)\left(\left(C_{2\phi}\right)_{T_{\sigma-}} - \left(C_{1\phi,II}\right)_{T_{\sigma-}}\right)$$
$$- x\frac{dT_\lambda}{dx}\left(1 - \frac{T}{T_\lambda}\right)\left(\left(C_{1\phi,II}\right)_{T_\lambda} - \left(C_{1\phi,I}\right)_{T_\lambda}\right) + \int_{T_{\sigma-}(x)}^{T_\lambda(x)} C_{1\phi,II}(x,T)dT - T\int_{T_{\sigma-}(x)}^{T_\lambda(x)} \frac{C_{1\phi,II}(x,T)}{T} dT$$

$$+\int_{T_\lambda(x)}^{T} C_{1\phi,I}(x,T)dT - T\int_{T_\lambda(x)}^{T}\frac{C_{1\phi,I}(x,T)}{T}dT - x\left(\int_{T_{\sigma-}(x)}^{T_\lambda(x)}\frac{\partial C_{1\phi,II}(x,T)}{\partial x}dT - T\int_{T_{\sigma-}(x)}^{T_\lambda(x)}\frac{1}{T}\frac{\partial C_{1\phi,II}(x,T)}{\partial x}dT\right)$$
$$-x\left(\int_{T_\lambda(x)}^{T}\frac{\partial C_{1\phi,I}(x,T)}{\partial x}dT - T\int_{T_\lambda(x)}^{T}\frac{1}{T}\frac{\partial C_{1\phi,I}(x,T)}{\partial x}dT\right) \quad \text{(B.19)}$$

$T_{\sigma-}(x)$, $h_{\sigma-}(x)$, $s_{\sigma-}(x)$, $\left(C_{1\phi,II}\right)_{T_{\sigma-}}$, $\left(C_{2\phi}\right)_{T_{\sigma-}}$, $\left(\frac{\partial h}{\partial x}\right)_{2\phi,T=T_{\sigma-}}$, and $\left(\frac{\partial s}{\partial x}\right)_{2\phi,T=T_{\sigma-}}$ have already been specified in Section B.2.2.

Note: The difference between the He-II specific heat and the He-I specific heat at the λ-transition temperature is a small non-zero value. To ensure consistency, we include the associated term in the expression for μ_4, even though it should really be zero.

B.3.2 Properties for ^{3}He concentrations of more than 67.4%

$$g(x,T) = h_{\sigma+}(x) - Ts_{\sigma+}(x) + \int_{T_{\sigma+}(x)}^{T} C_{1\phi,I}(x,T)dT - T\int_{T_{\sigma+}(x)}^{T}\frac{C_{1\phi,I}(x,T)}{T}dT \quad \text{(B.20)}$$

$$s(x,T) = s_{\sigma+}(x) + \int_{T_{\sigma+}(x)}^{T}\frac{C_{1\phi,I}(x,T)}{T}dT \quad \text{(B.21)}$$

$$h(x,T) = h_{\sigma+}(x) + \int_{T_{\sigma+}(x)}^{T} C_{1\phi,I}(x,T)dT \quad \text{(B.22)}$$

$$\mu_4(x,T) = \left(h_{\sigma+} - x\left(\frac{\partial h}{\partial x}\right)_{2\phi,T=T_{\sigma+}}\right) - T\left(s_{\sigma+} - x\left(\frac{\partial s}{\partial x}\right)_{2\phi,T=T_{\sigma+}}\right) - x\frac{dT_{\sigma+}}{dx}\left(1-\frac{T}{T_{\sigma+}}\right)\left(\left(C_{2\phi}\right)_{T_{\sigma+}} - \left(C_{1\phi,I}\right)_{T_{\sigma+}}\right)$$
$$+\int_{T_{\sigma+}(x)}^{T} C_{1\phi,I}(x,T)dT - T\int_{T_{\sigma+}(x)}^{T}\frac{C_{1\phi,I}(x,T)}{T}dT$$
$$-x\left(\int_{T_{\sigma+}(x)}^{T}\frac{\partial C_{1\phi,I}(x,T)}{\partial x}dT - T\int_{T_{\sigma+}(x)}^{T}\frac{1}{T}\frac{\partial C_{1\phi,I}(x,T)}{\partial x}dT\right) \quad \text{(B.23)}$$

$T_{\sigma+}(x)$, the temperature at which phase separation occurs at the given value of x, is obtained from Eq. A.2. $h_{\sigma+}(x)$ and $s_{\sigma+}(x)$, the enthalpy and entropy on the concentrated phase separation curve, are obtained by substituting $T = T_{\sigma+}(x)$ into Eqs. B.2 and B.1 respectively.

$\left(C_{1\phi,I}\right)_{T_{\sigma+}}$ is the specific heat in the 1-phase region at x and $T = T_{\sigma+}(x)$. $\left(C_{2\phi}\right)_{T_{\sigma+}}$ is the specific heat in the 2-phase region at x and $T = T_{\sigma+}(x)$:

$$\left(C_{2\phi}\right)_{T_{\sigma+}} = T_{\sigma+}\left[\frac{C_{2\phi,t}}{T} + (x-x_t)\left(\frac{1}{T}\frac{\partial C_{2\phi}}{\partial x}\right)\right]_{T=T_{\sigma+}} \quad \text{(B.24)}$$

The 2-phase-region derivatives can be obtained by taking the derivatives (at a constant temperature $T = T_{\sigma+}(x)$) of Eqs. B.2 and B.1, resulting in

$$\left(\frac{\partial h}{\partial x}\right)_{2\phi, T=T_{\sigma+}} = \left(\left(\frac{\partial h}{\partial x}\right)_{2\phi, 0K} + \int_0^{T_{\sigma+}} \frac{\partial C_{2\phi}}{\partial x} dT\right) \tag{B.25}$$

and

$$\left(\frac{\partial s}{\partial x}\right)_{2\phi, T=T_{\sigma+}} = \int_0^{T_{\sigma+}} \frac{1}{T} \frac{\partial C_{2\phi}}{\partial x} dT \tag{B.26}$$

Appendix C: Properties at non-zero pressure in terms of zero-pressure properties

Entropy:

$$s(x,T,p) = s(x,T,0) - \int_0^p \frac{\partial v}{\partial T} dp \tag{C.1}$$

Enthalpy:

$$h(x,T,p) = h(x,T,0) + \int_0^p \left(v - T\left(\frac{\partial v}{\partial T}\right)_{p,x} \right) dp \tag{C.2}$$

Gibbs free energy:

$$g(x,T,p) = g(x,T,0) + \int_0^p v dp \tag{C.3}$$

^{4}He chemical potential:

$$\mu_4(x,T,p) = \mu_4(x,T,0) + \int_0^p \left(v - x\left(\frac{\partial v}{\partial x}\right)_{T,p} \right) dp \tag{C.4}$$

Integrations in the single-phase region may be performed using Eq. A.20 in Appendix A.3.

In the two-phase region, the molar volume and its derivatives in terms of the single-phase molar volumes and volume derivatives are:

$$v(x,T,p) = v_{1\phi}(x_{\sigma+})\frac{(x - x_{\sigma-})}{(x_{\sigma+} - x_{\sigma-})} + v_{1\phi}(x_{\sigma-})\frac{(x_{\sigma+} - x)}{(x_{\sigma+} - x_{\sigma-})} \tag{C.5}$$

$$\frac{\partial v}{\partial x} = \frac{v_{1\phi}(x_{\sigma+}) - v_{1\phi}(x_{\sigma-})}{x_{\sigma+} - x_{\sigma-}} \tag{C.6}$$

$$\begin{aligned} \frac{\partial v}{\partial T} = &\left(\left(\frac{\partial v}{\partial T}\right)_{1\phi, x=x_{\sigma+}} + \left(\frac{\partial x_{\sigma+}}{\partial T}\right)_p \left[\left(\frac{\partial v}{\partial x}\right)_{1\phi, x=x_{\sigma+}} - \left(\frac{\partial v}{\partial x}\right)_{2\phi, x=x_{\sigma+}} \right] \right) \frac{(x - x_{\sigma-})}{(x_{\sigma+} - x_{\sigma-})} \\ &+ \left(\left(\frac{\partial v}{\partial T}\right)_{1\phi, x=x_{\sigma-}} + \left(\frac{\partial x_{\sigma-}}{\partial T}\right)_p \left[\left(\frac{\partial v}{\partial x}\right)_{1\phi, x=x_{\sigma-}} - \left(\frac{\partial v}{\partial x}\right)_{2\phi, x=x_{\sigma-}} \right] \right) \frac{(x_{\sigma+} - x)}{(x_{\sigma+} - x_{\sigma-})} \end{aligned} \tag{C.7}$$

Appendix D: Miscellaneous Stuff

D.1 Constraints on the specific heats

In the He-II region, properties at ^{3}He concentrations of less than about 8% are calculated by integrating up from the T = 0.15 K line. Properties at ^{3}He concentrations of greater than about 8% are calculated by integrating up from the dilute phase-separation line. (At a temperature of 0.15 K, phase separation occurs at x = 0.08014.) Since properties on the 0.15 K-line are obtained from Kuerten et al's model and properties on the phase-separation curve are based on data from several sources, it is not automatically ensured that the derivatives of entropy and enthalpy with respect to x will be continuous across the x = 0.08014 line.

In order to ensure that the 1st and 2nd derivatives of entropy and enthalpy (and thus the Gibbs free energy) are continuous across the x = 0.08014 line, the constraints listed below were applied to the specific heat fits determined from available experimental data.

In the following equations, the derivatives on the left hand side (the derivatives of the enthalpy and entropy at a temperature of 0.15 K) are evaluated from Kuerten et al's model at x = 0.08014. The quantities on the right are evaluated at x = 0.08014 (and $T_{\sigma-}$ = 0.15 K).

$$\frac{dh_{0.15}(x)}{dx} = \left(\frac{\partial h}{\partial x}\right)_{2\phi,0K} + \int_0^{T_{\sigma-}} \frac{\partial C_{2\phi}}{\partial x} dT + \frac{dT_{\sigma-}}{dx}\left[\left(C_{2\phi}\right)_{T_{\sigma-}} - \left(C_{1\phi,II}\right)_{T_{\sigma-}}\right] \tag{D.1}$$

$$\frac{ds_{0.15}(x)}{dx} = \int_0^{T_{\sigma-}} \frac{1}{T}\frac{\partial C_{2\phi}}{\partial x} dT + \frac{1}{T_{\sigma-}}\frac{dT_{\sigma-}}{dx}\left[\left(C_{2\phi}\right)_{T_{\sigma-}} - \left(C_{1\phi,II}\right)_{T_{\sigma-}}\right] \tag{D.2}$$

$$\frac{d^2h_{0.15}(x)}{dx^2} = \frac{d^2T_{\sigma-}}{dx^2}\left[\left(C_{2\phi}\right)_{T_{\sigma-}} - \left(C_{1\phi,II}\right)_{T_{\sigma-}}\right] + \frac{dT_{\sigma-}}{dx}\left[2\left(\left(\frac{\partial C_{2\phi}}{\partial x}\right)_{T_{\sigma-}} - \left(\frac{\partial C_{1\phi,II}}{\partial x}\right)_{T_{\sigma-}}\right)\right] + \left(\frac{dT_{\sigma-}}{dx}\right)^2\left(\left(\frac{\partial C_{2\phi}}{\partial T}\right)_{T_{\sigma-}} - \left(\frac{\partial C_{1\phi,II}}{\partial T}\right)_{T_{\sigma-}}\right) \tag{D.3}$$

$$\frac{d^2s_{0.15}(x)}{dx^2} = \frac{1}{T_{\sigma-}}\frac{d^2T_{\sigma-}}{dx^2}\left[\left(C_{2\phi}\right)_{T_{\sigma-}} - \left(C_{1\phi,II}\right)_{T_{\sigma-}}\right] + \frac{1}{T_{\sigma-}}\frac{dT_{\sigma-}}{dx}\left[2\left(\left(\frac{\partial C_{2\phi}}{\partial x}\right)_{T_{\sigma-}} - \left(\frac{\partial C_{1\phi,II}}{\partial x}\right)_{T_{\sigma-}}\right)\right] + \frac{1}{T_{\sigma-}}\left(\frac{dT_{\sigma-}}{dx}\right)^2\left[\left(\left(\frac{\partial C_{2\phi}}{\partial T}\right)_{T_{\sigma-}} - \left(\frac{\partial C_{1\phi,II}}{\partial T}\right)_{T_{\sigma-}}\right) - \frac{\left(C_{2\phi}\right)_{T_{\sigma-}} - \left(C_{1\phi,II}\right)_{T_{\sigma-}}}{T_{\sigma-}}\right] \tag{D.4}$$

Since properties for $x < 0.674$ were obtained by integrating up from the dilute phase separation curve and properties for $x > 0.674$ were obtained by integrating up from the concentrated phase separation curve, it is not automatically ensured that derivatives of enthalpy and entropy with respect to x will be continuous across the $x = 0.674$ line. Therefore, constraints were applied to ensure continuity of the 1st and 2nd derivatives of enthalpy and entropy across $x = 0.674$.

$$C_{1\phi,II}(x_t,T_t) = C_{1\phi,I}(x_t,T_t) = C_{2\phi}(x_t,T_t) \tag{D.5}$$

$$\begin{aligned} & 2\frac{dT_{\sigma+}}{dx}\left[\left(\frac{\partial C_{2\phi}}{\partial x}\right)_{x_t,T_t} - \left(\frac{\partial C_{1\phi,I}}{\partial x}\right)_{x_t,T_t}\right] + \left(\frac{dT_{\sigma+}}{dx}\right)^2\left[\left(\frac{\partial C_{2\phi}}{\partial T}\right)_{x_t,T_t} - \left(\frac{\partial C_{1\phi,I}}{\partial T}\right)_{x_t,T_t}\right] \\ = \quad & 2\frac{dT_{\sigma-}}{dx}\left[\left(\frac{\partial C_{2\phi}}{\partial x}\right)_{x_t,T_t} - \left(\frac{\partial C_{1\phi,II}}{\partial x}\right)_{x_t,T_t}\right] + \left(\frac{dT_{\sigma-}}{dx}\right)^2\left[\left(\frac{\partial C_{2\phi}}{\partial T}\right)_{x_t,T_t} - \left(\frac{\partial C_{1\phi,II}}{\partial T}\right)_{x_t,T_t}\right] \\ & + 2\frac{dT_{\lambda}}{dx}\left[\left(\frac{\partial C_{1\phi,II}}{\partial x}\right)_{x_t,T_t} - \left(\frac{\partial C_{1\phi,I}}{\partial x}\right)_{x_t,T_t}\right] + \left(\frac{dT_{\lambda}}{dx}\right)^2\left[\left(\frac{\partial C_{1\phi,II}}{\partial T}\right)_{x_t,T_t} - \left(\frac{\partial C_{1\phi,I}}{\partial T}\right)_{x_t,T_t}\right] \end{aligned} \tag{D.6}$$

D.2 Pressure derivatives of the phase-separation surfaces

Here we derive Eqs. 3.13 and 3.18, i.e.,

$$\frac{\partial x_{\sigma-}}{\partial p} = \frac{(\partial v/\partial x)_{2\phi,x=x_{\sigma-}} - (\partial v/\partial x)_{1\phi,x=x_{\sigma-}}}{\left(\partial^2 g/\partial x^2\right)_{x=x_{\sigma-}}} \tag{D.7}$$

and

$$\frac{\partial x_{\sigma+}}{\partial p} = \frac{(\partial v/\partial x)_{2\phi,x=x_{\sigma+}} - (\partial v/\partial x)_{1\phi,x=x_{\sigma+}}}{\left(\partial^2 g/\partial x^2\right)_{x=x_{\sigma+}}} \tag{D.8}$$

The pressure variation of the ^{4}He chemical potential along the dilute-phase surface, at constant temperature and x, is

$$\left(\frac{\partial \mu_4}{\partial p}\right)_{\sigma-} = \left[\left(\frac{\partial \mu_4}{\partial p}\right)_{x,T} + \left(\frac{\partial \mu_4}{\partial x}\right)_{p,T}\frac{\partial x_{\sigma-}(p,T)}{\partial p}\right]_{x=x_{\sigma-}} \tag{D.9}$$

Similarly, the pressure variation of μ_4 along the concentrated-phase surface is

$$\left(\frac{\partial \mu_4}{\partial p}\right)_{\sigma+} = \left[\left(\frac{\partial \mu_4}{\partial p}\right)_{x,T} + \left(\frac{\partial \mu_4}{\partial x}\right)_{p,T}\frac{\partial x_{\sigma+}(p,T)}{\partial p}\right]_{x=x_{\sigma+}} \tag{D.10}$$

Since the chemical potential of each species in a mixture is the same in all phases at the same temperature and pressure, the pressure variations $(\partial\mu_4/\partial p)_{\sigma-}$ and $(\partial\mu_4/\partial p)_{\sigma+}$ must be equal. Therefore, we can equate Eqs. D.9 and D.10 to get

$$\left(\frac{\partial \mu_4}{\partial p}\right)_{x=x_{\sigma-}} + \left(\frac{\partial \mu_4}{\partial x}\right)_{x=x_{\sigma-}} \frac{\partial x_{\sigma-}(p,T)}{\partial p} = \left(\frac{\partial \mu_4}{\partial p}\right)_{x=x_{\sigma+}} + \left(\frac{\partial \mu_4}{\partial x}\right)_{x=x_{\sigma+}} \frac{\partial x_{\sigma+}(p,T)}{\partial p}. \tag{D.11}$$

Using the relation between partial molar volume v_4 and the ^{4}He chemical potential,

$$v_4 = \frac{\partial \mu_4}{\partial p}, \tag{D.12}$$

the above equation becomes

$$(v_4)_{x=x_{\sigma-}} + \left(\frac{\partial \mu_4}{\partial x}\right)_{x=x_{\sigma-}} \frac{\partial x_{\sigma-}(p,T)}{dp} = (v_4)_{x=x_{\sigma+}} + \left(\frac{\partial \mu_4}{\partial x}\right)_{x=x_{\sigma+}} \frac{\partial x_{\sigma+}(p,T)}{\partial p}. \tag{D.13}$$

With a similar analysis using the ^{3}He chemical potential instead of the ^{4}He chemical potential, we get

$$(v_3)_{x=x_{\sigma-}} + \left(\frac{\partial \mu_3}{\partial x}\right)_{x=x_{\sigma-}} \frac{\partial x_{\sigma-}(p,T)}{dp} = (v_3)_{x=x_{\sigma+}} + \left(\frac{\partial \mu_3}{\partial x}\right)_{x=x_{\sigma+}} \frac{\partial x_{\sigma+}(p,T)}{\partial p}. \tag{D.14}$$

The definitions of the partial molar volumes are [18]

$$v_4 = v - x\left(\frac{\partial v}{\partial x}\right)_{p,T} \tag{D.15}$$

and

$$v_3 = v + (1-x)\left(\frac{\partial v}{\partial x}\right)_{p,T}. \tag{D.16}$$

Similarly, the definitions of the chemical potentials are [18]

$$\mu_4 = g - x\left(\frac{\partial g}{\partial x}\right)_{p,T} \tag{D.17}$$

and

$$\mu_3 = g + (1-x)\left(\frac{\partial g}{\partial x}\right)_{p,T}, \tag{D.18}$$

which give us:

$$\left(\frac{\partial \mu_4}{\partial x}\right) = -x\left(\frac{\partial^2 g}{\partial x^2}\right) \tag{D.19}$$

and

$$\left(\frac{\partial \mu_3}{\partial x}\right) = (1-x)\left(\frac{\partial^2 g}{\partial x^2}\right). \tag{D.20}$$

Substituting Eqs. D.15, D.16, D.19 and D.20 back into Eqs. D.13 and D.14 and rearranging, we get

$$\left(\frac{\partial^2 g}{\partial x^2}\right)_{x=x_{\sigma-}} \frac{\partial x_{\sigma-}(p,T)}{\partial p} = \frac{(v)_{x=x_{\sigma+}} - (v)_{x=x_{\sigma-}}}{x_{\sigma+} - x_{\sigma-}} - \left(\frac{\partial v}{\partial x}\right)_{x=x_{\sigma-}} \tag{D.21}$$

and

$$\left(\frac{\partial^2 g}{\partial x^2}\right)_{x=x_{\sigma+}} \frac{\partial x_{\sigma+}(p,T)}{\partial p} = \frac{(v)_{x=x_{\sigma+}} - (v)_{x=x_{\sigma-}}}{x_{\sigma+} - x_{\sigma-}} - \left(\frac{\partial v}{\partial x}\right)_{x=x_{\sigma+}} \tag{D.22}$$

Since the molar volume varies linearly with x in the two-phase region at a fixed pressure and temperature, the term $\left((v)_{x=x_{\sigma+}} - (v)_{x=x_{\sigma-}}\right)/(x_{\sigma+} - x_{\sigma-})$ is simply the slope of the molar volume in the two-phase region. (The quantities $(\partial v/\partial x)_{x=x_{\sigma-}}$ and $(\partial v/\partial x)_{x=x_{\sigma+}}$ are the slopes of the molar volume in the single-phase region.)

$$\frac{(v)_{x=x_{\sigma+}} - (v)_{x=x_{\sigma-}}}{x_{\sigma+} - x_{\sigma-}} = \left(\frac{\partial v}{\partial x}\right)_{2\phi, x=x_{\sigma-}} = \left(\frac{\partial v}{\partial x}\right)_{2\phi, x=x_{\sigma+}} \tag{D.23}$$

Substituting Eq. D.23 into Eqs. D.21 and D.22 results in the expressions in D.7 and D.8.

D.3 The specific heat at constant pressure and constant ^{4}He chemical potential

Here we show (mathematically) that Eqs. 4.2 and 4.8 are equivalent, i.e.,

$$\left(\frac{\partial h^{os}}{\partial T}\right)_{\mu_4,p} = T\left(\frac{\partial (s/x)}{\partial T}\right)_{\mu_4,p}, \tag{D.24}$$

The osmotic enthalpy is defined as (see Section 1.4.2):

$$h^{os} = \frac{h - (1-x)\mu_4}{x} \tag{D.25}$$

Using

$$h = g + Ts \tag{D.26}$$

and

$$g = x\mu_3 + (1-x)\mu_4, \tag{D.27}$$

the osmotic enthalpy can be rewritten as

$$h^{os} = \mu_3 + T\frac{s}{x} \tag{D.28}$$

Taking the derivative of this equation with respect to temperature, at constant μ_4 and p, we get

$$\left(\frac{\partial h^{os}}{\partial T}\right)_{\mu_4,p} = \left(\frac{\partial \mu_3}{\partial T}\right)_{\mu_4,p} + \frac{s}{x} + T\left(\frac{\partial (s/x)}{\partial T}\right)_{\mu_4,p}. \tag{D.29}$$

Now,

$$\left(\frac{\partial \mu_3}{\partial T}\right)_{\mu_4,p} = \left(\frac{\partial \mu_3}{\partial T}\right)_{x,p} + \left(\frac{\partial \mu_3}{\partial x}\right)_{T,p}\left(\frac{\partial x}{\partial T}\right)_{\mu_4,p}. \tag{D.30}$$

Using

$$\left(\frac{\partial \mu_3}{\partial T}\right)_{x,p} = -s - (1-x)\left(\frac{\partial s}{\partial x}\right)_{T,p}, \tag{D.31}$$

$$\left(\frac{\partial \mu_3}{\partial x}\right)_{T,p} = (1-x)\left(\frac{\partial^2 g}{\partial x^2}\right)_{T,p}, \tag{D.32}$$

and

$$\left(\frac{\partial x}{\partial T}\right)_{\mu_4,p} = \frac{-(\partial \mu_4 / \partial T)_{x,p}}{(\partial \mu_4 / \partial x)_{T,p}} = \frac{\left(s - x(\partial s / \partial x)_{T,p}\right)}{-x(\partial^2 g / \partial x^2)_{T,p}}, \tag{D.33}$$

Eq. D.30 becomes

$$\left(\frac{\partial \mu_3}{\partial T}\right)_{\mu_4,p} = -s - (1-x)\left(\frac{\partial s}{\partial x}\right)_{T,p} + (1-x)\left(\frac{\partial^2 g}{\partial x^2}\right)_{T,p}\left(\frac{\left(s - x(\partial s / \partial x)_{T,p}\right)}{-x(\partial^2 g / \partial x^2)_{T,p}}\right) \tag{D.34}$$

which simplifies to

$$\left(\frac{\partial \mu_3}{\partial T}\right)_{\mu_4,p} = -s - (1-x)\left(\frac{\partial s}{\partial x}\right)_{T,p} - \frac{(1-x)}{x}\left(s - x\left(\frac{\partial s}{\partial x}\right)_{T,p}\right) = -\frac{s}{x} \tag{D.35}$$

Substituting this back in Eq. D.29, we get Eq. D.24.

D.4 Errors associated with treating saturated-pressure molar volumes as zero pressure molar volumes

The error associated with the molar volume is:

$$v_{svp} - v_{p=0} = \left(\frac{\partial v}{\partial p}\right)_{x,T} p_{sat}$$

The error associated with the temperature-derivative of the molar volume is:

$$\left(\frac{\partial v}{\partial T}\right)_{svp} - \left(\frac{\partial v}{\partial T}\right)_{p=0} = \left(\frac{\partial v}{\partial p}\right)_{T}\left(\frac{\partial p_{sat}}{\partial T}\right)$$

The error associated with the x-derivative of the molar volume is:

$$\left(\frac{\partial v}{\partial x}\right)_{svp} - \left(\frac{\partial v}{\partial x}\right)_{p=0} = \left(\frac{\partial v}{\partial p}\right)_{x}\left(\frac{\partial p_{sat}}{\partial x}\right)$$

Over the range of interest, the maximum values of p_{sat}, $\partial p_{sat} / \partial T$ and $\partial p_{sat} / \partial x$ are about 6500 Pa, 15000 Pa/K and 6000 Pa respectively (as calculated from the vapour pressure data of Sydoriak and Roberts [7]). The maximum magnitude of $\partial v / \partial p$ is about 10^{-5} cm^3/mol-Pa. (This number is calculated from pure ^{3}He data [16, 59].) Therefore the maximum error associated with (a) the molar volume is about 0.065 cm^3/mol (as compared to typical values of 30 cm^3/mol), (b) $\partial v / \partial x$ is about 0.06 cm^3/mol (as compared to typical values of 10 cm^3/mol), and (c) $\partial v / \partial T$ is about 0.15 cm^3/mol (as compared to typical values of 1-2 cm^3/mol). Note that these are the maximum errors; the errors in most cases are much smaller than these values.

Appendix E: Property Tables

E.1 Properties at saturated pressure

Table 10: Kuerten et al's calculated values of the specific heat, entropy, enthalpy, ^{4}He chemical potential and osmotic enthalpy at low temperatures and low ^{3}He concentrations. These tables are a condensed version of their more extensive tables that can be found in Ref. 2.

C (J/mol-K)	T (K)	x	0.01	0.02	0.03	0.04	0.05	0.06
	0.01		0.0354	0.0454	0.0523	0.0578	0.0624	0.0665
	0.02		0.0641	0.0878	0.1027	0.1142	0.1237	0.1321
	0.05		0.1014	0.1694	0.2184	0.2561	0.2862	0.3113
	0.10		0.1155	0.2147	0.3012	0.3760	0.4417	0.5001
	0.15		0.1198	0.2296	0.3307	0.4248	0.512	0.5929
	0.20		0.1219	0.2367	0.3454	0.4485	0.5465	0.6403
	0.25		0.1235	0.2409	0.3539	0.4626	0.5674	0.6683
s (J/mol-K)	T (K)	x	0.01	0.02	0.03	0.04	0.05	0.06
	0.01		0.0360	0.0457	0.0525	0.0579	0.0625	0.0666
	0.02		0.0700	0.0905	0.1044	0.1154	0.1247	0.1329
	0.05		0.1470	0.2080	0.2485	0.2793	0.3046	0.3264
	0.10		0.2228	0.3428	0.4304	0.5000	0.5580	0.6079
	0.15		0.2706	0.4331	0.5589	0.6630	0.7522	0.8304
	0.20		0.3053	0.5002	0.6563	0.7888	0.9047	1.0081
	0.25		0.3327	0.5535	0.7344	0.8905	1.0291	1.1542
h (J/mol)	T (K)	x	0.01	0.02	0.03	0.04	0.05	0.06
	0.01		-0.0200	-0.0342	-0.0442	-0.0510	-0.0550	-0.0566
	0.02		-0.0195	-0.0335	-0.0435	-0.0501	-0.0540	-0.0556
	0.05		-0.0169	-0.0295	-0.0385	-0.0444	-0.0478	-0.0489
	0.10		-0.0114	-0.0196	-0.0251	-0.0282	-0.0291	-0.0280
	0.15		-0.0055	-0.0085	-0.0092	-0.0080	-0.0050	-0.0004
	0.20		0.0006	0.0032	0.0077	0.0139	0.0216	0.0305
	0.25		0.0067	0.0152	0.0252	0.0367	0.0495	0.0633
μ_4 (J/mol-^{4}He)	T (K)	x	0.01	0.02	0.03	0.04	0.05	0.06
	0.01		-0.0036	-0.0106	-0.0197	-0.0302	-0.0417	-0.0537
	0.02		-0.0040	-0.0111	-0.0202	-0.0308	-0.0423	-0.0544
	0.05		-0.0057	-0.0137	-0.0235	-0.0345	-0.0464	-0.0588
	0.10		-0.0093	-0.0203	-0.0323	-0.0452	-0.0587	-0.0725
	0.15		-0.0133	-0.0277	-0.0428	-0.0585	-0.0745	-0.0905
	0.20		-0.0173	-0.0354	-0.0540	-0.0729	-0.0919	-0.1108
	0.25		-0.0213	-0.0433	-0.0656	-0.0879	-0.1102	-0.1323
h^{os} (J/mol-^{3}He)	T (K)	x	0.01	0.02	0.03	0.04	0.05	0.06
	0.01		-1.6438	-1.1891	-0.8378	-0.5501	-0.3080	-0.1014
	0.02		-1.5599	-1.1338	-0.7953	-0.5149	-0.2777	-0.0746
	0.05		-1.1274	-0.8012	-0.5226	-0.2825	-0.0743	0.1071
	0.10		-0.2145	0.0117	0.2083	0.3812	0.5340	0.6687
	0.15		0.7629	0.9320	1.0782	1.2055	1.3159	1.4117
	0.20		1.7647	1.8945	2.0047	2.0986	2.1784	2.2454
	0.25		2.7805	2.8792	2.9615	3.0292	3.0841	3.1276

Table 11: Thermodynamic properties along the dilute and concentrated phase-separation lines.

Temp (K)	x (dil)	x (conc)	v (dil) cm^3/mol	v (conc) cm^3/mol	s (dil) J/mol K	s (conc) J/mol K	h (dil) J/mol	h (conc) J/mol	g (dil) J/mol	g (conc) J/mol	μ_4 J/mol-^{4}He	xh^{os} (dil) J/mol	xh^{os} (conc) J/mol
0.15	0.0801	1.0000	28.212	36.796	0.964	2.984	0.013	0.210	-0.132	-0.238	-0.122	0.126	0.210
0.175	0.0855	0.9995	28.250	36.779	1.117	3.381	0.037	0.274	-0.158	-0.317	-0.144	0.168	0.274
0.2	0.0915	0.9979	28.295	36.751	1.273	3.764	0.065	0.346	-0.190	-0.406	-0.168	0.217	0.347
0.225	0.0983	0.9953	28.346	36.714	1.434	4.136	0.097	0.426	-0.225	-0.504	-0.195	0.273	0.427
0.25	0.1058	0.9917	28.403	36.667	1.600	4.500	0.134	0.514	-0.266	-0.611	-0.225	0.335	0.516
0.275	0.1141	0.9872	28.467	36.609	1.775	4.859	0.177	0.610	-0.312	-0.726	-0.257	0.405	0.613
0.3	0.1231	0.9817	28.537	36.542	1.960	5.214	0.225	0.715	-0.363	-0.849	-0.293	0.482	0.720
0.325	0.1329	0.9753	28.614	36.465	2.155	5.564	0.280	0.828	-0.420	-0.980	-0.332	0.568	0.837
0.35	0.1435	0.9681	28.697	36.379	2.361	5.911	0.342	0.951	-0.484	-1.118	-0.374	0.662	0.963
0.375	0.1549	0.9600	28.788	36.283	2.580	6.254	0.412	1.081	-0.555	-1.264	-0.419	0.766	1.098
0.4	0.1670	0.9511	28.885	36.179	2.812	6.592	0.491	1.221	-0.634	-1.416	-0.468	0.880	1.244
0.425	0.1800	0.9415	28.990	36.065	3.058	6.923	0.578	1.368	-0.721	-1.575	-0.520	1.004	1.398
0.45	0.1938	0.9311	29.102	35.944	3.317	7.248	0.675	1.522	-0.817	-1.740	-0.575	1.139	1.562
0.475	0.2085	0.9199	29.221	35.815	3.591	7.564	0.783	1.683	-0.923	-1.910	-0.634	1.284	1.734
0.5	0.2241	0.9081	29.348	35.680	3.879	7.870	0.900	1.850	-1.039	-2.086	-0.696	1.440	1.913
0.525	0.2405	0.8956	29.482	35.537	4.181	8.166	1.029	2.021	-1.166	-2.266	-0.762	1.608	2.100
0.55	0.2580	0.8825	29.625	35.389	4.498	8.449	1.169	2.196	-1.305	-2.451	-0.832	1.786	2.294
0.575	0.2765	0.8688	29.775	35.236	4.830	8.719	1.320	2.374	-1.457	-2.639	-0.906	1.975	2.493
0.6	0.2960	0.8545	29.934	35.078	5.177	8.975	1.483	2.554	-1.623	-2.831	-0.983	2.175	2.697
0.625	0.3168	0.8397	30.103	34.916	5.539	9.216	1.658	2.735	-1.804	-3.025	-1.064	2.385	2.906
0.65	0.3389	0.8243	30.283	34.750	5.918	9.442	1.846	2.916	-2.000	-3.221	-1.148	2.606	3.118
0.675	0.3624	0.8085	30.474	34.581	6.314	9.651	2.048	3.096	-2.215	-3.418	-1.237	2.836	3.333
0.7	0.3877	0.7922	30.681	34.409	6.730	9.843	2.263	3.274	-2.448	-3.616	-1.329	3.076	3.550
0.725	0.4151	0.7755	30.905	34.235	7.168	10.018	2.493	3.448	-2.704	-3.815	-1.424	3.326	3.768
0.75	0.4451	0.7584	31.154	34.058	7.632	10.175	2.740	3.618	-2.984	-4.013	-1.523	3.585	3.986
0.775	0.4786	0.7409	31.435	33.880	8.131	10.314	3.006	3.783	-3.295	-4.210	-1.625	3.854	4.204
0.8	0.5170	0.7231	31.763	33.700	8.676	10.433	3.298	3.941	-3.643	-4.405	-1.730	4.134	4.420
0.825	0.5628	0.7050	32.167	33.518	9.293	10.532	3.625	4.091	-4.042	-4.598	-1.838	4.428	4.633
0.85	0.6213	0.6866	32.704	33.336	10.029	10.611	4.006	4.230	-4.519	-4.789	-1.949	4.744	4.841
0.867	0.6740	0.6740	33.211	33.211	10.651	10.651	4.319	4.319	-4.916	-4.916	-2.026	4.979	4.979

Table 12: Entropy per mole of mixture (J/mol K) as a function of temperature and ^{3}He mole fraction. The solid lines represent the transition from the He-II to the He-I region.

^{3}He mole fraction

Temp (K)	0	0.05	0.1	0.15	0.2	0.25	0.3	0.35	0.4	0.45	0.5	0.55	0.6	0.65	0.7	0.75	0.8	0.85	0.9	0.95	1
0.2	0.000	0.903																			3.730
0.25	0.000	1.026	1.550																		4.361
0.3	0.001	1.129	1.733																		4.902
0.35	0.001	1.219	1.892																		5.373
0.4	0.002	1.297	2.032	2.620																	5.791
0.45	0.002	1.367	2.157	2.790																7.017	6.168
0.5	0.003	1.430	2.269	2.944	3.581															7.383	6.511
0.55	0.004	1.487	2.372	3.085	3.757	4.399													8.316	7.717	6.828
0.6	0.006	1.539	2.466	3.214	3.919	4.595													8.659	8.024	7.123
0.65	0.007	1.587	2.552	3.335	4.071	4.779	5.444											9.359	8.971	8.311	7.401
0.7	0.010	1.632	2.633	3.447	4.215	4.955	5.654	6.294									9.845	9.691	9.261	8.582	7.664
0.75	0.013	1.675	2.709	3.554	4.352	5.125	5.859	6.535	7.143								10.205	9.994	9.532	8.838	7.915
0.8	0.018	1.717	2.782	3.657	4.485	5.291	6.059	6.773	7.418	7.995	8.512					10.538	10.530	10.275	9.788	9.084	8.155
0.85	0.024	1.759	2.853	3.756	4.616	5.454	6.258	7.008	7.691	8.305	8.857	9.362	9.834		10.707	10.890	10.827	10.537	10.032	9.319	8.387
0.9	0.034	1.801	2.924	3.855	4.745	5.617	6.457	7.244	7.964	8.613	9.199	9.736	10.237	10.717	11.091	11.207	11.101	10.784	10.265	9.546	8.611
0.95	0.046	1.846	2.996	3.955	4.875	5.781	6.657	7.481	8.238	8.922	9.541	10.108	10.638	11.140	11.435	11.498	11.357	11.020	10.489	9.764	8.830
1	0.064	1.895	3.071	4.057	5.008	5.948	6.860	7.721	8.513	9.232	9.884	10.482	11.042	11.523	11.747	11.767	11.598	11.244	10.705	9.976	9.042
1.05	0.087	1.948	3.150	4.164	5.146	6.119	7.067	7.965	8.794	9.547	10.232	10.862	11.453	11.865	12.034	12.019	11.827	11.460	10.914	10.182	9.250
1.1	0.118	2.009	3.237	4.278	5.291	6.298	7.282	8.216	9.080	9.869	10.588	11.252	11.850	12.176	12.301	12.257	12.046	11.669	11.117	10.382	9.454
1.15	0.156	2.078	3.332	4.402	5.445	6.486	7.506	8.476	9.376	10.200	10.956	11.661	12.197	12.462	12.553	12.484	12.257	11.870	11.315	10.578	9.654
1.2	0.204	2.156	3.439	4.536	5.611	6.686	7.741	8.746	9.683	10.546	11.344	12.080	12.509	12.729	12.791	12.702	12.461	12.066	11.508	10.769	9.851
1.25	0.263	2.247	3.558	4.686	5.792	6.901	7.990	9.032	10.006	10.910	11.756	12.440	12.794	12.981	13.019	12.912	12.658	12.257	11.696	10.957	10.046
1.3	0.335	2.351	3.693	4.852	5.991	7.133	8.257	9.335	10.349	11.299	12.197	12.754	13.060	13.221	13.239	13.115	12.850	12.444	11.881	11.141	10.237
1.35	0.421	2.471	3.845	5.037	6.210	7.386	8.544	9.660	10.717	11.719	12.580	13.037	13.310	13.452	13.452	13.312	13.037	12.628	12.064	11.324	10.427
1.4	0.523	2.608	4.018	5.245	6.453	7.663	8.857	10.010	11.114	12.178	12.902	13.297	13.549	13.674	13.658	13.504	13.221	12.810	12.245	11.504	10.614
1.45	0.643	2.766	4.214	5.479	6.723	7.968	9.198	10.393	11.549		13.187	13.541	13.777	13.889	13.858	13.692	13.403	12.990	12.426	11.684	10.799
1.5	0.782	2.945	4.436	5.743	7.025	8.306	9.572	10.811	12.027		13.447	13.772	13.997	14.098	14.053	13.876	13.582	13.170	12.607	11.865	10.981
1.55	0.944	3.150	4.687	6.038	7.361	8.680	9.985	11.273													
1.6	1.130	3.381	4.970	6.371	7.737	9.096	10.443	11.784													
1.65	1.343	3.644	5.289	6.744	8.158	9.558	10.950														
1.7	1.585	3.940	5.648	7.162	8.627	10.073	11.515														
1.75	1.861	4.273	6.050	7.631	9.151	10.647															
1.8	2.173	4.646	6.501	8.154	9.735																

Table 13: Enthalpy per mole of mixture (J/mol) as a function of temperature and ^{3}He mole fraction. The solid lines represent the transition from the He-II to the He-I region.

^{3}He mole fraction

Temp (K)	0	0.05	0.1	0.15	0.2	0.25	0.3	0.35	0.4	0.45	0.5	0.55	0.6	0.65	0.7	0.75	0.8	0.85	0.9	0.95	1
0.2	0.000	0.021																			0.340
0.25	0.000	0.049	0.124																		0.481
0.3	0.000	0.077	0.175																		0.630
0.35	0.000	0.106	0.226																		0.783
0.4	0.000	0.136	0.278	0.433																	0.939
0.45	0.001	0.165	0.331	0.505																1.402	1.099
0.5	0.001	0.195	0.385	0.578	0.792															1.576	1.262
0.55	0.002	0.225	0.439	0.652	0.883	1.129													2.095	1.751	1.428
0.6	0.003	0.255	0.493	0.726	0.977	1.242													2.292	1.928	1.598
0.65	0.004	0.285	0.547	0.801	1.072	1.357	1.640											2.804	2.487	2.107	1.772
0.7	0.005	0.315	0.601	0.877	1.169	1.475	1.782	2.069									3.253	3.028	2.682	2.289	1.949
0.75	0.008	0.347	0.656	0.955	1.268	1.599	1.930	2.244	2.523								3.514	3.247	2.879	2.475	2.131
0.8	0.011	0.379	0.713	1.034	1.372	1.727	2.086	2.428	2.737	3.004	3.230					3.928	3.765	3.465	3.077	2.665	2.317
0.85	0.017	0.413	0.771	1.117	1.479	1.862	2.250	2.623	2.962	3.259	3.515	3.734	3.928		4.257	4.218	4.010	3.681	3.278	2.860	2.508
0.9	0.025	0.451	0.833	1.203	1.592	2.004	2.424	2.829	3.201	3.529	3.814	4.061	4.281	4.483	4.593	4.496	4.250	3.897	3.482	3.058	2.705
0.95	0.037	0.492	0.900	1.295	1.713	2.156	2.609	3.048	3.454	3.815	4.130	4.406	4.652	4.875	4.911	4.765	4.487	4.115	3.690	3.260	2.906
1	0.054	0.540	0.973	1.395	1.842	2.319	2.807	3.282	3.723	4.118	4.464	4.770	5.045	5.248	5.215	5.027	4.722	4.334	3.901	3.467	3.114
1.05	0.078	0.595	1.055	1.505	1.983	2.495	3.020	3.532	4.010	4.440	4.821	5.160	5.468	5.598	5.509	5.285	4.957	4.555	4.115	3.678	3.327
1.1	0.110	0.660	1.148	1.627	2.139	2.687	3.250	3.802	4.318	4.786	5.204	5.580	5.893	5.932	5.796	5.541	5.192	4.779	4.333	3.893	3.546
1.15	0.154	0.737	1.255	1.766	2.313	2.898	3.502	4.094	4.651	5.159	5.619	6.040	6.284	6.253	6.079	5.796	5.429	5.006	4.555	4.113	3.771
1.2	0.210	0.829	1.380	1.925	2.508	3.133	3.778	4.412	5.012	5.565	6.073	6.532	6.650	6.567	6.359	6.052	5.668	5.236	4.781	4.337	4.003
1.25	0.283	0.940	1.526	2.107	2.730	3.396	4.084	4.762	5.408	6.012	6.578	6.972	7.000	6.876	6.639	6.309	5.910	5.470	5.012	4.567	4.241
1.3	0.375	1.073	1.698	2.319	2.983	3.693	4.424	5.148	5.845	6.508	7.142	7.373	7.339	7.182	6.919	6.568	6.155	5.709	5.249	4.803	4.485
1.35	0.489	1.232	1.900	2.565	3.274	4.028	4.805	5.579	6.332	7.064	7.649	7.747	7.670	7.488	7.201	6.829	6.403	5.952	5.491	5.044	4.736
1.4	0.629	1.421	2.138	2.852	3.608	4.409	5.234	6.061	6.879	7.695	8.091	8.105	7.998	7.793	7.484	7.093	6.656	6.202	5.740	5.293	4.993
1.45	0.799	1.646	2.417	3.185	3.993	4.844	5.721	6.606	7.498		8.496	8.452	8.323	8.100	7.770	7.361	6.914	6.458	5.997	5.549	5.257
1.5	1.005	1.911	2.745	3.573	4.438	5.342	6.273	7.224	8.204		8.880	8.793	8.647	8.407	8.057	7.633	7.179	6.724	6.265	5.815	5.526
1.55	1.252	2.222	3.127	4.025	4.952	5.913	6.904	7.928													
1.6	1.544	2.587	3.574	4.548	5.544	6.568	7.624	8.733													
1.65	1.890	3.014	4.092	5.155	6.227	7.320	8.449														
1.7	2.297	3.510	4.694	5.856	7.014	8.182	9.395														
1.75	2.773	4.084	5.388	6.664	7.918	9.172															
1.8	3.327	4.748	6.188	7.592	8.955																

Table 14: Gibbs free energy per mole of mixture (J/mol) as a function of temperature and ^{3}He mole fraction. The solid lines represent the transition from the He-II to the He-I region.

Temp (K)	^{3}He mole fraction																				
	0	0.05	0.1	0.15	0.2	0.25	0.3	0.35	0.4	0.45	0.5	0.55	0.6	0.65	0.7	0.75	0.8	0.85	0.9	0.95	1
0.2	0.000	-0.159																			-0.406
0.25	0.000	-0.208	-0.263																		-0.609
0.3	0.000	-0.262	-0.345																		-0.841
0.35	0.000	-0.320	-0.436																		-1.098
0.4	0.000	-0.383	-0.534	-0.615																	-1.377
0.45	0.000	-0.450	-0.639	-0.751																-1.756	-1.676
0.5	0.000	-0.520	-0.750	-0.894	-0.999															-2.116	-1.993
0.55	-0.001	-0.593	-0.866	-1.045	-1.183	-1.290													-2.479	-2.493	-2.327
0.6	-0.001	-0.668	-0.987	-1.202	-1.375	-1.515													-2.903	-2.887	-2.676
0.65	-0.001	-0.747	-1.112	-1.366	-1.574	-1.750	-1.898											-3.280	-3.344	-3.295	-3.039
0.7	-0.002	-0.827	-1.242	-1.536	-1.782	-1.993	-2.176	-2.337									-3.639	-3.756	-3.800	-3.718	-3.416
0.75	-0.002	-0.910	-1.375	-1.711	-1.996	-2.245	-2.464	-2.657	-2.834								-4.140	-4.248	-4.270	-4.153	-3.805
0.8	-0.003	-0.995	-1.513	-1.891	-2.217	-2.505	-2.762	-2.990	-3.198	-3.392	-3.580					-4.502	-4.659	-4.755	-4.753	-4.602	-4.207
0.85	-0.004	-1.082	-1.654	-2.076	-2.444	-2.774	-3.070	-3.335	-3.576	-3.800	-4.014	-4.223	-4.430		-4.844	-5.038	-5.193	-5.275	-5.249	-5.062	-4.621
0.9	-0.005	-1.171	-1.798	-2.267	-2.678	-3.051	-3.387	-3.691	-3.967	-4.223	-4.465	-4.701	-4.932	-5.162	-5.389	-5.591	-5.741	-5.809	-5.756	-5.533	-5.046
0.95	-0.007	-1.262	-1.946	-2.462	-2.919	-3.336	-3.715	-4.059	-4.372	-4.661	-4.934	-5.197	-5.454	-5.709	-5.952	-6.158	-6.302	-6.354	-6.275	-6.016	-5.482
1	-0.010	-1.355	-2.098	-2.662	-3.166	-3.629	-4.053	-4.439	-4.791	-5.115	-5.419	-5.711	-5.996	-6.276	-6.532	-6.740	-6.876	-6.910	-6.805	-6.510	-5.929
1.05	-0.014	-1.451	-2.253	-2.868	-3.420	-3.931	-4.401	-4.831	-5.223	-5.584	-5.922	-6.245	-6.558	-6.861	-7.127	-7.335	-7.462	-7.478	-7.345	-7.014	-6.386
1.1	-0.019	-1.550	-2.413	-3.079	-3.681	-4.241	-4.760	-5.236	-5.670	-6.070	-6.443	-6.798	-7.141	-7.462	-7.735	-7.942	-8.059	-8.056	-7.896	-7.528	-6.853
1.15	-0.026	-1.652	-2.577	-3.296	-3.949	-4.561	-5.130	-5.653	-6.132	-6.571	-6.981	-7.371	-7.743	-8.078	-8.356	-8.560	-8.666	-8.645	-8.457	-8.052	-7.331
1.2	-0.035	-1.758	-2.746	-3.519	-4.225	-4.890	-5.511	-6.083	-6.608	-7.090	-7.539	-7.964	-8.360	-8.708	-8.990	-9.190	-9.284	-9.243	-9.028	-8.585	-7.819
1.25	-0.046	-1.868	-2.921	-3.750	-4.510	-5.229	-5.904	-6.528	-7.100	-7.626	-8.116	-8.577	-8.993	-9.350	-9.635	-9.831	-9.912	-9.851	-9.608	-9.129	-8.316
1.3	-0.061	-1.983	-3.102	-3.988	-4.805	-5.580	-6.310	-6.987	-7.609	-8.181	-8.715	-9.207	-9.639	-10.01	-10.29	-10.48	-10.55	-10.47	-10.20	-9.681	-8.823
1.35	-0.080	-2.103	-3.291	-4.235	-5.110	-5.943	-6.730	-7.462	-8.135	-8.757	-9.335	-9.852	-10.30	-10.67	-10.96	-11.14	-11.20	-11.10	-10.80	-10.24	-9.340
1.4	-0.104	-2.230	-3.487	-4.492	-5.426	-6.319	-7.165	-7.953	-8.681	-9.354	-9.972	-10.51	-10.97	-11.35	-11.64	-11.81	-11.85	-11.73	-11.40	-10.81	-9.866
1.45	-0.133	-2.365	-3.693	-4.760	-5.755	-6.710	-7.616	-8.463	-9.247		-10.62	-11.18	-11.65	-12.04	-12.32	-12.49	-12.52	-12.38	-12.02	-11.39	-10.40
1.5	-0.168	-2.507	-3.909	-5.040	-6.099	-7.117	-8.085	-8.993	-9.837		-11.29	-11.86	-12.35	-12.74	-13.02	-13.18	-13.19	-13.03	-12.65	-11.98	-10.95
1.55	-0.211	-2.660	-4.137	-5.335	-6.459	-7.541	-8.574	-9.545													
1.6	-0.263	-2.823	-4.378	-5.645	-6.836	-7.985	-9.085	-10.12													
1.65	-0.325	-2.998	-4.634	-5.973	-7.233	-8.451	-9.619														
1.7	-0.398	-3.188	-4.908	-6.320	-7.652	-8.942	-10.18														
1.75	-0.484	-3.393	-5.200	-6.690	-8.097	-9.460															
1.8	-0.585	-3.616	-5.514	-7.084	-8.569																

Table 15: ^{4}He chemical potential (J/mol-^{4}He) as a function of temperature and ^{3}He mole fraction. The solid lines represent the transition from the He-II to the He-I region.

^{3}He mole fraction

Temp (K)	0	0.05	0.1	0.15	0.2	0.25	0.3	0.35	0.4	0.45	0.5	0.55	0.6	0.65	0.7	0.75	0.8	0.85	0.9	0.95
0.2	0.000	-0.092																		
0.25	0.000	-0.111	-0.214																	
0.3	0.000	-0.130	-0.249																	
0.35	0.000	-0.150	-0.286																	
0.4	0.000	-0.171	-0.324	-0.432																
0.45	0.000	-0.192	-0.363	-0.479																-1.378
0.5	0.000	-0.213	-0.404	-0.528	-0.642															-2.404
0.55	-0.001	-0.235	-0.446	-0.578	-0.697	-0.815													-1.268	-3.480
0.6	-0.001	-0.257	-0.489	-0.631	-0.753	-0.880													-2.113	-4.594
0.65	-0.001	-0.280	-0.533	-0.684	-0.812	-0.946	-1.072											-1.549	-3.014	-5.740
0.7	-0.002	-0.303	-0.577	-0.739	-0.871	-1.013	-1.153	-1.269									-1.401	-2.255	-3.961	-6.912
0.75	-0.002	-0.326	-0.622	-0.794	-0.931	-1.080	-1.234	-1.371	-1.471								-1.938	-3.018	-4.945	-8.107
0.8	-0.003	-0.349	-0.668	-0.850	-0.992	-1.147	-1.314	-1.472	-1.599	-1.682	-1.723					-1.880	-2.543	-3.829	-5.959	-9.321
0.85	-0.004	-0.373	-0.714	-0.907	-1.052	-1.214	-1.393	-1.572	-1.725	-1.836	-1.903	-1.936	-1.948		-1.976	-2.350	-3.203	-4.678	-6.998	-10.553
0.9	-0.005	-0.398	-0.761	-0.965	-1.113	-1.280	-1.472	-1.671	-1.850	-1.989	-2.083	-2.138	-2.165	-2.176	-2.328	-2.882	-3.908	-5.559	-8.059	-11.801
0.95	-0.007	-0.423	-0.809	-1.023	-1.174	-1.346	-1.549	-1.768	-1.974	-2.143	-2.265	-2.342	-2.385	-2.414	-2.750	-3.466	-4.651	-6.467	-9.139	-13.064
1	-0.010	-0.449	-0.859	-1.081	-1.235	-1.411	-1.625	-1.864	-2.097	-2.297	-2.447	-2.548	-2.608	-2.726	-3.230	-4.092	-5.426	-7.397	-10.236	-14.341
1.05	-0.014	-0.477	-0.909	-1.141	-1.297	-1.475	-1.701	-1.960	-2.221	-2.451	-2.631	-2.756	-2.834	-3.111	-3.758	-4.754	-6.229	-8.348	-11.349	-15.630
1.1	-0.019	-0.506	-0.961	-1.202	-1.359	-1.540	-1.776	-2.055	-2.344	-2.606	-2.816	-2.964	-3.103	-3.554	-4.326	-5.448	-7.055	-9.317	-12.476	-16.931
1.15	-0.026	-0.536	-1.014	-1.264	-1.421	-1.605	-1.851	-2.151	-2.468	-2.761	-3.000	-3.172	-3.458	-4.044	-4.930	-6.171	-7.903	-10.301	-13.615	-18.242
1.2	-0.035	-0.570	-1.070	-1.328	-1.486	-1.672	-1.927	-2.247	-2.592	-2.917	-3.184	-3.394	-3.875	-4.572	-5.564	-6.918	-8.770	-11.300	-14.767	-19.563
1.25	-0.046	-0.605	-1.129	-1.395	-1.552	-1.739	-2.005	-2.344	-2.717	-3.071	-3.363	-3.715	-4.339	-5.132	-6.226	-7.689	-9.655	-12.313	-15.931	-20.893
1.3	-0.061	-0.645	-1.191	-1.465	-1.622	-1.810	-2.085	-2.443	-2.842	-3.223	-3.539	-4.108	-4.839	-5.721	-6.914	-8.481	-10.557	-13.337	-17.105	-22.232
1.35	-0.080	-0.688	-1.258	-1.539	-1.695	-1.884	-2.168	-2.544	-2.967	-3.370	-3.811	-4.549	-5.368	-6.334	-7.624	-9.293	-11.474	-14.373	-18.289	-23.579
1.4	-0.104	-0.736	-1.329	-1.618	-1.773	-1.963	-2.255	-2.648	-3.091	-3.511	-4.173	-5.027	-5.920	-6.970	-8.357	-10.124	-12.404	-15.419	-19.482	-24.934
1.45	-0.133	-0.790	-1.405	-1.702	-1.856	-2.048	-2.348	-2.755	-3.213		-4.595	-5.532	-6.493	-7.627	-9.111	-10.973	-13.348	-16.474	-20.685	-26.299
1.5	-0.168	-0.850	-1.488	-1.793	-1.947	-2.140	-2.447	-2.865	-3.332		-5.060	-6.058	-7.084	-8.303	-9.884	-11.838	-14.302	-17.537	-21.896	-27.674
1.55	-0.211	-0.917	-1.578	-1.891	-2.046	-2.240	-2.553	-2.979												
1.6	-0.263	-0.993	-1.677	-1.999	-2.155	-2.351	-2.668	-3.096												
1.65	-0.325	-1.078	-1.785	-2.117	-2.276	-2.474	-2.793													
1.7	-0.398	-1.175	-1.904	-2.246	-2.409	-2.610	-2.928													
1.75	-0.484	-1.284	-2.036	-2.390	-2.558	-2.762														
1.8	-0.585	-1.407	-2.182	-2.548	-2.723															

Table 16: Osmotic enthalpy (J/mol-^{3}He) as a function of temperature and ^{3}He mole fraction.

Temp (K)	^{3}He mole fraction													
	0.025	0.05	0.1	0.15	0.2	0.25	0.3	0.35	0.4	0.45	0.5	0.55	0.6	0.65
0.2	1.955	2.174												
0.25	2.938	3.079	3.171											
0.3	3.943	4.017	3.986											
0.35	4.965	4.979	4.831											
0.4	5.999	5.959	5.699	5.331										
0.45	7.043	6.952	6.586	6.079										
0.5	8.096	7.955	7.488	6.844	6.524									
0.55	9.157	8.966	8.402	7.623	7.204	6.961								
0.6	10.230	9.985	9.326	8.415	7.897	7.605								
0.65	11.318	11.014	10.260	9.219	8.605	8.264	7.968							
0.7	12.432	12.056	11.204	10.035	9.328	8.939	8.630	8.268						
0.75	13.584	13.119	12.162	10.866	10.067	9.634	9.313	8.957	8.515					
0.8	14.798	14.214	13.139	11.714	10.824	10.349	10.019	9.671	9.240	8.730	8.183			
0.85	16.103	15.357	14.143	12.584	11.605	11.088	10.752	10.413	9.992	9.487	8.932	8.374	7.846	
0.9	17.541	16.570	15.186	13.485	12.414	11.857	11.514	11.185	10.776	10.274	9.712	9.133	8.578	8.068
0.95	19.166	17.882	16.284	14.428	13.260	12.660	12.310	11.992	11.595	11.096	10.525	9.926	9.343	
1	21.043	19.328	17.457	15.426	14.152	13.506	13.148	12.839	12.453	11.957	11.376	10.758	10.148	
1.05	23.253	20.950	18.727	16.495	15.103	14.404	14.034	13.732	13.356	12.863	12.273	11.636	11.002	
1.1	25.887	22.799	20.125	17.657	16.130	15.367	14.978	14.680	14.312	13.820	13.223	12.571		
1.15	29.054	24.931	21.681	18.936	17.249	16.409	15.992	15.691	15.329	14.839	14.237	13.576		
1.2	32.874	27.411	23.434	20.358	18.484	17.548	17.091	16.779	16.418	15.932	15.331			
1.25	37.484	30.313	25.426	21.955	19.859	18.804	18.290	17.959	17.595	17.113	16.520			
1.3	43.035	33.718	27.704	23.763	21.403	20.200	19.611	19.247	18.875	18.401				
1.35	49.698	37.717	30.321	25.822	23.148	21.764	21.075	20.664	20.280	19.818				
1.4	57.661	42.412	33.337	28.177	25.130	23.525	22.710	22.236	21.834	21.391				
1.45	67.137	47.915	36.818	30.878	27.392	25.521	24.547	23.991	23.566					
1.5	78.360	54.353	40.837	33.981	29.979	27.788	26.620	25.960	25.508					
1.55	91.596	61.866	45.476	37.548	32.943	30.373	28.969	28.183						
1.6	107.14	70.610	50.826	41.649	36.341	33.326	31.639	30.701						
1.65	125.32	80.761	56.988	46.361	40.238	36.700	34.681							
1.7	146.50	92.511	64.073	51.768	44.705	40.560	38.149							
1.75	171.09	106.08	72.204	57.965	49.819	44.972								
1.8	199.54	121.69	81.517	65.054	55.667									

Table 17: Lines of constant μ_4, and specific heats at constant μ_4 and constant pressure per mole of ^{3}He. The specific heats are in units of J/(mol-^{3}He K). T_{ps} is the temperature and x_{ps} the ^{3}He concentration at which the constant-μ_4 line intersects the dilute phase separation curve.

μ_4 = -0.2 J/mol-^{4}He x_{ps}= 0.0997, T_{ps}= 0.2297 K			μ_4 = -0.4 J/mol-^{4}He x_{ps}= 0.1501, T_{ps}= 0.3646 K			μ_4 = -0.6 J/mol-^{4}He x_{ps}= 0.2001, T_{ps}= 0.4608 K			μ_4 = -0.8 J/mol-^{4}He x_{ps}= 0.2499, T_{ps}= 0.5387 K			μ_4 = -1.0 J/mol-^{4}He x_{ps}= 0.3004, T_{ps}= 0.6054 K		
T (K)	x	C_{μ_4}	T (K)	x	C_{μ_4}	T (K)	x	C_{μ_4}	T (K)	x	C_{μ_4}	T (K)	x	C_{μ_4}
0.25	0.0924	16.216	0.4	0.1347	18.393	0.5	0.182	16.554	0.55	0.2435	15.357	0.65	0.2706	16.367
0.35	0.0674	19.183	0.5	0.0987	21.486	0.6	0.1376	23.524	0.65	0.1956	18.515	0.75	0.2238	18.065
0.45	0.0522	20.547	0.6	0.0801	21.807	0.7	0.1054	24.36	0.75	0.1521	25.241	0.85	0.1821	23.684
0.55	0.0424	21.211	0.7	0.0668	22.225	0.8	0.0885	22.363	0.85	0.1182	28.126	0.95	0.1431	31.367
0.65	0.0357	21.978	0.8	0.0574	23.557	0.9	0.0771	25.956	0.95	0.0985	27.788	1.05	0.1152	35.436
0.75	0.0307	23.765	0.9	0.0503	27.017	1	0.0675	30.971	1.05	0.0866	30.984	1.15	0.0982	40.636
0.85	0.0268	28.216	1	0.0445	34.615	1.1	0.0597	41.068	1.15	0.0768	43.371	1.25	0.0868	52.352
0.95	0.0236	38.48	1.1	0.0394	49.654	1.2	0.0528	59.578	1.25	0.0676	61.701	1.35	0.0765	80.351
1.05	0.0206	60.536	1.2	0.0345	78.175	1.3	0.0462	92.766	1.35	0.0592	93.619	1.45	0.0661	123.24
1.15	0.0176	107.25	1.3	0.0296	133.67	1.4	0.0395	154.75	1.45	0.0508	150.89	1.55	0.0558	201.41
1.25	0.0143	215.33	1.4	0.0241	253.78	1.5	0.0322	285.63	1.55	0.042	264.32	1.65	0.045	363.78
μ_4 = -1.2 J/mol-^{4}He x_{ps}= 0.3525, T_{ps}= 0.6647 K			μ_4 = -1.4 J/mol-^{4}He x_{ps}= 0.4081, T_{ps}= 0.7188 K			μ_4 = -1.6 J/mol-^{4}He x_{ps}= 0.4702, T_{ps}= 0.7690 K			μ_4 = -1.8 J/mol-^{4}He x_{ps}= 0.5456, T_{ps}= 0.8162 K			μ_4 = -2.0 J/mol-^{4}He x_{ps}= 0.6544, T_{ps}= 0.8612 K		
T (K)	x	C_{μ_4}	T (K)	x	C_{μ_4}	T (K)	x	C_{μ_4}	T (K)	x	C_{μ_4}	T (K)	x	C_{μ_4}
0.7	0.3185	18.567	0.75	0.3624	22.233	0.8	0.4007	26.323	0.85	0.4315	29.513	0.9	0.4546	31.234
0.8	0.2661	17.222	0.85	0.3018	17.682	0.9	0.332	18.699	0.95	0.3574	19.937	1	0.3785	21.251
0.9	0.2271	19.952	0.95	0.2641	18.909	1	0.2945	19.215	1.05	0.3196	20.155	1.1	0.3405	21.448
1	0.1886	27.119	1.05	0.2304	23.236	1.1	0.2639	22.364	1.15	0.2905	23.026	1.2	0.3121	24.457
1.1	0.1495	39.19	1.15	0.1932	34.436	1.2	0.2326	29.988	1.25	0.2629	29.387	1.3	0.2863	30.731
1.2	0.1198	49.301	1.25	0.1514	55.438	1.3	0.193	50.567	1.35	0.2303	44.18	1.4	0.2576	43.471
1.3	0.101	61.699	1.35	0.1194	74.237	1.4	0.1453	87.321	1.45	0.1811	89.631	1.5	0.2162	78.868
1.4	0.0882	83.395	1.45	0.0995	97.719	1.5	0.1129	116.95	1.55	0.1294	141.26	1.6	0.1503	170.2
1.5	0.0765	132.91	1.55	0.0857	138.16	1.6	0.0935	158.94	1.65	0.1014	187.75			
1.6	0.0642	214.1	1.65	0.0717	233.67									

μ_4 = -2.2 J/mol-^{4}He			μ_4 = -2.4 J/mol-^{4}He			μ_4 = -2.6 J/mol-^{4}He			μ_4 = -2.8 J/mol-^{4}He			μ_4 = -3.0 J/mol-^{4}He		
T (K)	x	C_{μ_4}	T (K)	x	C_{μ_4}	T (K)	x	C_{μ_4}	T (K)	x	C_{μ_4}	T (K)	x	C_{μ_4}
0.95	0.471	31.845	0.95	0.6293	134.65	1	0.5911	69.828	1.05	0.5751	53.64	1.1	0.566	46.63
1.05	0.3959	22.598	1.05	0.438	25.638	1.1	0.4487	26.785	1.15	0.4572	28.017	1.2	0.4643	29.432
1.15	0.3578	22.999	1.15	0.3892	23.934	1.2	0.4012	25.705	1.25	0.4113	27.723	1.3	0.4201	30.057
1.25	0.3298	26.394	1.25	0.3576	26.404	1.3	0.3699	28.819	1.35	0.3804	31.641	1.4	0.3898	34.937
1.35	0.3047	33.122	1.35	0.332	31.993	1.4	0.3444	35.297	1.45	0.355	39.2	1.5	0.3646	43.762
1.45	0.2778	45.774	1.45	0.3071	41.984	1.5	0.3196	46.496	1.55	0.3302	51.905	1.6	0.3395	58.244
1.55	0.2415	75.575	1.55	0.2781	60.935	1.6	0.2908	67.027	1.65	0.3354	89.542			

E.2 Properties at high pressures

Table 18: Properties at 2 bar. (h : J/mol, s : J/mol K, μ_4: J/mol-^{4}He, h^{os} : J/mol-^{3}He, v : cm^3/mol)

2 bar: x_t = 0.692, T_t = 0.809 K			x	0	0.1	0.2	0.3	0.4	0.5	0.6	0.7	0.8	0.9	1
T	*Dil-Φ*	*Conc-Φ*	T_λ	2.129	1.998	1.847	1.676	1.484	1.272	1.040				
0.2 K	5.692	7.483	h	5.453	5.679	5.884	6.086	6.287	6.488	6.689	6.891	7.092	7.293	7.480
	1.377	3.879	s	0.000	1.346	1.647	1.928	2.209	2.490	2.771	3.052	3.333	3.614	3.802
x_d = 0.104	5.265	5.265	μ_4	5.453	5.273	5.265	5.265	5.265	5.265	5.265	5.265	5.265	5.265	
x_c = 0.995	9.359	7.495	h^{os}		9.339	8.362	8.000	7.820	7.711	7.639	7.587	7.548	7.518	
	27.697	34.555	v	26.964	27.668	28.435	29.205	29.975	30.746	31.516	32.286	33.056	33.826	34.624
0.3 K	5.911	7.846	h	5.453	5.778	6.058	6.288	6.517	6.747	6.977	7.206	7.436	7.666	7.764
	2.087	5.418	s	0.001	1.744	2.341	2.736	3.131	3.526	3.921	4.316	4.711	5.106	4.953
x_d = 0.136	5.133	5.133	μ_4	5.452	5.203	5.133	5.133	5.133	5.133	5.133	5.133	5.133	5.133	
x_c = 0.979	10.858	7.905	h^{os}		10.958	9.757	8.981	8.593	8.361	8.205	8.095	8.011	7.947	
	27.913	34.343	v	26.964	27.661	28.403	29.166	29.928	30.691	31.454	32.217	32.979	33.742	34.596
0.4 K	6.252	8.292	h	5.453	5.882	6.310	6.576	6.842	7.108	7.374	7.640	7.906	8.172	8.066
	2.951	6.779	s	0.001	2.042	3.059	3.559	4.058	4.557	5.057	5.556	6.056	6.555	5.821
x_d = 0.178	4.953	4.953	μ_4	5.452	5.126	4.953	4.953	4.953	4.953	4.953	4.953	4.953	4.953	
x_c = 0.945	12.234	8.486	h^{os}		12.682	11.735	10.362	9.675	9.263	8.988	8.792	8.644	8.530	
	28.207	33.973	v	26.964	27.655	28.370	29.122	29.874	30.626	31.379	32.131	32.883	33.635	34.578
0.5 K	6.763	8.798	h	5.454	5.988	6.545	6.963	7.271	7.578	7.886	8.194	8.502	8.770	8.378
	4.034	7.950	s	0.003	2.279	3.592	4.418	5.010	5.603	6.195	6.787	7.379	7.893	6.516
x_d = 0.235	4.719	4.719	μ_4	5.452	5.045	4.804	4.719	4.719	4.719	4.719	4.719	4.719	4.584	
x_c = 0.896	13.416	9.270	h^{os}		14.470	13.512	12.199	11.098	10.438	9.998	9.683	9.447	9.235	
	28.601	33.536	v	26.964	27.649	28.352	29.085	29.832	30.578	31.324	32.070	32.816	33.568	34.568
0.6 K	7.495	9.335	h	5.455	6.094	6.734	7.411	7.803	8.154	8.505	8.855	9.206	9.147	8.700
	5.390	8.907	s	0.005	2.473	3.936	5.238	5.979	6.649	7.320	7.990	8.661	8.580	7.103
x_d = 0.312	4.423	4.423	μ_4	5.452	4.961	4.690	4.448	4.423	4.423	4.423	4.423	4.423	2.995	
x_c = 0.837	14.266	10.293	h^{os}		16.296	14.908	14.324	12.874	11.885	11.226	10.755	10.402	9.831	
	29.144	33.080	v	26.964	27.644	28.341	29.056	29.803	30.553	31.303	32.054	32.804	33.618	34.568
0.7 K	8.532	9.868	h	5.457	6.201	6.927	7.696	8.381	8.815	9.206	9.596	9.894	9.521	9.033
	7.137	9.641	s	0.008	2.638	4.234	5.676	6.871	7.667	8.399	9.132	9.726	9.156	7.616
x_d = 0.428	4.058	4.058	μ_4	5.451	4.873	4.573	4.281	4.079	4.058	4.058	4.058	3.869	1.189	
x_c = 0.770	14.522	11.608	h^{os}		18.152	16.346	15.663	14.833	13.572	12.638	11.970	11.400	10.447	
	29.988	32.612	v	26.965	27.639	28.331	29.046	29.782	30.544	31.311	32.078	32.854	33.680	34.579
0.8 K	10.173	10.352	h	5.463	6.311	7.129	7.999	8.796	9.424	9.929	10.359	10.387	9.893	9.379
	9.808	10.137	s	0.016	2.784	4.503	6.082	7.425	8.484	9.365	10.151	10.386	9.653	8.078
x_d = 0.656	3.621	3.621	μ_4	5.450	4.784	4.452	4.116	3.812	3.665	3.624	3.620	2.734	-0.767	
x_c = 0.698	13.615	13.262	h^{os}		20.054	17.834	17.060	16.271	15.184	14.132	13.247	12.301	11.078	
	31.781	32.121	v	26.965	27.637	28.324	29.039	29.784	30.554	31.340	32.136	32.938	33.754	34.601
0.9 K			h	5.477	6.428	7.345	8.330	9.250	9.994	10.587	11.032	10.844	10.270	9.741
			s	0.032	2.923	4.757	6.471	7.959	9.155	10.140	10.944	10.924	10.096	8.503
			μ_4	5.448	4.691	4.332	3.955	3.550	3.285	3.175	2.984	1.374	-2.824	
			h^{os}		22.063	19.397	18.540	17.799	16.703	15.529	14.481	13.211	11.724	
			v	26.966	27.636	28.321	29.040	29.796	30.586	31.398	32.219	33.037	33.843	34.635

1.0 K	h	5.506	6.565	7.586	8.698	9.749	10.615	11.316	11.616	11.277	10.651	10.119
	s	0.063	3.066	5.011	6.858	8.485	9.808	10.908	11.560	11.381	10.498	8.902
	μ_4	5.443	4.595	4.210	3.797	3.290	2.902	2.709	2.068	-0.136	-4.952	
	h^{os}		24.294	21.089	20.132	19.437	18.328	17.055	15.708	14.130	12.385	
	v	26.966	27.636	28.325	29.052	29.823	30.635	31.474	32.320	33.152	33.946	34.683
1.1 K	h	5.565	6.737	7.870	9.116	10.307	11.307	12.111	12.143	11.696	11.040	10.515
	s	0.119	3.230	5.282	7.256	9.016	10.467	11.665	12.062	11.780	10.868	9.280
	μ_4	5.434	4.494	4.087	3.641	3.031	2.514	2.194	0.961	-1.749	-7.133	
	h^{os}		26.925	23.004	21.891	21.222	20.100	18.722	16.934	15.057	13.059	
	v	26.965	27.639	28.337	29.079	29.872	30.709	31.575	32.444	33.287	34.066	34.744
1.2 K	h	5.668	6.967	8.222	9.608	10.947	12.109	12.794	12.632	12.107	11.435	10.931
	s	0.209	3.430	5.587	7.684	9.573	11.164	12.260	12.489	12.138	11.212	9.641
	μ_4	5.418	4.385	3.959	3.484	2.769	2.127	1.405	-0.279	-3.438	-9.353	
	h^{os}		30.207	25.277	23.899	23.214	22.091	20.386	18.166	15.993	13.745	
	v	26.963	27.644	28.359	29.126	29.947	30.813	31.706	32.596	33.443	34.203	34.820
1.3 K	h	5.838	7.283	8.675	10.206	11.707	13.087	13.384	13.098	12.513	11.840	11.366
	s	0.344	3.682	5.949	8.161	10.180	11.946	12.733	12.862	12.462	11.536	9.990
	μ_4	5.391	4.263	3.820	3.318	2.505	1.755	0.431	-1.620	-5.182	-11.602	
	h^{os}		34.462	28.095	26.278	25.512	24.419	22.020	19.406	16.936	14.445	
	v	26.959	27.650	28.393	29.196	30.054	30.955	31.874	32.779	33.625	34.357	34.912
1.4 K	h	6.100	7.721	9.271	10.954	12.648	13.921	13.919	13.546	12.916	12.259	11.821
	s	0.537	4.006	6.390	8.715	10.876	12.565	13.130	13.194	12.761	11.847	10.327
	μ_4	5.347	4.124	3.663	3.136	2.240	1.106	-0.653	-3.041	-6.969	-13.871	
	h^{os}		40.097	31.701	29.195	28.259	26.735	23.634	20.655	17.887	15.162	
	v	26.952	27.658	28.441	29.293	30.199	31.139	32.085	32.999	33.834	34.531	35.019
1.5 K	h	6.486	8.327	10.066	11.914	13.854	14.565	14.415	13.976	13.322	12.701	12.296
	s	0.803	4.423	6.937	9.377	11.707	13.010	13.472	13.490	13.042	12.151	10.654
	μ_4	5.281	3.962	3.481	2.930	1.981	0.208	-1.810	-4.527	-8.782	-16.153	
	h^{os}		47.616	36.407	32.878	31.665	28.922	25.232	21.906	18.848	15.907	
	v	26.942	27.667	28.504	29.421	30.387	31.373	32.344	33.260	34.073	34.725	35.144

Table 19: Properties at 4 bar. (h : J/mol, s : J/mol K, μ_4 : J/mol-^{4}He, h^{os} : J/mol-^{3}He, v : cm^3/mol)

4 bar: x_t = 0.698, T_t = 0.786 K			x	0	0.1	0.2	0.3	0.4	0.5	0.6	0.7	0.8	0.9	1
T	*Dil-Φ*	*Conc-Φ*	T_i	2.108	1.979	1.829	1.660	1.470	1.260	1.030				
0.2 K	11.203	14.250	h	10.791	11.155	11.509	11.855	12.201	12.547	12.893	13.238	13.584	13.930	14.260
	1.434	3.966	s	0.000	1.357	1.688	1.976	2.263	2.550	2.838	3.125	3.412	3.700	3.856
x_d = 0.112	10.594	10.594	μ_4	10.791	10.612	10.594	10.594	10.594	10.594	10.594	10.594	10.594	10.594	
x_c = 0.993	16.050	14.278	h^{os}		16.041	15.167	14.796	14.610	14.499	14.425	14.372	14.332	14.301	
	27.155	33.074	v	26.438	27.081	27.749	28.421	29.093	29.765	30.437	31.109	31.780	32.452	33.152
0.3 K	11.465	14.615	h	10.792	11.254	11.685	12.063	12.440	12.817	13.194	13.571	13.949	14.326	14.542
	2.154	5.606	s	0.001	1.757	2.395	2.809	3.222	3.636	4.049	4.462	4.876	5.289	4.995
x_d = 0.142	10.460	10.460	μ_4	10.791	10.541	10.460	10.460	10.460	10.460	10.460	10.460	10.460	10.460	
x_c = 0.977	17.556	14.714	h^{os}		17.670	16.586	15.801	15.409	15.174	15.017	14.905	14.821	14.756	
	27.341	32.902	v	26.438	27.075	27.730	28.396	29.062	29.728	30.394	31.060	31.726	32.392	33.131
0.4 K	11.864	14.990	h	10.792	11.358	11.936	12.348	12.760	13.172	13.584	13.996	14.408	14.820	14.839
	3.020	6.916	s	0.001	2.055	3.110	3.624	4.137	4.650	5.164	5.677	6.191	6.704	5.849
x_d = 0.182	10.278	10.278	μ_4	10.791	10.464	10.278	10.278	10.278	10.278	10.278	10.278	10.278	10.278	
x_c = 0.941	18.965	15.284	h^{os}		19.399	18.565	17.176	16.482	16.065	15.788	15.589	15.440	15.325	
	27.594	32.597	v	26.438	27.069	27.709	28.369	29.028	29.687	30.347	31.006	31.665	32.325	33.114
0.5 K	12.457	15.362	h	10.792	11.463	12.159	12.729	13.175	13.621	14.067	14.513	14.958	15.304	15.144
	4.111	7.949	s	0.002	2.291	3.614	4.471	5.060	5.649	6.237	6.826	7.415	7.799	6.530
x_d = 0.239	10.040	10.040	μ_4	10.791	10.383	10.138	10.040	10.040	10.040	10.040	10.040	10.040	9.684	
x_c = 0.891	20.160	16.016	h^{os}		21.187	20.242	19.005	17.878	17.202	16.752	16.430	16.188	15.928	
	27.942	32.241	v	26.439	27.063	27.695	28.346	29.005	29.665	30.324	30.984	31.643	32.310	33.102
0.6 K	13.326	15.744	h	10.793	11.569	12.347	13.159	13.703	14.179	14.655	15.131	15.608	15.670	15.457
	5.509	8.781	s	0.004	2.484	3.957	5.259	6.019	6.663	7.307	7.952	8.596	8.466	7.100
x_d = 0.321	9.734	9.734	μ_4	10.791	10.298	10.024	9.774	9.734	9.734	9.734	9.734	9.734	8.158	
x_c = 0.829	20.933	16.987	h^{os}		23.007	21.639	21.057	19.658	18.625	17.937	17.445	17.076	16.505	
	28.458	31.860	v	26.439	27.056	27.684	28.324	28.989	29.659	30.328	30.998	31.668	32.362	33.097
0.7 K	14.627	16.141	h	10.796	11.675	12.537	13.440	14.254	14.843	15.342	15.842	16.243	16.032	15.778
	7.390	9.453	s	0.007	2.648	4.250	5.691	6.873	7.684	8.365	9.046	9.579	9.024	7.596
x_d = 0.457	9.348	9.348	μ_4	10.790	10.211	9.905	9.603	9.389	9.348	9.348	9.348	9.130	6.414	
x_c = 0.760	20.902	18.289	h^{os}		24.851	23.065	22.391	21.552	20.337	19.339	18.626	18.021	17.100	
	29.352	31.444	v	26.439	27.050	27.675	28.315	28.971	29.650	30.341	31.032	31.726	32.421	33.098
0.8 K			h	10.801	11.783	12.732	13.733	14.657	15.408	16.028	16.573	16.726	16.392	16.110
			s	0.015	2.791	4.511	6.083	7.411	8.441	9.282	10.022	10.225	9.505	8.038
			μ_4	10.789	10.121	9.784	9.435	9.114	8.948	8.892	8.880	7.997	4.519	
			h^{os}		26.739	24.526	23.762	22.971	21.867	20.785	19.870	18.908	17.711	
			v	26.439	27.045	27.670	28.312	28.974	29.656	30.358	31.076	31.793	32.484	33.106
0.9 K			h	10.815	11.899	12.938	14.046	15.089	15.955	16.667	17.231	17.170	16.755	16.454
			s	0.032	2.928	4.753	6.452	7.919	9.086	10.034	10.798	10.748	9.933	8.443
			μ_4	10.787	10.028	9.661	9.270	8.845	8.558	8.426	8.229	6.642	2.522	
			h^{os}		28.733	26.046	25.190	24.454	23.353	22.162	21.088	19.802	18.337	
			v	26.440	27.040	27.670	28.319	28.986	29.676	30.392	31.126	31.859	32.548	33.123
1.0 K			h	10.847	12.033	13.166	14.388	15.556	16.543	17.368	17.794	17.589	17.124	16.811
			s	0.064	3.069	4.992	6.811	8.410	9.704	10.772	11.392	11.190	10.322	8.819
			μ_4	10.782	9.931	9.537	9.109	8.581	8.167	7.950	7.304	5.141	0.452	
			h^{os}		30.953	27.679	26.705	26.017	24.918	23.647	22.289	20.701	18.977	
			v	26.439	27.035	27.676	28.336	29.012	29.708	30.431	31.178	31.923	32.611	33.148

1.1 K	h	10.908	12.203	13.431	14.771	16.068	17.188	18.123	18.293	17.993	17.501	17.182
	s	0.122	3.231	5.245	7.176	8.898	10.319	11.492	11.868	11.575	10.680	9.173
	μ_4	10.773	9.828	9.410	8.949	8.319	7.777	7.434	6.198	3.543	-1.671	
	h^{os}		33.584	29.518	28.356	27.692	26.599	25.250	23.476	21.605	19.631	
	v	26.438	27.030	27.689	28.368	29.054	29.755	30.479	31.229	31.980	32.670	33.183
1.2 K	h	11.016	12.431	13.760	15.217	16.648	17.928	18.754	18.748	18.386	17.885	17.569
	s	0.216	3.429	5.531	7.564	9.402	10.962	12.042	12.265	11.918	11.014	9.509
	μ_4	10.757	9.715	9.275	8.786	8.056	7.395	6.654	4.972	1.879	-3.836	
	h^{os}		36.880	31.698	30.222	29.535	28.461	26.821	24.653	22.513	20.298	
	v	26.435	27.026	27.711	28.416	29.117	29.818	30.537	31.280	32.030	32.723	33.227
1.3 K	h	11.192	12.746	14.183	15.756	17.332	18.827	19.279	19.172	18.773	18.279	17.971
	s	0.357	3.681	5.869	7.995	9.949	11.681	12.462	12.604	12.227	11.330	9.831
	μ_4	10.729	9.588	9.128	8.614	7.794	7.036	5.703	3.661	0.171	-6.032	
	h^{os}		41.168	34.405	32.421	31.638	30.619	28.330	25.820	23.424	20.981	
	v	26.429	27.020	27.742	28.484	29.203	29.903	30.605	31.331	32.070	32.766	33.283
1.4 K	h	11.463	13.184	14.744	16.433	18.177	19.563	19.734	19.569	19.156	18.690	18.388
	s	0.557	4.004	6.284	8.496	10.575	12.228	12.799	12.899	12.511	11.634	10.140
	μ_4	10.683	9.443	8.960	8.425	7.534	6.409	4.657	2.289	-1.564	-8.250	
	h^{os}		46.857	37.882	35.120	34.142	32.717	29.784	26.975	24.336	21.683	
	v	26.420	27.014	27.784	28.572	29.316	30.010	30.687	31.379	32.098	32.797	33.350
1.5 K	h	11.860	13.790	15.497	17.308	19.269	20.089	20.132	19.939	19.540	19.124	18.819
	s	0.830	4.421	6.803	9.098	11.327	12.591	13.075	13.154	12.776	11.934	10.437
	μ_4	10.615	9.272	8.762	8.209	7.283	5.544	3.558	0.874	-3.308	-10.484	
	h^{os}		54.453	42.438	38.538	37.249	34.634	31.181	28.110	25.252	22.414	
	v	26.408	27.007	27.837	28.685	29.458	30.144	30.783	31.426	32.110	32.813	33.430

Table 20: Properties at 6 bar. (h : J/mol, s : J/mol K, μ_4 : J/mol-^{4}He, h^{os} : J/mol-^{3}He, v : cm^3/mol)

6 bar: x_t = 0.700, T_t = 0.772 K			x	0	0.1	0.2	0.3	0.4	0.5	0.6	0.7	0.8	0.9	1
T	*Dil-Φ*	*Conc-Φ*	T_i	2.092	1.962	1.813	1.644	1.456	1.248	1.020				
0.2 K	16.607	20.758	h	16.032	16.521	17.005	17.479	17.954	18.428	18.902	19.377	19.851	20.325	20.783
	1.467	4.032	s	0.000	1.367	1.713	2.006	2.299	2.592	2.885	3.178	3.471	3.764	3.899
x_d = 0.116	15.831	15.831	μ_4	16.032	15.853	15.831	15.831	15.831	15.831	15.831	15.831	15.831	15.831	
x_c = 0.991	22.518	20.801	h^{os}		22.539	21.701	21.325	21.138	21.025	20.950	20.896	20.856	20.824	
	26.671	31.951	v	25.980	26.576	27.178	27.781	28.385	28.988	29.591	30.194	30.798	31.401	32.028
0.3 K	16.907	21.108	h	16.032	16.621	17.184	17.691	18.198	18.705	19.212	19.719	20.226	20.733	21.063
	2.197	5.723	s	0.000	1.768	2.430	2.855	3.281	3.706	4.132	4.557	4.983	5.408	5.032
x_d = 0.145	15.696	15.696	μ_4	16.032	15.782	15.696	15.696	15.696	15.696	15.696	15.696	15.696	15.696	
x_c = 0.974	24.023	21.253	h^{os}		24.173	23.135	22.345	21.951	21.714	21.556	21.443	21.359	21.293	
	26.839	31.799	v	25.980	26.571	27.166	27.765	28.363	28.962	29.561	30.160	30.758	31.357	32.009
0.4 K	17.358	21.408	h	16.033	16.725	17.435	17.973	18.512	19.051	19.589	20.128	20.666	21.205	21.357
	3.073	6.956	s	0.001	2.068	3.146	3.662	4.179	4.695	5.212	5.728	6.245	6.761	5.878
x_d = 0.186	15.513	15.513	μ_4	16.032	15.705	15.513	15.513	15.513	15.513	15.513	15.513	15.513	15.513	
x_c = 0.938	25.448	21.800	h^{os}		25.905	25.124	23.716	23.011	22.589	22.307	22.106	21.955	21.837	
	27.067	31.551	v	25.980	26.565	27.152	27.748	28.344	28.941	29.537	30.133	30.730	31.326	31.993
0.5 K	18.031	21.662	h	16.033	16.831	17.652	18.356	18.919	19.483	20.047	20.611	21.175	21.617	21.658
	4.181	7.871	s	0.002	2.304	3.636	4.510	5.083	5.656	6.230	6.803	7.376	7.699	6.550
x_d = 0.243	15.269	15.269	μ_4	16.032	15.624	15.377	15.269	15.269	15.269	15.269	15.269	15.269	14.822	
x_c = 0.886	26.661	22.481	h^{os}		27.697	26.752	25.558	24.396	23.698	23.233	22.901	22.651	22.372	
	27.387	31.263	v	25.980	26.559	27.139	27.733	28.335	28.937	29.539	30.141	30.743	31.348	31.980
0.6 K	19.040	21.931	h	16.034	16.937	17.838	18.773	19.459	20.042	20.626	21.209	21.792	21.977	21.966
	5.625	8.643	s	0.004	2.498	3.976	5.280	6.063	6.672	7.281	7.889	8.498	8.356	7.110
x_d = 0.328	14.949	14.949	μ_4	16.032	15.539	15.261	15.007	14.949	14.949	14.949	14.949	14.949	13.357	
x_c = 0.824	27.417	23.425	h^{os}		29.521	28.145	27.562	26.224	25.136	24.410	23.892	23.503	22.935	
	27.878	30.936	v	25.980	26.552	27.129	27.712	28.321	28.938	29.555	30.172	30.789	31.402	31.971
0.7 K	20.613	22.240	h	16.036	17.043	18.025	19.048	19.984	20.743	21.333	21.923	22.415	22.337	22.280
	7.613	9.321	s	0.007	2.661	4.263	5.703	6.879	7.749	8.369	8.989	9.461	8.911	7.594
x_d = 0.478	14.537	14.537	μ_4	16.031	15.451	15.141	14.834	14.609	14.537	14.537	14.537	14.316	11.668	
x_c = 0.754	27.246	24.759	h^{os}		31.371	29.558	28.881	28.046	26.948	25.864	25.089	24.439	23.523	
	28.773	30.544	v	25.980	26.545	27.122	27.704	28.298	28.914	29.557	30.200	30.844	31.457	31.966
0.8 K			h	16.042	17.150	18.214	19.331	20.376	21.248	21.986	22.642	22.907	22.702	22.602
			s	0.015	2.804	4.516	6.081	7.402	8.423	9.243	9.950	10.119	9.397	8.025
			μ_4	16.030	15.360	15.018	14.664	14.331	14.144	14.061	14.031	13.174	9.820	
			h^{os}		33.267	30.998	30.221	29.443	28.352	27.270	26.333	25.340	24.133	
			v	25.980	26.538	27.117	27.702	28.296	28.910	29.553	30.222	30.892	31.506	31.966
0.9 K			h	16.057	17.266	18.411	19.629	20.791	21.785	22.626	23.312	23.368	23.077	22.934
			s	0.032	2.940	4.749	6.431	7.891	9.056	9.996	10.739	10.663	9.839	8.416
			μ_4	16.028	15.265	14.893	14.498	14.062	13.751	13.586	13.365	11.809	7.856	
			h^{os}		35.277	32.486	31.602	30.884	29.819	28.652	27.575	26.258	24.768	
			v	25.980	26.531	27.116	27.706	28.300	28.914	29.560	30.240	30.925	31.544	31.971
1.0 K			h	16.090	17.401	18.627	19.949	21.234	22.357	23.326	23.892	23.815	23.468	23.277
			s	0.067	3.082	4.976	6.768	8.358	9.658	10.733	11.351	11.134	10.251	8.777
			μ_4	16.023	15.165	14.764	14.335	13.801	13.366	13.111	12.432	10.297	5.801	
			h^{os}		37.525	34.080	33.048	32.384	31.348	30.136	28.803	27.195	25.430	
			v	25.980	26.524	27.120	27.719	28.314	28.921	29.561	30.242	30.936	31.566	31.982

1.1 K	h	16.154	17.572	18.879	20.304	21.716	22.981	24.081	24.415	24.259	23.876	23.631
	s	0.128	3.245	5.215	7.106	8.816	10.252	11.453	11.850	11.556	10.640	9.114
	μ_4	16.014	15.058	14.631	14.174	13.546	12.990	12.608	11.330	8.690	3.670	
	h^{os}		40.201	35.870	34.609	33.970	32.972	31.730	30.023	28.151	26.121	
	v	25.977	26.516	27.130	27.742	28.337	28.932	29.556	30.225	30.921	31.567	31.999
1.2 K	h	16.267	17.802	19.190	20.715	22.256	23.695	24.712	24.902	24.706	24.305	23.998
	s	0.226	3.445	5.485	7.463	9.286	10.872	12.003	12.274	11.945	11.013	9.433
	μ_4	15.997	14.940	14.489	14.010	13.296	12.633	11.857	10.121	7.018	1.471	
	h^{os}		43.566	37.994	36.361	35.696	34.757	33.282	31.237	29.128	26.842	
	v	25.973	26.507	27.145	27.778	28.373	28.949	29.542	30.185	30.874	31.540	32.024
1.3 K	h	16.451	18.121	19.593	21.211	22.891	24.560	25.237	25.366	25.162	24.759	24.376
	s	0.372	3.699	5.807	7.860	9.793	11.564	12.423	12.646	12.310	11.376	9.736
	μ_4	15.967	14.806	14.331	13.836	13.050	12.310	10.951	8.844	5.306	-0.790	
	h^{os}		47.951	40.638	38.421	37.651	36.810	34.760	32.447	30.126	27.598	
	v	25.967	26.497	27.168	27.827	28.424	28.971	29.520	30.119	30.788	31.481	32.056
1.4 K	h	16.731	18.564	20.129	21.837	23.677	25.254	25.690	25.813	25.631	25.244	24.766
	s	0.579	4.027	6.204	8.323	10.375	12.080	12.760	12.977	12.658	11.735	10.025
	μ_4	15.920	14.652	14.151	13.644	12.812	11.733	9.972	7.526	3.572	-3.109	
	h^{os}		53.769	44.043	40.952	39.973	38.775	36.169	33.651	31.146	28.394	
	v	25.956	26.485	27.197	27.892	28.490	29.001	29.487	30.023	30.658	31.385	32.096
1.5 K	h	17.140	19.176	20.853	22.650	24.698	25.731	26.089	26.244	26.120	25.772	25.166
	s	0.861	4.448	6.703	8.883	11.078	12.409	13.035	13.274	12.995	12.099	10.301
	μ_4	15.849	14.470	13.937	13.426	12.590	10.934	8.963	6.188	1.833	-5.484	
	h^{os}		61.525	48.518	44.172	42.860	40.527	37.506	34.839	32.192	29.245	
	v	25.942	26.470	27.235	27.973	28.574	29.040	29.444	29.892	30.478	31.245	32.144

Table 21: Properties at 8 bar. (h : J/mol, s : J/mol K, μ_4 : J/mol-^{4}He, h^{os} : J/mol-^{3}He, v : cm^3/mol)

8 bar: x_t = 0.699, T_t = 0.764 K			x	0	0.1	0.2	0.3	0.4	0.5	0.6	0.7	0.8	0.9	1
T	*Dil-Φ*	*Conc-Φ*	T_λ	2.075	1.945	1.795	1.627	1.439	1.233	1.007				
0.2 K	21.908	27.064	h	21.187	21.793	22.393	22.984	23.575	24.165	24.756	25.347	25.937	26.528	27.100
	1.484	4.105	s	0.000	1.375	1.731	2.031	2.331	2.631	2.932	3.232	3.532	3.832	3.938
x_d = 0.118	20.986	20.986	μ_4	21.187	21.008	20.986	20.986	20.986	20.986	20.986	20.986	20.986	20.986	
x_c = 0.991	28.810	27.121	h^{os}		28.856	28.023	27.646	27.458	27.345	27.270	27.216	27.175	27.144	
	26.228	31.015	v	25.572	26.130	26.678	27.227	27.775	28.324	28.872	29.421	29.969	30.517	31.092
0.3 K	22.250	27.377	h	21.187	21.893	22.573	23.197	23.820	24.444	25.067	25.691	26.315	26.938	27.379
	2.227	5.793	s	0.000	1.779	2.452	2.886	3.319	3.753	4.187	4.620	5.054	5.488	5.066
x_d = 0.148	20.850	20.850	μ_4	21.187	20.937	20.850	20.850	20.850	20.850	20.850	20.850	20.850	20.850	
x_c = 0.970	30.294	27.576	h^{os}		30.497	29.463	28.671	28.275	28.037	27.879	27.766	27.681	27.615	
	26.387	30.857	v	25.572	26.125	26.669	27.213	27.756	28.300	28.844	29.387	29.931	30.474	31.073
0.4 K	22.758	27.596	h	21.187	21.998	22.826	23.476	24.126	24.777	25.427	26.077	26.727	27.378	27.671
	3.119	6.922	s	0.001	2.080	3.172	3.684	4.195	4.706	5.217	5.728	6.240	6.751	5.908
x_d = 0.190	20.665	20.665	μ_4	21.187	20.860	20.665	20.665	20.665	20.665	20.665	20.665	20.665	20.665	
x_c = 0.934	31.706	28.089	h^{os}		32.238	31.468	30.035	29.318	28.888	28.601	28.397	28.243	28.124	
	26.603	30.644	v	25.572	26.119	26.660	27.203	27.746	28.289	28.832	29.376	29.919	30.462	31.057
0.5 K	23.513	27.749	h	21.187	22.104	23.040	23.864	24.530	25.197	25.864	26.531	27.197	27.742	27.970
	4.254	7.738	s	0.002	2.318	3.656	4.543	5.091	5.639	6.188	6.736	7.284	7.582	6.574
x_d = 0.247	20.414	20.414	μ_4	21.187	20.778	20.531	20.414	20.414	20.414	20.414	20.414	20.414	19.950	
x_c = 0.883	32.939	28.723	h^{os}		34.037	33.073	31.912	30.704	29.980	29.497	29.152	28.893	28.608	
	26.903	30.412	v	25.573	26.112	26.650	27.194	27.746	28.298	28.851	29.403	29.955	30.508	31.043
0.6 K	24.659	27.939	h	21.188	22.210	23.225	24.273	25.098	25.774	26.450	27.126	27.802	28.103	28.273
	5.753	8.496	s	0.003	2.512	3.994	5.299	6.121	6.686	7.251	7.816	8.381	8.239	7.127
x_d = 0.335	20.078	20.078	μ_4	21.186	20.693	20.415	20.158	20.078	20.078	20.078	20.078	20.078	18.552	
x_c = 0.820	33.752	29.661	h^{os}		35.869	34.465	33.873	32.628	31.470	30.698	30.146	29.732	29.164	
	27.362	30.135	v	25.573	26.105	26.640	27.174	27.733	28.305	28.876	29.447	30.019	30.574	31.032
0.7 K	26.496	28.189	h	21.190	22.316	23.409	24.543	25.591	26.546	27.206	27.867	28.432	28.472	28.582
	7.831	9.222	s	0.006	2.674	4.277	5.716	6.891	7.872	8.415	8.957	9.357	8.808	7.603
x_d = 0.492	19.631	19.631	μ_4	21.186	20.604	20.293	19.984	19.749	19.631	19.631	19.631	19.419	16.919	
x_c = 0.749	33.571	31.061	h^{os}		37.725	35.871	35.183	34.355	33.461	32.257	31.397	30.685	29.756	
	28.222	29.769	v	25.573	26.098	26.632	27.165	27.705	28.268	28.871	29.475	30.080	30.632	31.025
0.8 K			h	21.196	22.423	23.593	24.819	25.979	26.968	27.820	28.584	28.950	28.855	28.898
			s	0.015	2.818	4.524	6.085	7.408	8.428	9.236	9.914	10.049	9.319	8.025
			μ_4	21.185	20.511	20.168	19.813	19.470	19.257	19.136	19.080	18.264	15.109	
			h^{os}		39.629	37.294	36.501	35.741	34.678	33.609	32.656	31.622	30.382	
			v	25.573	26.092	26.625	27.158	27.698	28.261	28.860	29.492	30.123	30.677	31.021
0.9 K			h	21.212	22.538	23.784	25.106	26.385	27.505	28.475	29.284	29.452	29.262	29.222
			s	0.033	2.953	4.748	6.422	7.886	9.061	10.007	10.740	10.640	9.798	8.406
			μ_4	21.183	20.415	20.040	19.646	19.203	18.865	18.654	18.397	16.880	13.160	
			h^{os}		41.651	38.757	37.844	37.156	36.145	35.022	33.950	32.595	31.051	
			v	25.573	26.087	26.622	27.156	27.692	28.253	28.855	29.497	30.142	30.702	31.021
1.0 K			h	21.247	22.673	23.991	25.410	26.814	28.075	29.194	29.907	29.957	29.700	29.555
			s	0.070	3.095	4.966	6.742	8.338	9.661	10.764	11.397	11.171	10.259	8.757
			μ_4	21.178	20.312	19.909	19.484	18.948	18.488	18.183	17.457	15.349	11.090	
			h^{os}		43.920	40.318	39.237	38.611	37.662	36.535	35.243	33.608	31.767	
			v	25.571	26.082	26.623	27.159	27.692	28.244	28.838	29.478	30.129	30.702	31.026

1.1 K	h	21.315	22.845	24.231	25.745	27.276	28.695	29.973	30.485	30.476	30.173	29.897
	s	0.134	3.258	5.194	7.061	8.778	10.251	11.506	11.948	11.667	10.709	9.083
	μ_4	21.168	20.202	19.772	19.324	18.704	18.131	17.699	16.360	13.721	8.909	
	h^{os}		46.632	42.068	40.726	40.132	39.258	38.155	36.539	34.665	32.535	
	v	25.569	26.078	26.629	27.170	27.698	28.234	28.808	29.431	30.079	30.669	31.036
1.2 K	h	21.434	23.077	24.528	26.129	27.790	29.402	30.631	31.042	31.022	30.686	30.249
	s	0.237	3.459	5.452	7.395	9.225	10.866	12.080	12.433	12.141	11.156	9.389
	μ_4	21.149	20.080	19.624	19.162	18.470	17.805	16.984	15.172	12.030	6.617	
	h^{os}		50.050	44.146	42.387	41.771	40.998	39.730	37.843	35.770	33.361	
	v	25.564	26.075	26.641	27.191	27.713	28.226	28.765	29.354	29.985	30.597	31.051
1.3 K	h	21.626	23.398	24.914	26.594	28.393	30.257	31.189	31.591	31.601	31.247	30.611
	s	0.390	3.716	5.761	7.766	9.707	11.549	12.527	12.873	12.604	11.604	9.679
	μ_4	21.119	19.941	19.459	18.990	18.247	17.526	16.135	13.937	10.299	4.215	
	h^{os}		54.510	46.736	44.335	43.612	42.987	41.226	39.158	36.926	34.251	
	v	25.556	26.072	26.659	27.224	27.739	28.220	28.708	29.242	29.840	30.479	31.072
1.4 K	h	21.917	23.844	25.431	27.180	29.139	30.938	31.682	32.141	32.220	31.864	30.982
	s	0.605	4.046	6.143	8.200	10.259	12.056	12.893	13.280	13.063	12.062	9.953
	μ_4	21.069	19.779	19.269	18.801	18.037	17.010	15.235	12.683	8.548	1.700	
	h^{os}		60.426	50.081	46.731	45.793	44.867	42.647	40.481	38.138	35.216	
	v	25.544	26.070	26.685	27.269	27.778	28.219	28.637	29.091	29.638	30.311	31.098
1.5 K	h	22.339	24.460	26.132	27.946	30.112	31.397	32.125	32.694	32.888	32.551	31.360
	s	0.896	4.470	6.626	8.728	10.929	12.373	13.198	13.662	13.524	12.535	10.214
	μ_4	20.995	19.588	19.044	18.585	17.849	16.287	14.330	11.434	6.797	-0.930	
	h^{os}		68.305	54.487	49.789	48.506	46.507	43.988	41.805	39.411	36.271	
	v	25.528	26.068	26.718	27.330	27.832	28.223	28.551	28.900	29.374	30.084	31.131

Table 22: Properties at 10 bar. (h : J/mol, s : J/mol K, μ_4 : J/mol-^{4}He, h^{os} : J/mol-^{3}He, v : cm^3/mol)

10 bar: x_t = 0.697, T_t =0.757 K			x	0	0.1	0.2	0.3	0.4	0.5	0.6	0.7	0.8	0.9	1
T	*Dil-Φ*	*Conc-Φ*	T_λ	2.057	1.925	1.775	1.607	1.420	1.215	0.992				
0.2 K	27.155	33.216	h	26.264	26.980	27.688	28.386	29.085	29.784	30.482	31.181	31.880	32.578	33.247
	1.511	4.233	s	0.000	1.383	1.750	2.064	2.378	2.691	3.005	3.319	3.633	3.947	3.981
x_d = 0.124	26.066	26.066	μ_4	26.264	26.088	26.066	26.066	26.066	26.066	26.066	26.066	26.066	26.066	
x_c = 0.991	34.866	33.279	h^{os}		35.009	34.175	33.801	33.614	33.502	33.427	33.373	33.333	33.302	
	25.851	30.245	v	25.206	25.732	26.238	26.744	27.251	27.757	28.264	28.770	29.277	29.784	30.329
0.3 K	27.552	33.462	h	26.264	27.081	27.866	28.597	29.327	30.057	30.788	31.518	32.248	32.979	33.525
	2.277	5.860	s	0.000	1.790	2.467	2.910	3.353	3.796	4.238	4.681	5.124	5.567	5.104
x_d = 0.157	25.931	25.931	μ_4	26.264	26.015	25.931	25.931	25.931	25.931	25.931	25.931	25.931	25.931	
x_c = 0.966	36.258	33.726	h^{os}		36.668	35.607	34.816	34.421	34.184	34.025	33.912	33.828	33.762	
	26.014	30.043	v	25.206	25.727	26.228	26.726	27.224	27.722	28.220	28.718	29.216	29.714	30.307
0.4 K	28.129	33.592	h	26.264	27.186	28.120	28.871	29.621	30.372	31.123	31.874	32.624	33.375	33.816
	3.196	6.853	s	0.001	2.094	3.190	3.693	4.195	4.698	5.200	5.703	6.205	6.708	5.939
x_d = 0.201	25.745	25.745	μ_4	26.264	25.938	25.745	25.745	25.745	25.745	25.745	25.745	25.745	25.745	
x_c = 0.929	37.596	34.193	h^{os}		38.424	37.621	36.165	35.437	35.000	34.708	34.500	34.344	34.223	
	26.229	29.845	v	25.206	25.720	26.223	26.720	27.217	27.714	28.211	28.707	29.204	29.701	30.289
0.5 K	28.972	33.654	h	26.265	27.293	28.334	29.267	30.024	30.781	31.538	32.295	33.052	33.689	34.111
	4.368	7.567	s	0.002	2.332	3.674	4.569	5.087	5.604	6.121	6.639	7.156	7.425	6.599
x_d = 0.261	25.487	25.487	μ_4	26.264	25.855	25.610	25.487	25.487	25.487	25.487	25.487	25.487	25.003	
x_c = 0.879	38.836	34.774	h^{os}		40.233	39.230	38.087	36.830	36.076	35.573	35.213	34.944	34.654	
	26.519	29.656	v	25.206	25.712	26.217	26.716	27.223	27.731	28.238	28.745	29.253	29.766	30.275
0.6 K	30.242	33.782	h	26.265	27.399	28.520	29.671	30.631	31.385	32.139	32.893	33.647	34.058	34.411
	5.923	8.326	s	0.003	2.525	4.014	5.319	6.187	6.699	7.211	7.722	8.234	8.097	7.145
x_d = 0.348	25.132	25.132	μ_4	26.264	25.769	25.492	25.237	25.132	25.132	25.132	25.132	25.132	23.696	
x_c = 0.818	39.801	35.708	h^{os}		42.065	40.633	40.017	38.881	37.639	36.811	36.219	35.776	35.210	
	26.939	29.430	v	25.206	25.705	26.207	26.701	27.213	27.743	28.274	28.804	29.334	29.853	30.264
0.7 K	32.279	33.985	h	26.267	27.503	28.703	29.943	31.093	32.212	32.959	33.668	34.293	34.445	34.715
	8.044	9.114	s	0.006	2.686	4.295	5.739	6.911	7.973	8.471	8.916	9.232	8.692	7.614
x_d = 0.504	24.641	24.641	μ_4	26.263	25.680	25.370	25.060	24.816	24.653	24.641	24.641	24.446	22.135	
x_c = 0.745	39.791	37.189	h^{os}		43.911	42.036	41.338	40.508	39.771	38.504	37.537	36.755	35.812	
	27.730	29.101	v	25.206	25.699	26.196	26.688	27.187	27.707	28.276	28.846	29.417	29.927	30.258
0.8 K			h	26.274	27.608	28.884	30.217	31.482	32.575	33.526	34.386	34.849	34.857	35.025
			s	0.015	2.826	4.537	6.104	7.431	8.444	9.230	9.873	9.974	9.242	8.028
			μ_4	26.262	25.587	25.245	24.888	24.533	24.288	24.123	24.041	23.279	20.372	
			h^{os}		45.792	43.443	42.651	41.906	40.861	39.796	38.820	37.741	36.467	
			v	25.206	25.696	26.186	26.673	27.173	27.704	28.276	28.881	29.478	29.982	30.256
0.9 K			h	26.291	27.719	29.068	30.497	31.885	33.118	34.203	35.126	35.402	35.307	35.341
			s	0.035	2.957	4.754	6.433	7.905	9.084	10.026	10.746	10.626	9.772	8.400
			μ_4	26.260	25.490	25.117	24.722	24.265	23.891	23.629	23.339	21.883	18.440	
			h^{os}		47.779	44.875	43.970	43.315	42.346	41.252	40.177	38.782	37.181	
			v	25.206	25.696	26.179	26.659	27.157	27.694	28.279	28.900	29.509	30.013	30.258
1.0 K			h	26.328	27.849	29.266	30.789	32.305	33.690	34.944	35.796	35.973	35.805	35.665
			s	0.074	3.094	4.962	6.741	8.347	9.685	10.806	11.452	11.228	10.295	8.742
			μ_4	26.255	25.388	24.986	24.562	24.013	23.516	23.157	22.393	20.339	16.355	
			h^{os}		50.005	46.386	45.319	44.742	43.864	42.802	41.540	39.882	37.966	
			v	25.204	25.701	26.177	26.650	27.144	27.682	28.271	28.896	29.508	30.013	30.265

1.1 K	h	26.400	28.016	29.493	31.105	32.749	34.305	35.744	36.431	36.579	36.357	35.998
	s	0.142	3.252	5.178	7.043	8.770	10.271	11.568	12.057	11.805	10.821	9.058
	μ_4	26.244	25.277	24.849	24.404	23.775	23.170	22.686	21.305	18.702	14.119	
	h^{os}		52.667	48.071	46.741	46.211	45.440	44.449	42.913	41.048	38.828	
	v	25.201	25.710	26.181	26.648	27.138	27.673	28.255	28.870	29.470	29.979	30.277
1.2 K	h	26.526	28.241	29.774	31.465	33.238	35.000	36.424	37.054	37.230	36.971	36.338
	s	0.251	3.448	5.422	7.355	9.195	10.875	12.161	12.600	12.371	11.355	9.355
	μ_4	26.225	25.153	24.701	24.245	23.551	22.865	22.002	20.148	17.008	11.731	
	h^{os}		56.032	50.066	48.311	47.769	47.135	46.038	44.300	42.286	39.776	
	v	25.196	25.724	26.194	26.656	27.144	27.671	28.237	28.822	29.393	29.904	30.293
1.3 K	h	26.726	28.555	30.139	31.896	33.805	35.835	37.002	37.681	37.937	37.657	36.687
	s	0.411	3.699	5.714	7.700	9.648	11.543	12.624	13.102	12.937	11.903	9.634
	μ_4	26.192	25.013	24.535	24.077	23.343	22.620	21.206	18.967	15.284	9.185	
	h^{os}		60.435	52.555	50.140	49.498	49.051	47.532	45.702	43.601	40.820	
	v	25.187	25.743	26.216	26.679	27.166	27.683	28.218	28.752	29.272	29.783	30.314
1.4 K	h	27.028	28.994	30.631	32.440	34.504	36.487	37.513	38.320	38.710	38.425	37.043
	s	0.634	4.023	6.077	8.102	10.165	12.028	13.003	13.575	13.509	12.472	9.897
	μ_4	26.141	24.850	24.344	23.892	23.152	22.150	20.383	17.798	13.553	6.475	
	h^{os}		66.289	55.777	52.386	51.531	50.825	48.932	47.116	44.999	41.975	
	v	25.174	25.769	26.249	26.717	27.208	27.712	28.202	28.661	29.104	29.610	30.341
1.5 K	h	27.465	29.600	31.301	33.155	35.416	36.906	37.972	38.974	39.558	39.291	37.404
	s	0.935	4.441	6.539	8.594	10.794	12.317	13.320	14.026	14.094	13.070	10.147
	μ_4	26.063	24.656	24.117	23.680	22.989	21.489	19.584	16.669	11.839	3.593	
	h^{os}		74.099	60.036	55.263	54.057	52.323	50.230	48.533	46.488	43.258	
	v	25.156	25.801	26.295	26.776	27.276	27.763	28.193	28.548	28.886	29.380	30.372

References

1. Radebaugh, R. , "Thermodynamic properties of ^{3}He-^{4}He solutions with applications to the 3He-4He dilution refrigerator", NBS Tech note 362:19 (1967).

2. Kuerten, J.G.M. , Castelijns, C.A.M. , de Waale, A.T.A.M. , and Gijsman, H.M. , "Thermodynamic properties of ^{3}He-^{4}He mixtures at zero pressure for temperatures below 250 mK and ^{3}He concentrations below 8%", *Cryogenics* **24**, pp. 419-443 (1985).

3. Miller, F.K., and Brisson, J.G., "Measurements of the Superfluid Joule-Thomson Refrigerator Using High Concentration ^{3}He-^{4}He Mixtures", *Journal of Low Temperature Physics* **147**, pp. 559-578 (2007).

4. Miller, F.K., "The Development of a Proof of Principle Superfluid Joule-Thomson refrigerator for cooling below 1 K", Ph.D. Thesis, Massachusetts Institute of Technology (2005).

5. Miller, F.K., and Brisson, J.G., "Proof-of-principle measurements of the superfluid Joule-Thomson refrigerator concept", *Journal of Low Temperature Physics* **141**, pp. 179-190 (2005).

6. Brisson, J.G., "Cold-Cycle Dilution Refrigeration", *Journal of Low Temperature Physics* **111**, pp. 181-199 (1998).

7. Sydoriak, S.G., and Roberts, T.R., "Vapor pressures of ^{3}He-^{4}He mixtures", *Physical Review* **118**, pp. 901-912 (1960).

8. Sommers, H.S., "Vapor pressures of ^{3}He-^{4}He mixtures below the Lambda-Point", *Physical Review* **88**, pp. 113-127 (1952).

9. Sreedhar, A.K., and Daunt, J.G., "Vapor pressures of ^{3}He-^{4}He mixtures", *Physical Review* **117**, pp. 891-896 (1960).

10. de Bruyn Ouboter, R., Taconis, K.W., le Pair, C., and Beenakker, J.J.M., "Thermodynamic properties of liquid ^{3}He-^{4}He mixtures derived from specific heat measurements between 0.4 K and 2 K over the complete concentration range", *Physica* **26**, pp. 853-888 (1960).

11. London, H., Clarke, G.R., and Mendoza, E., "Osmotic Pressure of ^{3}He in Liquid ^{4}He, with Proposals for a Refrigerator to Work below 1 K", *Physical Review* **128**, pp. 1992-2005 (1962).

12. Islander, S. T., and Zimmermann Jr., W., "Specific Heat of Liquid He^3/He^4 Mixtures near the Junction of the λ and Phase-Separation Curves. II", *Physical Review A* **7**, pp. 188-197 (1973).

13. Goellner, G., Behringer, R., and Meyer, H., "Thermodynamic Properties of Liquid ^{3}He-^{4}He mixtures near the tricritical point. I. Vapor pressure measurements and their thermodynamic analysis", *Journal of Low Temperature Physics* **13**, pp. 113-147 (1973).

14. Alvesalo, T.A., Bergland, P.M., Islander, S.T., Pickett, G.R., and Zimmermann Jr., W., "Specific Heat of Liquid He^3/He^4 Mixtures near the Junction of the λ and Phase-Separation Curves. I", *Physical Review A* **4**, pp. 2354-2368 (1971).

15. Arp, V., McCarty, R.D., and Hands, B.A., computer code HEPAK ver 3.30, CRYODATA, Niwot, CO (1994).

16. Abraham, B.M., and Osborne, D.W., "Experimental determination of the molar volume and derivation of the expansion coefficient, entropy change on compression, compressibility, and first-sound velocity for liquid ^{3}He from 35 to 1200 mK and from the saturation pressure to 24 atm", *Journal of Low Temperature Physics* **5**, pp. 335-352 (1971).

17. Lemmon, E.W., McLinden, M.O., and Huber, M.L., computer code REFPROP (NIST Standard Reference Database 23, Version 7.0), Physical and Chemical Properties Division, NIST, Boulder, CO (2002).

18. Smith, J.M., Van Ness, H.C., and Abbott, M.M., Introduction to Chemical Engineering Thermodynamics, 6th ed., McGraw-Hill, pp. 368-380 (2001).

19. Wilks, J., The Properties of Liquid and Solid Helium, Clarendon Press, p. 247 (1967).

20. Ebner, C., and Edwards, D.O., "The low temperature thermodynamic properties of superfluid solutions of ^{3}He in ^{4}He", *Physics Reports* **2**, pp. 77-154 (1971).

21. Miller, F.K., and Brisson, J.G., "A simple method for the analysis of sub-Kelvin refrigerators that use a dilute superfluid ^{3}He-^{4}He mixture as a working fluid", *Cryogenics* **41**, pp. 311-318 (2001).

22. Kierstead, H.A., "Dielectric Constant, Molar Volume, and Phase Diagram of Saturated Liquid ^{3}He-^{4}He Mixtures", *Journal of Low Temperature Physics* **24**, pp. 497-512 (1976).

23. He, J., Culman, T.G., Hjort, H.H., and Edwards, D.O., "^{4}He in liquid ^{3}He below 0.1 K : Measurements of the solubility and prewetting transition", *Journal of Low Temperature Physics* **119**, pp. 533-588 (2000).

24. Nakamura, M., Fujii, Y., Shigi, T., and Nagao, K., "Solubility of ^{4}He in Liquid ^{3}He at Very Low Temperatures", *Journal of the Physical Society of Japan* **57**, pp. 1676-1680 (1988).

25. Landau, J., Tough, J.T., Brubaker, N.R., and Edwards, D.O., "Temperature, Pressure and Concentration Dependence of the Osmotic Pressure of Dilute ^{3}He-^{4}He Mixtures", *Physical Review A* **2**, pp. 2472-2482 (1970).

26. Wilson, M.F., and Tough, J.T., "Osmotic pressure of dilute solutions of ^{3}He in ^{4}He", *Physics Review A* **1**, pp. 914-922 (1970).

27. Qin, X., Howald, C., and Meyer, H., "Shear viscosity measurements of liquid ^{3}He-^{4}He mixtures above 0.5 K", *Journal of Low Temperature Physics* **87**, pp. 731-752 (1992).

28. Kierstead, H.A., "Phase diagram and Concentration Susceptibility of ^{3}He-^{4}He mixtures near the tricritical point", *Journal of Low Temperature Physics* **35**, pp. 25-39 (1978).

29. Roe, D.B., Rupperiner, G., and Meyer, H., "Ultrasonic propagation in ^{3}He-^{4}He mixtures near the tricritical point", *Journal of Low Temperature Physics* **27**, pp. 747-776 (1977).

30. Yorozu, S., Hiroi, M., Fukuyama, H., Akimoto H., Ishimoto, H., and Ogawa, S., "Phase-separation curves of ^{3}He-^{4}He mixtures under pressure", *Physical Review B* **45**, pp. 12942-12948 (1992).

31. Ahlers, G., and Greywall, D.S., "Second-sound velocity and superfluid density near the tricritical point in ^{3}He-^{4}He mixtures", *Physics Review Letters* **29**, pp. 849-852 (1972).

32. Lahuerte, J.P., "Phase separation under pressure in dilute liquid mixtures of ^{4}He in ^{3}He", *Journal of Low Temperature Physics* **12**, pp. 127-144 (1973).

33. Roberts, T.R., and Sydoriak, S.G., "Sound velocity, phase separation and Lambda-transitions of ^{3}He-^{4}He mixtures", *Physics of Fluids* **3**, pp. 895-902 (1960).

34. Anderson, A.C., Edwards, D.O., Roach, W.R., Sarwinski, R.E. and Wheatley, J.C., "Thermal and Magnetic Properties of Dilute Solutions of ^{3}He in ^{4}He at Low Temperatures", *Physical Review Letters* **17**, pp. 367-372 (1966).

35. Edwards, D.O., Brewer, D.F., Seligman, P., Skertic, M., and Yakub, M., "Solubility of He^3 in liquid He^4 at 0 K", *Physical Review Letters* **15**, pp. 773-775 (1960).

36. Gasparini, F., and Moldover, M.R., "Specific Heat of ^{3}He-^{4}He mixtures very near the λ line", *Physical Review Letters* **23**, pp. 749-752 (1969).

37. Reif, F., Fundamentals of Statistical and Thermal Physics, McGraw-Hill, pp. 119-121 (1965).

38. Lounasmaa, O.V., Experimental Principles and Methods below 1 K, Academic Press, pp. 21-22 (1974).

39. Greywall, D.S., "Specific Heat of Dilute Solutions of ^{3}He in ^{4}He and the ^{3}He-Quasiparticle Excitation Spectrum", *Physical Review Letters* **41**, pp. 177-180 (1978).

40. Greywall, D.S., "Specific heat of normal liquid ^{3}He", *Physical Review B* **27**, pp. 2747-2766 (1983).

41. Khalatnikov, I.M., An Introduction to the Theory of Superfluidity, W.A. Benjamin Inc., pp. 11-12 (1965).

42. Greywall, D.S., "Specific heat and phonon dispersion of liquid ^{4}He", *Physical Review B* **18**, pp. 2127-2144 (1978).

43. Brisson, J.G., and Patel, A.B., "A Simple Model for a Superfluid Stirling Refrigerator at High Operating Temperature", *Journal of Low Temperature Physics* **116**, pp. 443-475 (1999).

44. Arp, V.D., "State Equation of Liquid Helium-4 from 0.8 to 2.5 K", *Journal of Low Temperature Physics* **79**, pp. 93-114 (1990).

45. Polturak, E., and Rosenbaum, R., "Specific Heat of 5% and 3% ^{3}He-^{4}He solutions under pressure", *Journal of Low Temperature Physics* **43**, pp. 477-498 (1981).

46. Deng, W., "Studies of Wall-Film Superfluidity in ^{3}He/^{4}He mixtures", Ph.D. Thesis, University of Minnesota (2007).

47. Hoffer, J.K., and Sinha, D.N., "Dynamics of binary phase separation in liquid ^{3}He-^{4}He mixtures", *Physical Review A* **33**, pp. 1918-1940 (1986).

48. del Cueto, J., Johnson, R.L., Rohde, T., Wirth, F.H., and Graf, E.H., "Experiments in ^{3}He-^{4}He liquid mixtures near the tricritical point", *Journal de Physique* **C7**, pp. 133-136 (1980).

49. Hatakeyama, K., Noma, S., Tanaka, E., Burmistrov, S.N., and Satoh, T., "Molar volume of superfluid ^{3}He-^{4}He mixtures: The dependence of the Bardeen-Baym-Pines parameter on temperature, pressure and ^{3}He concentration", *Physical Review B* **67**, 094503 (2003).

50. Watson, G.E., Reppy, J.D., and Richardson, R.C., "Low-Temperature Density and Solubility of ^{3}He in Liquid ^{4}He under Pressure", *Physical Review* **188**, pp. 384-396 (1969).

51. Zinov'eva, K.N., "Diagram of state for ^{3}He-^{4}He solutions: phase stratification and solidification curves", *Soviet Physics JETP* **17**, pp. 1235-1241 (1963).

52. Beal, B.T., Hatton, J., and Harrison, R.B., "Investigation of the λ-point of ^{3}He-^{4}He mixtures by NMR", *Physics Letters* **21**, pp. 142-144 (1966).

53. Vignos, J.H. and Fairbank, H.A., "Sound Measurements in Liquid and Solid He^3, He^4, and He^3-He^4 Mixtures", *Physical Review* **147**, pp. 185-198 (1966).

54. Le Pair, C., Taconis, K.W., de Bruyn Ouboter, R., Das, P. and de Jong, E., "The phase diagram of ^{3}He-^{4}He mixtures at pressures larger than the saturated vapour pressure", *Physica* **31**, pp. 764-812 (1965).

55. Boghosian, C., and Meyer, H., "Density of a dilute ^{3}He-^{4}He solution under pressure", *Physical Letters A* **25**, pp. 352-353 (1967).

56. Kerr, E.C., "Temperatures of the volume minima and stratification regions for ^{3}He-^{4}He mixtures", *Physical Review Letters* **12**, pp. 185-187 (1964).

57. Tanaka, E., Hatakeyama, K., Noma, S., and Satoh, T., "Molar volume of pure liquid ^{4}He: dependence on temperature (50-1000 mK) and pressure (0-1.57 MPa)", *Cryogenics* **40**, pp. 365-377 (2000).

58. Brooks, J.S., and Donnelly, R.J., "The Calculated Thermodynamic Properties of Superfluid Helium-4", *Journal of Physical and Chemical Reference Data* **6**, pp. 51-104 (1977).

59. Kollar, M., and Vollhardt, D., "Thermodynamically consistent equilibrium properties of normal-liquid ^{3}He", *Physical Review B* **61**, pp. 15347-15360 (2000).

60. Sherman, R.H., and Edeskuty, F.J., "Pressure-Volume-Temperature relations of liquid ^{3}He from 1.0 to 3.3 K", *Annals of Physics* **9**, pp. 522-547 (1960).

61. Khalatnikov, I.M., An Introduction to the Theory of Superfluidity, W.A. Benjamin Inc., pp. 149-152 (1965).

62. Zeegers, J.C.H., "Critical Velocities and Mutual Friction in ^{3}He-^{4}He mixtures at temperatures below 100 mK", Ph.D. Thesis, Eindhoven University of Technology (1991).

63. Mudde, R.F., "Thermal Counterflow in ^{3}He-^{4}He mixtures", Ph.D. Thesis, Leiden University (1989).

64. Miller, F.K., and Brisson, J.G., "Development of a low-temperature ^{3}He compressor for superfluid ^{3}He-^{4}He mixtures", *Cryogenics* **47**, pp. 67-80 (2007).